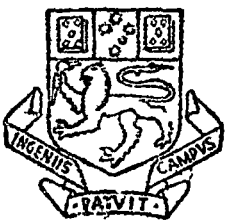

The University of Tasmania

SOLAR RADIO EMISSIONS

by

Wan Kwan Yip, B.Sc. (Hon.)

A thesis submitted in fulfillment of

the requirements for the Degree of

Doctor of Philosophy

in the

University of Tasmania

HOBART

January, 1970

ACKNOWLEDGEMENTS

I am indebted to my supervisor Professor G.R.A. Ellis for his encouragement, criticism and advice through the period of my study. In particular, Professor Ellis suggested the investigation of the origin of solar drift pair burst and hook burst emissions.

Apart from the acknowledgements made above and in the body of the text the material presented in this thesis is my own work.

During the course of this study, I have been awarded the Research Scholarship from the University of Tasmania.

Yip Wai Kwan

W.K. Yip (葉雲鈞)

January, 1970.

CONTENTS

CHAPTER 1

INTRODUCTION

A. Solar Radio Emissions

During the last two solar cycles, solar radio emissions in the observable frequency range have been observed to come from both thermal and nonthermal sources in the solar atmosphere. The thermal emission consists of two components (Kundu, 1965):

(1) The quiet sun component, the radiation emitted in the absence of localized sources in the solar atmosphere and originating in the corona where the temperature is of the order of 10^6 ^oK, or from the chromosphere whose temperature varies between 6,000 ^oK and 30,000 ^oK;

(2) The slowly varying component which originates thermally from high density regions of the corona with a temperature of about $2x10^6$ ^oK; these regions exist over sunspots and plage regions. The nonthermal emissions are generally associated with solar flares and originate from all levels of the solar atmosphere between the lower chromosphere (millimetre and centimetre waves) and the outer corona to heights of several solar radii (metre and decametre waves). The equivalent brightness temperature of the nonthermal emission source can reach as high as 10^{12} ^oK. The bursts at centimetre wavelengths are simplest in spectral appearance and consist of three distinct types: impulsive burst, post burst and gradual rise and fall. The bursts in decimetre wavelength region show a great variety of fast drifting elements

superimposed on a background continuum. The bursts at metre and decametre wavelengths are characterized by great variety and complexity. Depending on their spectral characteristics, they are designated as types I, II, III, IV and V (Wild et al., 1963). Examples of the principal spectral types of solar radio bursts are illustrated in Fig. 1.1. The main characteristics of these radio bursts are summarized in the figure captions.

To utilize radio observations for studying the structures and processes in the upper layers of the solar atmosphere, it is necessary to develop consistent theories of solar radio emissions. The thermal radio emission theory proposed by Ginzburg (1946), Shklovskii (1946) and Martyn (1946) explains a series of phenomena related to the radio emission of the quiet Sun and gives important information on the temperature and density of the solar corona and chromosphere (Kundu, 1965). However, theories of many observed solar burst emissions have not yet been fully developed although many suggestions have been put forward. Many existing theories of solar radio burst emissions are either based on some assumptions that require both experimental and theoretical verifications or lack quantitative analysis. Consequently, many of these theories are speculative only.

To put forward a successful theory, we need to study the theory in great detail and in a quantitative way. Since most of the observed burst emissions come from the corona which is

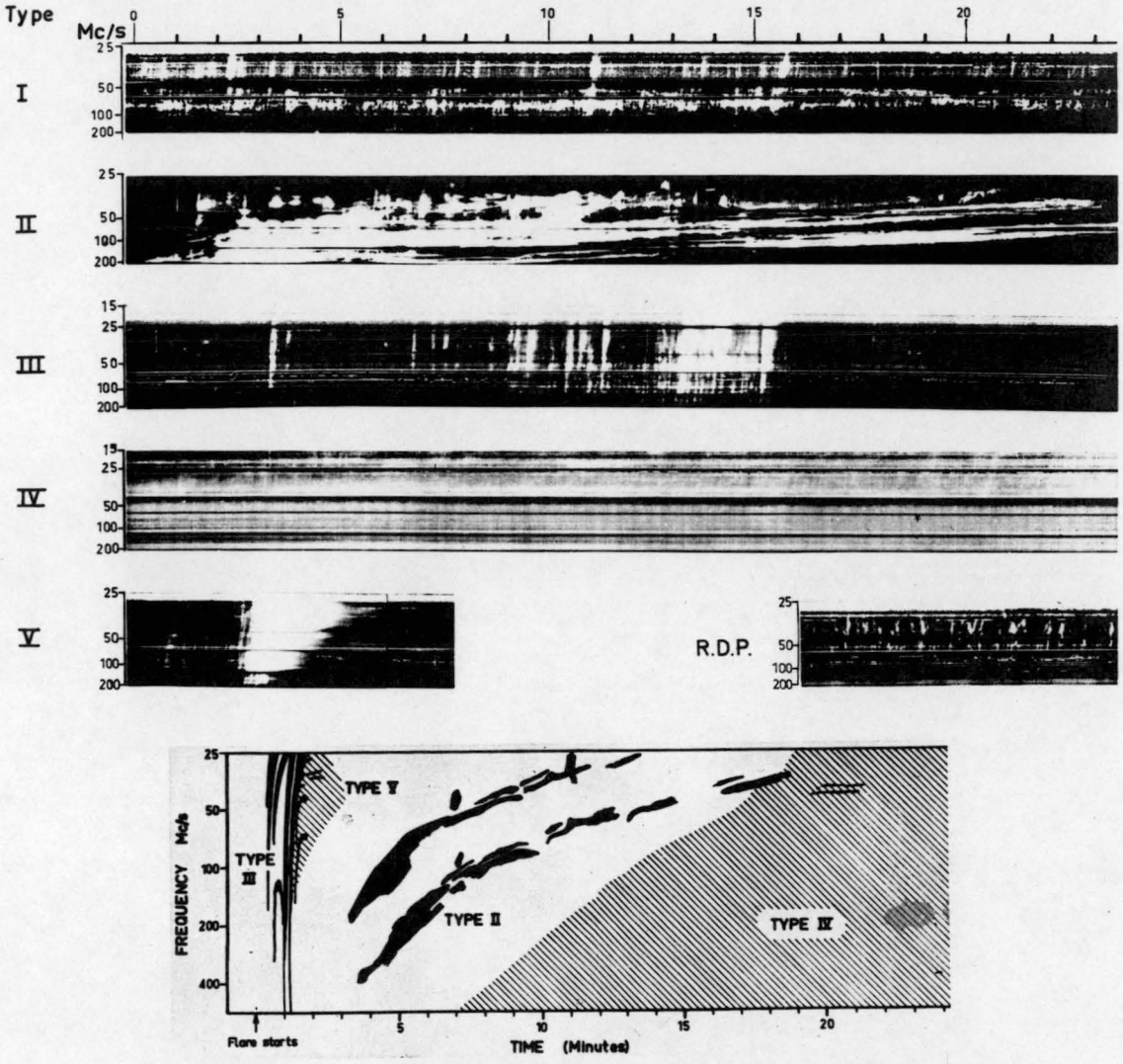

FIG. 1·1 EXAMPLES OF THE PRINCIPAL SPECTRAL TYPES OF SOLAR RADIO BURSTS AT METER WAVELENGTHS

The main figure shows records taken with the Dapto Solar Radio Spectrograph (near Sydney, Australia). The records chosen show typical examples of the six main types of events observable at meter wavelengths. Frequency is measured vertically and time horizontally, the intensity is given by the shade: intense bursts appear white, weak ones grey, and the background is black. The bright lines which are observed at a constant frequency are interference from radio transmitters.

The bottom figure shows in the same form, an idealization of the most complete sequence of events which can follow a major flare. Other details of the particular events are as follows:

Type I (22–12–59 record starts 0210 U.T.). This is a typical "noise storm" which may last for hours. This particular event occurred simultaneously with a large number of type III bursts (see below) which should not be confused with the type I.

Type II (30–11–59 record starts 0251 U.T.) This is also called a slow-drift burst. The direction of drift is always the same and the rate of drift does not vary greatly. Note, particularly near the end, the two pairs of bands, one at twice the frequency of the other.

Type III (7–10–60 record starts 0547 U.T.) These are also called fast-drift bursts. Each of the individual, almost vertical lines is a separate burst. The direction of drift is the same as for type II bursts.

Type IV (11–11–60 record starts 0408 U.T.) The example shows a form of continuum radiation (so called for its slow variation with frequency and time) which commonly follows type II bursts. It is sometimes called "type IV," but the term has been loosely applied to various forms of continuum.

Type V (4–2–60 record starts 0422 U.T.) This is a continuum event, of much shorter duration, which follows immediately after a group of type III bursts.

Drifting pairs (*D.P.*) (12–2–60 record starts 0422 U.T.) A *drifting pair* is a pair of short-duration, narrow-bandwidth bursts, very similar to one another, which occur separated in time by about two seconds. Both parts drift rapidly in frequency, either from high to low frequencies ("forward-drift pairs") or from low to high ("reverse-drift pairs"). This record shows a portion of a particularly dense storm of drifting pairs and includes drifts of both senses.

(Recorded with the Dapto Radio Spectrograph of the Division of Radiophysics C. S. I. R. O., University Grounds, Sydney, Australia. Courtesy, Paul Wild.) (After Aller, 1963).

a fully ionized gas, any interpretation of the observed solar radio emissions is tightly linked to the consideration of generation and propagation of radio waves in a fully ionized plasma. Therefore, in this chapter we shall describe briefly the propagation and generation of electromagnetic waves in a fully ionized plasma. Gaussian units will be used in this thesis.

B. Propagation of Electromagnetic Waves in A Magnetoactive Plasma

A plasma may be defined as an electrically charged gas consisting of ions and electrons. It is macroscopically neutral but microscopically ionized. When the plasma is located in a constant magnetic field, the plasma is said to be magnetoactive. A fully ionized plasma consists of ions and electrons the sum of whose charges gives zero.

(a) Dielectric Tensor and Dispersion Equation

The propagation of small amplitude waves results in small amplitude variations in the physical quantities characterizing the plasma. To obtain waves that can propagate in a plasma, one must require that the electromagnetic field associated with the wave is caused by current and space charge which, in turn, result from the action of these fields on the plasma. Therefore, the study of the behaviour of the propagating waves in a plasma is a self-consistent electromagnetic field problem.

When the particle interactions are neglected, the collisionless Boltzmann equation which describes the time behaviour of the distribution function of the plasma particles of species i in the phase space and time $f_i(\bar{r},\bar{v},t)$ under the action of an external electromagnetic field can be written as (Delcroix, 1965, p.165)

$$\frac{\partial f_i}{\partial t} + \bar{v} \cdot \frac{\partial f_i}{\partial \bar{r}} + \frac{\bar{F}}{m_i} \cdot \frac{\partial f_i}{\partial \bar{v}} = 0, \qquad (1.1)$$

where $\bar{F} = q_i \left[\bar{E} + \frac{1}{c} \bar{v} \times (\bar{B} + \bar{B}_o)\right]$.

q_i and m_i are the charge and the mass of the particle of species i. $\bar{B}_o$ is the static magnetic induction of the magnetoactive plasma. The equation (1.1) is obtained by assuming that the particle densities are low enough not to affect the external field. The macroscopic current density $\bar{j}$ and space charge density ρ representing the respond of the plasma to the electromagnetic field of the wave are determined by

$$\bar{j}(\bar{r},t) = \sum_i q_i \int \bar{v}(\bar{r},t)\, f_i(\bar{r},\bar{v},t)\, d\bar{v}$$

and $$\rho = \sum_i q_i \int f_i(\bar{r},\bar{v},t)\, d\bar{v} \qquad (1.2)$$

respectively, while the electromagnetic field itself satisfies the Maxwell's equations

$$\nabla \times \bar{B} = \frac{4\pi}{c} \bar{j} + \frac{1}{c} \frac{\partial \bar{E}}{\partial t} ,$$

$$\nabla\times\bar{E} = -\frac{1}{c}\frac{\partial\bar{B}}{\partial t}\,,$$

$$\nabla.\bar{B} = 0, \tag{1.3}$$

$$\nabla.\bar{E} = 4\pi\rho,\ \bar{B} = \bar{H}\ .$$

For small amplitude waves, the system of equations (1.1) - (1.3) can be linearized and, in a number of cases, these equations can be solved by means of Fourier methods. In the perturbation treatment, the distribution function and other physical quantities in the plasma are written in the form of plane waves*

$$f_1 = f_o + f'$$

and $$f'(\bar{r},\bar{v},t) = f'(\bar{v},\bar{k},\omega)\exp(i\bar{k}.\bar{r} - i\omega t)$$

where f_o is the unperturbed distribution function, $\bar{k}$ is the wave vector and ω is the angular wave frequency. The perturbation f' due to the presence of the wave is assumed to be much smaller than the unperturbed value, i.e. $f' << f_o$. Then the electric field vector associated with the wave can be written as

$$\bar{E}(\bar{r},t) = \bar{E}(\bar{k},\omega)\exp\left[i(\tilde{k}z - \tilde{\omega}t) + (qz - \delta t)\right]\,,$$

where $\tilde{k}$ denotes the wave number and is related to the wavelength λ and the refractive index n by

---

* In this thesis, unless otherwise stated, we assume that the wave is in the form $\exp(i\bar{k}.\bar{r} - i\omega t)$ with wave vector $\bar{k}$ lying on x-z plane of a Cartesian coordinate system and the static magnetic field directs along the z-axis.

$$\tilde{k} = \frac{2\pi}{\lambda} = \frac{n\tilde{\omega}}{c} ,$$

$\tilde{\omega}$ being the real part of the angular wave frequency. q and δ are the imaginary parts of the complex quantities k, ω respectively, z is the path length in the direction of propagation. The phase velocity and the group velocity for the wave are given by (Ginzburg, 1964, p.262)

$$v_{ph} = \frac{\tilde{\omega}}{\tilde{k}} , \text{ and } v_g = \left| \frac{\partial \tilde{\omega}}{\partial \underline{\tilde{k}}} \right|$$

respectively.

Having determined f' from (1.1) and (1.3), we can express the Fourier component of the current density resulting from the action of the electromagnetic field in a homogeneous unbounded plasma as

$$j_\alpha (\bar{k},\omega) = -i\omega K_{\alpha\beta} E_\beta(\bar{k},\omega) \qquad (1.4)$$

where $K_{\alpha\beta}(\bar{k},\omega) = \sum - i \frac{e^2 n_o}{\omega} \int d\bar{p}_o \int v_\alpha (t) \left[(1 - \frac{\bar{k}.\bar{v}_o}{\omega}) \frac{\partial F_o}{\partial p_\beta^o} + \frac{v_\beta^o}{\omega} \bar{k} . \frac{\partial F_o}{\partial \bar{p}_o} \right]$

$$\times \exp \left[i\omega t - i\bar{k} . \int_o^t \bar{v}(t')dt' \right] dt \qquad (1.5)$$

is the polarizability tensor (Shafranov, 1967, p.79). The summation is carried out over all particle species (electrons and ions). The subscript "o" denotes the quantity at the time t = 0. e is the charge of an electron and n_o is the

particle number density. The unperturbed distribution function in the momentum space $F_o(\bar{p})$ is normalized to unity, i.e. $\int F_o(\bar{p})d\bar{p} = 1$, where $\bar{p}$ is the momentum of the particle. Usually, the electromagnetic properties of the plasma is characterized by the dielectric tensor $\varepsilon_{\alpha\beta}(\bar{k},\omega)$ which is related to the current density j_α through the equation

$$D_\alpha = 4\pi \int j_\alpha \, dt + E_\alpha = \varepsilon_{\alpha\beta} \, E_\beta \, , \tag{1.6}$$

where D_α is the electric induction. From (1.4), (1.5) and (1.6), it can be found that

$$\varepsilon_{\alpha\beta} \quad (\bar{k},\omega) = \delta_{\alpha\beta} + 4\pi \, K_{\alpha\beta}(\bar{k},\omega), \tag{1.7}$$

where $\delta_{\alpha\beta}$ is the Kronecker's delta. The dependence of the dielectric tensor on the frequency defines the frequency dispersion while the dependence on the wave vector $\bar{k}$ defines the spatial dispersion of the plasma.

Now, Maxwell's equations (1.3) can be reduced to three linear homogeneous equations for the three components of $E_\alpha \, (\bar{k},\omega)$. These equations have non-trivial solutions only if the determinant of their coefficients vanishes. This statement gives the most general dispersion equation which relates the angular wave frequency ω and the wave vector $\bar{k}$ in the form

$$|\wedge_{\alpha\beta}(\bar{k},\omega)| = \left|k^2 \, \delta_{\alpha\beta} - \frac{\omega^2}{c^2} \varepsilon_{\alpha\beta} - k_\alpha k_\beta\right| = 0 \, . \tag{1.8}$$

In general, $|\Lambda_{\alpha\beta}(\bar{k},\omega)|$ is a complex quantity; the imaginary part is associated with the absorption or growth of the electromagnetic wave in the plasma and arises from the anti-hermitian part of the dielectric tensor (Rukhadze and Silin, 1962; Sitenko and Kirochkin, 1966). In the transparency region of the plasma (i.e. the region of ω and $\bar{k}$ in which the anti-hermitian part of the dielectric tensor is small compared with the hermitian part), the dispersion equation can be approximately written in the form

$$\text{Re}\ |\Lambda_{\alpha\beta}(\bar{k},\omega)| = 0 \ . \qquad (1.9)$$

Since the dispersion equation involves only the dielectric tensor, once the distribution functions for the constituent plasma particles are known, the wave modes and the behaviour of the waves in a plasma will be well defined. Such a description of the electromagnetic phenomena in a plasma by means of the Boltzmann equation and the self-consistent field equations is the most rigorous and complete one. However, these equations are extremely complicated and may not always be necessary in many cases of practical interest. For a qualitative description of the relation between ω and $\bar{k}$, a macroscopic approach is sufficient.

In the macroscopic approach, the plasma is treated as a continuous fluid and its state is specified by certain macroscopic quantities such as density, mean particle velocity vector.

The changes of these macroscopic parameters due to the presence of an external electromagnetic field are described by the two basic transport equations obtained by taking the first two moments of the linearized Boltzmann-Vlasov equation (Delcroix, 1965, p.210).

The macroscopic theory does not reveal those electromagnetic phenomena which depend on the microscopic distribution of particle velocity; in particular, the Landau damping and the cyclotron resonance absorption of waves due to the thermal motions of the plasma particles (see Chapter VI). Moreover, it gives qualitatively correct description of the behaviour of the waves in a plasma only if the phase velocities of the waves are greater than the mean thermal speed of the plasma particles such that the number of resonant particles moving in synchronism with the wave is small and hence the damping is weak.

(b) High Frequency Waves in A Magnetoactive Plasma

In the Cartesian coordinate system in which the static magnetic field $\bar{B}_o$ is along the z-axis and $\bar{k}$ lies on the x-z plane, the dispersion equation (1.8) can be expanded as

$$An^4 + Bn^2 + C = 0 \qquad (1.10)$$

or $$A\left(\frac{ck}{\omega}\right)^4 + B\left(\frac{ck}{\omega}\right)^2 + C = 0,$$

where $A = \varepsilon_{11} \sin^2\theta + 2\,\varepsilon_{13} \sin\theta \cos\theta + \varepsilon_{33} \cos^2\theta$,

$$B = -\varepsilon_{11}\,\varepsilon_{33} - (\varepsilon_{22}\,\varepsilon_{33} + \varepsilon_{23}^2)\cos^2\theta + \varepsilon_{13}^2 - (\varepsilon_{11}\,\varepsilon_{22} + \varepsilon_{12}^2)\sin^2\theta + 2(\varepsilon_{12}\,\varepsilon_{23} - \varepsilon_{13}\,\varepsilon_{22})\cos\theta \sin\theta ,$$

$$C = \det(\varepsilon_{\alpha\beta}) = \varepsilon_{33}(\varepsilon_{11}\,\varepsilon_{22} + \varepsilon_{12}^{2}) + \varepsilon_{11}\,\varepsilon_{23}^{2}$$

$$+ 2\,\varepsilon_{12}\,\varepsilon_{13}\,\varepsilon_{23} - \varepsilon_{22}\,\varepsilon_{13}^{2}\ ,$$

and θ is the wave-normal angle; angle between $\bar{k}$ and $\bar{B}_o$.

For cold and collisionless homogeneous magnetoactive plasma, the dielectric tensor components (1.7) are functions of wave frequency only and the dispersion equation (1.10) is quadratic in n^2. The plasma transmits only four different waves; two hydromagnetic waves in the low frequency region ($f < f_{Hi}$, where $f = \omega/2\pi$ and f_{Hi} is the ion gyrofrequency) and two high frequency electromagnetic waves ($f \gg f_{Hi}$). When the plasma temperature is not absolutely zero, two additional longitudinal waves (or pressure waves) may propagate in a magnetoactive plasma. These longitudial waves depend partly on the elastic force resulting from compression of the plasma (either as a whole or the electron gas alone) and make their appearance when the thermal motions of the plasma particles are taken into account. One of these longitudinal waves appears at hydromagnetic frequencies and the other occurs in the high frequency domain.

Although low frequency waves may be important in the solar physics, they are not important in the study of generation and propagation of solar radio emissions observed on the Earth since the electromagnetic radiation in the low frequency region is unable to escape from the Sun. Therefore only the high frequency waves will be considered in this thesis.

In the high frequency domain, the effects of the ions on the propagation of waves in the magnetoactive plasma can be neglected and only the electron component of the plasma needs to be taken into account in the dispersion equation. In the solar corona, the mean thermal speed of the plasma electrons is small, i.e. $\beta_T = (\kappa T/m_o c^2)^{\frac{1}{2}} << 1$, where κ is the Boltzmann constant, T is the plasma temperature in degree Kelvin and m_o is the electron rest mass, the coronal plasma can be considered as cold and collisionless almost everywhere. With this assumption, the dispersion equation (1.10) gives two roots of n^2 for the two normal waves; extraordinary wave (n_1^2) and ordinary wave (n_2^2).

For $\theta \neq 0, \pi/2$, the polarization of the normal wave is elliptical. The polarization ellipses associated with the extraordinary and ordinary waves are identical in shape with the major and the minor axes interchanged and the senses of rotation reversed. The sense of rotation of the electric field vector of the extraordinary wave is that of the electron relative to the static magnetic field, i.e. right-handed sense relative to the direction of propagation. For longitudinal propagation ($\theta = 0$), the characteristic polarization of the two normal two waves is circular while for transverse propagation ($\theta = \pi/2$), the two waves are linearly polarized.

With the spatial dispersion of the plasma taken into account, a third wave known as a longitudinal plasma wave (n_3^2)

appears in the regions near the plasma resonance where n_1^2 or n_2^2 tends to infinity as $\beta_T \to 0$ (Gershman, 1953; 1957; Sitenko and Stepanov, 1957). Strictly speaking, electromagnetic waves in a magnetoactive plasma cannot be separated into longitudinal and transverse components except where $\theta = 0$ (Shafranov, 1967, p.7). However, in the regions near the plasma resonance, the electromagnetic wave becomes almost a pure longitudinal electric wave even for $\theta \neq 0$ (Sitenko and Kirochkin, 1966).

The dispersion curves of the three high frequency waves are illustrated in Fig. 1.2 for $Y = f_H/f = \frac{1}{2}$ and $T = 10^6\ ^oK$ and for arbitrary angle of propagation θ, where $f_H = |e|\ H_o/2\pi m_o c$ is the magnitude of the electron gyrofrequency and H_o is the static magnetic field intensity. The full and dashed lines of Fig. 1.2 represent the limiting cases corresponding to longitudinal and transverse propagation. Intermediate values of θ give dispersion curves lying in the shaded area between.

The propagation regions are $n^2 \geq 0$. For $n^2 \gg 1$, the dispersion curves represent the longitudinal plasma waves. It can be seen that the plasma wave gradually changes its physical character from a pure longitudinal wave ($n^2 \gg 1$) to a transverse electromagnetic wave. When the phase velocity of the plasma wave is reduced to the point where the wavelength becomes about as small as the Debye length D given by

$$D = \left(\frac{\kappa T}{4\pi e^2 n_o} \right)^{\frac{1}{2}} ,$$

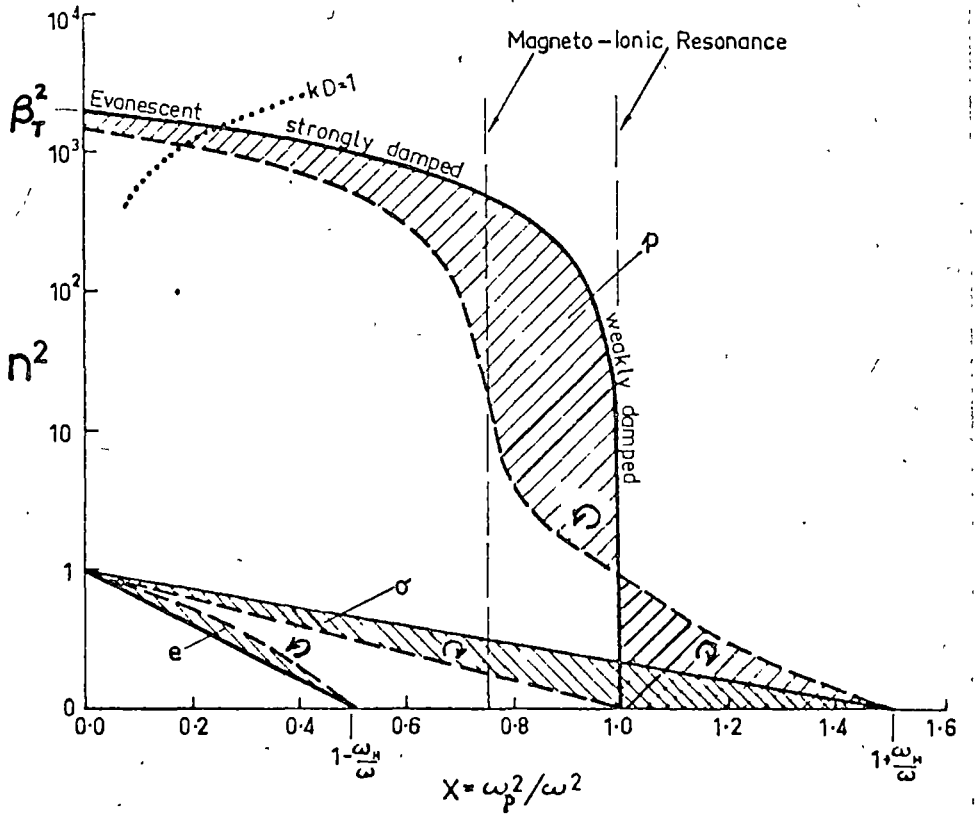

Fig.1.2 The dispersion curves for the ordinary (o), extraordinary (e) and plasma (p) waves in a plasma, assuming $T = 10^6$ °K and $Y = \frac{1}{2}$. Longitudinal propagation is shown thus ——— ; transverse thus ------. In general the curves lie in the hatched areas. The line kD = 1 corresponds to the wave number equal to the reciprocal of the Debye length.

(Wild et al., 1963, with modifications)

where n_o is the electron number density, then the wave becomes completely disorganized by the thermal motions and can no longer be supported.

For wave-normal angles different from zero, the refractive indices for the extraordinary and ordinary waves (n_1^2 and n_2^2) vanish at the points $X = f_p^2/f^2 = 1 \pm Y$ and $X = 1$ respectively; the electron plasma frequency f_p is given by $f_p = (e^2 n_o/\pi m_o)^{\frac{1}{2}}$. Hence, the critical frequencies of a layer for the two normal waves will be

$$f_1 = \pm \tfrac{1}{2} f_H + \tfrac{1}{2}(f_H^2 + 4f_p^2)^{\frac{1}{2}} \quad \text{(extraordinary)}$$

and $$f_2 = f_p \quad \text{(ordinary)} \; . \qquad (1.12)$$

Moreover, along each branch of dispersion curve, the sense of polarization reverses on passing through the point $X = 1$ (Ginzburg, 1964, p.104).

For a given homogeneous magnetoactive plasma characterized by the quantities $A = f_p^2/f_H^2$ and β_T, the dispersion curves can also be presented as n_j vs $\xi = f/f_H$ (normalized frequency) (see Fig. 2.1). It is found that for a given wave-normal angle θ, each wave is represented by two branches of dispersion curves; each branch can be labelled as a mode. Hence electromagnetic waves in six different modes in different frequency regions can propagate in a magnetoactive plasma; these are the z-mode and the x-mode (extraordinary wave), the whistler mode and the o-mode (ordinary wave) and the two longitudinal p-modes (plasma

wave) appearing in the vicinities of the plasma resonance frequencies.

For transverse electromagnetic waves, the plasma behaves as a dielectric and the waves can exist outside of the plasma. The propagation of longitudinal plasma waves is connected to the energy transport of the plasma particles and hence the longitudinal plasma waves cannot exist in the vacuum (Denisse and Delcroix, 1963, p.54).

C. Generation of High Frequency Waves in A Magnetoactive Plasma (Wild et al., 1963; Smerd, 1968)

The solar radio emissions observed on the Earth are the distant fields due to currents in the coronal plasma. The radiation processes can be classified as radiation from uniformly moving electrons and radiation due to electron acceleration.

(a) Radiation from uniformly moving Electrons

A charged particle moving with constant velocity through a medium (such as a plasma) along a rectilinear trajectory can radiate if its velocity exceeds the phase velocity of light in the medium. The radiation process is called Cerenkov radiation. Owing to its faster-than-light motion, the charged particle temporarily produces an asymmetric polarized wake in the medium which radiates the electromagnetic energy.

The direction of emission is governed by the Cerenkov condition

$$\cos \theta = \frac{c}{v n_j} , \qquad (1.13)$$

where v is the magnitude of the charged particle velocity (For a gyrating charged particle, v is taken to be the speed of the guiding centre motion.), θ is the angle between the direction of the emission and that of the charged particle motion (or guiding centre motion). For $v < c$, the Cerenkov radiation can be emitted only in the electron plasma mode, z-mode and the whistler mode and in the forward hemisphere with respect to the electron motion (or the guiding centre motion).

(b) Radiation from accelerated electrons

At large distances from an accelerated electron, the acceleration field makes the main contribution to the observed radiation intensity which is proportional to the square of the electron's acceleration (Jackson, 1962, p.464). The radiation processes due to the electron acceleration are bremsstrahlung, cyclotron radiation and synchrotron radiation.

The bremsstrahlung emission (or braking radiation) occurs when the Coulomb force of individual ions deflects the electron in electron-ion encounters. Because of the random motion of the electrons, the observed bremstrahlung emission will be randomly polarized.

A single electron gyrating along a helical path in a magnetoactive plasma will experience centrifugal acceleration and emit electromagnetic radiation at harmonics of the Doppler-shifted gyrofrequency f_H',

$$f = sf_H' = \frac{s\gamma f_H}{1 - n_j\beta \cos\theta \cos\phi} \qquad (1.14)$$

where $\gamma = (1 - \beta^2)^{-\frac{1}{2}}$, $\beta = v/c$ is the normalized speed of the electron and ϕ is the electron pitch angle; angle between the electron velocity vector and the magnetic field line. s is the harmonic number.

When the electron speed is mildly relativistic (electron energy covering a range between a few keV to a few hundreds of keV), the radiation energy is concentrated within the first few harmonics which may be clearly resolved. For $s \neq 0$, the radiation from this mildly relativistic gyrating electron is generally called cyclotron radiation (or gyro-radiation). The anomalous Doppler-shifted radiation ($s < 0$) is emitted when the electron guiding centre velocity is greater than the wave phase velocity, as for Cerenkov radiation (Ginzburg, 1960; Ginzburg et al., 1962). Hence, the Cerenkov and anomalous cyclotron radiations do not occur in the vacuum.

When the speed increases to highly relativistic (electron energy greater than 1 MeV), the emission is mainly concentrated within a cone of half-angle $\sim \gamma$; the axis of the emission cone is along the instantaneous velocity vector of the electron. An observer located in the orbital plane of the electron will receive short sharp pulse, each of duration $\Delta\tau \sim \gamma^2/2\pi f_H \sin\phi$, only when the instantaneous velocity of the electron is towards him. These pulses recur with a frequency $\sim \gamma f_H/\sin^2\phi$.

The macroscopic spectrum emitted from an assemblage of highly relativistic electrons is essentially a continuum. This radiation usually known as synchrotron radiation (Wild et al., 1963).

A group of radiating electrons, under favourable conditions, radiate electromagnetic energy coherently rather than individually. The intensity level, the polarization character and the polar diagram of the coherent radiation from a system of radiating electrons may differ greatly from those of the summation of radiation powers from all individual electrons. Therefore, in this thesis, coherent radiation processes will be considered.

D. Outline of The Thesis

All radiation processes described above can take place in the solar corona, depending on different physical characters of the radiating electrons and the coronal plasma, such as electron energy, electron pitch angle and the magnitude of the ratio f_p^2/f_H^2 of the medium in the region where the radiators reside. On the other hand, the observed spectral features of a solar radio emission are determined by both the mechanism responsible for the emission and the propagation conditions of electromagnetic waves in the solar corona. Thus, the observed dynamic spectra of the solar radio emissions reveal essentially the physical conditions of the solar corona during the emission

periods.

The emissions of narrow bandwidth type III bursts and drift pair bursts have been proposed as the consequence of plasma radiation caused by electron streams in the isotropic corona, which is understood to refer to electromagnetic radiation extracted from Cerenkov plasma waves through scattering or wave-mode coupling (Ginzburg and Zheleznyakov, 1958; Roberts, 1958; Wild et al., 1963; Zheleznyakov, 1965). However, many observed spectral characteristics of the type III bursts and its related U bursts, the drift pairs and the newly discovered hook bursts clearly indicate that it is necessary that the sunspot magnetic field be taken into account in the theories. So far the conditions of plasma radiation by electron streams in a magnetoactive plasma have not been investigated in detail and consequently, many characteristics of these emission events remain unexplained. In this thesis, we begin by formulating the theory of plasma radiation in a magnetoactive plasma (Chapter II and Chapter V). The theory is then applied to the interpretation of the polarized type III burst and U burst emission event and the drift pair and hook burst emission event in Chapter VI and Chapter VII respectively.

The origins of various components of the complicated type IV emission have been interpreted as the results of synchrotron radiation by relativistic electrons trapped in the sunspot magnetic field configurations (Boischot and Denisse, 1957;

Takakura and Kai, 1961; Kai, 1964; etc.). However, without taking into account the effects of the medium on the radiation process, previous theories encounter various difficulties and fail to account for the outstanding polarization characters of the type IV emission. In order to set up a satisfactory theory of type IVA emission, we study, for the x-mode and the o-mode, the power spectra from single electrons, the process of amplification of cyclotron radiation in a stream-plasma system and the escape conditions in detail in Chapter III and Chapter VIII. Cyclotron radiation of electromagnetic waves in the x-mode and the o-mode and the Cerenkov excitation of plasma waves by helical electron streams moving at the base of the solar corona is proposed as the origin of the type IVA emission. It is found that most of the important characteristics of the emission can be well accounted for by the theory.

In Chapter IX, coherent synchrotron radiation from a system of relativistic electrons is studied taking into account the effects of the ambient plasma. The origins of some broad band solar continuum emissions are also discussed.

In the final chapter, a conclusion of the thesis is given and further researches are suggested.

CHAPTER II

RADIATION OF PLASMA WAVES BY AN ELECTRON STREAM IN A MAGNETOACTIVE PLASMA

A. Introduction

The radiation of electromagnetic waves in various modes by charged particles in the magnetoactive plasma is of great importance to the study of radio emissions from the Earth's magnetosphere and the solar corona. By assuming that the magnetoactive plasma is cold and collisionless, Eidmman (1958, 1959) obtained both the frequency spectra and the polar diagrams of the radiation power emitted from a single charged particle based on the fundamental Hamiltonian method. Eidman's theory was subsequently revised by Liemohn (1965) who included relativistic effects in the calculation*. On the other hand, Mansfield (1967) treated the problem by means of the Fourier method in which the fields are expanded in plane waves via Fourier transforms.

When spatial dispersion of the plasma is taken into account, radiation of plasma waves by a moving electron is also possible. The general form of the dispersion equation (1.10) is

---

* Using the Eidman-Liemohn theory, the characteristics of the cyclotron radiation in the x-mode and the o-mode from a single electron will be studied in Chapter VIII.

extremely complicated. However, under the typical solar corona conditions, ($\beta_T \simeq 10^{-2}$) weakly damped plasma waves with phase velocities which satisfy the inequality $n^2 \beta_T^2 \cos^2\theta << 1$ can be generated by mildly relativistic electrons and the dispersion equation for such weakly damped plasma waves can be greatly simplified except for the case of double resonance (see discussion in Section F). Although Eidman (1962), using the Fourier transform method, obtained expressions for the total energy loss of a moving charged particle due to emission of weakly damped plasma waves, the numerical study of the characteristics of the radiation in the weakly damped plasma mode has not been attempted. Moreover, when the charged particles are organized as a stream with small momentum spread, they will radiate coherently with a radiation intensity much higher than the sum of the individual particle radiations.

In an isotropic plasma, weakly damped plasma waves are emitted only at the frequencies close to the plasma frequency by an electron stream through the Cerenkov process (Ginzburg and Zheleznyakov, 1958). In a magnetoactive plasma, weakly damped plasma waves at frequencies in the vicinities of the plasma resonance frequencies which are in general different from the plasma frequency can be excited by helical electron streams through the Cerenkov and cyclotron processes. Therefore, interpretation of the solar radio burst emission as the consequence of the generation of plasma waves by electron streams in the

magnetoactive coronal plasma requires a quantitative study of the angular and frequency spectra of the plasma waves excited by helical electron streams.

In the present chapter, after briefly reviewing the theory of propagation of plasma waves in a magnetoactive plasma in Section B, we derive the angular and frequency spectra of the weakly damped plasma waves emitted by a single electron and the rate of growth of the weakly damped plasma wave in the stream-plasma system explicitly in Section C and Section D. The expressions obtained are studied numerically with parameters appropriate to the active solar corona conditions in section E. Finally, a short discussion on the limitation of the theory is given in Section F.

B. Propagation of Longitudinal Plasma Waves in A Magnetoactive Plasma

The high frequency longitudinal plasma waves will be weakly damped when the following conditions are satisfied (Ginzburg, 1964, p.140):

$$(kv_T \sin\theta/\omega_H)^2 << 1, \; n^2 \beta_T^2 \cos^2\theta << 1, \qquad (2.1)$$

$$(1 - \omega_H^2/\omega^2)^3 >> \beta_T^2, \quad (1 - 4\omega_H^2/\omega^2) >> \beta_T^2 . \qquad (2.2)$$

In general, the conditions (2.1) are satisfied simultaneously in a plasma with fairly strong magnetic field. The conditions (2.2) indicate that only those plasma waves with frequencies

sufficiently far from the resonances $f = f_H$ and $f = 2f_H$ will be weakly attenuated. When (2.1) and (2.2) hold and for very large value of refractive index, the dispersion equation (1.10) is approximated by (Sitenko and Stepanov, 1957; Sitenko and Kirochkin, 1966)

$$\varepsilon_{\parallel}(k,\omega) = 1 - \frac{\omega_p^2 \sin^2\theta}{\omega^2-\omega_H^2} - \frac{\omega_p^2 \cos^2\theta}{\omega^2} - \frac{k^2 v_T^2 \omega_p^2 \cos^2\theta}{\omega^2} R_1 = 0 \quad (2.3)$$

where $$R_1 = \frac{3\omega^2 \sin^2\theta \tan^2\theta}{(\omega^2-\omega_H^2)(\omega^2-4\omega_H^2)} + \frac{(6\omega^4-3\omega^2\omega_H^2+\omega_H^4)\sin^2\theta}{(\omega^2-\omega_H^2)^3} + \frac{3\cos^2\theta}{\omega^2} .$$

The refractive index for the weakly damped plasma wave will be

$$n_3^2 = [\omega^4 - (\omega_p^2+\omega_H^2)\omega^2 + \omega_p^2\omega_H^2\cos^2\theta] / \beta_T^2\omega_p^2\omega^2(\omega^2-\omega_H^2)R_1 \cos^2\theta . \quad (2.4)$$

From (2.1), (2.2) and (2.3), we can see that the weakly damped plasma waves exist at the frequencies near the plasma resonance frequencies

$$f_{\pm}^2 = \tfrac{1}{2}(f_p^2 + f_H^2) \pm \tfrac{1}{2}[(f_p^2 + f_H^2)^2 - 4f_p^2 f_H^2 \cos^2\theta]^{\frac{1}{2}} \quad (2.5)$$

only. However, from (2.4), when $f \simeq f_{\pm}$, n_3 will tend to zero and the approximate dispersion equation (2.3) will no longer be valid. On the other hand, when the plasma wave frequency differs from $f_{\pm}$ greatly, the weakly damped condition $n_3^2 \beta_T^2 \cos^2\theta \ll 1$ may not hold. Therefore, in order that (2.3) and (2.4) may be

applicable, it is necessary that (2.1) and (2.2) are satisfied with the condition (Gershman, 1957; Sitenko and Stepanov, 1957)

$$\beta_T^2 << \left| 1 - \frac{\omega_p^2 \sin^2\theta}{\omega^2 - \omega_H^2} - \frac{\omega_p^2 \cos^2\theta}{\omega^2} \right| << 1. \qquad (2.6)$$

The variation of the refractive index $n_j (j = 1,2,3)$ with normalized frequency $\xi = f/f_H$ for various cases is given in Fig. 2.1. For convenience, those plasma waves with normalized frequency $\xi > 1$ will be designated as upper p-mode while those with $\xi < 1$ as lower p-mode. The dispersion curve of the upper p-mode goes asymptotically over into the dispersion curve of the z-mode while that of the lower p-mode into the whistler mode dispersion curve. For a given wave-normal angle, the phase velocities of the upper p-mode and the lower p-mode waves are always less than those of the z-mode and the whistler mode waves respectively.

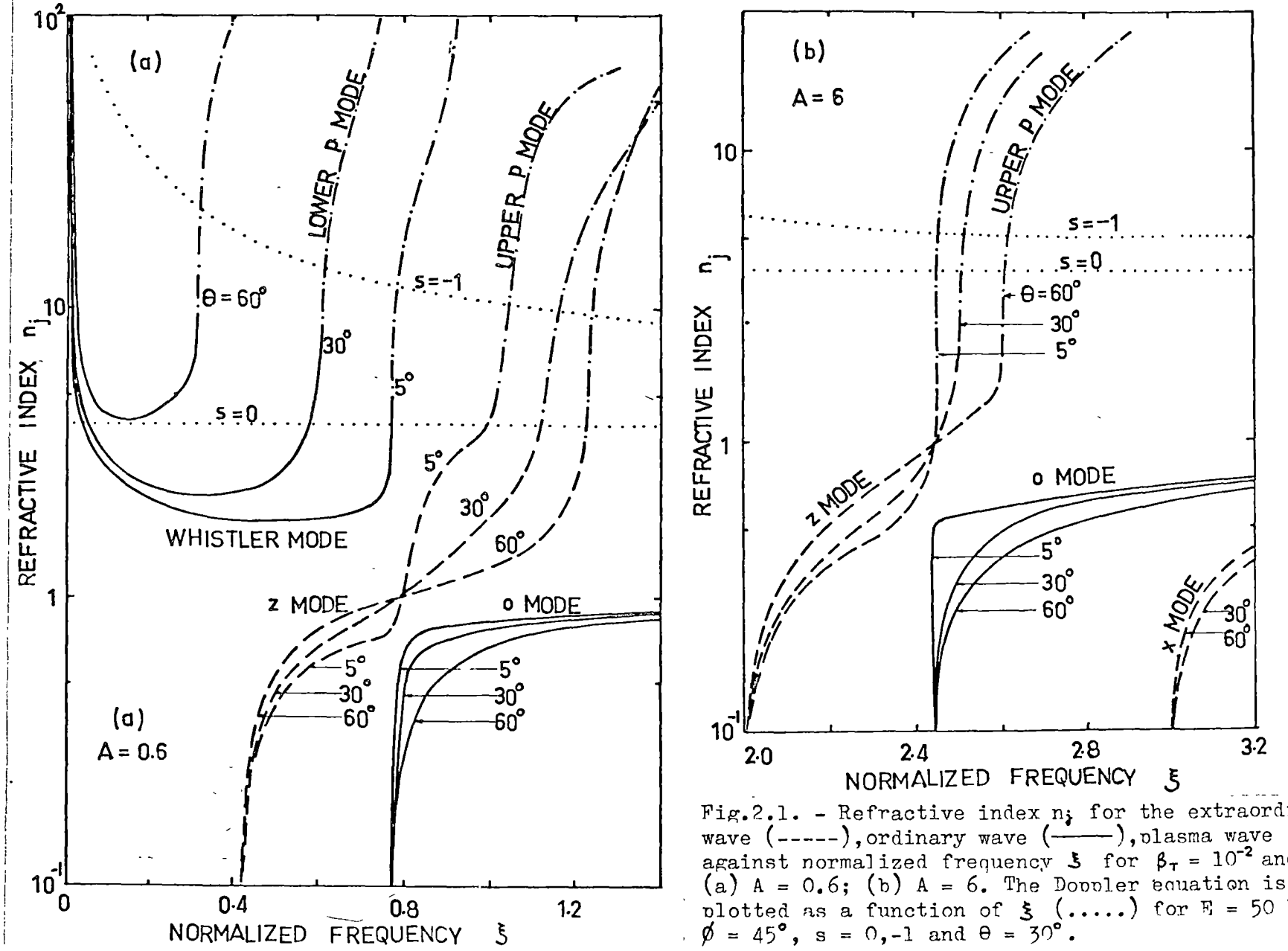

Fig.2.1. - Refractive index n_j for the extraordinary wave (-----), ordinary wave (———), plasma wave (-.-.-) against normalized frequency ξ for $\beta_T = 10^{-2}$ and (a) A = 0.6; (b) A = 6. The Doppler equation is also plotted as a function of ξ (.....) for E = 50 keV, $\phi = 45°$, s = 0,-1 and $\theta = 30°$.

C. Radiation of Plasma Waves by A Single Charged Particle moving in A Magnetoactive Plasma

In deriving the plasma wave power spectra radiated by a single charged particle moving in a homogeneous magnetoactive plasma, we neglect the effects of the presence of the source charges on the description of the plasma and the interaction between the plasma particles. We further assume that the velocity vector of the moving charged particle is constant in time and space.

The average instantaneous radiated power from a gyrating charged particle is given by (Shafranov, 1967, p.104)

$$\tilde{P} = -2\mathrm{Re} \int_0^{\infty} \int_{-\infty}^{\infty} G_{\beta\alpha}(\vec{k},\omega)\, L_{\alpha\beta}(\vec{k},\omega)\, d\tilde{k}d\omega \ , \qquad (2.7)$$

where, for longitudinal plasma waves,

$$L_{\alpha\beta}(\vec{k},\omega) = -i4\pi\kappa_\alpha\kappa_\beta/\omega\varepsilon_{\parallel} \ ,$$

$\varepsilon_{\parallel}(\vec{k},\omega)$ is the longitudinal component of the dielectric constant and $\kappa_\alpha = k_\alpha/k$ the polarization vector for the longitudinal plasma wave. For a single gyrating charged particle,

$$G_{\alpha\beta}(\bar{k},\omega) = \frac{q^2}{8\pi^3} \sum_{s=-\infty}^{\infty} \delta(\omega - k_{\parallel} v_{\parallel} - s\gamma\omega_H)\pi_{\alpha\beta}^{(s)} \quad , \qquad (2.8)$$

where $\pi_{xx}^{(s)} = \frac{s^2}{X^2} v_\perp^2 J_s^2(X)$, $\pi_{xy}^{(s)} = -\pi_{yx}^{(s)} = i\frac{s}{X} v_\perp^2 J_s(X)J_s'(X)$,

$$\pi_{yy}^{(s)} = v_\perp^2 J_s'^2(X), \qquad \pi_{yz}^{(s)} = -\pi_{zy}^{(s)} = -iv_\perp v_{\parallel} J_s(X)J_s'(X), \qquad (2.9)$$

$$\pi_{zz}^{(s)} = v_{\parallel}^2 J_s^2(X), \qquad \pi_{xz}^{(s)} = \pi_{zx}^{(s)} = \frac{s}{X} v_{\parallel} v_\perp J_s^2(X) \ .$$

$J_s(X)$ and $J_s'(X)$ are Bessel function and its first derivative with the argument $X = k_\perp v_\perp/\gamma\omega_H$. s is the harmonic number and $\gamma = (1 - v_\perp^2/c^2 - v_{\parallel}^2/c^2)^{\frac{1}{2}} = (1 - \beta_\perp^2 - \beta_{\parallel}^2)^{\frac{1}{2}}$ is the relativistic correction factor. The subscripts $\perp$, $\parallel$ indicate the perpendicular and parallel components of the particle velocity with respect to the static magnetic field. In (2.7), the element of the wave vector space $d\bar{k}$ is replaced by $k^2\, dk d\cos\theta\, d\psi$, where ψ is the azimuthal angle, and the delta function can be reduced to

$$\delta(\omega - kv_{\parallel}\cos\theta - s\gamma\omega_H) = \frac{\delta(\cos\theta - \cos\theta_s)}{\left| v_{\parallel} k\left(1 - \frac{\partial k}{\partial\theta}/k\tan\theta\right)\right|_{\theta=\theta_s(\omega_s)}} \qquad (2.10)$$

with $\omega_s - kv_{\parallel}\cos\theta_s - s\gamma\omega_H = 0$.

When the weakly damped conditions (2.1) and (2.2) are met, the real part of $\epsilon_{\parallel}(\bar{k},\omega)$ is given by the left handed side of (2.3). Then after integration over $\cos\theta$ and k by using the delta function (2.10) and the equality $\mathrm{Re}\left(\frac{i}{\epsilon_{\parallel}}\right) = \pi\delta(\epsilon_{\parallel})$, the frequency power spectrum of the plasma wave for the s-th harmonic

radiated by a single electron is readily obtained,

$$\frac{d\tilde{P}_s}{df} = 2\pi e^2 \omega J_s^2(X)/c \left| n_3^2 \beta_{\parallel} A_1 \left(1 - \frac{\partial n_3}{\partial \theta}/n_3 \tan\theta\right) \right|_{\theta=\theta_s(\omega_s)} , \quad (2.11)$$

where $A_1 = \beta_T^2 \omega_p^2 \cos^2\theta R_1$,

and ω_s and θ_s have to satisfy the equation (Doppler equation)

$$\omega_s = \frac{s\gamma\omega_H}{1 - n_3\beta_{\parallel} \cos\theta_s} \quad (2.12)$$

or $\omega_s - n_3 \beta_{\parallel} \omega_s \cos\theta_s - s\gamma\omega_H = 0$,

simultaneously. (2.11) can also be obtained from the expression (17) of Eidman (1962).

The angular spectrum of the radiation in the plasma mode, $\frac{d\tilde{P}_s}{d\Omega}$, i.e. the power density in watts per steradian, can be obtained by carrying out the integration over frequency in (2.7). Writing the element of the wave vector space $d\bar{k}$ as $k^2 dk d\Omega$ and carrying out integration over frequency and over wave number k, we find

$$\frac{d\tilde{P}_s}{d\Omega} = e^2\omega^2 J_s^2(X)/2\pi c n_3 \left| A_1 \left[1 - n_3\beta_{\parallel} \cos\theta \left(1 + \frac{\omega}{n_3} \frac{\partial n_3}{\partial \omega}\right)\right] \right|_{\omega=\omega_s(\theta_s)} , \quad (2.13)$$

where $\omega_s(\theta_s)$ satisfies (2.12).

For an electron travelling along the external magnetic field, $\beta_{\perp} = 0$, there are no normal and anomalous cyclotron

radiations. The Cerenkov radiation angular power spectrum, in this case, is

$$\frac{d\tilde{P}_s}{d\Omega} = e^2\omega^2/2\pi c n_3 \left| A_1 \left[1-n_3\beta_{\parallel} \cos\theta\left(1 + \frac{\omega}{n_3}\frac{\partial n_3}{\partial \omega}\right)\right] \right|_{\omega=\omega_s(\theta_s)} . \quad (2.14)$$

In the other limiting case, $\beta_{\parallel} = 0$, radiation of weakly damped plasma wave occurs at the frequency and the wave-normal angle θ_s such that $\omega_s = s\gamma\omega_H \simeq \omega_{\pm}(\theta_s)$ is due to normal cyclotron effect ($s > 0$). Then (2.11) and (2.13) are applicable only for $s\gamma \simeq \xi_{\pm} \neq 1,2$. When the intensity of the static magnetic field is small, the radius of curvature of the electron's rotation is sufficiently large, the radiation for $\beta_{\perp} n_3 > 1$ and $\beta_{\parallel} = 0$ can be approximated as Cerenkov radiation of plasma wave in an isotropic plasma.

D. Excitation of Plasma Waves in A Charged Particle Stream-Plasma System

In the presence of a charged particle stream in the ambient plasma, waves in various modes emitted by individual stream charged particles in this stream-plasma system would be unstable. Autoexcitation results in the amplification of amplitudes of the waves. The excitation of longitudinal plasma waves in the stream-plasma system in the isotropic corona has been discussed by Ginzburg and Zheleznyakov (1958). Recently,

Zayed and Kitsenko (1968a), assuming a system comprising the cold and collisionless magnetoactive plasma and a helical charged particle stream, obtained the rate of growth for the longitudinal plasma oscillation. In this section, taking into account of the effect of the stream particle's longitudinal temperature, we calculate the rate of growth for the plasma wave in the helical electron stream-plasma system. We assume that the density of the electron stream is very small compared with that of the ambient plasma and the whole is electrically neutral. We consider excitation of the weakly damped plasma waves in the stream-plasma system during the initial stage of the process so that the linearized kinetic equation can be employed to find the rate of growth (see Section D, Chapter III).

Based on the classical kinetic equation, the problem of instability in a charged particle stream-plasma system is solved by writing the dielectric tensor for the stream-plasma system in the form (Stepanov and Kitsenko, 1961):

$$\varepsilon_{\alpha\beta}(\bar{k},\omega) = \varepsilon^{(o)}_{\alpha\beta}(\bar{k},\omega) + \varepsilon'_{\alpha\beta}(\bar{k},\omega) - \delta_{\alpha\beta}, \quad (2.15)$$

where $\varepsilon^{(o)}_{\alpha\beta}(\bar{k},\omega)$ is the dielectric tensor for the ambient plasma and $\varepsilon'_{\alpha\beta}(\bar{k},\omega) - \delta_{\alpha\beta}$ is due to the presence of the charged particle stream. The dispersion equation for the longitudinal plasma wave in the stream-plasma system becomes

$$\varepsilon^{(o)}_{||}(\bar{k},\omega) + \varepsilon'_{||}(\bar{k},\omega) - 1 = 0. \quad (2.16)$$

For weakly damped plasma waves, $\varepsilon_{ij}^{(o)}(\bar{k},\omega)$ is given by the left-handed side of (2.3) and

$$\varepsilon'_{ij}(\bar{k},\omega) = \varepsilon'_{xx}\sin^2\theta + \varepsilon'_{zz}\cos^2\theta + 2\,\varepsilon'_{xz}\sin\theta\cos\theta\ .$$

Making use of the integration by parts and assuming that the unperturbed charged particle distribution function $F_o(\bar{p})$ tends to zero as the transverse momentum component $p_\perp$ or the absolute value of the longitudinal momentum component $|p_{||}|$ tends to infinity, from (1.7) we obtain the dielectric tensor components for the growing waves in the stream:

$$\varepsilon'_{xx} = 1-4\pi\int_{-\infty}^{\infty}\int_{o}^{\infty}\frac{s^2 m_o\omega_H\omega_p'^2(\omega m-k_{||}\,p_{||})J_sJ_s'F_o}{k_\perp\omega^2R}\,dp_\perp\,dp_{||}$$

$$-2\pi\int_{-\infty}^{\infty}\int_{o}^{\infty}\frac{s^2m_o^2\omega_H^2\omega_p'^2J_s^2p_\perp(k_{||}^2-\omega^2/c^2)F_o}{k_\perp^2\omega^2R^2}\,dp_\perp\,dp_{||}\ ,$$

$$\varepsilon'_{yy} = 1-4\pi\int_{-\infty}^{\infty}\int_{o}^{\infty}\frac{\omega_p'^2p_\perp J_s'^2(\omega m-k_{||}\,p_{||})F_o}{\omega^2R}\,dp_\perp\,dp_{||}$$

$$-4\pi\int_{-\infty}^{\infty}\int_{o}^{\infty}\frac{\omega_p'^2p_\perp^2J_sJ_s''(\omega m-k_{||}\,p_{||})F_o}{\omega^2m_o\omega_HR}dp_\perp\,dp_{||}$$

$$-2\pi\int_{-\infty}^{\infty}\int_{o}^{\infty}\frac{\omega_p'^2p_\perp^3J_s'^2(k_{||}^2-\omega^2/c^2)F_o}{\omega^2R^2}\,dp_\perp\,dp_{||}\ ,$$

$$\varepsilon'_{zz} = 1-4\pi \int_{-\infty}^{\infty}\int_{0}^{\infty} \frac{\omega_p'^2 k_\perp p_\perp^2 J_s J_s'(\omega m - k_\parallel p_\parallel) F_o}{\omega^2 m_o \omega_H R}\, dp_\perp\, dp_\parallel$$

$$- 4\pi \int_{-\infty}^{\infty}\int_{0}^{\infty} \frac{\omega_p'^2 k_\parallel p_\parallel p_\perp J_s^2 F_o}{\omega^2 R}\, dp_\perp\, dp_\parallel$$

$$- 2\pi \int_{-\infty}^{\infty}\int_{0}^{\infty} \frac{\omega_p'^2 p_\parallel^2 p_\perp (k_\parallel^2 - \omega^2/c^2) J_s^2 F_o}{\omega^2 R^2}\, dp_\perp\, dp_\parallel \quad ,$$

$$\varepsilon'_{xy} = -i2\pi \int_{-\infty}^{\infty}\int_{0}^{\infty} \frac{s\omega_p'^2 p_\perp (\omega m - k_\parallel p_\parallel)(J_s J_s'' + J_s'^2) F_o}{\omega^2 R}\, dp_\perp\, dp_\parallel \qquad (2.17)$$

$$- i2\pi \int_{-\infty}^{\infty}\int_{0}^{\infty} \frac{s m_o \omega_H \omega_p'^2 (\omega m - k_\parallel p_\parallel) J_s J_s' F_o}{k_\perp \omega^2 R}\, dp_\perp\, dp_\parallel$$

$$- i2\pi \int_{-\infty}^{\infty}\int_{0}^{\infty} \frac{s m_o \omega_H \omega_p'^2 p_\perp^2 (k_\parallel^2 - \omega^2/c^2) J_s J_s' F_o}{k_\perp \omega^2 R^2}\, dp_\perp\, dp_\parallel \quad ,$$

$$\varepsilon'_{xz} = -4\pi \int_{-\infty}^{\infty}\int_{0}^{\infty} \frac{s\omega_p'^2 p_\parallel J_s J_s' (\omega m - k_\parallel p_\parallel) F_o}{\omega^2 R}\, dp_\perp\, dp_\parallel - 2\pi \int_{-\infty}^{\infty}\int_{0}^{\infty} \frac{s m_o \omega_H \omega_p'^2 k_\parallel p_\parallel J_s^2 F_o}{\omega^2 k_\perp R}\, dp_\perp\, dp_\parallel$$

$$- 2\pi \int_{-\infty}^{\infty}\int_{0}^{\infty} \frac{s m_o \omega_H \omega_p'^2 p_\parallel p_\perp J_s^2 (k_\parallel^2 - \omega^2/c^2) F_o}{k_\perp \omega^2 R^2}\, dp_\perp\, dp_\parallel \quad ,$$

$$\varepsilon'_{yz} = i2\pi \int_{-\infty}^{\infty}\int_{0}^{\infty} \frac{\omega_p'^2 k_\perp p_\parallel p_\perp (J_s'^2 + J_s J_s'')\ (\omega m - k_\parallel p_\parallel) F_o}{\omega^2 m_o \omega_H R}\, dp_\perp\, dp_\parallel$$

$$+i2\pi \int_{-\infty}^{\infty}\int_{o}^{\infty} \frac{\omega_p'^2 p_{\parallel}(\omega m - k_{\parallel} p_{\parallel}) J_s J_s' F_o}{\omega^2 R} \, dp_{\perp} dp_{\parallel}$$

$$+i2\pi \int_{-\infty}^{\infty}\int_{o}^{\infty} \frac{\omega_p'^2 k_{\parallel} p_{\perp}^2 J_s J_s' F_o}{\omega^2 R} \, dp_{\perp} dp_{\parallel}$$

$$+ i2\pi \int_{-\infty}^{\infty}\int_{o}^{\infty} \frac{\omega_p'^2 p_{\perp}^2 p_{\parallel} J_s J_s' (k_{\parallel}^2 - \omega^2/c^2) F_o}{\omega^2 R^2} \, dp_{\perp} dp_{\parallel} \ ,$$

$$\varepsilon'_{zx} = \varepsilon'_{xz} \ , \ \varepsilon'_{zy} = -\varepsilon'_{yz} \ , \ \varepsilon'_{yx} = -\varepsilon'_{xy} \ ,$$

where $R = \omega m - k_{\parallel} p_{\parallel} - s m_o \omega_H$; ω_p' is the angular plasma frequency of the stream particle; $k_{\parallel}$ and $k_{\perp}$ are the wave vector components along and perpendicular to the static magnetic field. J_s, J_s' are the Bessel function and its first derivative with respect to the argument $X = k_{\perp} p_{\perp} / m_o \omega_H$. When the relativistic effects are included the mass of the charged particle is a function of its momentum components

$$m^2 = m_o^2 + p_{\perp}^2/c^2 + p_{\parallel}^2/c^2 \ .$$

A general form of the unperturbed distribution function for a helical charged particle stream can be represented by

$$F_o(\bar{p}) d\bar{p} = C \exp[-(p_{\perp} - p_{\perp}^o)^2/a_{\perp}^2 - (p_{\parallel} - p_{\parallel}^o)^2/a_{\parallel}^2] \, d\bar{p}, \quad (2.18)$$

where $a_{\perp}^2 = 2\pi m_o T_{\perp}'$, $a_{\parallel}^2 = 2\pi m_o T_{\parallel}'$, $T_{\perp}'$, $T_{\parallel}'$ are the transverse and

longitudinal temperatures of the stream particles. $p_{\perp}^{o}$ and $p_{\parallel}^{o}$ are the values of $p_{\perp}$ and $p_{\parallel}$ at which the distribution function reaches its maximum. The constant C is determined by the normalization condition $\int F_o(\bar{p})d\bar{p} = 1$. The momentum spread of the stream is specified by the parameters $a_{\perp}$ and $a_{\parallel}$. When $T_{\perp}'$ and $T_{\parallel}'$ are sufficiently small, each exponential function involved in (2.18) can be approximated by the delta function $\delta(p - p^{o})$. For the sake of simplicity, we assume that $a_{\perp} \simeq 0$ and $T_{\parallel}' = T' \leq T$, where T is the ambient plasma temperature. Then (2.18) can be approximated by

$$F_o(\bar{p})d\bar{p} = \frac{1}{2\pi^{3/2}a_{\parallel}p_{\perp}^{o}} \delta(p_{\perp} - p_{\perp}^{o}) \exp[-(p_{\parallel} - p_{\parallel}^{o})^2/a_{\parallel}^2] \, d\bar{p}. \quad (2.19)$$

Substituting (2.18) into (2.17), we carry out integration over $p_{\perp}$ along the real axis from 0 to ∞ and over $p_{\parallel}$ along the real axis from $-\infty$ to ∞ bypassing from above or below the poles of the integrand. Since we assume the density of the stream is very small in comparison with the ambient plasma density, from (2.16) and (2.17), it can be seen that $\varepsilon_{\parallel}'(\bar{k},\omega)$ should be necessarily taken into account only when the term $\omega - k_{\parallel}v_{\parallel} - s\gamma\omega_H$ is small. In the real k-method, i.e. we assume the wave vector is real and the frequency is complex in order to find the growth rate of the electromagnetic wave , we let

$$\omega - k_{\parallel}v_{\parallel} - s\gamma\omega_H = \alpha, \quad (2.20)$$

where α is a complex quantity with very small magnitude compared with $|\omega|$. For an electron stream with small momentum spread, the method of carrying out the integration over the longitudinal momentum component involved in (2.17) has been developed by Zheleznyakov (1960). Then, adopting Zheleznyakov's method, we carry out the integration over the longitudinal momentum component in (2.17) and retain terms proportional to $(\omega - k_{\parallel} v_{\parallel} - s\gamma\omega_H)^{-2}$ and the number $\wedge 1$. Making use of the approximation (2.19), we evaluate the integrals over transverse momentum component and finally get the expressions for the dielectric tensor components of a helical electron stream

$$\varepsilon'_{xx} = 1 - \frac{s^2\omega_H^2\omega_p'^2\gamma^2(k_{\parallel}^2 - \omega^2/c^2)}{k_{\perp}^2\omega^2\alpha^2} J_s^2(1 - \tfrac{1}{2}\gamma^2\beta_T'^2) ,$$

$$\varepsilon'_{zz} = 1 - \frac{\omega_p'^2 v_{\parallel}^2(k_{\parallel}^2 - \omega^2/c^2)}{\omega^2\alpha^2} J_s^2 \left[(1-\frac{5}{2}\gamma^2\beta_T'^2) + \frac{\gamma^2\beta_T'^2}{\beta_{\parallel}^2}(1-\frac{3}{2}\gamma^2\beta_T'^2)\right], \tag{2.21}$$

$$\varepsilon'_{xz} = -\frac{s\gamma\omega_H\omega_p'^2 v_{\parallel} J_s^2(k_{\parallel}^2 - \omega^2/c^2)}{k_{\perp}\omega^2\alpha^2}(1 - \frac{3}{2}\gamma^2\beta_T'^2) ,$$

where $\beta_T' = (\kappa T'/m_o c^2)^{\frac{1}{2}}$ is the normalized thermal speed of the stream electron. The angular plasma frequency ω_p' in the laboratory system has been replaced by $\omega_p' = (4\pi e^2 n_o'/m_o)^{\frac{1}{2}}$, where n_o' is the number density of the stream electrons in the system of

reference in which the electron stream is at rest, since the plasma frequency is a Lorentz-invariant quantity(Chawla and Unz,1966).

From (2.3), (2.15) and (2.21), we write the dispersion equation in the form

$$A^P(\bar{k},\omega) + A^S(\bar{k},\omega) = 0 \quad , \tag{2.22}$$

$$\text{with} \quad A^P(\bar{k},\omega) = 1 - \frac{\omega_p^2 \sin^2\theta}{\omega^2-\omega_H^2} - \frac{\omega_p^2\cos^2\theta}{\omega^2} - \frac{k^2 v_T^2 \omega_p^2 \cos^2\theta}{\omega^2} R_1, \tag{2.23}$$

$$\text{and} \quad A^S(\bar{k},\omega) = -\frac{\omega_p'^2 J_s^2 (k_{||}^2 - \omega^2/c^2)}{\omega^2 \alpha^2} \{[\frac{s\gamma\omega_H}{k}(1-\tfrac{1}{4}\gamma^2\beta_T'^2) + v_{||}\cos\theta(1-\frac{5}{4}\gamma^2\beta_T'^2)]^2$$

$$+ (\frac{\beta_T'}{\beta_{||}})^2 \gamma^2 (1 - \frac{3}{2}\gamma^2\beta_T'^2) v_{||}^2 \cos^2\theta\} \; . \tag{2.24}$$

In writing down (2.24), we have used the assumption $\beta_T' \leq \beta_T$. In the absence of the stream, for weakly damped plasma waves, we have

$$A^P(\bar{k}_o,\omega_s) = 0.$$

Now we expand the left-handed side of (2.22) in the neighbourhood of the point $\omega = \omega_s + \delta$ and $k = k_o + \eta$, where δ is assumed to be complex and η real and $|\delta| << |\omega|$, $\eta \to 0$ and $|\delta| \to 0$ as $\omega_p' \to 0$,

$$A^P(\bar{k}_o,\omega_s) + A^S(\bar{k}_o,\omega_s) + (\delta\frac{\partial}{\partial\omega} + \eta\frac{\partial}{\partial k})\,[A^P(\bar{k},\omega) + A^S(\bar{k},\omega)] = 0. \tag{2.25}$$

The derivatives are evaluated at $\omega = \omega_s$ and $k = k_o$. Eliminating δ in (2.25) by the relation $\alpha = \delta - \eta\, v_{||} \cos\theta$, we get a cubic equation with real coefficients for α,

$$\alpha^3 + \alpha^2\eta(v_{||}\cos\theta+v_g') + \frac{\alpha N}{\left(\frac{\partial A^P}{\partial\omega}\right)} + \frac{(W\eta+\eta v_{||}\cos\theta\ N+U)}{\left(\frac{\partial A^P}{\partial\omega}\right)} = 0 \ , \qquad (2.26)$$

where $W = \alpha^2\left(\frac{\partial A^S}{\partial k}\right)$, $N = \alpha^2\left(\frac{\partial A^S}{\partial\omega}\right)$, $U = \alpha^2 A^a(\bar{k}_o,\omega)$ and $v_g' = \left(\frac{\partial A^P}{\partial k}\right) / \left(\frac{\partial A^P}{\partial\omega}\right)$ is the component of the group velocity of the plasma wave in the direction of wave propagation. Assuming this equation has complex roots for α, the rate of growth of the plasma wave is given by the absolute value of the imaginary part of α at a real wave vector. Solving (2.26) for α by Carden's method, we find the second term in (2.26) is unimportant, and hence for simplicity we put $\eta = 0$ and rewrite (2.26) in the form

$$\left(\frac{\delta}{\omega_s}\right)^3 + a\left(\frac{\delta}{\omega_s}\right) + b = 0 \ , \qquad (2.27)$$

where $a = \sigma J_s^2\cos^2\theta G/\xi^2 K$, $b = -\sigma J_s^2(\cos^2\theta - 1/n_3^2)G/2\xi^2 K$,

$$K = \frac{\xi^4\sin^4\theta+(\xi^2-1)^2\cos^2\theta+n_3^2\beta_T^2\cos^2\theta\xi^2 B}{\xi^2\ (\xi^2-1)^2} \ ,$$

$$B = \frac{3\xi^4(2\xi^2-5)\sin^4\theta}{(\xi^2-4)^2\cos^2\theta} + \frac{(12\xi^6-3\xi^4+4\xi^2-1)\sin^2\theta}{(\xi^2-1)^2} + \frac{6(\xi^2-1)^2\cos^2\theta}{\xi^2} \ ,$$

$$G = [(1 - \tfrac{1}{4}\gamma^2\beta_T'^2) - n_3\beta_{||}\cos\theta\gamma^2\beta_T'^2]^2 \ ,$$

$$\sigma = \frac{\omega_p'^2}{\omega_p^2} = \frac{n_o'}{n_o} \quad \text{and} \quad \xi = \frac{f_s}{f_H} \ .$$

The rate of growth of the plasma wave can then be solved from (2.27):

$$\text{Im}\left(\frac{\delta}{\omega_s}\right) = \pm \frac{\sqrt{3}}{2}\left(D^{1/3} - F^{1/3}\right), \qquad (2.28)$$

where $D = -\frac{b}{2} + \left(\frac{b^2}{4} + \frac{a^3}{27}\right)^{\frac{1}{2}}$, $F = -\frac{b}{2} - \left(\frac{b^2}{4} + \frac{a^3}{27}\right)^{\frac{1}{2}}$.

For sufficiently small streams density $\sigma << 1$, then

$$\text{Im}\left(\frac{\delta}{\omega_s}\right) \simeq \frac{\sqrt{3}\sigma^{1/3}}{2}[J_s^2(\cos^2\theta - 1/n_3^2)G/2\xi^2K]^{1/3}. \qquad (2.29)$$

Thus, the growth factor for the plasma wave radiated by a single electron of the stream is $\exp(|\text{Im}\delta|t)$, where t is the interaction time*. We should remark that the method of obtaining the dielectric tensor components (2.21) is applicable under the condition $m|\text{Im}\delta| >> ka$ (Zheleznyakov, 1960). In other words, the rate of growth must be very much greater than kv_T' . Since $|\text{Im}\frac{\delta}{\omega_s}|$ is proportional to $\sigma^{1/3}$, this imposes a restriction on the density of the stream. For example if $\sigma \simeq 10^{-4}$

---

* We assume that the interaction time is of the same order of magnitude of the characteristic time for non-linear transfer of the plasma wave across the spectrum (see Section G of Chapter VI).

and $n_3 \simeq 10$, then β_T' cannot exceed 10^{-3} in order that (2.28) is valid. It is obvious that (2.21) is applicable only to the initial stage of the excitation process during which the stream can be assumed to be cold (Shapiro, 1963).

E. Numerical Illustrations

In this section, we make use of the expressions (2.11), (2.13) and (2.28) to study the characteristics of the plasma waves excited by electron streams moving in the magnetoactive corona.

(a) Emitted Frequency Range from Electrons

The emitted frequency and the wave-normal angle θ can be determined by solving a quartic equation which is obtained by substituting the refractive index n_3 (expression (2.4)) into (2.12),

$$A_o \cos^4\theta + B_o \cos^2\theta + C_o = 0, \qquad (2.30)$$

where $$A_o = \frac{\beta_T^2 A(\xi - s\gamma)^2 (3\xi^6 - 21\xi^4 + 10\xi^2 - 4)}{(\xi^2-4)\ (\xi^2-1)^2} - \frac{3\beta_T^2 A(\xi - s\gamma)^2 (\xi^2-1)}{\xi^2} + A\beta_{11}^2,$$

$$B_o = \beta_{11}^2 \xi^2 (\xi^2 - A - 1) + \beta_T^2 A(\xi - s\gamma)^2 \left[\frac{15\xi^4 - 7\xi^2 + 4}{(\xi^2-4)(\xi^2-1)^2}\right],$$

and $$C_o = -\frac{3\xi^2 \beta_T^2 A(\xi - s\gamma)^2}{(\xi^2-4)}.$$

The square of the cosine of the emission angle is given by

$$\cos^2\theta_s^{\pm} = [- B_o \pm (B_o^2 - 4A_oC_o)^{\frac{1}{2}}] /2A_o \ . \qquad (2.31)$$

For a given set of parameters $\beta_{\parallel}$, β_T, A, E and s, the permissible emission frequency ξ must satisfy the condition that $\cos^2\theta_s^{\pm}$ is real, positive and ≤ 1. For anomalous cyclotron and Cerenkov radiation ($s \leq 0$), the wave-normal angle is $0 \leq \theta_s^{\pm} \leq \pi/2$. For normal cyclotron radiation, $\theta_s \leq \pi/2$ for $\xi > s\gamma$ and $\theta_s \geq \pi/2$ for $\xi < s\gamma$. We should emphasize that in some cases, the solutions given by (2.31) would violate the condition $n^2 >> 1$ and are not applicable.

The solutions for θ and ξ from (2.30) with parameters $A = 0.6$, $\beta_T = 10^{-2}$, $\beta_{\parallel} = 0.1$, $\beta_{\perp} = 0.2$, $s = 0, -1$ are shown in Fig. 2.2. The plasma resonance frequencies $\xi_{\pm}$ with the same value A are also plotted against the wave-normal angle θ.

(b) The Power Spectra in The p-Mode Radiated by A Single Electron

The normalized emitted frequency and the corresponding wave-normal angle θ obtained from (2.30) are used to calculate the frequency and angular power spectra in the plasma mode radiated from a single electron moving in the magnetoactive plasma. For electron energy E = 50 keV, A = 0.6,6, s = 0,±1,2,3 and electron pitch angle $\phi = 0^o$, 30^o, 45^o, 60^o, the polar

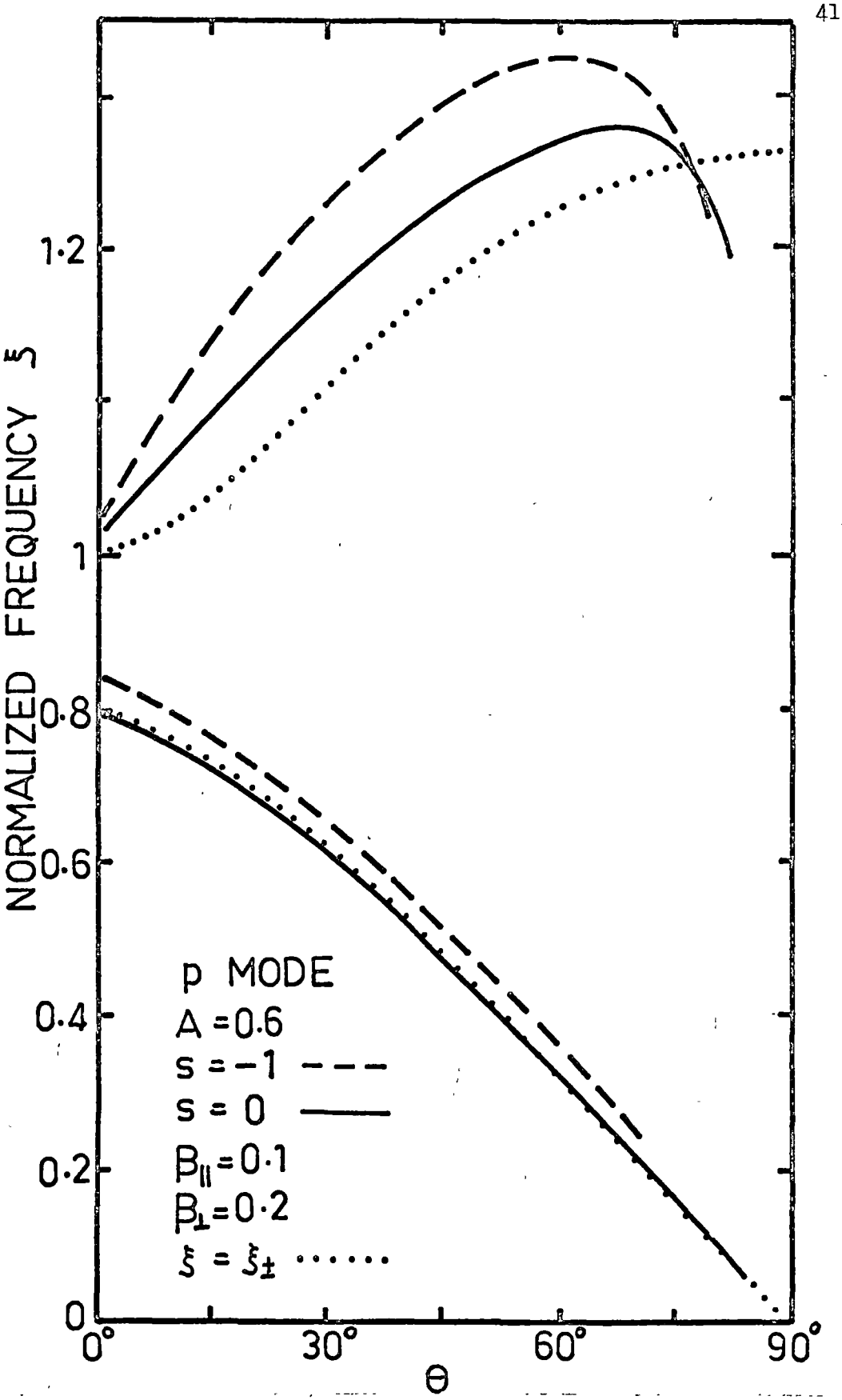

Fig.2.2 - Relation between normalized emitted frequency and wave-normal angle Θ for the plasma mode when A = 0.6, $\beta_T = 10^{-2}$, s = 0,-1, $\beta_{\parallel} = 0.1$, $\beta_{\perp} = 0.2$.

diagrams and the frequency power spectra, (2.13) and (2.11), are presented in Fig. 2.3 and Fig. 2.4 respectively. The gyrofrequency is taken to be 100 MHz for A = 0.6 and 20 MHz for A = 6. In Fig. 2.4(d), the fluctuation parts of the frequency spectra of the backward normal cyclotron radiation in the plasma mode have been smoothed out by taking the mean values of the power. In these spectra, the minima should go to zero. For the sake of clarity, the lines are drawn continuously.

These spectra demonstrate several properties of the emission power in the plasma mode. Firstly, the main plasma wave power is radiated within a cone whose thickness is inversely proportional to the electron pitch angle. Secondly, in the case $\beta_\perp = 0$, the Cerenkov radiation has a very broad polar diagram. Thirdly, there is no cyclotron radiation in the plasma mode in the direction around the static magnetic field line. However, Cerenkov radiation in the plasma mode is always emitted in the direction parallel to the static magnetic field line and at the frequency in the neighbourhood of the plasma frequency f_p. For $s \leq 0$, the phase velocity of the plasma wave emitted from the electron decreases to velocities comparable to the mean thermal speed of the plasma electrons as $\theta \to \pi/2$ and emission of weakly damped plasma waves will no longer be possible since the plasma can support only those plasma waves with phase velocities greater than the mean thermal speed of the plasma electrons.

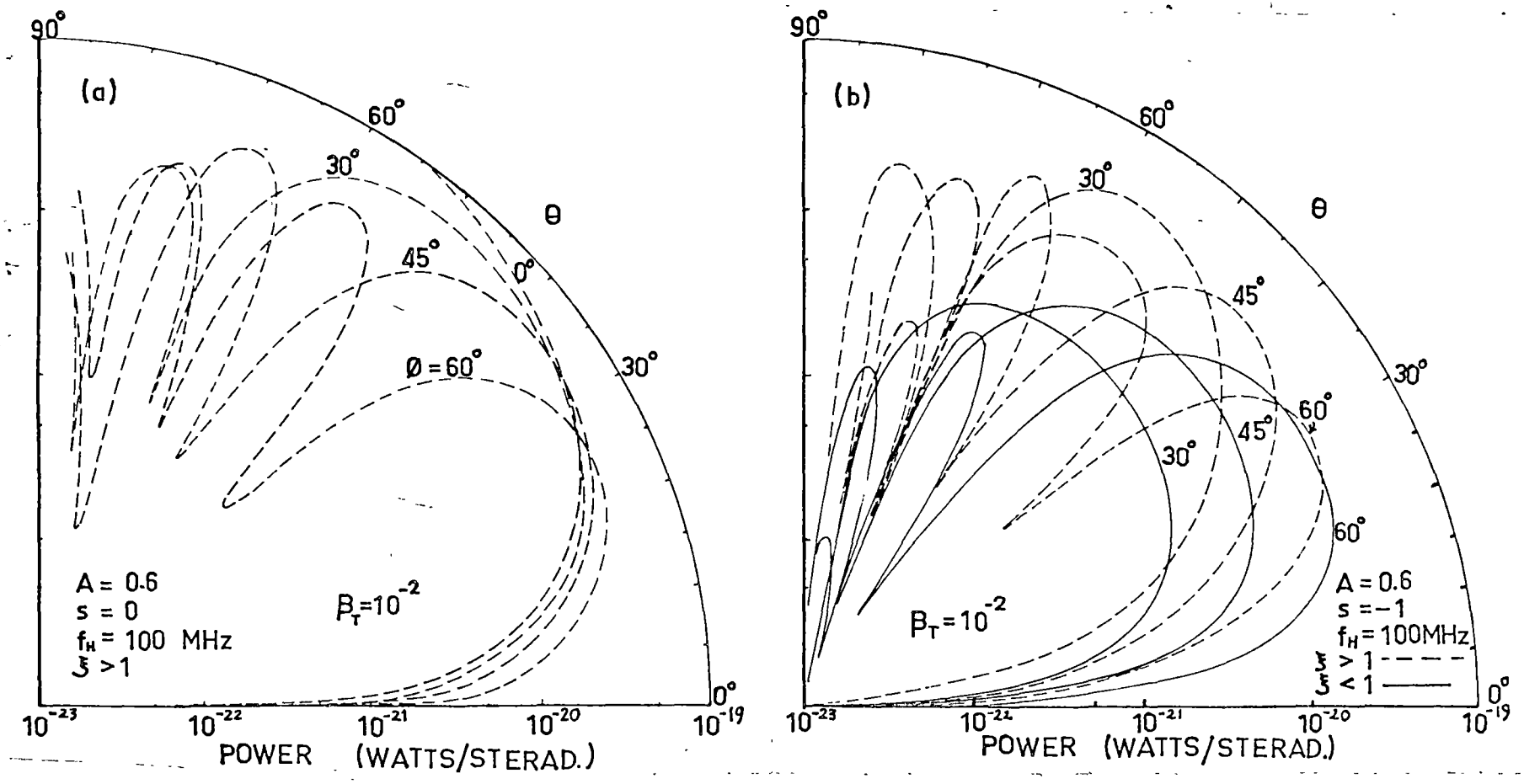

Fig.2.3. - Angular power spectra in the p-mode from a single electron with energy E = 50 keV and electron pitch angle $\emptyset = 0^\circ, 30^\circ, 45^\circ, 60^\circ$ for

(a) A=0.6, s = 0 and f_H = 100 MHz; (b) A = 0.6, s = -1 and f_H = 100 MHz.

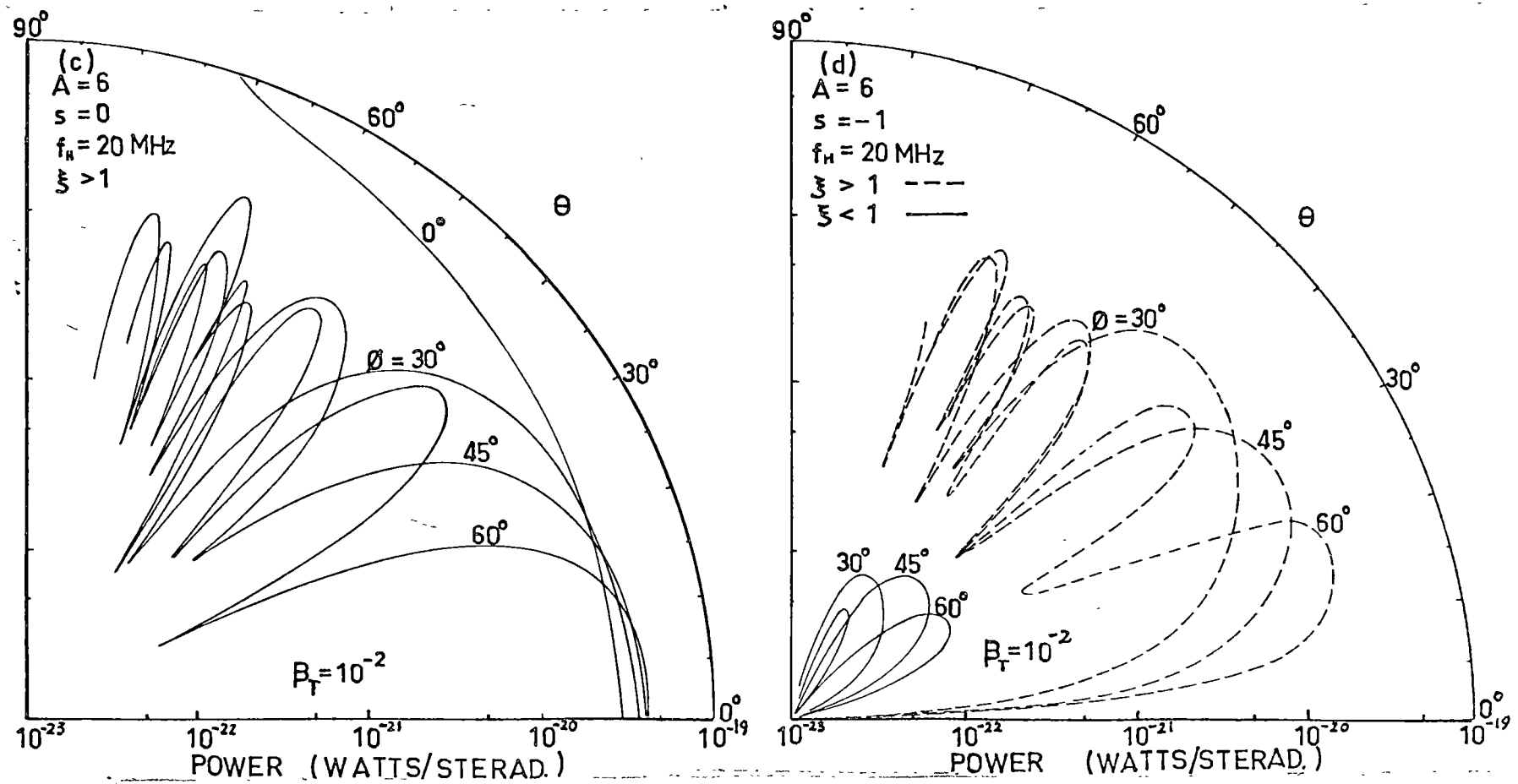

Fig.2.3. - Angular power spectra in the o-mode from a single electron with energy E = 50 keV and electron pitch angle Ø = 0°,30°,45°,60° for

(c) A = 6, s = 0 and f_H = 20 MHz; (d) A = 6, s = -1 and f_H = 20 MHz.

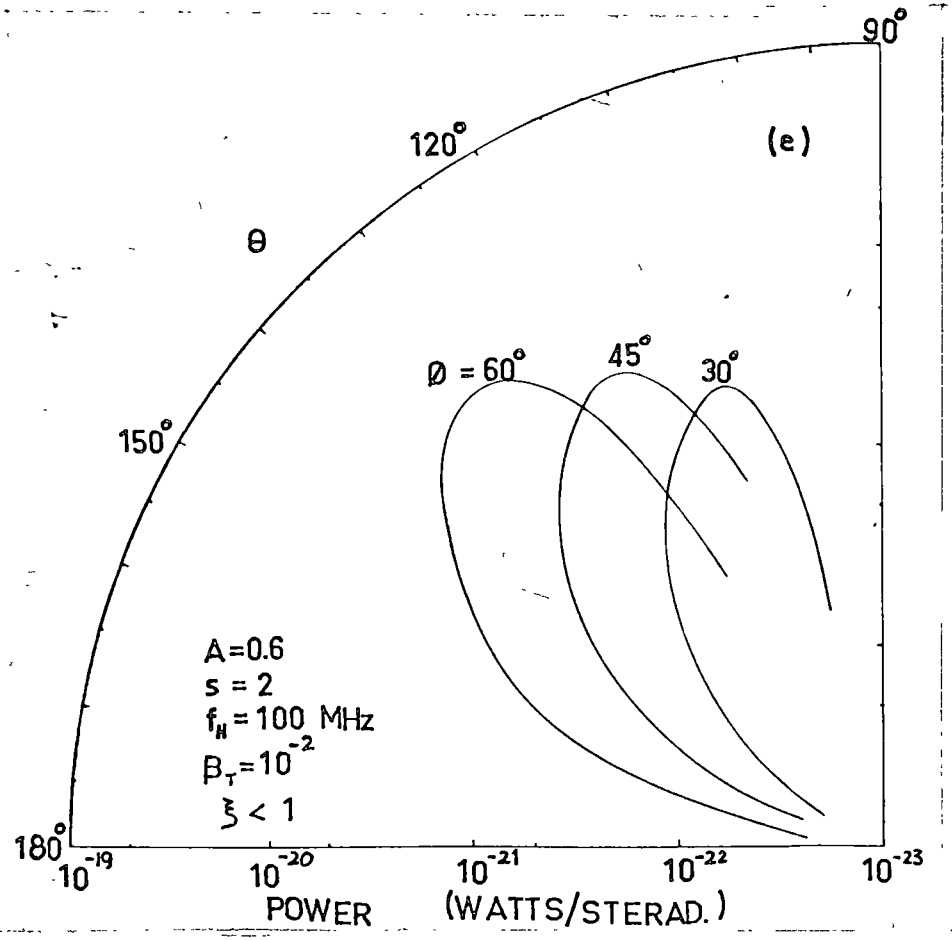

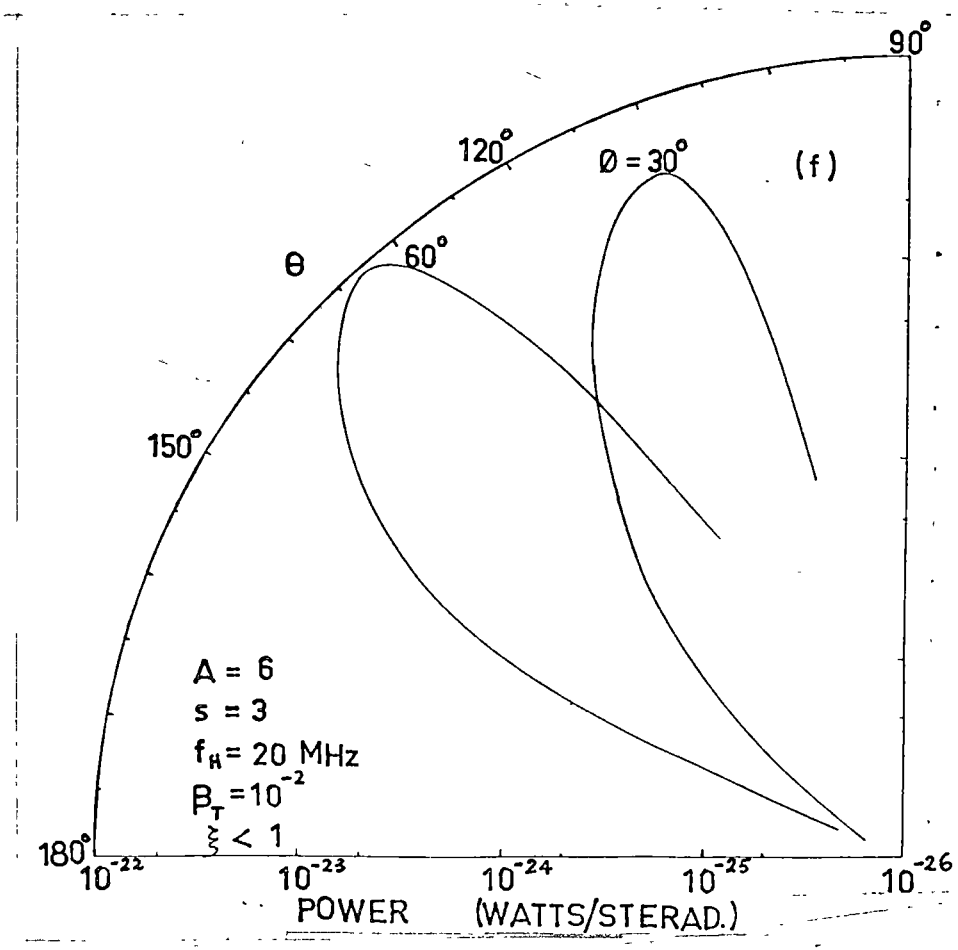

Fig.2.3. - Angular power spectra in the o-mode from a single electron with energy E = 50 keV and electron pitch angle $\emptyset = 0^\circ, 30^\circ, 45^\circ, 60^\circ$ for

(e) A =0.6, s = 2 and f_H = 100 MHz; (f) A = 6, s = 3 and f_H = 20 MHz.

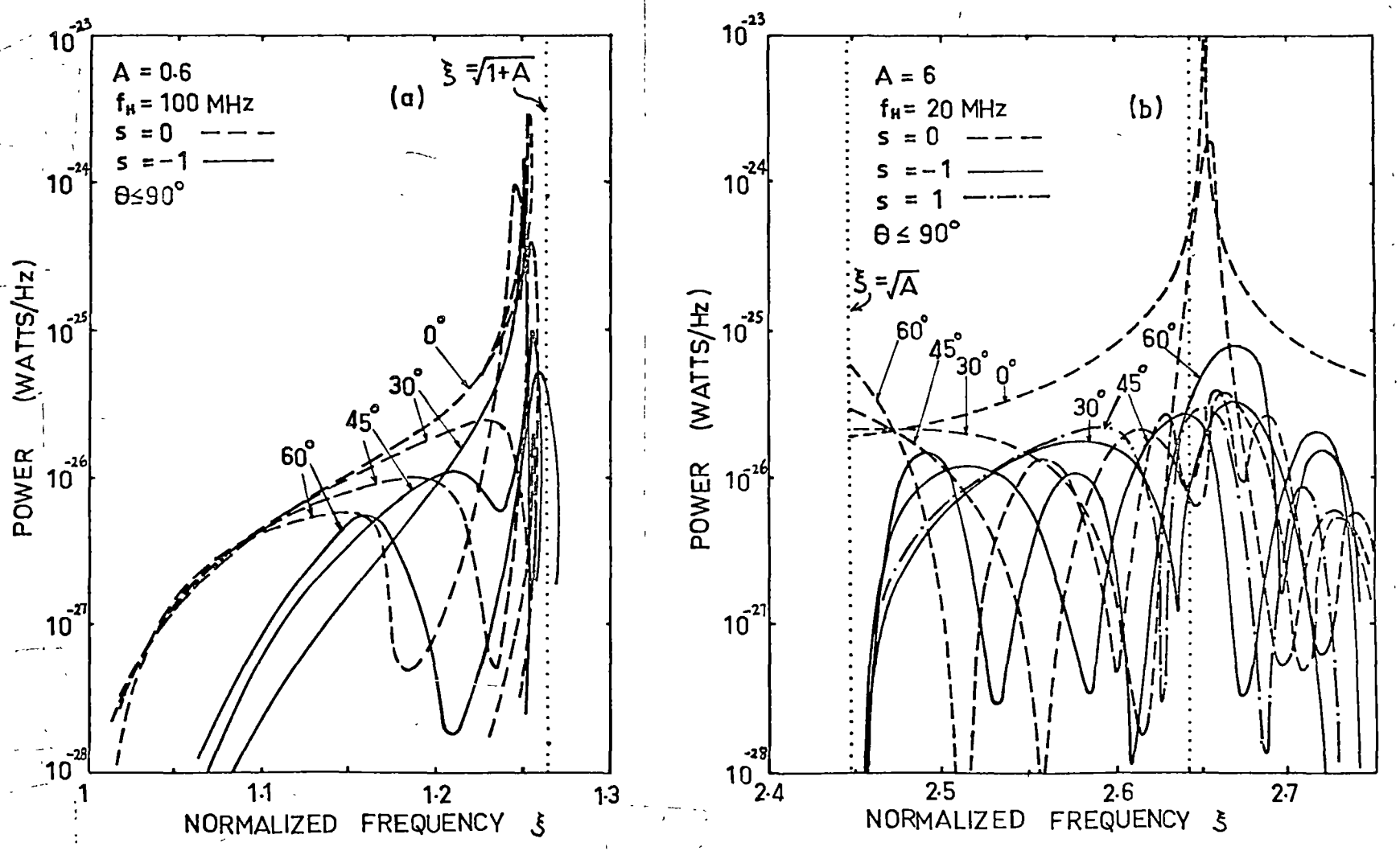

Fig.2.4. - Frequency spectra in the p-mode from a single electron with energy E = 50 keV and electron pitch angle ϕ = 0°,30°,45°,60° for $\beta_T = 10^{-2}$ and for

(a) A = 0.6 and f_H = 100 MHz; (b) A = 6 and f_H = 20 MHz.

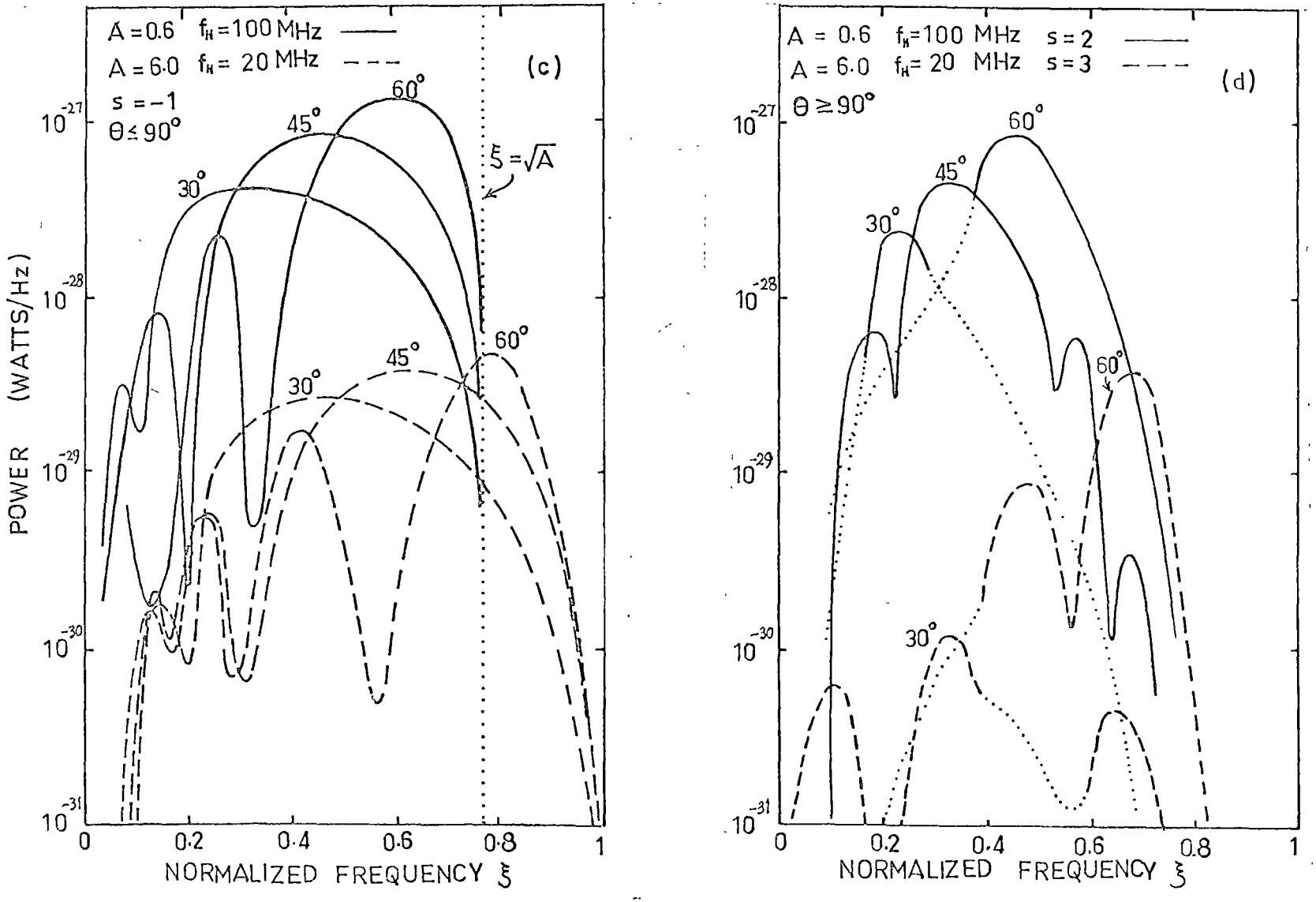

Fig.2.4. - (c) s = -1, A = 6, f_H = 20 MHz (– – – –); s = -1, A = 0.6, f_H = 100 MHz (———);
(d) s = 2, A = 0.6, f_H = 100 MHz (———); s = 3, A = 6, f_H = 20 MHz (- - - - - -).

(c) Growth of Plasma Waves in The Stream-Plasma System

At the onset of the excitation process, the rate of growth of the plasma wave with time in the stream-plasma system can be computed by (2.28) with $\beta_T' = 0$. The variation of the growth rate $\left| \mathrm{Im} \frac{\delta}{\omega_H} \right|$ with the wave-normal angle for the upper p-mode and the lower p-mode is demonstrated in Fig. 2.5 with parameters as given in Fig. 2.3 and Fig. 2.4. It can be seen that, in general, the growth rate peaks in the vicinity of the direction in which the single electron radiation in the plasma mode reaches its maximum. Studying the cases for $s = 0, \pm 1, 2, 3$, we can conclude that under the same conditions,

(i) the Cerenkov radiation in the plasma mode grows more rapidly than the corresponding anomalous and normal cyclotron radiations;

(ii) in general, the rate of growth for the Cerenkov radiation in the plasma mode increases with the electron's longitudinal velocity component, while for the cyclotron radiation in the plasma mode with the electron's transverse velocity component.

Whenever generation of the Cerenkov radiation in both the upper and lower plasma modes is possible, the plasma waves at the frequencies near the plasma frequency and propagating in the directions around the magnetic field line will grow at the greatest rate (Fig.2.5(c) and Fig.2.6). On the other hand, when A is large, Cerenkov plasma waves can be emitted only at the frequencies

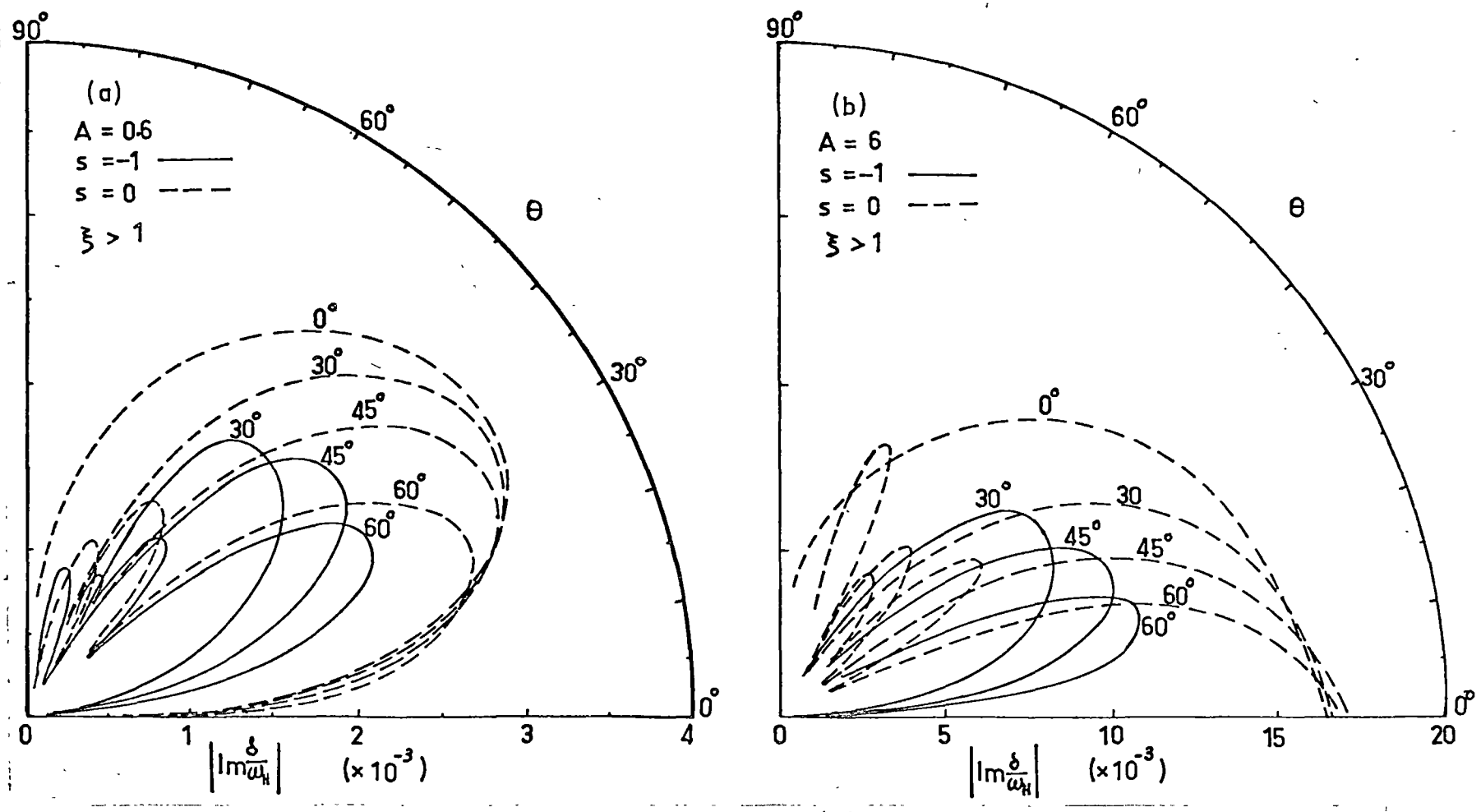

Fig.2.5. - The dependence of the growth rate $\left|\mathrm{Im}\frac{\delta}{\omega_H}\right|$ on wave-normal angle θ for $\beta'_T = 0$, $\beta_T = 10^{-2}$, $\sigma = 10^{-6}$, electron energy E = 50 keV, electron pitch angle $\phi = 0^\circ, 30^\circ, 45^\circ, 60^\circ$ and for

(a) A = 0.6; (b) A = 6.

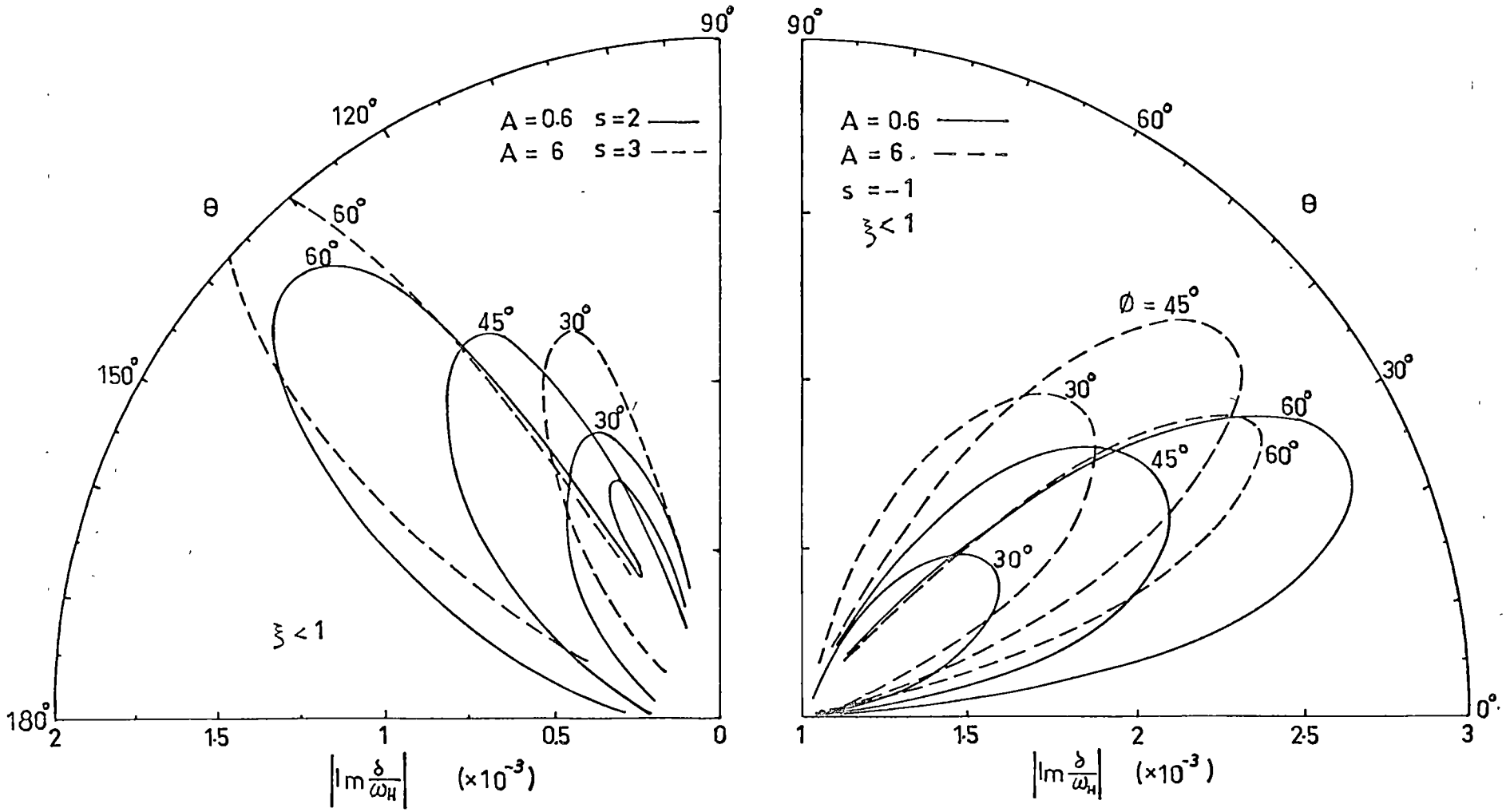

Fig.2.5. - The dependence of the growth rate $\left|\mathrm{Im}\frac{\delta}{\omega_H}\right|$ on wave-normal angle θ for $\beta_T' = 0$, $\beta_T = 10^{-2}$, $\sigma = 10^{-6}$, electron energy E = 50 keV, electron pitch angle $\emptyset = 0^\circ, 30^\circ, 45^\circ, 60^\circ$ and for

(c) s = 2, A = 0.6 (———) and s = 3, A = 6 (------).
(d) s = −1, A = 0.6 (———), A = 6 (-----).

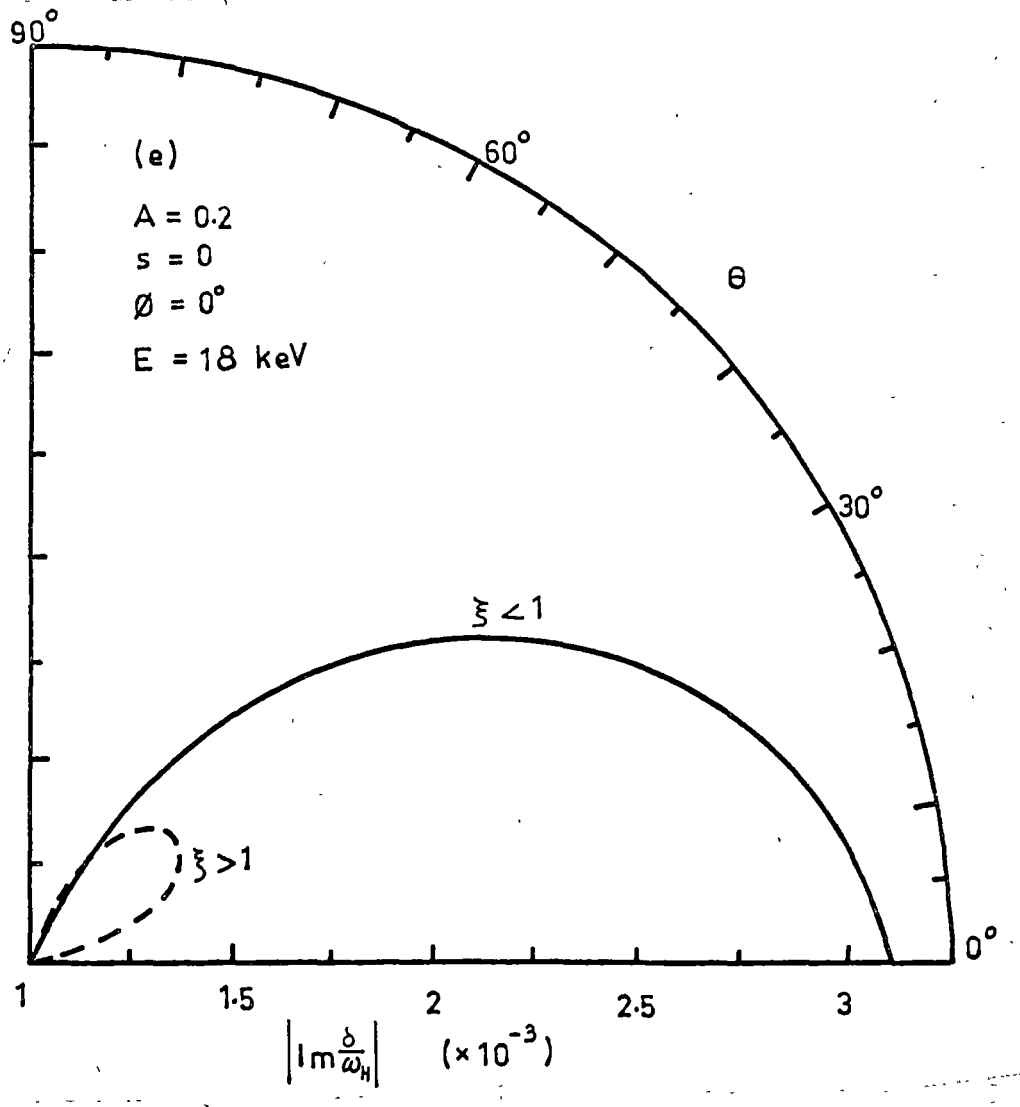

Fig.2.5 (e) The dependence of the growth rate $\left|\mathrm{Im}\frac{\delta}{\omega_H}\right|$ on wave-normal angle θ for $\beta_T' = 0$, $\beta_T = 10^{-2}$, $\sigma = 10^{-6}$, electron energy E = 18 keV, electron pitch angle $\emptyset = 0°, 30°, 45°, 60°$ and for lower p-mode (————) and upper p-mode (-------), A = 0.2, s = 0

Fig. 2.6 Power gain versus normalized frequency ξ for electron energy E = 50 keV and electron pitch angle $\phi = 0^{o}$, 30^{o}, 45^{o}, 60^{o}, $\beta_T' = 0$, $\beta_T = 10^{-2}$, $\sigma = 10^{-6}$ and interaction time $t = 5 \times 10^{-5}$ sec and for

(a) A = 0.6, f_H = 100 MHz, s = 0,-1;

(b) A = 6, f_H = 20 MHz, s = 0,-1,1.

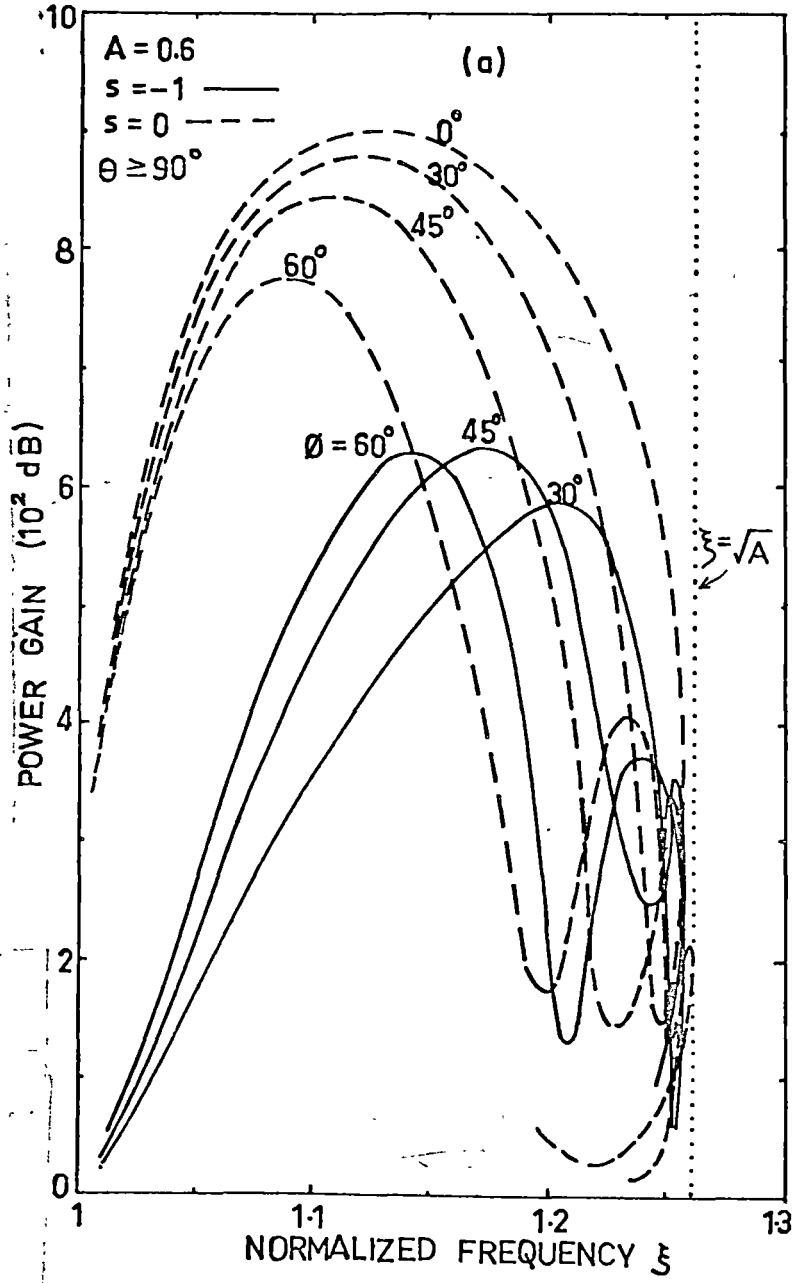
A = 0.6
s = −1
s = 0
θ ≥ 90°
(a)
0°
30°
45°
60°
Ø = 60°
45°
30°
ξ = √A
POWER GAIN (10² dB)
NORMALIZED FREQUENCY ξ
10
8
6
4
2
0
1
1·1
1·2
1·3

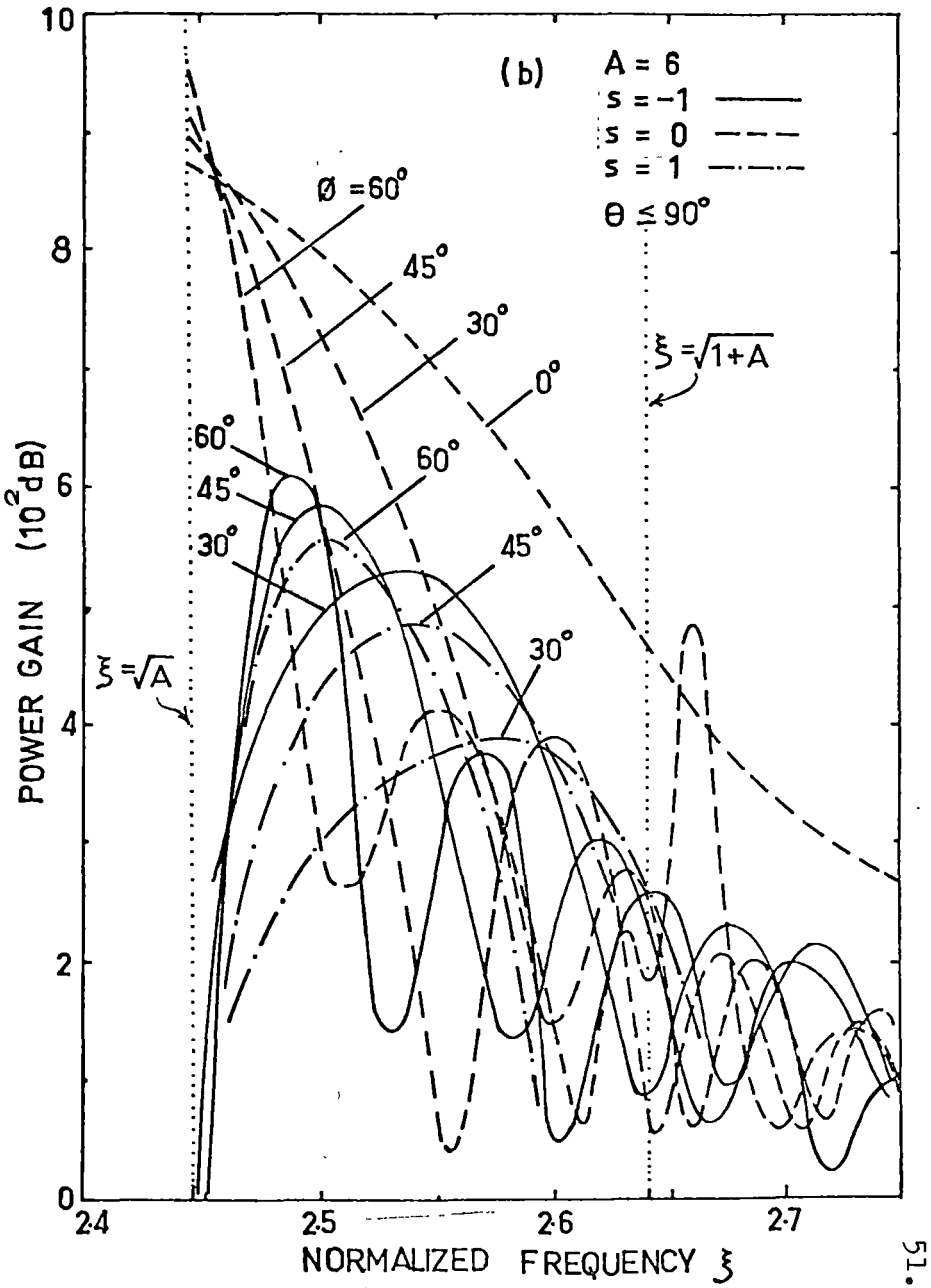
(b)
A = 6
s = −1
s = 0
s = 1
θ ≤ 90°
Ø = 60°
45°
30°
0°
ξ = √(1+A)
ξ = √A
60°
45°
30°
60°
45°
30°
POWER GAIN (10² dB)
NORMALIZED FREQUENCY ξ
10
8
6
4
2
0
2·4
2·5
2·6
2·7

Fig. 2.6

Fig. 2.6 Power gain versus normalized frequency ξ for electron energy E = 50 keV and electron pitch angle $\phi = 0^{o}$, 30^{o}, 45^{o}, 60^{o}, $\beta_T^i = 0$, $\beta_T = 10^{-2}$, $\sigma = 10^{-6}$ and interaction time $t = 5 \times 10^{-5}$ sec and for

(c) A = 0.6, f_H = 100 MHz, s = 0,-1,2;

(d) A = 6, f_H = 20 MHz, s = -1,3.

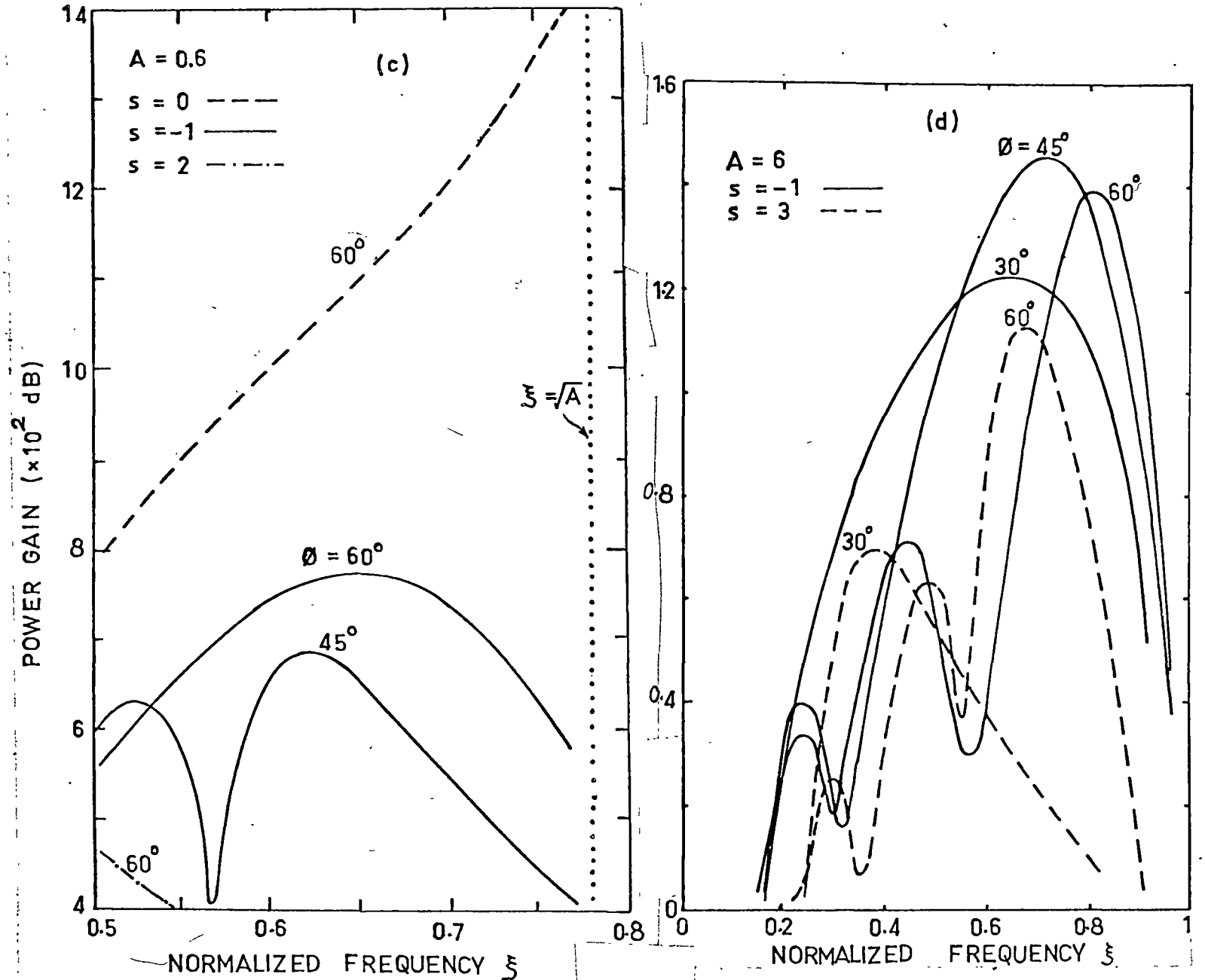
(c)
A = 0.6
s = 0
s = -1
s = 2
60°
ξ = √A
Ø = 60°
45°
60°
POWER GAIN (×10² dB)
NORMALIZED FREQUENCY ξ
(d)
A = 6
s = -1
s = 3
Ø = 45°
60°
30°
60°
30°
NORMALIZED FREQUENCY ξ

Fig.2.6

$f > f_H$ and maximizes at the frequency $f \simeq f_p$. Thus, we can conclude that even in the presence of the static magnetic field, most of the energy of the radiation in the plasma mode from an electron stream will be emitted in the direction of the electron guiding centre motion and at the frequency near the plasma frequency through the Cerenkov process.

F. Conclusion

Using the linearized kinetic equation approach, the rate of growth of the plasma wave in a stream-plasma system has been studied in previous sections. It is found that the intensity of the coherent radiation in the plasma mode is greater than that in the x-mode and the o-mode (see Chapter VIII). Hence it is believed that generation of plasma waves by electron streams in the active solar corona will play an important part in the solar radio emissions.

However, the expressions obtained in this chapter are applicable only to the case of excitation of weakly damped plasma waves by the low density electron stream during the initial stage of the process (see Section D, Chapter III). When the weak damping conditions (2.2) are violated, double resonances (i.e. $f \simeq f_{\pm} = sf_H$, $s = 1,2$) occur and the dispersion equation (2.3) and hence the theories given in sections C and D can no longer be valid. The dispersion equation for the plasma wave and the generation of plasma waves in the case of double

resonances have been studied by Stepanov (1960) and by Pakhomov and Stepanov (1963) respectively. However, since weakly damped plasma waves at the frequencies $f \simeq f_p$ emitted by an electron stream are of greatest intensity, it is not difficult to see that the theories given in this chapter can be applied to the consideration of coherent generation of plasma waves by low density electron streams everywhere in the active solar corona except the layers where $A \simeq 1{,}4$.

CHAPTER III

EXCITATION OF CYCLOTRON RADIATION IN THE SUBLUMINOUS* MODE IN A STREAM-PLASMA SYSTEM

A. Introduction

In Chapter II, we have studied the excitation of longitudinal plasma waves with phase velocities less than the free space light speed in a system comprising a low density helical electron stream and the background magnetoactive plasma. In such a combined system, excitation of electromagnetic radiation in the subluminous mode can also occur and is very important for the theory of solar radio emission, since radiation with $0 < n < 1$ can escape from the solar corona directly without preliminary transformation into other types of normal waves.

The problem of radiative instability in a stream-plasma system can be studied by assuming the wave vector to be real and solving the dispersion equation for complex wave frequency; separating the dielectric tensor components of the system into two parts - one due to the ambient magnetoactive plasma and the other due to the presence of the stream. This method was initiated by Stepanov and Kitsenko (1961) and recently adopted by Zayed and Kitsenko (1968a, 1968b) to investigate the excitation of cyclotron harmonics in various cases.

Since the general form of the dispersion equation for the electromagnetic wave in a helical stream-plasma system is

---

*The subluminous mode of the electromagnetic wave is defined here as the electromagnetic wave whose phase velocity v_p in the medium is greater than the guiding centre speed of the electron who generates it (i.e. in the region of normal Doppler effect).

extremely complicated, Zayed and Kitsenko (1968a) obtained only the rate of growth of the electromagnetic wave in the combined system for certain particular cases in which the dispersion equation can be simplified. However, in order to study the characteristics of the cyclotron radiation in the subluminous mode from a gyrating electron stream, one requires an explicit expression for the rate of growth of electromagnetic radiation in the combined system which is applicable to general cases. In this chapter, we derive the essential mathematical expression explicitly. The expression obtained will be applied in the theory of solar type IVA burst emission in Chapter VIII.

B. Formulation

For small amplitude waves of the form $\exp(i\bar{k}.\bar{r} - i\omega t)$ in an unbounded homogeneous medium consisting of a cold and collisionless magnetoactive plasma and a system of non-equilibrium electrons, the dispersion equation for the wave is given by (1.10) with the dielectric tensor components (2.15). We assume the whole system is electrically neutral and the number density of the non-equilibrium electrons is much smaller than that of the ambient plasma.

The dielectric tensor components for the cold and collisionless magnetoactive plasma alone, $\varepsilon_{\alpha\beta}^{(o)}$, are given by

$$\varepsilon_{11}^{(o)} = \varepsilon_{22}^{(o)} = 1 - \frac{\omega_p^2}{\omega^2-\omega_H^2}\,, \quad \varepsilon_{33}^{(o)} = 1 - \frac{\omega_p^2}{\omega^2}\,, \quad \varepsilon_{12}^{(o)} = \frac{i\omega_H\omega_p^2}{\omega(\omega^2-\omega_H^2)}\,, \tag{3.1}$$

$$\varepsilon_{13}^{(o)} = \varepsilon_{23}^{(o)} = 0 \quad .$$

The components $\varepsilon'_{\alpha\beta} - \delta_{\alpha\beta}$ are the small corrections to the dielectric tensor components of the ambient plasma due to the presence of non-equilibrium electrons. If the non-equilibrium electrons form a stream with a sufficiently small momentum spread, the distribution function for the electron stream (2.18) can be approximated by

$$F_o(\bar{p})d\bar{p} = \frac{1}{2\pi p_\perp^o}\,\delta(p_\perp - p_\perp^o)\;\delta(p_{||} - p_{||}^o)d\bar{p}. \tag{3.2}$$

Using (3.2) in (2.17), we obtain the dielectric tensor components for the electron stream

$$\varepsilon'_{11} = 1 - \frac{2s^2\gamma\omega_H\omega'^2_p(\omega - k_{||}v_{||})J_sJ'_s}{k_\perp\omega^2 v_\perp\alpha} - \frac{s^2\gamma^2\omega_H^2\omega'^2_p J_s^2(k_{||}^2 - \omega^2/c^2)}{k_\perp^2\omega^2\alpha^2} \quad ,$$

$$\varepsilon'_{22} = 1 - \frac{2\omega'^2_p J'^2_s(\omega - k_{||}v_{||})}{\omega^2\alpha} + \frac{2\omega'^2_p v_\perp J'_s J''_s k_\perp(\omega - k_{||}v_{||})}{\omega^2\gamma\omega_H\alpha}$$

$$- \frac{\omega'^2_p v_\perp^2 J'^2_s(k_{||}^2 - \omega^2/c^2)}{\omega^2\alpha^2} \quad ,$$

$$\varepsilon'_{33} = 1 - \frac{2\omega'^2_p k_\perp v_{||}^2 J_sJ'_s(\omega - k_{||}v_{||})}{\omega^2\gamma\omega_H v_\perp\alpha} - \frac{2\omega'^2_p k_{||}v_{||}J_s^2}{\omega^2\alpha} - \frac{\omega'^2_p v_{||}^2 J_s^2(k_{||}^2 - \omega^2/c^2)}{\omega^2\alpha^2} \quad ,$$

$$\varepsilon'_{12} = \frac{is\omega_p'^2(J_sJ_s''+J_s'^2)(\omega-k_{\parallel}v_{\parallel})}{\omega^2\alpha} + \frac{is\gamma\omega_H\omega_p'^2J_sJ_s'(\omega-k_{\parallel}v_{\parallel})}{k_{\perp}v_{\perp}\omega^2\alpha} \qquad (3.3)$$

$$+ \frac{is\gamma\omega_H\omega_p'^2v_{\perp}J_sJ_s'(k_{\parallel}^2-\omega^2/c^2)}{k_{\perp}\omega^2\alpha^2}$$

$$\varepsilon'_{13} = -\frac{2s\omega_p'^2v_{\parallel}J_sJ_s'(\omega-k_{\parallel}v_{\parallel})}{\omega^2v_{\perp}\alpha} - \frac{s\gamma\omega_H\omega_p'^2k_{\parallel}J_s^2}{\omega^2k_{\perp}\alpha}$$

$$- \frac{s\gamma\omega_H\omega_p'^2v_{\parallel}J_s^2(k_{\parallel}^2-\omega^2/c^2)}{k_{\perp}\omega^2\alpha^2} ,$$

$$\varepsilon'_{23} = -\frac{i\omega_p'^2k_{\perp}v_{\parallel}(J_sJ_s''+J_s'^2)(\omega-k_{\parallel}v_{\parallel})}{\omega^2\gamma\omega_H\alpha} - \frac{i\omega_p'^2v_{\parallel}J_sJ_s'(\omega-k_{\parallel}v_{\parallel})}{\omega^2v_{\perp}\alpha}$$

$$- \frac{i\omega_p'^2k_{\parallel}v_{\perp}J_sJ_s'}{\omega^2\alpha} - \frac{i\omega_p'^2v_{\perp}v_{\parallel}J_sJ_s'(k_{\parallel}^2-\omega^2/c^2)}{\omega^2\alpha^2} ,$$

$$\varepsilon'_{31} = \varepsilon'_{13} , \quad \varepsilon'_{32} = -\varepsilon'_{23} , \quad \varepsilon'_{21} = -\varepsilon'_{12} ,$$

where $\alpha = \omega - k_{\parallel}v_{\parallel} - s\gamma\omega_H$. For cyclotron radiation in the subluminous mode, the harmonic number s is a non-zero positive integer. $\omega'_p = \left(\frac{4\pi e^2n'_o}{m_o}\right)^{\frac{1}{2}}$ is the angular plasma frequency of the stream electron, n'_o being the stream electron density in system of reference in which the electron stream is at rest. J_s, J'_s and J''_s are the Bessel function and its first two

derivatives of s-th order with the argument $X = k_{\perp} v_{\perp}/\gamma\omega_H$.

For a single electron gyrating in the magnetoactive plasma, the frequency ω_s and the wave-normal angle θ of the normal cyclotron radiation satisfy the Doppler equation simultaneously,

$$\omega_s - k_o v_{\parallel} \cos\theta - s\gamma\omega_H = 0 \ . \qquad (3.4)$$

We assume that the number density of the stream electrons is much smaller than that of the ambient plasma while the magnitude of α is a very small quantity compared with the magnitude of the angular wave frequency ω . The presence of the electron stream introduces only very small corrections to the dielectric tensor components for the ambient plasma.

Neglecting the terms proportional to the second and third powers of $\omega_p'^2$, we express the dispersion equation of the stream-plasma system as

$$F(\bar{k},\omega) + F'(\bar{k},\omega) = 0 \ , \qquad (3.5)$$

where $F(\bar{k},\omega) = A_o n^4 + B_o n^2 + C_o$,

$$A_o = \varepsilon_{11}^{(o)} \sin^2\theta + \varepsilon_{33}^{(o)} \cos^2\theta$$

$$B_o = - [\varepsilon_{11}^{(o)} \varepsilon_{33}^{(o)} (1 + \cos^2\theta) + (\varepsilon_{11}^{(o)2} + \varepsilon_{12}^{(o)2}) \sin^2\theta] \ ,$$

$$C_o = \varepsilon_{33}^{(o)} (\varepsilon_{12}^{(o)2} + \varepsilon_{11}^{(o)2}) \ ,$$

$$F'(\bar{k},\omega) = (\varepsilon'_{11}\sin^2\theta + \varepsilon'_{33}\cos^2\theta + 2\varepsilon'_{13}\sin\theta\cos\theta)n^4$$

$$+[2\cos\theta\sin\theta(\varepsilon^{(o)}_{12}\varepsilon'_{23}-\varepsilon^{(o)}_{22}\varepsilon'_{13}) - \varepsilon^{(o)}_{11}\varepsilon'_{33}(1+\cos^2\theta)$$

$$- \varepsilon^{(o)}_{33}(\varepsilon'_{11}+\varepsilon'_{22}\cos^2\theta) - \varepsilon^{(o)}_{11}(\varepsilon'_{11}+\varepsilon'_{22})\sin^2\theta-2\varepsilon^{(o)}_{12}\varepsilon'_{12}\sin^2\theta]n^2$$

$$+ \varepsilon'_{33}(\varepsilon^{(o)2}_{11}+\varepsilon^{(o)2}_{12})+ \varepsilon^{(o)}_{33}\varepsilon^{(o)}_{11}(\varepsilon'_{11}+\varepsilon'_{22}) + 2\varepsilon^{(o)}_{33}\varepsilon^{(o)}_{12}\varepsilon'_{12} .$$

By direct substitution and rearrangement, we express F' as a sum of D'_1 and D'_2, where D'_1 takes the terms proportional to α^{-1} while D'_2 takes those proportional to α^{-2} , i.e.

$$F' = D'_1 + D'_2 \quad ,$$

where $$D'_2 = A'n^4 + B'n^2 + C' \quad ,$$

$$D'_1 = A''n^4 + B''n^2 + C'',$$

with $$A' = -\frac{\omega'^2_p h_4}{\omega^2\alpha^2} J_s^2 h_3^2 \quad ,$$

$$B' = \frac{\omega'^2_p h_4}{\omega^2\alpha^2}\left[\frac{2\omega^2_p\omega_H v_\perp \sin\theta}{\omega(\omega^2-\omega_H^2)} h_3 J_s J'_s - \frac{\omega^2_p}{(\omega^2-\omega_H^2)}(\ell+v_\perp^2 J'^2_s\sin^2\theta)\right.$$

$$\left. - \frac{\omega^2_p}{\omega^2} h_1 + h_2 + \ell \right],$$

$$C' = -\frac{\omega_p'^2 h_4}{\omega^2\alpha^2}\left[v_{\parallel}^2 J_s^2(\varepsilon_{11}^{(o)2}+\varepsilon_{12}^{(o)2}) + \varepsilon_{33}^{(o)}\varepsilon_{11}^{(o)}h_2 \right.$$

$$\left. - i2\,\varepsilon_{33}^{(o)}\varepsilon_{12}^{(o)}\frac{s\gamma\omega_H}{k_\perp}v_\perp J_s J_s' \right],$$

$$A'' = -\frac{2\omega_p'^2 J_s J_s' h_5 h_3^2 k_\perp}{\omega^2\alpha\, v_\perp \gamma\omega_H} - \frac{2\omega_p'^2 k_{\parallel}\cos\theta\, J_s^2 h_3}{\omega^2\alpha}$$

$$B'' = \frac{2\omega_p'^2\sin\theta\cos\theta}{\omega^2\alpha}\left\{-i\varepsilon_{12}^{(o)}\left[\frac{k_\perp v_{\parallel}(J_s J_s''+J_s'^2)h_5}{\gamma\omega_H} + \frac{v_{\parallel}J_s J_s' h_5}{v_\perp} + k_{\parallel}v_\perp J_s J_s'\right]\right.$$

$$\left. +\varepsilon_{22}^{(o)}\left[\frac{2sv_{\parallel}J_s J_s' h_5}{v_\perp} + \frac{s\gamma\omega_H k_{\parallel}}{k_\perp}J_s^2\right]\right\}$$

$$+\frac{2\omega_p'^2}{\omega^2\alpha}\varepsilon_{11}^{(o)}(1+\cos^2\theta)\left[\frac{k_\perp v_{\parallel}^2 J_s J_s' h_5}{\gamma\omega_H v_\perp}\right.$$

$$\left. + k_{\parallel}v_{\parallel}J_s^2\right] + \varepsilon_{33}^{(o)}\frac{2\omega_p'^2 h_5}{\omega^2\alpha}\left(\frac{s^2\gamma\omega_H}{k_\perp v_\perp}J_s J_s' + \cos^2\theta\, J_s'^2\right.$$

$$\left. + \frac{k_\perp v_\perp\cos^2\theta}{\gamma\omega_H}J_s' J_s''\right)$$

$$+\frac{2\omega_p'^2 h_5}{\omega^2\alpha}\varepsilon_{11}^{(o)}\left(\frac{s^2\gamma\omega_H}{k_\perp v_\perp}J_s J_s' + J_s'^2 + \frac{k_\perp v_\perp}{\gamma\omega_H}J_s' J_s''\right)\sin^2\theta$$

$$- 2\frac{is\omega_p'^2 h_5}{\omega^2\alpha}\varepsilon_{12}^{(o)}\left(J_s J_s'' + J_s'^2 + \frac{\gamma\omega_H}{k_\perp v_\perp}J_s J_s'\right)\sin^2\theta \quad ,$$

$$C'' = -\frac{2\omega_p'^2}{\omega^2\alpha}(\varepsilon_{11}^{(o)2}+\varepsilon_{12}^{(o)2})\left[\frac{k_\perp v_{||}^2 J_s J_s' h_5}{\gamma\omega_H v_\perp} + k_{||} v_{||} J_s^2\right]$$

$$-\frac{2\omega_p'^2}{\omega^2\alpha}(\varepsilon_{33}^{(o)}\varepsilon_{11}^{(o)})h_5\left(\frac{s^2\gamma\omega_H}{k_\perp v_\perp} J_s J_s' + J_s'^2 + \frac{k_\perp v_\perp}{\gamma\omega_H} J' J_s''\right)$$

$$+ i2\varepsilon_{33}^{(o)}\varepsilon_{12}^{(o)}\frac{s\omega_p'^2 h_5}{\omega^2\alpha}\left(J_s J_s'' + J_s'^2 + \frac{\gamma\omega_H}{k_\perp v_\perp} J_s J_s'\right) ,$$

$$h_1 = \frac{s^2\gamma^2\omega_H^2}{k_\perp^2} J_s^2 + v_\perp^2\cos^2\theta\, J_s'^2 , \quad h_2 = \frac{s^2\gamma^2\omega_H^2}{k_\perp^2} J_s^2 + v_\perp^2 J_s'^2 ,$$

$$h_3 = \frac{s\gamma\omega_H}{k} + v_{||}\cos\theta , \qquad h_4 = k_{||}^2 - \omega^2/c^2 ,$$

$$h_5 = \omega - k_{||} v_{||} , \qquad \ell = (h_3^2 + v_{||}^2) J_s^2 .$$

In the absence of the electron stream, $F(\bar{k},\omega) = 0$ and the refractive index of the two characteristic waves $n_j (j = 1,2)$ in the cold and collisionless ambient magnetoactive plasma will be given by

$$n_{1,2}^2 = 1 - \frac{2A(\xi^2 - A)}{2\xi^2(\xi^2-A) - \xi^2\sin^2\theta \mp \sqrt{\xi^4\sin^4\theta + 4\xi^2(\xi^2-A)^2\cos^2\theta}} . \quad (3.6)$$

Now, taking (3.2) and (3.4) into account, we expand the left-handed side of the dispersion equation (3.5) by Taylor series in the neighbourhood of the point k_o, ω_s and obtain a cubic equation in $\frac{\alpha}{\omega_s}$,

$$\left(\frac{\alpha}{\omega_s}\right)^3 + p\left(\frac{\alpha}{\omega_s}\right)^2 + a\left(\frac{\alpha}{\omega_s}\right) + b = 0 \ , \qquad (3.7)$$

where $p = \frac{\eta}{\omega_s}(v_{\parallel}\cos\theta + v_g') + \frac{H_1}{V}$,

$$a = \frac{1}{\omega_s V}(F_1+H_2) + \frac{\eta}{\omega_s V}(H_1 v_{\parallel}\cos\theta + L_1) \ ,$$

$$b = \frac{F_2}{\omega_s^2} + \frac{\eta}{\omega_s}\left(\frac{L_2}{\omega_s} + \frac{H_2}{\omega_s} v_{\parallel}\cos\theta\right) ,$$

$$F_1 = \alpha D_1' \ , \ F_2 = \alpha^2 D_2' \ ,$$

$$L_1 = \alpha \frac{\partial D_1'}{\partial k} \ , \quad L_2 = \alpha^2 \frac{\partial D_2'}{\partial k} \ ,$$

$$H_1 = \alpha \frac{\partial D_1'}{\partial \omega} \ , \ H_2 = \alpha^2 \frac{\partial D_2'}{\partial \omega} \ ,$$

$$V = \omega_s \frac{\partial F}{\partial \omega} \qquad v_g' = \frac{\frac{\partial F}{\partial k}}{\frac{\partial F}{\partial \omega}} \ .$$

The derivatives are evaluated at the point k_o, ω_s. In the real

k-method, we assume $\eta = k - k_o$ is real and $\delta = \omega - \omega_s$ is complex. We also assume that $|\delta| << |\omega|$ and $|\frac{\eta}{k}| << 1$, and $|\delta| \to 0$, $\eta \to 0$ as $\omega_p'^2 \to 0$. In (3.7), we have eliminated δ by the relation $\alpha = \delta - \eta v_{||}\cos\theta$. Thus, all the coefficients a,b and p in the equation (3.7) are real. Assuming that the equation (3.7) has complex roots for $\frac{\alpha}{\omega_s}$, then the imaginary part of α gives the temporal rate of growth of electromagnetic radiation in the stream-plasma system. However, we cannot obtain the rate of growth in an explicit form from (3.7) directly without further simplification of the equation. We note that the quantities $\frac{F_2}{\omega_s^2}$, $\frac{F_1}{\omega_s}$, $\frac{H_2}{\omega_s}$ and H_1 are proportional to $\frac{\sigma\omega_p^2}{\omega_s^2}$, L_2 proportional to $\frac{\sigma\omega_p^2}{k_o}$ and L_1 to $\frac{\sigma\omega_p^2}{\omega_s k_o}$, where $\sigma = n_o'/n_o$.

It is not difficult to see that each of the coefficients p,a,b consists of two types of terms; one proportional to $\sigma\frac{\omega_p^2}{\omega_s^2}$ and the other proportional to $\frac{\eta}{k_o}(\sigma\frac{\omega_p^2}{\omega_s^2})$ or $\frac{\eta}{k_o}$. With the present assumption that $|\frac{\eta}{k}| << 1$ and $\sigma << 1$, we can omit terms proportional to $(\sigma\frac{\omega_p^2}{\omega_s^2})\frac{\eta}{k_o}$ in the coefficients a,b and p. The complex roots of the equation (3.7) are determined by the

coefficients a,b and p. However, solving the equation (3.7), we find that the coefficient p is unimportant. In view of these facts, for simplicity, we assume $\eta = 0$ and omit the second term in (3.7). Then, after some tedious evaluations, we express (3.7) as

$$\left(\frac{\delta}{\omega_s}\right)^3 + a\left(\frac{\delta}{\omega_s}\right) + b = 0 \ , \qquad (3.8)$$

where $a = U/V$, $b = M/V$,

$$U = \frac{2\sigma A}{\xi^2}\{n_j^2\cos^2\theta\ [n_j^2(J_s^2-H)+W\ ]+Q_4[\ n_j^2(2J_s^2-S-Y)-Z\ ]\} + a'n^4+b'n^2+c',$$

$$M = \frac{\sigma A}{\xi^2}\ [n_j^2(S-J_s^2)-W]\ Q_4, \quad V = (T-4A_o)n_j^4 + (L-2B_o)n_j^2 + K,$$

$$H = 2A\sin\theta\beta_\perp J_s J_s'/n_j\xi h^2 - AQ_3/h - AQ_2/\xi^2 + Q_1 + (1/n_j^2+\beta_{\|}^2)J_s^2 \ ,$$

$$Y = A\sin\theta(3\xi^2-1)\beta_\perp J_s J_s'/n_j\xi h^2 - A\xi^2 Q_3/h^2 - AQ_2/\xi^2 \ ,$$

$$Z = \frac{\beta_{\|}^2 A J_s^2}{h^3}\ [2\xi^2 Q_5 + \frac{A}{\xi^2}(3\xi^2-1)\ ] + \frac{Q_1}{h}[Q_6 - \varepsilon_{33}^{(o)}\varepsilon_{11}^{(o)}(2\xi^2-1)]$$

$$- \frac{A(3\xi^4-\xi^2-5A\xi^2+3A)}{\xi^3 h^2}\left(\frac{s\ \gamma\beta_\perp}{n_j\xi\sin\theta}\right)J_s J_s' \ ,$$

$$W = \beta_{\|}^2 J_s^2(\varepsilon_{11}^{(o)2} + \varepsilon_{12}^{(o)2} + \varepsilon_{11}^{(o)}\varepsilon_{33}^{(o)}Q_1 - i2\varepsilon_{33}^{(o)}\varepsilon_{12}^{(o)}\left(\frac{s\gamma\beta_\perp}{n_j\xi\sin\theta}\right)J_s J_s' \ ,$$

$$S = 2A\sin\theta\beta_\perp J_s J_s'/n_j\xi h \ - AQ_3/h - AQ_2/\xi^2 + Q_1 \ ,$$

$$T = 2A[\ \xi^4\sin^2\theta + h^2\cos^2\theta\ ]/\xi^2h^2\ ,$$

$$L = -2\{\frac{(1+\cos^2\theta)}{\xi^2h^2}\ [\xi^2hQ_6-(\xi^2-A)Q_5(2\xi^2-1)] + \frac{\sin^2\theta A}{h^3}\ [\ 2\xi^2Q_5 + \frac{A}{\xi^2}\ (3\xi^2-1)]\},$$

$$K = 2\ \{\frac{A}{\xi^2}\ (\varepsilon_{11}^{(o)2}+\varepsilon_{12}^{(o)2}) + \frac{A}{h^3}\ \varepsilon_{33}^{(o)}[2\xi^2Q_5+\frac{A}{\xi^2}(3\xi^2-1)]\}\ ,$$

$$A_o = \varepsilon_{11}^{(o)}\sin^2\theta + \varepsilon_{33}^{(o)}\ \cos^2\theta\ ,$$

$$B_o = -[\ \varepsilon_{11}^{(o)}\varepsilon_{33}^{(o)}(1+\cos^2\theta) + (\varepsilon_{11}^{(o)2}+\varepsilon_{12}^{(o)2})\sin^2\theta\ ],$$

$$a' = -\frac{2\sigma A}{\xi^2}\ (\ \frac{\sin\theta J_s J_s'}{n_j\beta_\perp}\ + \cos^2\theta\ J_s^2\ ),$$

$$b' = \frac{2\sigma A}{\xi}\ \{\sin\theta\ \cos\theta\ [-i\varepsilon_{12}^{(o)}K_5+\varepsilon_{33}^{(o)}\ \frac{s\gamma}{\xi}(2s\beta_{||}J_sJ_s'/\beta_\perp+\cot\theta J_s^2)]$$

$$+\ \varepsilon_{11}^{(o)}(1+\cos^2\theta)n_j\beta_{||}\cos\theta K_1 + \frac{s\gamma}{\xi}\ \varepsilon_{33}^{(o)}K_2+\frac{s\gamma}{\xi}\varepsilon_{11}^{(o)}\sin^2\theta K_3$$

$$- i\ \frac{s^2\gamma}{\xi}\ \varepsilon_{12}^{(o)}\sin^2\theta K_4\}\ ,$$

$$c' = -\frac{2\sigma A}{\xi^2}\ [\ (\varepsilon_{11}^{(o)2}+\varepsilon_{12}^{(o)2})n_j\beta_{||}\cos\theta K_1+\varepsilon_{11}^{(o)}\varepsilon_{33}^{(o)}\ \frac{s\gamma}{\xi}K_3$$

$$- i\varepsilon_{33}^{(o)}\varepsilon_{12}^{(o)}\ \frac{s^2\gamma}{\xi}\ K_4\ ],$$

$$Q_1 = s^2\gamma^2J_s^2/n_j^2\xi^2\sin^2\theta+\beta_\perp^2J_s'^2,\quad Q_2 = s^2\gamma^2J_s^2/n_j^2\xi^2\sin^2\theta+\beta_\perp^2J_s'^2\cos^2\theta,$$

$$Q_3 = (1/n_j^2+\beta_{||}^2)J_s^2+\beta_\perp^2\sin^2\theta J_s'^2\ ,\quad Q_4 = n_j^2\cos^2\theta - 1\ ,$$

$$Q_5 = \xi^2 - A - 1, \quad Q_6 = 2\xi^2 - 2A - 1, \quad h = \xi^2 - 1,$$

$$K_1 = \frac{s\tan\theta\beta_{\parallel}}{\beta_{\perp}} J_s J_s' + J_s^2 , \quad K_2 = \frac{s^2}{X} J_s J_s' + (J_s'^2 + XJ_s'J_s'')\cos^2\theta ,$$

$$K_3 = \frac{s^2}{X} J_s J_s' + J_s'^2 + XJ_s'J_s'' , \quad K_4 = J_s'^2 + J_s J_s'' + \frac{1}{X} J_s J_s' ,$$

$$K_5 = sn_j\beta_{\parallel} \sin\theta(J_s'^2 + J_s J_s'') + J_2 J_s'(s\gamma\beta_{\parallel}/\beta_{\perp} + n_j\beta_{\perp}\cos\theta) ,$$

$$X = n_j\xi\beta_{\perp}\sin\theta/\gamma .$$

The temporal rate of growth (normalized by the angular gyrofrequency) is readily obtained

$$\left| \mathrm{Im}\frac{\delta}{\omega_H} \right| = \frac{\sqrt{3}}{2}\xi \left| M_p^{\frac{1}{3}} - N_p^{\frac{1}{3}} \right| , \qquad (3.9)$$

where $M_p = -\frac{b}{2} + \sqrt{\frac{b^2}{4} + \frac{a^3}{27}}$,

$$N_p = -\frac{b}{2} - \sqrt{\frac{b^2}{4} + \frac{a^3}{27}} .$$

The cubic equation (3.8) yields complex solution for $\frac{\delta}{\omega_s}$ only when $\frac{b^2}{4} + \frac{a^3}{27} > 0$. We should remark that, in obtaining the dispersion equation (3.5), we have omitted terms proportional to $\frac{\omega_p'^4}{\alpha^4}$, $\frac{\omega_p'^4}{\omega\alpha^3}$ and the other higher order terms.

This is possible provided that

$$\left(\frac{\delta}{\omega_s}\right) > \sigma^{2/3} \quad \text{or} \quad \left(\frac{\delta}{\omega_H}\right) > \xi\sigma^{2/3} \qquad (3.10)$$

Therefore, the present formulation of the rate of growth of electromagnetic radiation in the stream-plasma system is valid only when the number density of the stream electrons is very small compared with that of the ambient plasma.

The distribution function (3.2) is the idealized one and more convenient in application due to the simplicity of the corresponding dispersion equation (3.5). A more realistic distribution function for a helical electron stream will be of the form (2.18). However, it is expected that if the dispersion of momentum is sufficiently small, the general behaviour of the stream-plasma system in the real situation will not differ from that given by the present formulation significantly.

C. Negative Absorption Coefficient and Conditions for Amplification

Using the classical kinetic approach, we have studied the radiative instability of a system comprising the ambient plasma and an ensemble of non-equilibrium electrons in Section B and in Chapter II (Section D). The same problem can also be solved by means of the quantum treatment*.

---

* The quantum treatment of the synchrotron instability of a system consisting of the background magnetoactive plasma and a group of relativistic electrons is illustrated in Chapter IX.

The interaction of a radiation field with a system, consisting of a set of incoherent radiating centres with two states, may be characterized by three elementary processes: spontaneous emission, stimulated absorption and stimulated (induced) emission. The absorption coefficient for a radiation field in this system can be derived by using the Einstein transition probabilities and the relations for spontaneous emission, stimulated absorption and stimulated emission (Wild et al., 1963). In this treatment, the absorption coefficient is the algebraic sum of all stimulated transitions between energy states whose energy difference is $\hbar\omega$, where $\hbar$ is Planck's constant. Amplification of waves occurs when the absorption coefficient is negative, i.e. the processes of the stimulated emission of photons (or plasmons) prevail over the stimulated absorption of photons (or plasmons). In this case, the system of charged particles does not take in energy from the waves, on the contrary, it gives the energy to them (negative absorption).

Smerd (1963) derived the general expression for the absorption coefficient and obtained conditions for negative absorption in terms of energy distribution of the radiating electrons and the mean emissivity. Hence Smerd found that the bremsstrahlung cannot lead to amplification regardless of any energy distribution and that for thermodynamic equilibrium plasma, the absorption coefficient is always positive for any

emitting process. Therefore, corresponding to various types of spontaneous emission processes, collisional and non-collisional absorptions of electromagnetic waves can take place in a Maxwellian magnetoactive plasma (cf. Chapter VI and Chapter VII).

For other types of energy distribution, negative absorption would occur under favourable condition. Amplification of Cerenkov plasma waves in an electron stream is due to the fact that the longitudinal plasma waves are compressional waves in which at any instant, the electrons are bunched around the peaks of the wave. The electrons trapped by such wave through the electrostatic force $e\bar{E}$ transfer energy to the wave when the electron velocity exceeds the wave phase velocity. Hence in an isotropic plasma (or electrons moving along magnetic field), the condition for wave growth is that there should be more fast particles than slow particles for a given velocity range, i.e.

$$\frac{\partial F_o(v_k)}{\partial v_k} > 0 \qquad \text{at } v_{ph} = v_k \tag{3.11}$$

where v_{ph} is the phase velocity of the plasma wave and $F_o(v_k)$ is the distribution function of the electrons in the stream for the projection v_k of the velocity $\bar{v}$ in the direction of wave vector $\bar{k}$ (Ginzburg and Zheleznyakov, 1958). The strong wave-particle interaction is carried out by the resonant

particles with velocities $v \approx v_{ph}$.

In the case of amplification of cyclotron radiation from electrons in helical orbit along the static magnetic field, the Lorentz force involved in the wave-particle interactions is $e\,[\bar{E} + (\bar{v}\times\bar{B})/c]$ and the condition for negative absorption is (Smerd, 1963; 1968)

$$\Delta p_{\perp} \frac{\partial F_o}{\partial p_{\perp}} + \Delta p_{\parallel} \frac{\partial F_o}{\partial p_{\parallel}} < 0. \qquad (3.12)$$

The changes of momentum components $\Delta p_{\parallel}$, $\Delta p_{\perp}$ due to the emission of a single quantum must satisfy the conservation of energy and momentum (cf. Bekefi, 1966, p.60). Only those resonant electrons which find the wave frequency in their frame of reference to be a multiple integral of the Doppler-shifted electron gyrofrequency f'_H will participate in the strong wave-particle interaction. Thus, the cyclotron resonant velocity of the electron will be

$$v_{\parallel} = [\omega_s - s\gamma\omega_H]\,/k_o \cos\theta \ .$$

For a helical electron stream with momentum distribution function given by (2.18), the condition of amplification (3.12) becomes (Smerd, 1968)

$$(1-n_j\beta_{\parallel}\cos\theta)\,\frac{(p_{\perp}-p_{\perp}^o)}{a_{\perp}^2} + n_j\beta_{\perp}\cos\theta\,\frac{(p_{\parallel}-p_{\parallel}^o)}{a_{\parallel}^2} < 0 \qquad (3.13)$$

According to this condition (3.13), it can be shown that negative absorption of waves occurs not only in the stream-plasma system but also in a system consisting of electrons with temperature anisotropy (i.e. $T_{\perp} \neq T_{\parallel}$). The instability of a homogeneous plasma due to temperature anisotropy has been investigated by Sagdeev and Shafranov (1961).

D. Conclusion

Both the quantum treatment and classical linearized kinetic approach of solving the problem of the instability of the homogeneous and unbounded stream-plasma system suffer the same limitations; they are valid only for the onset of the instability and for the system comprising an ambient plasma and a low density stream.

In the quantum treatment, one derives the absorption coefficient under the condition that the initial state is incoherent; this allows one to sum the number of the radiated and absorbed quanta when determining the radiated and absorbed energy in the system of particles (Zheleznyakov, 1959; Ginzburg and Zheleznyakov, 1965). The increase of the amplitude of the passing wave may be caused only by a change in the electron motions under the action of the wave field, and therefore result in a distortion of the initial incoherent character of the electron radiation process. Moreover, it is assumed that the emission and absorption take place in a

medium with real refractive index n_j, i.e. the contribution of the stream electrons to n_j is disregarded. Therefore, the quantum approach is useful to the study of the radiation instability of a system consisting of an ambient plasma and a very low density stream (or ensemble of non-equilibrium electrons) in the incoherent initial state.

On the other hand, in the linear kinetic approach, one has to assume that the perturbation of distribution function is small compared with the unperturbed distribution function $f_o(\bar{p})$, and that $f_o(\bar{p})$ does not change with time. These assumptions hold only for the onset of the excitation process during which the growth (or damping) is small and the energy of the electrons in the stream is practically constant. Moreover, the dispersion equation for the wave in the stream-plasma system can be simplified only if the number density of the stream electrons is much smaller than that of the ambient plasma (SectionB). Under the assumption $\left|(\omega - kv)/k\beta_T'\right|^2 \ll 1$, it has been shown that for the case of excitation of Cerenkov plasma waves in a stream-isotropic plasma system both the quantum approach and the classical kinetic approach give the same instability criteria and the same amplifieation factor (Ginzburg and Zheleznyakov, 1958; 1965). However, in the case that $m|\mathrm{Im}\delta| \gg ka$ (p.38), the rate of growth cannot be treated by the quantum approach.

The strong wave-particle interaction predicted from the linear theory leads to the growth of the amplitude of the passing wave in the stream-plasma system without limit. In

fact, as the wave grows, it is important to take the nonlinear effect into account. In the absence of static magnetic field, it has been shown that during the initial stage the stream can be assumed to be cold and the passing wave grows in time with the growth rate obtained from the linear theory. However, the development of the instability causes the kinetic energy of the resonant electrons to be converted into electrostatic energy associated with the plasma waves and into thermal energy of the plasma electrons (Shapiro, 1963). Meanwhile, a small part of the energy lost by the stream goes into increasing the thermal energy of the stream electrons themselves. As the amplitudes of the growing waves increase, the non-linear interaction between modes becomes important. For small interaction time during the initial stage, the amplitudes of the waves grow exponentially with time; when interaction time reaches a certain limit, the non-linear mode interaction retards the exponential growth.

Owing to the feed-back effect of the growing waves, there is a diffusion of electrons in the stream and in the plasma in the velocity space; this tends to smooth the distribution function in the region where the wave diffusion coefficient is nonvanishing and hence to reduce the growth rate and to increase the width of the spectrum. The quasi-linear theory (Vedenov, Velikhov and Sagdeev, 1961) predicts that the wave growth and the diffusion of resonant

electrons continue until a plateau is formed on the distribution function for the stream-plasma system. After this point the waves no longer grow and a stationary state is established.

Instability of stream-plasma system leading to coherent radiation of electromagnetic waves by electron streams can explain the high intensities of various solar radio burst emissions that cannot plausibly be accounted for as a result of radiation from thermal or non-thermal plasma by non-coherent mechanism. . However, in applying the results obtained from linear theory to interpretation of the solar radio emissions, one has to assume the existence of an effective process for preventing the plateau formation in the distribution function for the stream-plasma system (see Section G of Chapter VI).

CHAPTER IV

THE SOLAR ATMOSPHERE AND MODELS OF THE SOLAR CORONA

In order to study the generation and propagation of electromagnetic waves in the solar corona in a quantitative manner, we need some suitable models for the electron density distribution and the sunspot magnetic field configurations in the solar atmosphere. In the present chapter, we shall briefly describe the observed features of the solar atmosphere and hence suggest models for the background corona and the active corona.

A. Radial Distribution of Electron Density in The Solar Corona

The solar atmosphere consists of three main layers - the photosphere, the chromosphere and the corona. The medium of the upper chromosphere and the corona is a fully ionized plasma though neutral on a large scale. The well known conventional model for the radial distribution of electron density in the background (normal, regular) corona is given by the Baumbach-Allen formula (Allen, 1947):

$$N = 10^8(1.55\ \rho^{-6} + 2.99\ \rho^{-16})\ \text{cm}^{-3} \qquad (4.1)$$

where $\rho = R/R_o$, R is the distance from the centre of the Sun and $R_o = 6.95 \times 10^5$ km the photospheric radius. This formula

was derived by assuming the spherical symmetry of the corona and based on many years' optical observational data.

The corona overlying the optical centre of activity (sunspots and plages) in the photosphere and the chromosphere is called the active region. The active region is permeated by the sunspot magnetic field and contains enhanced plasma density. From optical observations, Newkirk (1961) found that the coronal streamer* contains enhanced electron densities about two to five times the local background out to the altitude $R \simeq 2R_o$ (Fig. 4.1(a)).

As is well known, the drifts of the type III and type II bursts towards lower frequency with increasing time are attributed to the excitation of electromagnetic waves at the plasma frequency by electron streams travelling upward through the corona and by outward moving hydromagnetic shock waves respectively (Wild et al., 1963). Radio-interferometer observations of the type III and type II burst source positions suggest that type II and type III burst emission sources

---

* Coronal streamers are formations of plasma emerging radially from the Sun in the active regions and can be observed during an eclipse up to ~ $12R_o$ (Kundu, 1965, p.17).

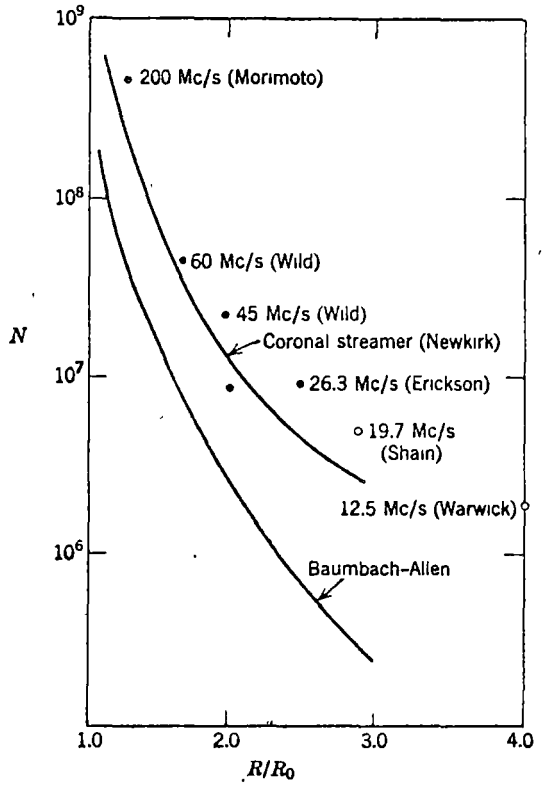

Fig. 4·1(a) The electron densities deduced from different radio observations compared with those of the Baumbach-Allen model and coronal streamer model of Newkirk (after Wild, Sheridan, and Neylan 1959; Morimoto and Kai 1962; Erickson 1962; and Warwick 1964).

(After Kundu, 1965, p. 324)

may travel physically out along coronal streamers where the electron densities increase by a factor about ten over the values given by the Baumbach-Allen formula (Shain and Higgins, 1959; Wild, Sheridan and Neylan, 1959; Morimoto and Kai, 1962; Weiss, 1963a; etc.) (Fig. 4.1(a)). Since during the past sunspot maximum, the background corona electron densities were observed to be some two times the Baumbach-Allen values (Newkirk, 1961), the electron densities of the coronal streamers are only five times over the background electron densities.

For the transition region between the upper layer of the chromosphere and the base of the solar corona, the radial electron density gradient is very large. From a detailed analysis of the observational data on the extreme ultraviolet solar radiation, Ivanov-Kholodnyi and Nikol'skii (1962) constructed a purely empirical model of the radial distribution of the electron density with height in the active and undistrubed regions of the solar atmosphere. This empirical model is shown in Fig. 4.1(b). Alternatively, using the results of the eclipse observations in Sr II lines and in the Balmer continuum (Thomas and Athay, 1961), Gulyaev, Nikol'skaya and Nikol'skii (1963) obtained the radial electron density distribution in the lower layer of the solar atmosphere for the altitude greater than 1,000 km above the photosphere (Table 4.1). The models obtained by both techniques are in

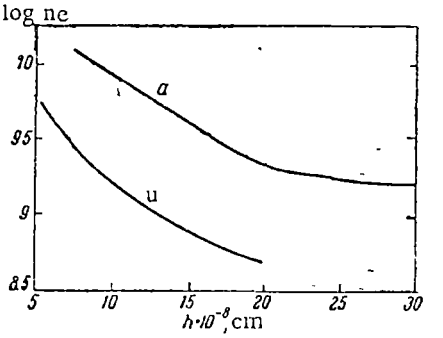

Fig.4.1 (b) Distribution of electron concentration in the transition region; a, u : model for active and unperturbed regions.
(After Ivanov-Kholodyni and Nikol'skii, 1962)

Table 4.1 Distribution of Temperature and the Concentration of H and He in the Solar Atmosphere (After Gulyaev et al., 1963)

h, km	log T	log n_e	log n_{HI}	log n_{HeI}	log n_{HeII}	log $n_{He\ III}$
			Active region			
1000	3.74	11.42	14.35	13 36		
2000	3.74	11.21	13.80	12.82		
3000	3.75	10.89	13,35	12.35		
4000	3.76	10.75	12.80	11.80		
5000	3.78	10.54	12.10	11 10		
6000	3.79	10.35	11.30	10.35		
7000	3.82	10.19	10.35	9.64	1.30	−0.10
8000	3.89	10.07	9.50	8.40	9.05	+7.83
9000	4.14	9.98	8.75	7.31	9.00	8.01
10000	4.36	9.90	7.90	6.88	8.85	8.10
12000	4.67	9.77	6.15	5.60	8.58	8.20
14000	4.95	9.64	5.00	3.76	7.98	8.47
16000	5.20	9.53	4.25	1.46	6.48	8.53
18000	5.39	9.42	3.65	0.03	5.55	8.42
20000	5.56	9.34	3.25		4.81	8.34
25000	5.91	9.23	2.70		3.67	8.24
30000	6.20	9.21	2.30		2.85	8.21
			Undisturbed region			
1000	3.74	11.41	14.20	13.19		
2000	3 74	11.00	13.55	12.55		
3000	3.75	10.73	12.75	11.75		
4000	3.76	10.25	11.80	10.80	0.00	
5000	3.78	9.94	10.70	9.78	8.50	5.94
6000	3.82	9.68	9.55	8.39	8.74	6 42
7000	4.20	9.51	8.10	7.67	8.41	6.48
8000	4.55	9.39	6.30	6.23	8.33	6.76
9000	4.83	9.29	5.00	4.42	8.14	7.48
10000	5.06	9.20	4.25	2.39	6.97	8.08
12000	5.45	9.05	3.25	−0.68	4.93	7.97
14000	5.74	8.93	2.65		3.87	7.87
16000	5.94	8.83	2.25		3.21	7.76
18000	6.07	8.75	2.10		2.79	7.67
20000	6.20	8.68	1.80		2.49	7.60

good agreement with each other.

B. Magnetic Fields of The Sun

(a) Magnetic Fields of Sunspots

A sunspot consists of a dark core, an umbra and a brighter "Penumbra" surrounding the core. Hale and Nicholson (1938) made extensive observation and first discovered intense magnetic field exists in the sunspots. The classical picture of magnetic field configuration inside the surface of a regular, single spot can be described as (Bray and Loughhead, 1964):

(1) The magnetic field is symmetrical around the axis of the spot.

(2) It has its maximum value at the centre of the umbra, the lines of force at this point being perpendicular to the solar surface.

(3) Away from the centre of the umbra, the field becomes smaller and inclined to the vertical. In fact, recent measurements led to the conclusion that the field in the penumbra is almost everywhere horizontal. Thus, only those field lines emerging from the central area of the umbra can extend to the outer layers of the solar corona.

The magnetic field intensity of the sunspot is proportional to the area of the spot. Hale and Nicholson (1938) found that the observed intensities range from a maximum

of about 4,000 gauss for the largest spots down to values of the order of 100 gauss for the smallest spots. In general, the field intensity decreases only slowly across the umbra and drops very sharply across the penumbra (von Klüber, 1948; Bumba, 1960).

A number of single sunspots with the same magnetic polarity form a unipolar sunspot group. However, in majority of cases, sunspots form bipolar groups which are systems of two spots in which the leading spot has a polarity opposite to that of the following spot. The leading spots of such pairs are of opposite polarity in the two hemispheres and these polarities are reversed in successive eleven years solar cycle. On the average, the magnetic field intensity of the leading spot is stronger than that of the following spot. The two principal spots of a bipolar group separate in longitude to a distance of 10° or more (Chapman, 1943). In complex spot groups, spots of opposite polarity are mixed together. The bipolar pair appears to be the fundamental type. It has been pointed out by Bray and Loughhead (1962, 1964) that experimental results have indicated that regions of opposite polarity may frequently appear even within a single isolated spot. No matter how complicated the structure of the sunspot's field is, the field line issuing from one spot can only either stretch straight into the corona as coming from a unipolar spot, or go up and curve down to join a spot in a bipolar

spot group or a region in some spot nearby, or in the leading spot itself.

The observed radial gradient of the sunspot magnetic field intensity in the photosphere is very large (cf. Bray and Loughhead, 1964, p.212; Severnyi, 1966). So far measurements of the radial gradient of the sunspot magnetic field at the corona height are subject to uncertainty. Nevertheless, optical observation as well as the measurements of the radio-wave spectrum of circular polarization radio waves (Hewish, 1962; Molechanov, 1962) indicate that it is possible that the field in the chromosphere and the corona does not vary as rapidly with height as in the photosphere itself. The intensity of coronal magnetic fields at various coronal heights in the active region inferred from various theories of solar radio bursts is illustrated in Fig. 4.2.

(b) The General Magnetic Field of The Sun

Outside the active regions, there is a weak magnetic field which is somewhat stronger at polar latitudes; an upper limit of about 2.5 gauss on the photosphere at the high latitude (Hogbom, 1960). This field is sometimes called the general magnetic field of the Sun since its nature resembles the dipole field of the Earth. The effects of the weak general magnetic field on the propagation of high frequency electromagnetic waves in the solar corona is insignificant and will be neglected.

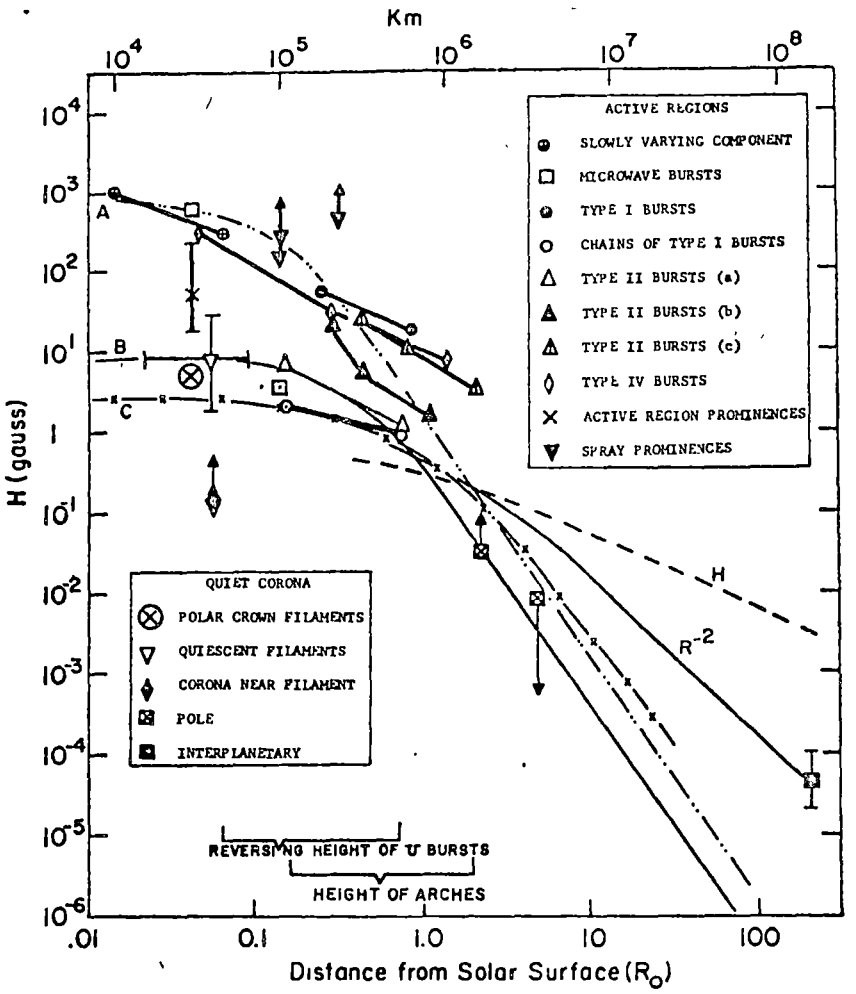

FIG.4.2 The strength of coronal magnetic fields as a function of height above the photosphere as estimated by various techniques. Values referring to active regions appear as heavy lines. Simple models for the potential field above an active region (*A*), an extended dipole region (*B*), and the general solar field at the equator (*C*) appear for comparison. The curve *H* represents the field required for pressure equilibrium with the solar wind.

(After Newkirk, 1967)

C. Models of Sunspot Magnetic Field Configurations

Referring to Fig. 4.3, we assume an imaginary dipole buried at a point about 0.1 solar radius beneath the photosphere. The axis of the dipole inclines to the radial line of the Sun at an angle 70°. The magnetic field lines originating from the dipole pass through the umbral area of the sunspot and the intensity along a field line is given by the dipole field equation

$$H = \frac{M}{r^3}(1 + 3\sin^2\ell)^{\frac{1}{2}} \qquad (4.2)$$

where M is the magnetic moment of the dipole and ℓ is the latitude angle with respect to the centre of the dipole. If the field line passing through the photosphere at r=d and ℓ=L, then $M = H_s d^3/(1 + 3\sin^2 L)^{\frac{1}{2}}$ gauss-(solar radius)^3 where H_s is the magnetic field intensity of the sunspot at the surface of the Sun. For a dipole field model, we also have

$$r = r_o \cos^2\ell \ , \qquad (4.3)$$

and

$$\frac{ds}{d\ell} = r_o \cos\ell(1 + 3\sin^2\ell)^{\frac{1}{2}} \ , \qquad (4.4)$$

where $r_o = d/\cos^2 L$ and ds is the length of a small segment of the field line and $d\ell$ is the corresponding small angular interval at latitude ℓ(Fig. 4.3). The relation between r and ρ is given by

$$\rho^2 = (0.1)^2 + r^2 - 0.2r\cos\mu \ , \qquad (4.5)$$

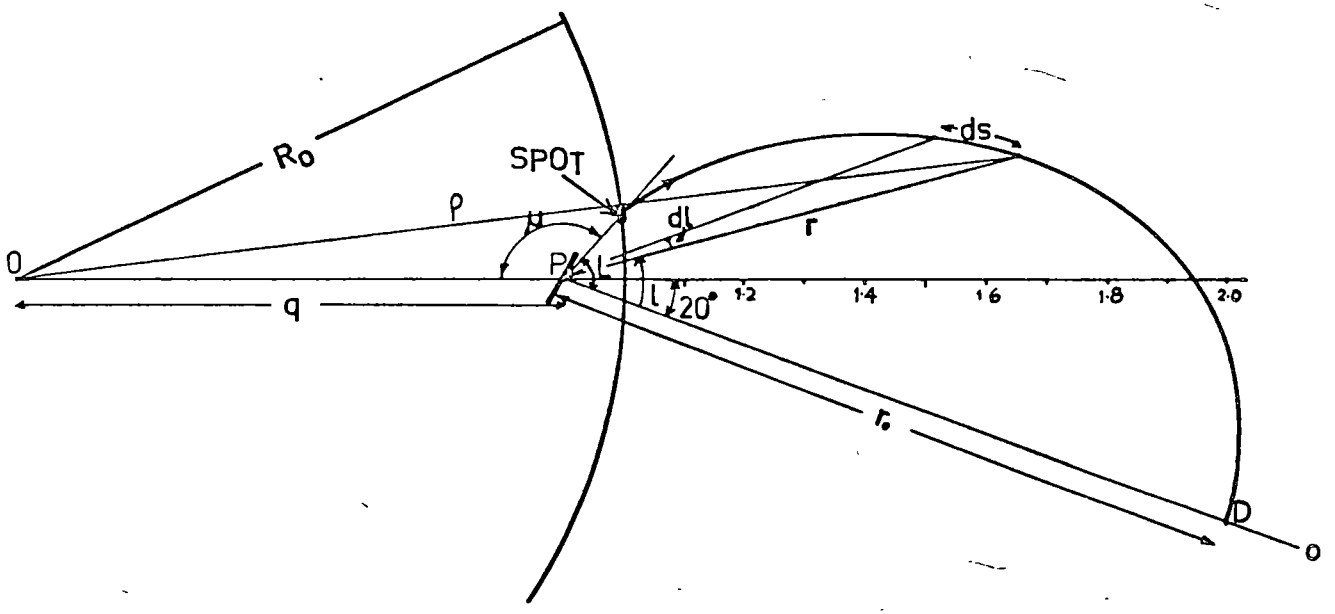

Fig.4.3. - Geometry illustrating the calculation of a theoretical sunspot magnetic field configuration. O is the centre of the Sun and P is the centre of the dipole. r_o is the maximum height of the field line above the centre of the dipole.

where $\mu = 180^{\circ} - |\ell - 20^{\circ}|$.

The magnetic field intensity along a field line emerging from the centre of a unipolar sunspot is plotted against the distance from the centre of the Sun in term of gyrofrequency f_H(in MHz) in Fig. 4.4(a) where $L = 82^{\circ}$ and H_s = 1,000 gauss. We assume two field lines originating from two single spots of opposite polarity joint together at the coronal height and form an arch in the solar corona. Taking $L = 69^{\circ}$, 75° and H_s = 2,000, 150 gauss for the field lines emerging from the leading spot and the following spot respectively, we show the variation of the magnetic field intensity along a bipolar field line in Fig. 4.4(b) (the dashed curve). A similar model for a bipolar field line with turning point at $\rho = 1.62$ is also shown in this figure (the solid curve). Since the radial gradient of the sunspot magnetic field intensity near the solar surface is very large, the surface field intensity H_s may be higher than 2,000 gauss. (In Fig. 4.5(b), the value of H_s has been raised to 3,000 gauss.) Similarly, other field lines originating from different points on the umbral areas of a bipolar pair can also be constructed.

Assuming the Baumbach-Allen formula (4.1), the variations of the electron density (in term of plasma frequency f_p) and the value $A = f_p^2/f_H^2$ with distance from the centre of the Sun along the background corona and the coronal streamer are also shown in Fig. 4.4.

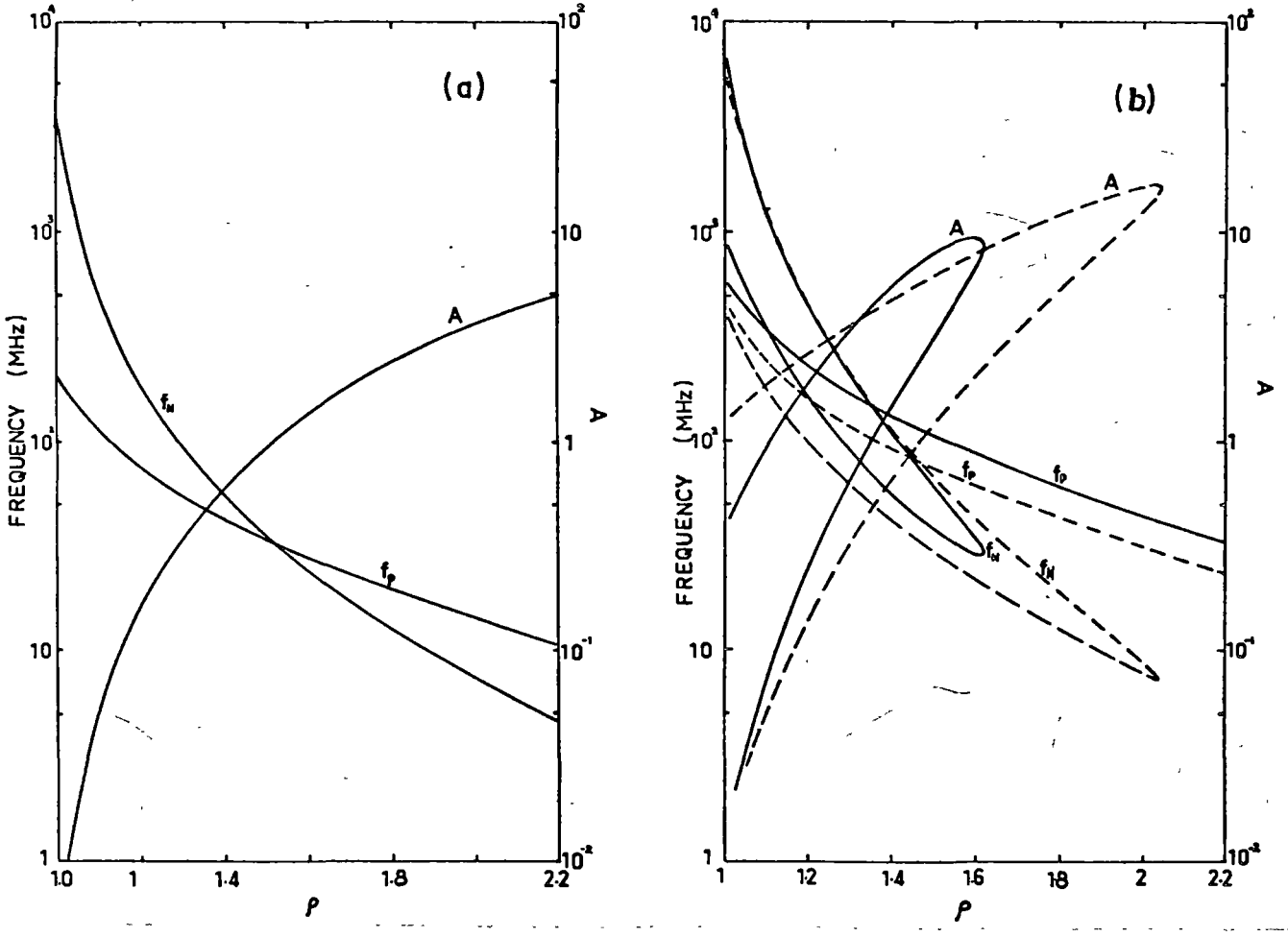

Fig.4.4.- Variation of plasma frequency f_p, gyrofrequency f_H and A along the strongest field line of

(a) a unipolar sunspot specified by H_S = 1000 G in the regular corona;
(b) a bipolar spot group with the maximum leading spot magnetic field intensity on the photosphere H_S = 3000 G in the coronal streamer where the electron density is given by 5xBaumbach-Allen model (--------); 10xBaumbach-Allen model (————).

For unipolar spot magnetic field, a simple theoretical model has been proposed by Ginzburg and Zheleznyakov (1959). The axis of the imaginary dipole is assumed to be coincident with the radial line of the Sun and only some lines of force from the pole near the photosphere will emerge through the umbral area of the spot. The sunspot field line passing through the centre of the sunspot will be the strongest field line whose intensity at a height $\rho-1$ above the photosphere is given by

$$H = H_s\left(1 - \frac{\rho-1}{\sqrt{(\rho-1)^2+b^2}}\right) \qquad (4.6)$$

where b is the radius of sunspot in units of solar radius and H_s is the maximum surface field intensity of the spot. According to Ginzburg and Zheleznyakov (1959), b is taken to be 0.05.

We should remark that the models of the sunspot magnetic field configurations given above are empirical only, since at present there is no observational data giving the magnitude and the exact nature of the sunspot magnetic field above the photosphere.

D. The Temperature of the Coronal Plasma

The coronal temperature has been determined by optical and radio observations. The detailed studies of the thermal

radio emission spectrum in combination with simultaneously optical measurements of coronal electron density showed that the coronal plasma temperature ranges from 1 to 2×10^6 ^oK (Christiansen et al., 1960; Newkirk, 1961). Recent investigations by various authors lead to the conclusion that in general the corona maintains a temperature of approximately 1.5×10^6 ^oK with an increase by 20% during sunspot maximum (Newkirk, 1967). For the active regions, both the optical measurement and the analysis of brightness temperatures associated with slowly varying component of radio emissions suggest the coronal plasma temperature can reach as high as 2×10^6 ^oK (Newkirk, 1967, p.248). Thus for altitude within one solar radius above the photosphere, the coronal plasma temperature is almost constant in the range approximately from $T = 10^6$ ^oK to 2×10^6 ^oK. This is equivalent to the normalized mean thermal speed of the plasma electrons $\beta_T = v_T/c$ from 1.3×10^{-2} to 1.85×10^{-2} .

CHAPTER V

INTERACTION OF NORMAL WAVES AND TRANSFORMATION OF PLASMA WAVES IN THE SOLAR CORONA

A. Introduction

Electromagnetic waves originating in the active solar corona may be prevented from leaving the Sun through collisional and gyro-resonance absorption or through Landau damping in the layers where their phase velocities become close to the mean thermal speed of the plasma electrons. The coupling between different wave modes can, in certain circumstances, increase the probability of escape. We shall examine various possible coupling processes and their effects on the wave propagation.

Since each wave is represented by two branches of the refractive index curves corresponding to two different modes (Fig. 2.1), electromagnetic waves in six different modes can propagate in different layers of the solar corona. Assuming a unipolar magnetic field model (4.6) with H_s = 3,500 gauss (1,500 gauss) and $\beta_T = 10^{-2}$ and the electron density distribution given by five (two) times the background coronal density, we show the variation of the square of refractive index along a radial line passing through the centre of the sunspot in Fig. 5.1. The whistler mode (n_2) and the lower p-mode (n_3) propagate in the layers where $f < f_H$ (i.e. $Y > 1$) and the

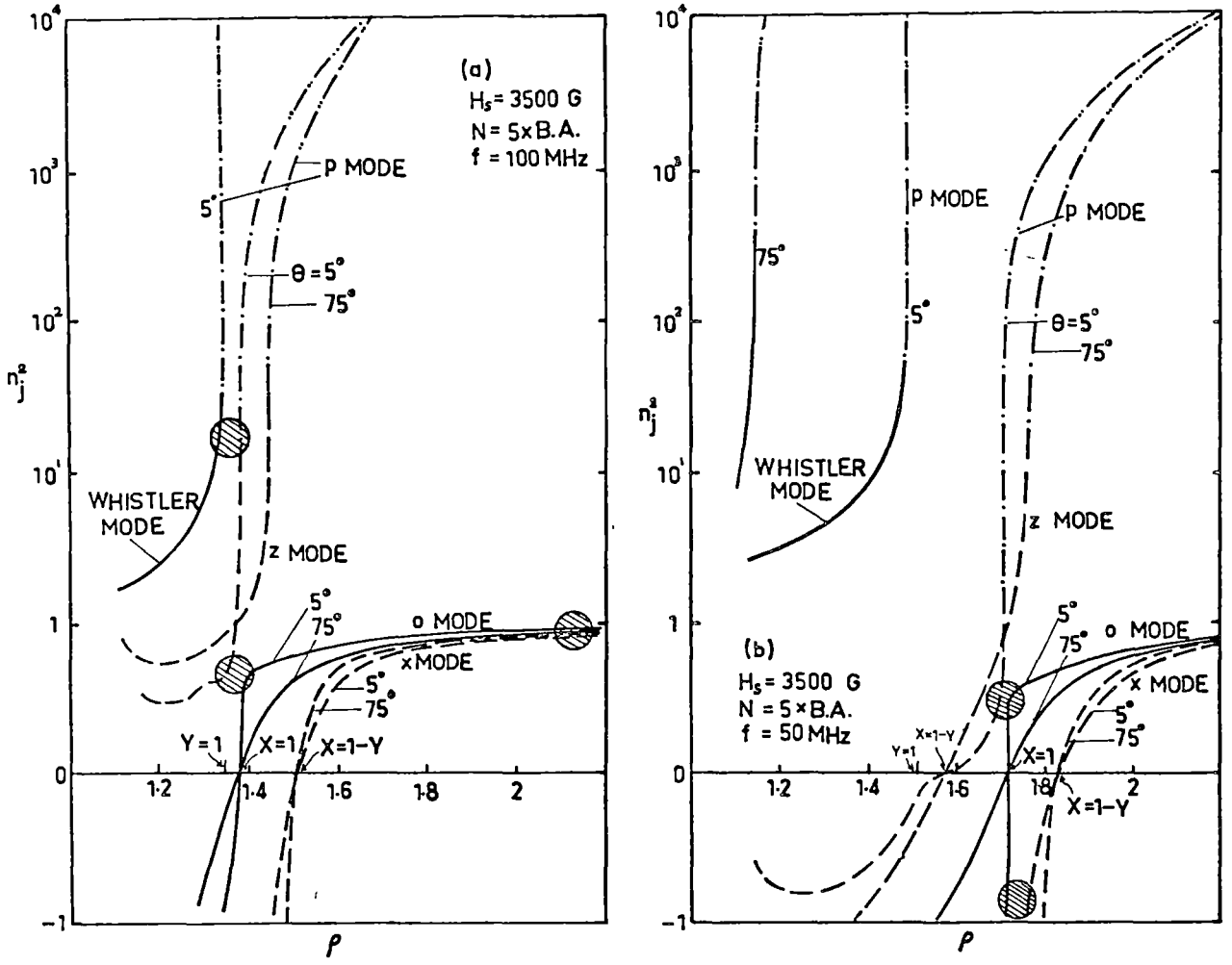

Fig. 5·1 - The variation of refractive index squared n_j^2 along the radial line ρ passing through the centre of the strong unipolar spot (H_s = 3500 G.) for (a) f = 100 MHz (b) f = 50 MHz when the electron density distribution is given by the five times the Baumbach-Allen's formula.

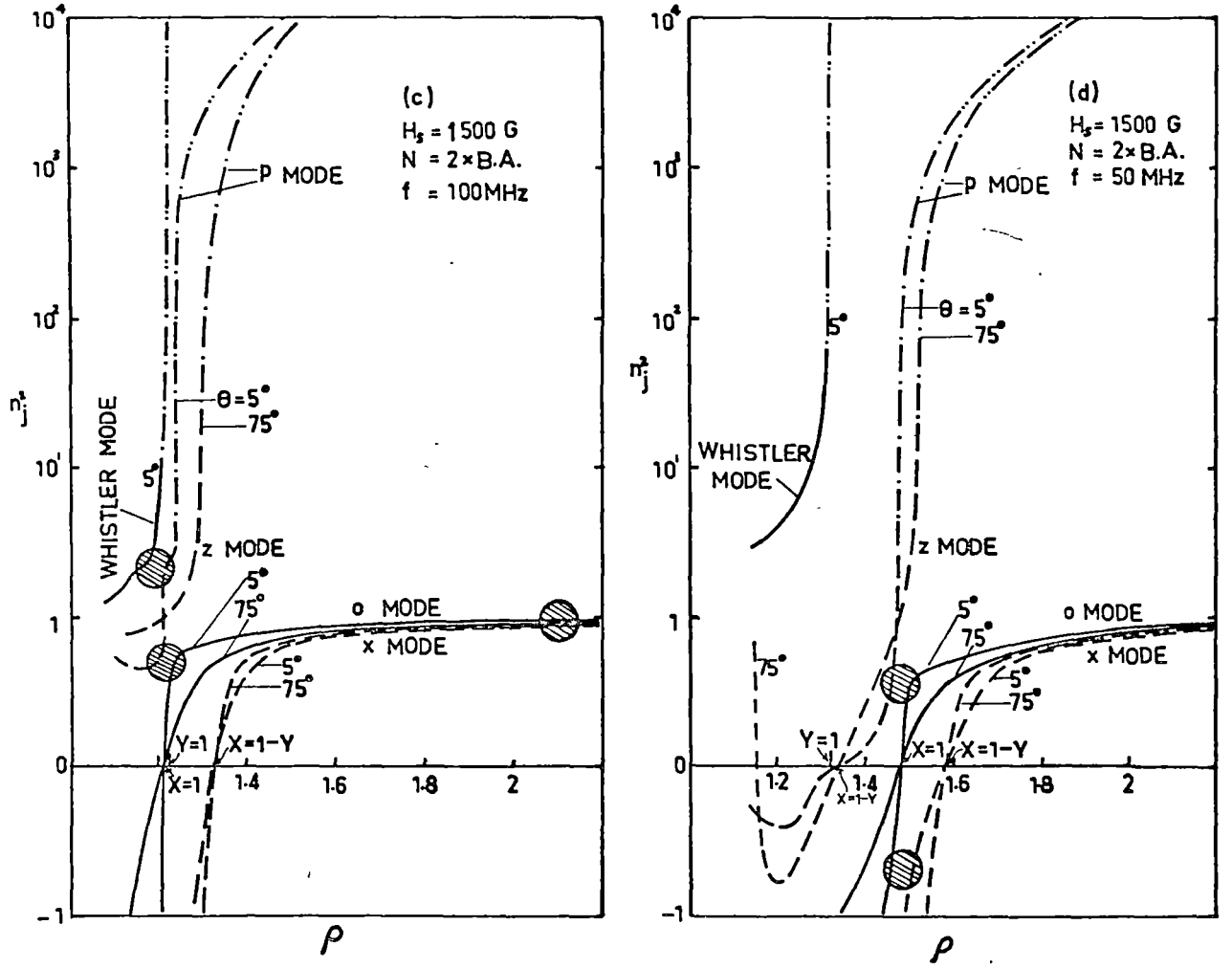

Fig.5·1 - The variation of refractive index squared n_j^2 along the radial line ρ passing through the centre of the strong unipolar spot (H_s = 1500 G.) for (c) f = 100 MHz (d) f = 50 MHz when the electron density distribution is given by the two times the Baumbach-Allen's formula.

o-mode (n_2) and x-mode(n_1) in the layers where

$$f > f_o = f_p \text{ and } f > f_x = \tfrac{1}{2}f_H + \tfrac{1}{2}(f_H^2 + 4f_p^2)^{\frac{1}{2}} \qquad (5.1)$$

respectively. The z-mode wave (n_1) propagates only in the layers where $f \leq f_x$. The upper p-mode (n_3) wave exists within the layer $f_p \lesssim f \lesssim f_x$. If the sunspot magnetic field intensity is very weak such that $f_p >> f_H$, the whistler mode and the lower p-mode waves propagate with very small phase velocities and the layers $f = f_x$ and $f = f_p$ are close to one another. Therefore, in the outer layers where $f_p >> f_H$, the coronal plasma tends to be isotropic and only the longitudinal plasma wave and the transverse electromagnetic wave can propagate. From the refractive index curves, we can see that the x-mode wave and the o-mode wave are able to traverse through the solar corona freely* while the z-mode wave, the whistler mode wave and the p-mode wave can leave the Sun only if they can be coupled to the x-mode and the o-mode waves.

---

* The x-mode and the o-mode waves can escape from the solar corona only if the resonance absorptions at the harmonic layers ($f = sf_H$, $s = 1,2,3,...$) are insignificant (see Chapter VI).

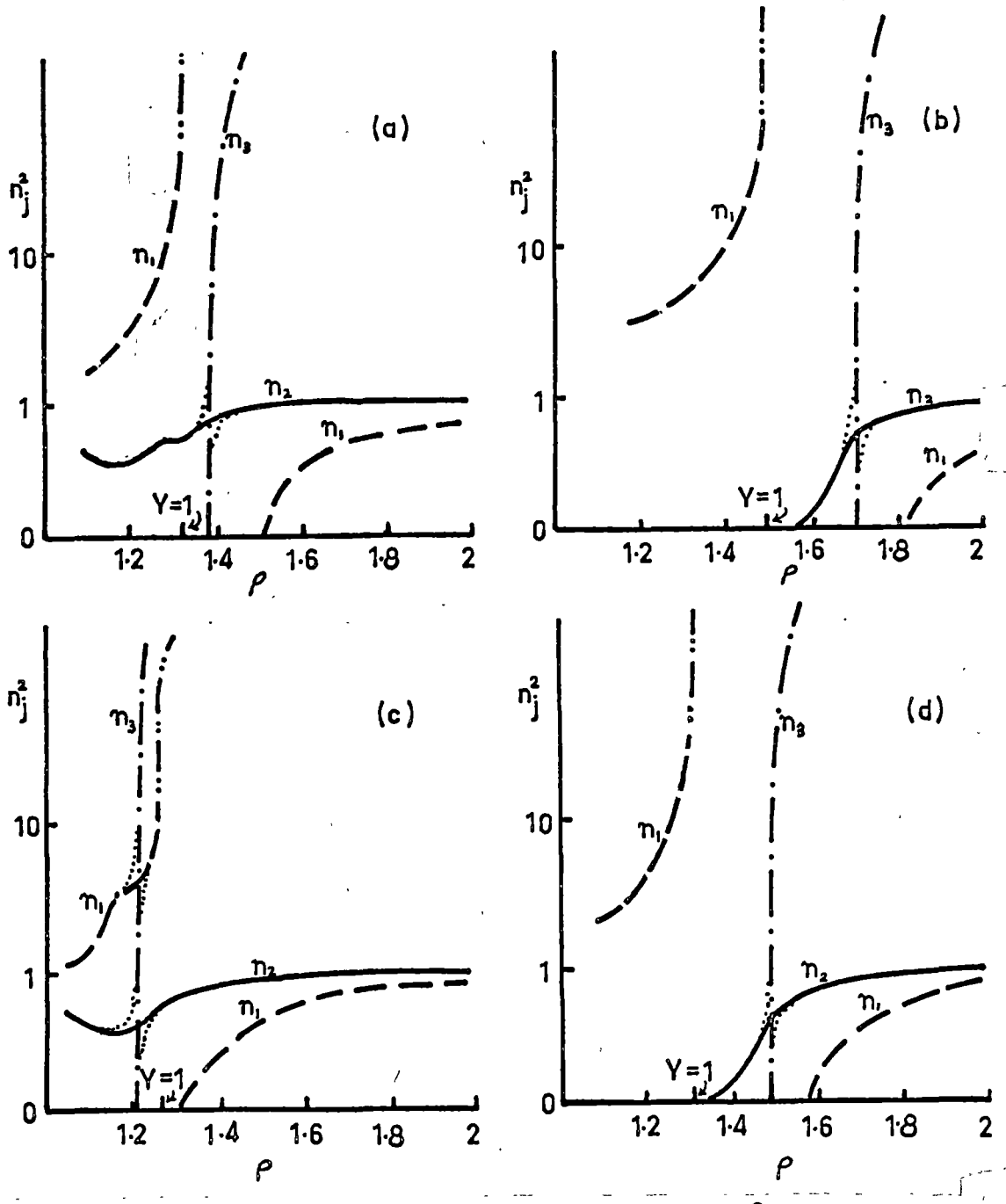

Fig.5.? - The variation of refractive index squared n_j^2 along the radial line ρ in the coronal streamer for the wave frequency f = 100 MHz ((a),(c)), 50 MHz ((b),(d)) and for the wave normal-angle $\theta = 0^o$. The models of the sunspot magnetic field and electron density distribution along the coronal streamer correspond to those shown in Fig.5.1 (a)-(d). The double dotted-dashed curves indicate the occurrence of strong attenuation due to double resonsnces and the dotted curves show the variation of refractive index squared when θ departs slightly from zero.

B. Coupling of Normal Waves in The Solar Corona

The wave equation describing the propagation of the electromagnetic wave in an inhomogeneous magnetoactive plasma involves a dielectric tensor $\varepsilon_{\alpha\beta}(\omega,\bar{r})$, where $\bar{r}$ is the position vector with respect to some origin. The exact solutions of this equation, in general, are either entirely unkown or of little practical value. However some approximate solutions have been obtained and these reveal the physical phenomenon of the propagation of waves in an inhomogeneous magnetoactive plasma. The most important method of solving the wave equations is based on the use of the approximation of geometrical optics. The applicability of this approximation requires the satisfaction of the inequality (Ginzburg, 1964, p.256),

$$\frac{\lambda_o}{2\pi}\left|\frac{dn_j}{dr}\Big/ n_j^2\right| \ll 1, \qquad (5.2)$$

where $\frac{dn_j}{dr}$ is the spatial gradient of the refractive index in the direction of wave propagation and $\lambda_o = 2\pi c/\omega$ is the wavelength in vacuum. For the most part of the solar corona, the properties of the plasma vary slowly in space, the refractive index changes very little over distance of the order of the wavelength, and the inequality (5.2) is generally satisfied. Thus for propagation of waves in any relatively small region, the layer may then be regarded as being a homogeneous medium with the corresponding values of n_j^2 in that region. When (5.2)

holds, the two normal waves are entirely independent and so are waves of the same type propagating in opposite directions.

From (5.2), it is obvious that the geometrical optics is invalid when

$$n_j^2 \to 0, \tag{5.3}$$

$$\frac{\lambda_o}{2\pi}\frac{dn_j}{dr} \gg 1 . \tag{5.4}$$

The inapplicability of geometrical optics in the layer where $n_j \simeq 0$ indicates the possibility of total reflection of waves (in the absence of absorption), since in this layer the field almost completely disappears at a distance of a few wavelengths beyond the point $n_j = 0$ and it is clear all the energy must be totally reflected. Accordingly, the x-mode, o-mode and z-mode waves propagate towards the surface of the Sun will be reflected from the layers $f=f_x$, $f=f_o = f_p$ and $f_z = -\frac{1}{2}f_H+\frac{1}{2}(f_H^2+4f_p^2)^{\frac{1}{2}}$ respectively.

For θ is not too small, geometrical optics is inapplicable only to the o-mode wave at the layer $f \simeq f_p$ and so reflection of the o-mode wave does not affect the other waves. The same phenomenon will also happen for the waves of other modes. However, when the angle θ decreases to small values (but not exactly equal to zero), geometrical optics becomes inapplicable to both o-mode and z-mode waves and also to whistler mode and z-mode waves in the region $f \simeq f_o = f_p$. Both the o-mode and

the z-mode waves (or whistler mode and z-mode waves) possess not only similar phase velocities but also similar states of polarization (Fig. 5.1; Fig. 11.12 of Ginzburg, 1964, p.108). Thus, as one of the normal waves (o-mode, say) approaches to the layer $f=f_p$, its polarization has to change rapidly in order to remain a characteristic o-mode wave, but with a small change of polarization, it could propagate as a z-mode wave (Ratcliffe, 1959, p.162). Then an o-mode wave (or a whistler mode wave) on passing through the points near $f=f_p$ will partially transform into the z-mode and continue to propagate with that mode. A similar phenomenon also occurs when the z-mode wave passing through the layers near the point $f=f_p$ with small wave-normal angle. The parameters determining the efficiency of the interaction between normal waves near the point $f=f_p$ have been calculated by means of the method of phase integrals (Ginzburg, 1964, p.320) and given by

$$2\,\delta_{o1} = \frac{\pi\omega\theta^2}{2ca(1+\omega/\omega_H)^{3/2}} \quad \text{and} \quad 2\delta_{o2} = \frac{\pi\omega\theta^2}{2ca(1-\omega/\omega_H)^{3/2}}\,, \qquad (5.5)$$

where $a = \left|\frac{1}{n_o}\,\frac{\partial n_o}{\partial r}\right|_{n_o=N_c}$, N_c is the electron density in the coupling region, and θ is in radian. The expressions for the transmission coefficient $|D|^2$ and reflection coefficient $|R|^2$ in various cases are shown in Fig. 5.3. These expressions are valid only for

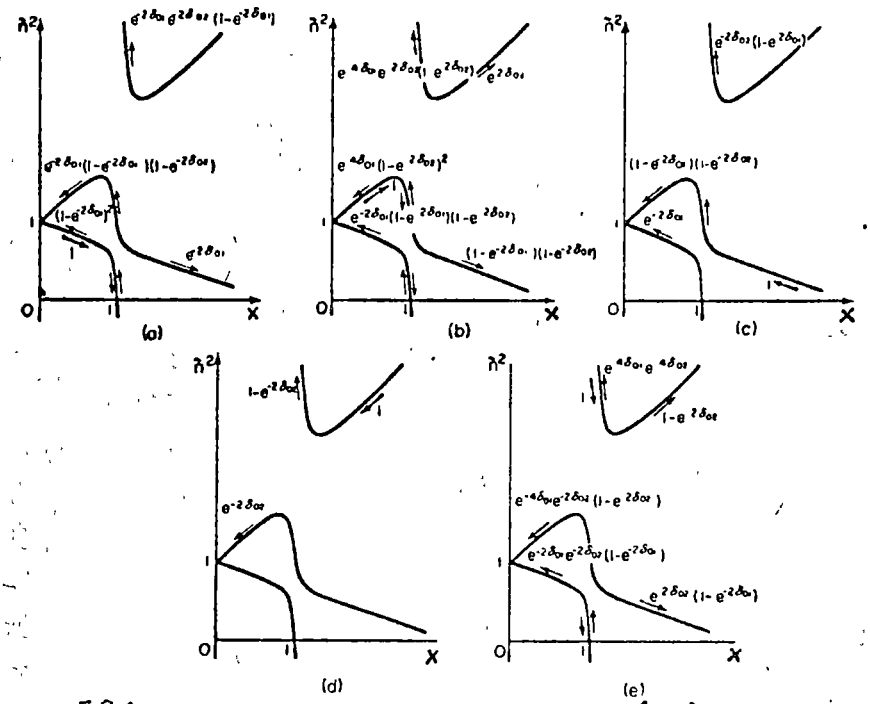

FIG. 5·3 A Various cases of interaction of waves with $\gamma_L^2 = \gamma^2 \cos^2\theta > 1$. The diagrams show the squared moduli of the wave amplitudes, with the amplitude of the incident wave (shown by the thick arrow) taken as unity.

Reflection from the point X = 1 + Y is neglected.

(After Ginzburg, 1964, p.320)

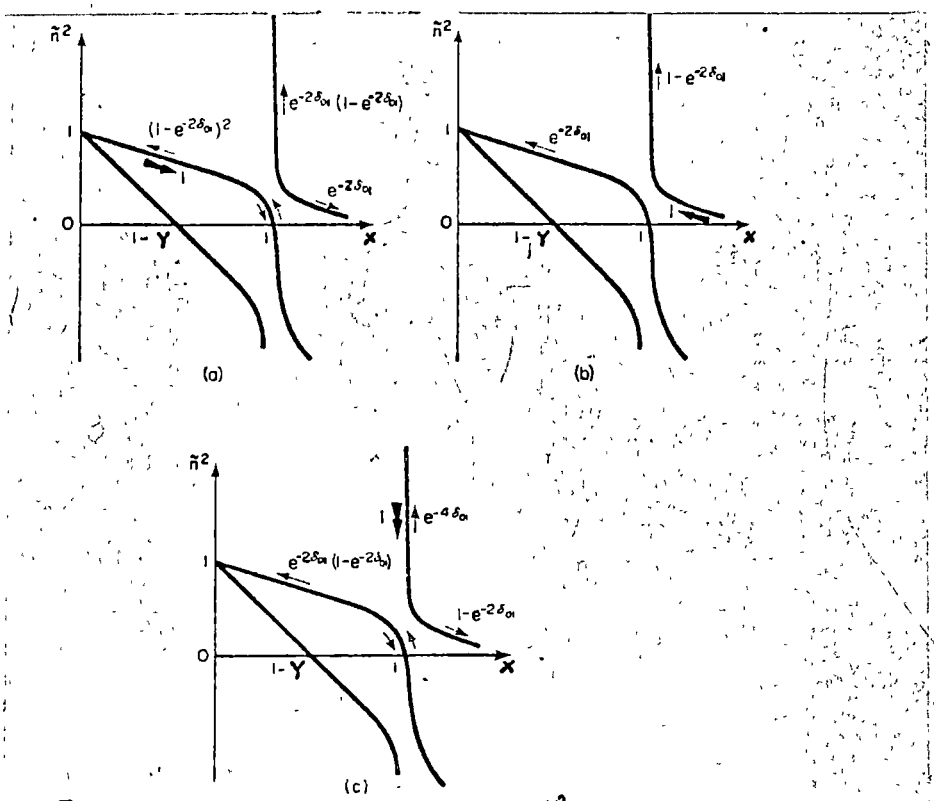

FIG. 5·3 B Various cases of interaction of waves with $\gamma^2 < 1$. The notation and conditions are the same as in Fig. 5·3 A.

(After Ginzburg, 1964, p.321)

$$\nu_{eff} << f_H \sin^2\theta/2\cos\theta \quad , \qquad (5.6)$$

where ν_{eff} is the effective collision frequency. For the solar corona, ν_{eff} is given by (Ginzburg, 1964; Wild et al., 1963):

$$\nu_{eff} = 5.5 n_o \ln(220T/n_o^{\frac{1}{3}})/T^{3/2} \quad ,$$

$$\simeq 50\, n_{o\,(cm^{-3})}\, T^{-3/2}_{(^oK)}\ sec^{-1} \quad . \qquad (5.7)$$

In the active solar corona, if the electron density distribution is given by the Newkirk model and $\beta_T \simeq 10^{-2}$, ν_{eff} varies from 50 Hz to 2 Hz for $\rho = 1.1$ to $\rho = 2$. So the condition (5.6) is satisfied even for extremely small values of θ (but $\theta \neq 0$).

The most interesting case is the coupling of the z-mode wave to the o-mode wave in the active solar corona. For the wave frequency f = 50 MHz, the interaction between the z-mode wave and the o-mode wave takes place at the layer $\rho \simeq 1.7$ (Fig. 5.1(b)) where $f_p \simeq f$, $f_H \simeq 30$ MHz, $N_c \simeq 6\times10^7 (cm^{-3})$ $\left|\frac{\partial n_o}{\partial r}\right|_{n_o=N_c} \leq 2\times10^{-4}(cm^{-3})/cm$. If the amplitude of the z-mode wave is taken to be unity, the square of the amplitude of the o-mode wave leaving the interaction region will be (Fig. 5.3(B)(b))

$$|D|^2_{z\Leftrightarrow 0} \simeq \exp\left[\frac{-\pi^2 f\theta^2}{ca\,|1+f/f_H|^{3/2}}\right] \qquad (\theta \text{ in radian}) \ .$$

If $\theta = 0.5^{o}$ and 5^{o}, then $\log_{10}|D|^2 \simeq -4\times10^4$ and -4×10^6 respectively. Hence, under the normal active solar corona condition, coupling the z-mode wave to the o-mode wave is entirely inefficient. However, if there are some local inhomogeneities, e.g. "electron hills" or sharp shock front, in the interaction region such that the value of $\left| \frac{\partial n_o}{\partial r} \right|_{n_o=N_c}$ can reach $1.4\times10 - 1.4\times10^2$ $(cm^{-3})/cm$, o-mode radiation with the intensity about 10^{-7} of that of the incident z-mode radiation will emerge from the interaction region.

As shown in Chapter II, the coherent Cerenkov plasma wave emitted by an electron stream is of greatest intensity in the direction of the electron guiding centre motion. Thus, the Cerenkov plasma wave excited by a stream moving towards the Sun will change its physical character from a longitudinal plasma wave to electromagnetic wave in the z-mode ($n_1 \gtrsim 1$) near the point $f=f_p$, then part of its energy will couple to the o-mode wave which after being reflected at $f=f_p$ will leave the Sun. From Fig. 5.3(B)(c), the efficiency of this coupling will be given by $|D|^2_{p\to o} = |D|^2_{z\leftrightarrow o}\ (1 - |D|^2_{z\leftrightarrow o})$. Since for normal active corona conditions, $|D|^2_{z\leftrightarrow o}$ is very small, no significant o-mode radiation arising from coupling between the p-mode and o-mode waves in the region $f \simeq f_p$ will emerge from the solar corona.

Interaction between normal waves also occurs in those

shaded regions in Fig. 5.1 (a), (c) and (d).

When $\theta = 0$, the waves are to some extent renamed. This is illustrated in Fig. 5.2 where n_j^2 is plotted against the radial distance from the centre of the Sun for wave frequencies f=50 MHz and 100 MHz. From this figure, we see that the geometrical optics approximation will be inapplicable only to the p-mode at the layer $f \simeq f_p$, hence the p-mode and o-mode waves propagate independently.

C. Interaction of Normal Waves in The Region Near The Boundary of A Layer

The boundary of a layer is defined as the region where $f_p^2/f^2 \to 0$ and beyond which the effect of the medium on the propagation of electromagnetic waves is insignificant. It has been shown that near the boundary of a layer the approximation of geometrical optics is also invalid for the x-mode and o-mode waves through the occurrence of polarization degeneracy in the vacuum (Ginzburg, 1964, p.257). The condition for the approximation of geometrical optics to be valid, in the present case, is

$$\frac{\lambda_o}{2\pi} \frac{d\Delta n}{dr} \Big/ \Delta n \ll 1, \qquad (5.8)$$

where $\Delta n = n_2 - n_1$. Near the boundary of a layer, $n_{1,2} \to 1$, (5.8) will then be violated. For transverse propagation, $\Delta n \to 0$ even in the region where f_p^2/f^2 is not vanishingly small.

Cohen (1960) suggested that a breakdown of the geometrical optics approximation due to transverse propagation would result in an effective interaction between normal waves. This interaction is characterized by a coupling parameter

$$2\delta_o = \frac{e^5 n_o H_o^3 L_H}{32\pi^2 m_o^4 c^4 f^4} \quad , \tag{5.9}$$

which is obtained by means of phase integral method (Zheleznyakov and Zlotnik, 1964). Here L_H is the characteristic scale of the magnetic field and for typical solar active region, $L_H \simeq 10^9 - 10^{10}$ cm .

Since the magnetic field intensity and the electron density in the solar corona decreases away from the Sun, electromagnetic waves (x-mode and o-mode) emitted from a source embedded in the active region will traverse the solar corona with the quasi-longitudinal propagation condition $\left|\frac{2\cos\theta(1-X)}{Y\sin^2\theta}\right|^2 \gg 1$ under which the waves are circularly polarized. However, when the waves pass through the magnetic field with wave-normal angles in the vicinity of $\pi/2$, the quasi-transverse propagation condition $\left|\frac{2\cos\theta(1-X)}{Y\sin^2\theta}\right|^2 \ll 1$ holds and the waves are linearly polarized (Piddington and Minnett, 1951). According to Zheleznyakov and Zlotnik (1964), for circularly polarized radiation of unit intensity which penetrates into the quasi-transverse propagation region (QT region), the emerging

radiation will consist of a circularly component and a linearly polarized component whose degrees of polarization are respectively given by

$$\rho_{cir} = 2e^{-2\delta_o} - 1, \qquad (5.10)$$

$$\rho_{lin} = 2\,[e^{-2\delta_o}(1 - e^{-2\delta_o})]^{\frac{1}{2}}, \qquad (5.11)$$

where $\rho_{cir}^2 + \rho_{lin}^2 = 1$. Strong coupling occurs when δ_o is small. This requires that the characteristic polarizations change substantially in a distance comparable with that required for a Faraday rotation of one radian (Cohen, 1960).

In general, interaction of normal waves in the region $f \simeq f_p$ does not give rise to the x-mode wave. However, since the approximation of geometrical optics is also invalid for both z-mode and x-mode waves near the point $f = f_x$, the z-mode wave can transmit part of its energy to the x-mode wave. This transmission process will be efficient only when $\theta \simeq \pi/2$ (Ginzburg, 1964, p.287). The sense of polarization of the transmitted x-mode wave is the same as that of the original z-mode wave.

D. Transformation of Plasma Waves into Electromagnetic Waves by Scattering on Fluctuations of Electron Density in The Solar Corona

(a) Introduction

The high intensity Cerenkov plasma waves which are

excited by electron streams in the solar corona (Chapter II) are important in connection with the observed solar radio emission only when these plasma waves can be transformed efficiently into electromagnetic waves in the o-mode and the x-mode. It has been shown in Section B that under normal active solar corona conditions, the transformation of plasma waves into o-mode waves through wave-mode coupling in the region near $f \simeq f_p$ is quite inefficient. Alternatively, the plasma waves can also be transformed into the x-mode and o-mode waves through scattering on the fluctuations of electron density and magnetic field intensity existing in a homogeneous magnetoactive plasma*.

The problem of scattering and conversion of waves in the equilibrium and non-equilibrium plasmas has been dealt with by many authors (e.g. Akhiezer, Prokhoda and Sitenko, 1958; Akhiezer and Sitenko, 1962; Rosenbluth and Rostoker, 1962; Bass and Blank, 1963; Daneliya and Tsintsadze, 1965; Tsintsadze, 1965; Sitenko and Radzieveskii, 1966; etc.). Quantitative application of these theories to the study of radio

---

* The term "homogeneous plasma" means that a plasma is homogeneous "on the average" (in the absence of fluctuations or local inhomogeneities).

emissions from the planetary atmospheres, however, is still rare. Ginzburg and Zheleznyakov (1958) and Smerd, Wild and Sheridan (1962) have studied the efficiency of the transformation of longitudinal plasma waves radiated by electron streams and applied to the interpretation of unpolarized type III bursts. Tidman, Birmingham and Stainer (1966) showed that the solar type II emission could be the consequence of conversion of the plasma wave excited by energetic electrons into electromagnetic radiation by scattering on the low frequency ion density fluctuations and high frequency electron plasma oscillations in a plasma consisting of a thermal electron component co-existing with a flux of energetic electrons.

On the other hand, Zaitsev (1966, 1967) has considered that the type II bursts and the drifting bursts superimposed on the type IV continuum at decimetre wavelengths are the consequences of conversion of plasma waves generated in the shock front which propagates through the solar corona. Ondoh (1966) has suggested that the very low frequency hiss emitted in the Earth's magnetosphere may be attributed to the emission of the plasma waves by fast electron streams travelling along the geomagnetic field line. However, most of these applications are limited to the case of isotropic plasma. In the presence of a magnetic field, coherent fluctuation of electron density occurs at frequencies close to plasma resonance frequencies (2.5) which, in the general case, do not

coincide with the plasma frequency. Furthermore, the intensity of the radiation resulting from transformation of a given incident plasma wave depends strongly on the wave-normal angle of the transformed emission. Therefore, in the present section we formulate the coefficients for the transformation of plasma waves into electromagnetic waves by thermal fluctuations of electron density in a magnetoactive plasma.

(b) Fluctuations of Electron Density in a Magnetoactive Plasma

We consider an unbounded and spatial homogeneous fully ionized two component plasma (electrons and ions). The state of the plasma is assumed to be stationary with a fairly strong imposed magnetic field whose direction is along the z-axis. Taking into account of self-consistent interaction between electrons and ions, the spectral distribution for the electron density fluctuations in the isothermal Maxwellian plasma is given by (Sitenko and Kirochkin, 1966)*:

$$\langle \delta n^2 \rangle_{\bar{k},\omega} = \frac{k^2}{e^2\omega^2 |\varepsilon_{||}(\bar{k},\omega)|^2} \left[|1+4\pi K^i_{||}|^2 G^e_{||} + 16\pi^2 |K^e_{||}|^2 G^i_{||} \right], \quad (5.12)$$

where $\bar{k}$ and ω are the vector and frequency of the fluctuation. $G^e_{\alpha\beta}$ and $G^i_{\alpha\beta}$ are the spectral correlation functions of microcurrent density for uncorrelated electrons and ions respectively. $K^e_{\alpha\beta}$ and $K^i_{\alpha\beta}$ are the polarizability tensors of the electron and ion components in the plasma and they are related to the

---

* A detailed derivation of (5.12) is given in Appendix B.

dielectric tensor by

$$\varepsilon_{\alpha\beta}(\bar{k},\omega) = \delta_{\alpha\beta} + 4\pi K^{e}_{\alpha\beta} + 4\pi K^{i}_{\alpha\beta} \ . \qquad (5.13)$$

The subscript $||$ represents the longitudinal component of the corresponding tensor. For an isothermal plasma, the spectral correlation functions of the microcurrent density for independent electrons and for independent ions can be expressed in terms of dielectric tensor as

$$G^{e}_{\alpha\beta} = \frac{\kappa T\omega}{(2\pi)^5} \frac{(\varepsilon^{e}_{\alpha\beta} - \varepsilon^{e*}_{\beta\alpha})}{2i} \ , \ G^{i}_{\alpha\beta} = \frac{\kappa T\omega}{(2\pi)^5} \frac{(\varepsilon^{i}_{\alpha\beta} - \varepsilon^{i*}_{\beta\alpha})}{2i} \qquad (5.14)$$

where $\varepsilon^{\alpha}_{\alpha\beta} = \delta_{\alpha\beta} + 4\pi K^{\alpha}_{\alpha\beta}$ (α = i.e). Thus, the electron density fluctuation spectrum for an isothermal magnetoactive plasma is completely determined by the dielectric tensor for the plasma.

The electron density fluctuation spectrum consists of a central broad maximum about the origin $\omega = 0$ of approximate width proportional to kv^{i}_{T}, where v^{i}_{T} is the mean thermal speed of the ions. When $k < k_D = \left(\frac{4\pi e^2 n_o}{\kappa T}\right)^{\frac{1}{2}}$, in addition to the central maximum, there are also side bands occurring at frequencies ω and vectors $\bar{k}$ for which Re $\varepsilon_{||}(\bar{k},\omega) = 0$, the dispersion equation for weakly damped plasma waves* ($T=T^{i}=T^{e}$ is the

---

* For an isothermal magnetoactive plasma, the electron density fluctuation spectrum for a given wave-normal angle θ is essentially the same as that for an isotropic plasma except that the sharp maximum occurs near $\omega = \omega_{\pm}(\theta)$ instead of $\omega = \omega_p$.

plasma temperature). The sharp delta-like maximum arises from the long range Coulomb interaction. The central maximum is associated with electrons in the shield clouds around the ions of velocities close to zero. Hence the fluctuations with frequencies in the central maximum of the spectrum are associated with the random motion of the individual ions and, for a given $\bar{k}$, the frequency of the fluctuation is not restricted by the dispersion equation for the low frequency wave.

Owing to the relatively large ion mass, the effect of the ions on the dielectric tensor and hence on the electron density fluctuation can be neglected in the high frequency region. That is, the ions serve merely to neutralize the electron charge density. The spectral distribution for coherent fluctuations of electron density is then

$$\langle \delta n^2 \rangle_{\bar{k},\omega} = \frac{n_o k^2 [\delta(\omega-\omega_s) + \delta(\omega+\omega_s)]}{2(2\pi)^3 k_D^2 \omega^2 \left| \frac{\partial}{\partial \omega^2} \mathrm{Re}\ \varepsilon_{||}(\bar{k},\omega) \right|_{\omega=\pm\omega_s}} \tag{5.15}$$

where Re $\varepsilon_{||}(\bar{k},\omega)$ is given by the left-handed side of (2.3) and

$$\omega_s \simeq 2\pi f_{\pm} \tag{5.16}$$

is the angular frequency at which the sharp delta-like maximum occurs and satisfies the dispersion equation Re $\varepsilon_{||}(\bar{k},\omega_s) = 0$. Then the magnitude of the fluctuation vector becomes

$k = \frac{n_3 \omega_s}{c}$ with n_3 given by (2.4).

The total electron density fluctuation, obtained by integration of $< \delta n^2 >_{\bar{k},\omega}$ over all frequencies, is

$$< \delta n^2 >_{\bar{k}} = \frac{n_o(1+k_D^2/k^2)}{(2\pi)^3(1+2k_D^2/k^2)} \quad . \tag{5.17}$$

From (5.15) and (5.17), it can be seen that coherent fluctuation of electron density at frequency ω and vector $\bar{k}$ yields only a small fraction, of the order of k^2/k_D^2 , of the total electron density fluctuation.

(c) Transformation of Plasma Waves in A Magnetoactive Plasma

The use of the linearized kinetic equation and the Maxwell's equations to describe the electromagnetic properties of the plasma leads to the independent propagation of waves in various modes. On the other hand, the non-linearity of the kinetic equation leads to the possibility that each of these waves may be scattered or transformed into waves in other modes by scattering on the electron density fluctuations of either thermal or nonthermal origin existing in the plasma. The interaction between the incident wave of frequency ω_o and wave vector $\bar{k}_o$ with the electron density fluctuation at frequency $\tilde{\omega}$ and wave vector $\bar{q}$ would give rise to waves whose frequencies and wave vectors are given by

$$\omega = \omega_o + \tilde{\omega} \ , \ \bar{k} = \bar{k}_o + \bar{q} \ . \tag{5.18}$$

Since ω_o, $\bar{k}_o$ and $\omega,\bar{k}$ have to satisfy their own dispersion equations $\omega_o(\bar{k}_o)$ and $\omega(\bar{k})$ respectively, scattering or conversion of the incident wave can take place only when the equation

$$\omega(\bar{k}) = \omega_o(\bar{k}_o) + \tilde{\omega}(\bar{k} - \bar{k}_o)$$

has real solution for $\bar{k}$ (Bass and Blank, 1963; Sitenko, 1967, p.152). Therefore, owing to the existence of a broad maximum about $\tilde{\omega} = 0$ and side maxima at frequencies equal to electron plasma wave frequencies in the electron density fluctuation spectrum for the isothermal plasma, the incident plasma wave may be transformed into electromagnetic waves by incoherent scattering with a small frequency change and by coherent (combination) scattering with a change in frequency by an amount equal to the plasma wave frequency (5.16).

Actually, in a magnetoactive plasma, fluctuations of electron density and magnetic field will result in fluctuations of the dielectric tensor, i.e.

$$\varepsilon'_{\alpha\beta} = \varepsilon_{\alpha\beta} + \delta\varepsilon_{\alpha\beta}$$

where $\varepsilon_{\alpha\beta}$ is the dielectric tensor of the plasma in the absence of fluctuations and is determined by the system of linearized kinetic equation and Maxwell's equations (Chapter I, Section B). Thus, propagation of an incident wave $E_{o\beta}$ (assumed to be a first order quantity) in a plasma with fluctuations gives rise not only to a linear induced current density signifying

the propagation of the incident wave but also to a non-linear current density which is proportional to the product $\delta\varepsilon_{\alpha\beta} E_{o\beta}$ and reveals the possibility of formation of the scattered or transformed waves from the incident wave*. Since $\delta\varepsilon_{\alpha\beta} E_{o\beta}$ is a second order quantity**, it is expected that the non-linear current density can be sought from the Maxwell's equations for the second order wave field (i.e. scattered or transformed wave field) and the second order approximated kinetic equation which describes the perturbation of the state of the plasma under the action of the second order wave field and the action of the incident wave field (cf. Akhiezer, Daneliya and Tsintsadze, 1964; Daneliya and Tsintsadze, 1965).

Now the phase velocities of the weakly damped plasma waves generated by electron streams moving in the solar corona

---

* Scattering of electromagnetic waves with fluctuations of plasma temperature taken into account has been discussed by Sitenko and Gurin (1966). It was found that the fluctuations in temperature have a significant effect on long-wavelength scattering characterized by small frequency change (i.e. the case $k_D^2/k^2 \gg 1$), when the effective collision frequency is very large.

** We assume that there are only small random fluctuations existing in the plasma, the electromagnetic radiation resulting from multiple scattering is insignificant.

greatly exceed the mean thermal speed of the plasma electrons. Moreover, the collision frequency of the coronal plasma is negligibly small, being of the order of 10 Hz. In this case, we can make use of the hydrodynamic equation to find the current responsible for the transformation. In the absence of external current, the system of equations describing the behaviour of a homogeneous magnetoactive plasma under the action of the electromagnetic field will be

$$\text{curl } \bar{H} - \frac{1}{c}\frac{\partial \bar{E}}{\partial t} = \frac{4\pi}{c}\bar{j}\,(\bar{E}) ,$$

$$\text{curl } \bar{E} + \frac{1}{c}\frac{\partial \bar{H}}{\partial t} = 0, \quad \bar{j}(\bar{E}) = en\,\bar{v}(\bar{E}), \tag{5.19}$$

$$\text{div } \bar{E} = 4\pi en(\bar{E}), \qquad \text{div } \bar{H} = 0,$$

$$m_o n\left[\frac{\partial \bar{v}}{\partial t} + (\bar{v}.\nabla)\,\bar{v}\right] + \nabla p = en(\bar{E} + \frac{1}{c}\,\bar{v}\times\bar{H}),$$

$$\frac{\partial n}{\partial t} + \nabla.(n\bar{v}) = 0, \qquad p = 3\kappa nT, \tag{5.20}$$

where $\bar{v}$, n, T and p are the electron velocity, electron density, temperature and electron pressure of the plasma respectively. $\bar{E}$, $\bar{H}$ and $\bar{j}(\bar{E})$ are the electric field, magnetic field and the total current density in the plasma due to the presence of the wave. By writing

$$\bar{E} = \sum_{i=1} \epsilon^i \bar{E}^{(i)} \; ; \quad \bar{H} = \sum_{i=0} \epsilon^i \bar{H}^{(i)} \; , \quad p = \sum_{n=0} \epsilon^i p^{(i)} \; ,$$

$$\bar{v} = \sum_{i=1} \varepsilon^i \bar{v}^{(i)}, \quad n = \sum_{i=0} \varepsilon^i n^{(i)}, \quad \bar{j} = \sum_{i=1} \varepsilon^i \bar{j}^{(i)},$$

where ε is a small parameter, in (5.19) and (5.20), we obtain the equations of the i-th approximation as:

$$\begin{aligned}
&\operatorname{curl} \bar{H}^{(i)} = \frac{1}{c} \frac{\partial \bar{E}^{(i)}}{\partial t} + \frac{4\pi}{c} \bar{j}^{(i)}(\bar{E}^{(i)}), \\
&\operatorname{curl} \bar{E}^{(i)} = -\frac{1}{c} \frac{\partial \bar{H}^{(i)}}{\partial t}, \\
&\operatorname{div} \bar{H}^{(i)} = 0, \quad \operatorname{div} \bar{E}^{(i)} = 4\pi e n^{(i)}(\bar{E}^{(i)}), \\
&\bar{j}^{(i)}(\bar{E}^{(i)}) = e n_o \bar{v}^{(i)}(\bar{E}^{(i)}),
\end{aligned} \tag{5.19a}$$

$$\begin{aligned}
&n_o \left[\frac{\partial \bar{v}^{(i)}}{\partial t} + \sum_{j=1}^{i-1} (\bar{v}^{(j)} \cdot \nabla)\bar{v}^{(i-j)}\right] + \sum_{j=1}^{i-1} n^{(j)} \left[\frac{\partial \bar{v}^{(i-j)}}{\partial t}\right. \\
&\left. + \sum_{k=1}^{i-j-1} (\bar{v}^{(k)} \cdot \nabla)\bar{v}^{(i-j-k)}\right] + \frac{1}{m_o} \nabla p^{(i)} - \frac{e n_o}{m_o c}(\bar{E}^{(i)} + \frac{1}{c} \bar{v}^{(i)} \times \bar{H}_o) \\
&- \frac{e n_o}{m_o c} \sum_{j=1}^{i-1} \bar{v}^{(i-j)} \times \bar{H}^{(j)} - \frac{e}{m_o} \sum_{j=1}^{i-1} n^{(j)}(\bar{E}^{(i-j)} + \frac{1}{c} \bar{v}^{(i-j)} \times \bar{H}_o \\
&+ \frac{1}{c} \sum_{k=1}^{i-j-1} \bar{v}^{(i-j-k)} \times \bar{H}^{(k)}) = 0,
\end{aligned} \tag{5.20a}$$

$$\begin{aligned}
&p^{(i)} = 3\kappa n^{(i)} T, \\
&\frac{\partial n^{(i)}}{\partial t} + n_o \operatorname{div} \bar{v}^{(i)} = -\sum_{j=1}^{i-1} \nabla \cdot (n^{(j)} \bar{v}^{(i-j)}).
\end{aligned}$$

The last equation specifies the conservation of the i-th order electron density in the plasma. Now let the incident wave and the scattered (or transformed) wave be in the forms

$$\bar{E}_o(\bar{r},t) = \sum_{\bar{k}_o} \sum_{\omega_o} \bar{E}_o(\bar{k}_o,\omega_o) \exp(i\bar{k}_o.\bar{r}-i\omega_o t),$$

$$\bar{E}'(\bar{r},t) = \sum_{\bar{k}} \sum_{\omega} \bar{E}'(\bar{k},\omega) \exp(i\bar{k}.\bar{r}-i\omega t),$$

where $\bar{E}_o(\bar{k}_o,\omega_o)$ and $\bar{E}'(\bar{k},\omega)$ are the Fourier components of electric field vectors of the waves. $\bar{E}'(\bar{r},t)$ arises due to scattering the indicent wave $\bar{E}_o(\bar{r},t)$ by the fluctuations with frequency $\tilde{\omega}$ and vector $\bar{q}$ in the plasma. Solving (5.19a) and (5.20a) by the Fourier method and taking (5.18) into account, we obtain the equation of the second approximation for the scattered (or transformed) wave $\bar{E}'(\bar{k},\omega)$ as

$$\left.\begin{aligned} k^2\bar{E}' - \bar{k}(\bar{k},\bar{E}') - \frac{\omega^2}{c^2}\bar{E}' &= i\frac{4\pi}{c^2}\omega\bar{j}', \\ \bar{j}' &= en_o\bar{v}', \end{aligned}\right\} \qquad (5.21)$$

$$-i\omega\bar{v}' + \frac{3\kappa T}{m_o\omega}\nabla(\bar{k},\bar{v}') - \frac{e}{m_o}\left[\bar{E}' + \frac{1}{c}\bar{v}'\times\bar{H}_o\right] - \bar{P} = 0, \qquad (5.22)$$

where $\bar{P}(\bar{k},\omega) = -\left\{\frac{im_o}{e}(\delta\bar{v}.\bar{k}_o)\bar{v} + \frac{m_o\delta n}{en_o}\left[-i\omega_o\bar{v} - \frac{e}{m_o}(\bar{E}_o + \frac{1}{c}\bar{v}\times\bar{H}_o)\right]\right.$

$$\left. - \frac{1}{c}\bar{v}\times\delta\bar{H} + \frac{k_o p^{(1)}}{n_o e\omega}\left[i\delta n\left(\frac{-4\pi\omega_o q}{n_o k_o}\tilde{\kappa}\,\hat{\bar{K}}^o\,\bar{\kappa}^o + \frac{\omega_o}{n_o}\right) + i(\bar{k}_o.\delta\bar{v} + \frac{\tilde{\omega}}{n_o}\delta n)\right]\bar{\kappa}^o\right\}.$$

$\bar{v}(\bar{k}_o,\omega_o)$, $n(\bar{k}_o, \omega_o)$ are the electron velocity, induced electron density associated with the incident wave. $\bar{v}'(\bar{k},\omega)$ and $n'(\bar{k},\omega)$ are associated with the transformed wave. $\delta\bar{v}(\bar{q},\tilde{\omega})$, $\delta n(\bar{q},\tilde{\omega})$ and $\delta\bar{H}(\bar{q},\tilde{\omega})$ are the fluctuations of electron velocity, electron density and magnetic field in the plasma respectively. $\delta n(\bar{q},\tilde{\omega})$ and $\delta\bar{v}(\bar{q},\tilde{\omega})$ are related by the first order approximation of the equation of continuity.

The solution for $\bar{v}'(\bar{k},\omega)$ of (5.22) is, then,

$$\bar{v}'(\bar{k},\omega) = -\frac{i\omega}{n_o e}\,\underline{\hat{K}}\,\bar{E}' - \frac{i\omega}{n_o e}\,\underline{\hat{K}}\,\bar{P} \quad ,$$

where $K_{\alpha\beta}(\bar{k},\omega)$ is defined in (5.14) and $\tilde{\kappa} = \bar{q}/q$, $\bar{\kappa}^o = \bar{k}^o/k^o$. The high frequency dielectric tensor $\varepsilon_{\alpha\beta}(\bar{k},\omega)$ in the hydrodynamic approximation, taking account of the gas-kinetic pressure of the charged particles, is given by (Shafranov, 1967, p.37)

$$\begin{aligned}
\varepsilon_{xx} &= 1 - \chi(1 - 3k^2v_T^2\cos^2\theta/\omega^2), \\
\varepsilon_{yy} &= 1 - \chi(1 - 3k^2v_T^2/\omega^2) , \\
\varepsilon_{zz} &= 1 - \chi[\,1 - (\omega_H^2 + 3k^2v_T^2\sin^2\theta)/\omega^2] , \\
\varepsilon_{xy} &= -\varepsilon_{yx} = -i\chi\,\frac{\omega_H}{\omega}\,(1-3k^2v_T^2\cos^2\theta/\omega^2), \\
\varepsilon_{xz} &= \varepsilon_{zx} = \chi(3k^2v_T^2\sin\theta\,\cos\theta/\omega^2) , \\
\varepsilon_{yz} &= -\varepsilon_{zy} = i\chi(\omega_H k^2v_T^2\sin\theta\,\cos\theta/\omega^3) ,
\end{aligned} \tag{5.23}$$

where $$\chi = \frac{\omega_p^2}{\omega^2-\omega_H^2-3k^2v_T^2(1-\omega_H^2\cos^2\theta/\omega^2)} \quad .$$

Then the equation (5.21) becomes

$$k^2\bar{E}' - \bar{k}(\bar{k}.\bar{E}') - \frac{\omega^2}{c^2}\hat{\underline{\varepsilon}}\,\bar{E}' = i\,\frac{4\pi}{c^2}\,\omega\bar{j}^{(n)}(\bar{E}_o), \qquad (5.24)$$

$$\text{with } \bar{j}^{(n)}(\bar{E}_o) = i\omega\hat{\underline{K}}\left\{\frac{im_o}{e}(\delta\bar{v}.\bar{k}_o)\bar{v} + \frac{m_o\delta n}{en_o}\left[-i\omega_o\bar{v} - \frac{e}{m_o}(\bar{E}_o + \frac{1}{c}\bar{v}\times\bar{H}_o)\right]\right.$$

$$- \frac{1}{c}\bar{v}\times\delta\bar{H} + \frac{k_o p^{(1)}}{n_o e\omega}\left[i\delta n\left(\frac{-4\pi\omega_o q}{n_o k_o}\tilde{\kappa}.\hat{\underline{K}}^o\,\bar{\kappa}^o + \frac{\omega_o}{n_o}\right)\right.$$

$$\left.\left. + i(\bar{k}_o.\delta\bar{v} + \frac{\tilde{\omega}\delta n}{n_o})\right]\bar{\kappa}^o\right\}\ ,$$

$$p^{(1)} = 3\kappa T n(\bar{k}_o, \omega_o)\ . \qquad (5.25)$$

The non-linear current element $\bar{j}^{(n)}(\bar{E}_o)$ arises due to the propagation of the incident wave in a plasma with small random fluctuations and is responsible for scattering or transforming the incident wave.

Since we confine ourselves to ~~consider~~ the consideration of the transformation of plasma waves into electromagnetic waves by the thermal fluctuations of electron density, we assume that there exists a longitudinal electric field which induces fluctuations of electron density δn in the plasma. So that the term proportional to $\delta\bar{H}$ is neglected. Making use of the first approximation of (5.20a), we find $\bar{k}_o.\delta\bar{v} = \tilde{\omega}k_o\delta n(\bar{\kappa}^o.\underline{\tilde{K}}\tilde{\kappa})/n_o q\tilde{K}_{\parallel}$, where $\tilde{K}_{\parallel} = \tilde{\kappa}.\underline{\tilde{K}}\,\tilde{\kappa}$ is the longitudinal component of the polarizability tensor $\underline{\tilde{\chi}}(\bar{q},\tilde{\omega})$,

and we can then express the non-linear current density in terms of the product of the fluctuation of electron density and the incident wave electric field vector,

$$\bar{j}^{(n)}(\bar{E}_o) = \frac{i\omega^2\omega_o m_o}{e^2 n_o^2}\,\delta n\underline{\hat{K}}\left[\frac{\tilde{\omega}k_o}{\omega q}\left(\frac{\bar{\kappa}^o.\underline{\tilde{K}}\,\tilde{\kappa}}{\tilde{K}_{||}}\right)\underline{\hat{K}}^o + \frac{3n_3^{o2}\beta_T^2\omega_o}{4\pi\omega}(1-U)\right]\bar{E}_o\,, \quad (5.26)$$

where $U = \frac{\omega_o}{\omega}\left[1 + \frac{q}{k_o}(-4\pi\tilde{\kappa}.\underline{\hat{K}}^o\,\bar{\kappa}^o)\right] + \frac{\tilde{\omega}}{\omega}\left[1+\frac{k_o}{q}(\bar{\kappa}^o.\underline{\tilde{K}}\,\tilde{\kappa}/\tilde{K}_{||})\right]$.

$\underline{\hat{K}}(\bar{k},\omega)$, $\underline{\hat{K}}^o(k_o, \omega_o)$ are the polarizability tensors with frequencies ω, ω_o and wave vectors $\bar{k}$, $\bar{k}_o$ respectively. The refractive index n_3^o for the incident plasma wave in hydrodynamic approximation is given by

$$n_3^{o2} = [\omega_o^4-(\omega_p^2+\omega_H^2)\omega_o^2 + \omega_p^2\omega_H^2\cos^2\theta_o]/3\beta_T^2\omega_o^2(\omega_o^2-\omega_H^2\cos^2\theta_o). \quad (5.27)$$

We note that the term associated with $\delta\bar{v}.\bar{k}_o$ has the magnitude proportional to $\frac{\tilde{\omega}\delta n}{\omega n_o}\left(\frac{k_o}{q}\right)$ and can be omitted in (5.26) when $\tilde{\omega} \to 0$ and $\omega_o >> \tilde{\omega}$. In the following, we make use of (5.26) to consider the efficiency of transformation of plasma waves in a magnetoactive plasma by combination scattering and incoherent scattering processes respectively.

(i) Transformation of Plasma Waves by Combination Scattering

For high frequency weakly damped waves, we can omit terms proportional to $k^2v_T^2/\omega^2$ ($<< 1$) in $\underline{\hat{K}}$,$\underline{\tilde{K}}$ and $\underline{\hat{K}}^o$. The average power of the electromagnetic wave in the j-mode emitted from unit volume of plasma is (Shafranov, 1967, p.104)

$$P = -\int \; <\bar{j}^{(n)*}.\bar{E}_j' > \; _{\bar{k},\omega} \; d\bar{k}d\omega \; , \qquad (5.28)$$

where the angular bracket denotes the ensemble average and $<\bar{j}^{(n)}.\bar{E}_j' >_{\bar{k},\omega} \; \underline{\underline{def}} \; <\bar{j}^{(n)*}(\bar{k},\omega).\bar{E}_j'(\bar{k},\omega) >$. From (5.21), the Fourier component of the electric field of the transformed wave is determined by

$$\bar{E}_j'(\bar{k},\omega) = i4\pi \left[\bar{a}_j^*.\bar{j}^{(n)}\right] \; \bar{a}_j/\omega(k^2c^2/\omega^2-n_j^2) \qquad (5.29)$$

where n_j^2 is the square of the refractive index for extraordinary wave (j=1) and ordinary wave (j=2) in the cold collisionless magnetoactive plasma and $\bar{a}_j$ is the polarization vector of the j normal wave given by (Shafranov, 1967, p.56);

$$\begin{aligned} a_{jx}(\psi) &= K_j(i\alpha_x \cos\psi - \sin\psi \,), \\ a_{jy}(\psi) &= K_j(i\alpha_x \sin\psi + \cos\psi \,), \qquad (5.30) \\ a_{jz}(\psi) &= iK_j\alpha_z \quad , \end{aligned}$$

where $K_j = (1 + \alpha_{\theta j})^{-\frac{1}{2}}$,

$$\alpha_x = \alpha_{\theta j}\cos\theta + \alpha_{kj}\sin\theta \ , \quad \alpha_z = \alpha_{kj}\cos\theta - \alpha_{\theta j}\sin\theta \ ,$$

$$\alpha_{\theta j} = -\xi\cos\theta/[\xi^2 + A/(n_j^2-1)] \ ,$$

$$\alpha_{kj} = -(n_j^2-1)\xi\sin\theta/(A-\xi^2) \ .$$

Thus, the average energy of the transformed wave radiated into the solid angle $d\Omega$ per unit time from unit volume of plasma becomes

$$dP = -i4\pi \int_{-\infty}^{\infty}\int_{o}^{\infty} \frac{k^2 < |\bar{a}_j^* . \bar{j}^{(n)}|^2 >_{\bar{k},\omega}}{\omega(k^2c^2/\omega^2 - n_j^2)} \, dk d\omega \, d\Omega \ . \qquad (5.31)$$

Making use of the relation $-i(k^2c^2/\omega^2 - n_j^2)^{-1} \rightarrow \pi\delta(k^2c^2/\omega^2 - n_j^2)$, we carry out integration over k and obtain

$$dP_\omega = \frac{2\pi^2\omega_o^2 m^2 E_o^2}{n_o^4 e^4 c^3} \ <\delta n^2>_{\bar{q},\omega} \ \omega^6 n_j \ |\bar{a}_j^* . \bar{Q}|^2 \ d\omega d\Omega \ , \qquad (5.32)$$

where E_o is the amplitude of the electric field of the incident plasma wave, and

$$|\bar{a}_j^* . \bar{Q}|^2 = |\frac{\tilde{\omega}}{\omega}(\bar{\kappa}^o . \underline{\hat{K}}\tilde{K}/\tilde{K}_{||})\bar{a}_j^* . \underline{\hat{K}}^o \ \bar{\kappa}^o + \frac{3n_3^{o2}\beta_T^2\omega_o}{4\pi\omega}(1-U)\bar{a}_j^* . \underline{\hat{K}} \ \bar{\kappa}^o|^2 \ .$$

The differential scattering cross-section is defined as ratio of the average transformed wave intensity to the incident wave

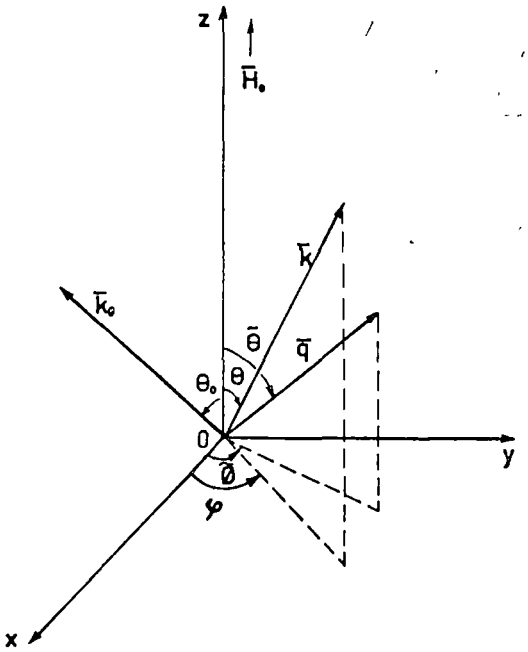

Fig.5.4 Coordinate system for transformation of waves in a magnetoactive plasma.

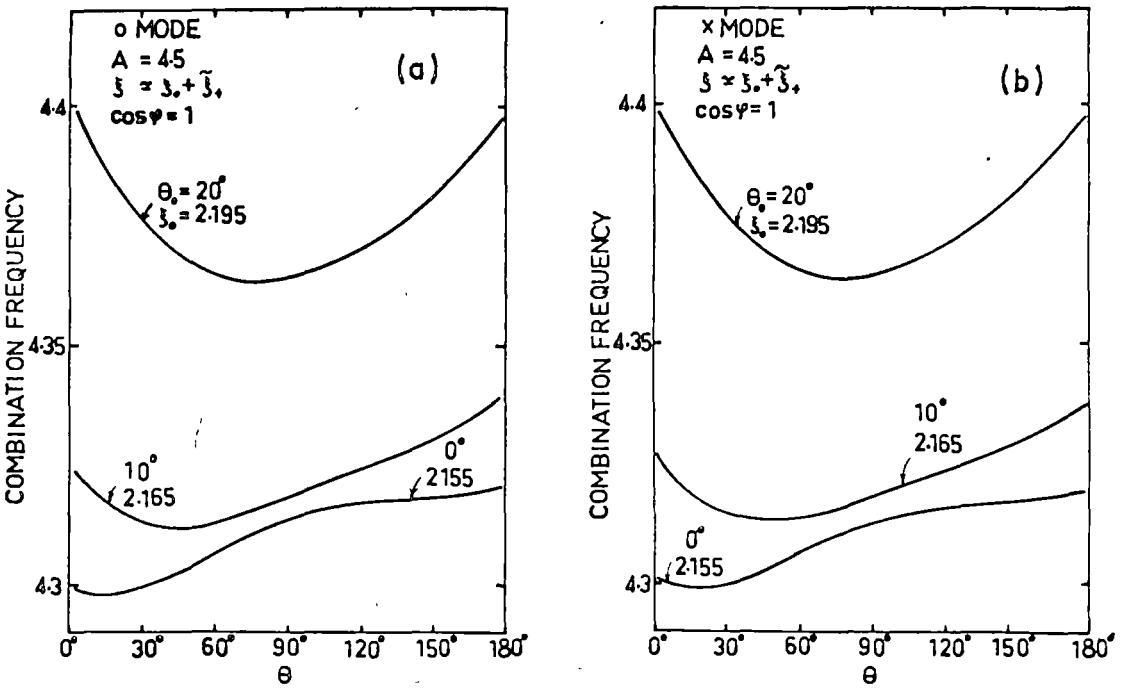

Fig. 5.5 Dependence of normalized combination frequency $\xi \simeq \xi_0 + \tilde{\xi}$ on the emission wave-normal angle θ for $\beta_T = 10^{-2}$, A = 4.5, cosφ = 1 and for (a) the o-mode; (b) the x-mode. The numbers on each curve represent the wave-normal angle θ_0 and the normalized frequency ξ_0 of the incident plasma wave.

energy flux density in the incident wave vector direction. For the incident longitudinal plasma wave, the energy flux density is given by

$$S_o = -\frac{\omega E_o^2}{16\pi}\frac{\partial}{\partial k_o}\,\mathrm{Re}\;\varepsilon_{\shortparallel}(\bar{k}_o,\omega_o) = \frac{3n_3^o\beta_T^2\omega_o^2 cE_o^2}{8\pi\omega_p^2}\quad . \tag{5.33}$$

That is, from (5.32), (5.33) and (5.15), the differential scattering cross-section, $\sigma_{j\omega}$, for combination scattering will be

$$\frac{dP_\omega}{d\Omega}/S_o = \sigma_{j\omega}(\theta)d\omega$$

$$= \frac{16\pi^2 n_j\tilde{n}_3^2\omega^6\tilde{\omega}^2|\bar{a}_j^*\cdot\bar{Q}|^2\;[\delta(\tilde{\omega}-\omega_s)+\delta(\tilde{\omega}+\omega_s)]\;d\omega}{3n_3^o n_o c^4\omega_p^4\;|\tilde{\omega}^2\frac{\partial}{\partial\tilde{\omega}^2}\,\mathrm{Re}\;\varepsilon_{\shortparallel}(\bar{q},\tilde{\omega})|_{\tilde{\omega}=\pm\omega_s}}\;(\mathrm{cm}^2\;\mathrm{cm}^{-3}\;\mathrm{sr}^{-1}), \tag{5.34}$$

where $\omega=\omega_o+\tilde{\omega}$ and ω_s is the plasma wave frequency. Now, we define the transformation coefficient as

$$\eta_j(\omega,\theta) = \sigma_{j\omega}(\theta)\,\frac{V}{L^2}\quad(\mathrm{sr}^{-1}), \tag{5.35}$$

where V is the volume of the plasma in which the scattering takes place and L is its linear size. We note that $\eta_j(\omega,\theta)$ is a dimensionless quantity which specifies the efficiency of the transformation.

(ii) Transformation of Plasma Waves by Incoherent Scattering

Conversion of plasma waves into electromagnetic waves with small frequency change in an isothermal plasma is the result of scattering of the incident plasma waves by fluctuations of electron density with frequencies about the origin $\tilde{\omega} = 0$ where $< \delta n^2 >_{\bar{q}, \tilde{\omega}}$ exhibits a broad maximum. Then, as $\omega \simeq \omega_o >> \tilde{\omega}$, we have

$$\bar{j}^{(n)}(\bar{E}_o) = i \frac{3\omega m_o \omega_o^2 n_3^{o2} \beta_T^2}{4\pi e^2 n_o^2} E_o \delta n (1 - U) \hat{\underline{K}} \bar{\kappa}^o \quad , \qquad (5.36)$$

where $U = \frac{\omega_o}{\omega} [1 + \frac{q}{k_o} (-4\pi\tilde{\kappa}.\hat{\underline{K}}^o \bar{\kappa}^o)]$. The average electromagnetic energy radiated per unit time per unit solid angle from unit volume of plasma is obtained by inserting (5.36) into (5.31) and carrying out integration over k,

$$\frac{dP}{d\Omega} = \frac{9\omega_o^4 m_o^2 n_3^{o4} \beta_T^4 E_o^2}{8 n_o^4 e^4 c^3} \int_{-\infty}^{\infty} n_j \omega^4 < \delta n^2 >_{\bar{q}, \omega} |\bar{a}_j^*.\bar{Q}|^2 \, d\omega \quad , \qquad (5.37)$$

where $|\bar{a}_j^*.\bar{Q}|^2 = |\bar{a}_j^*.\hat{\underline{K}}\bar{\kappa}^o|^2 \, |1-U|^2$. In order to find the integral scattering cross-section, we replace the frequency ω in (5.37) by $\omega = \omega_o + \tilde{\omega}$ and write the electron density fluctuation spectrum (5.12) in the form

$$< \delta n^2 >_{\bar{q},\tilde{\omega}} = \frac{q^2 \kappa T}{e^2 (2\pi)^5} \, \mathrm{Im} \, \frac{(\epsilon_{\parallel}^{e} - 1)\epsilon_{\parallel}^{i}}{\tilde{\omega}\, \epsilon_{\parallel}}$$

Then, after carrying out complex integration over $\tilde{\omega}$ (Shafranov, 1967, p.134), we obtain the integral scattering cross-section and the corresponding transformation coefficient as

$$\sigma_j = \frac{dP}{d\Omega}/S_o = \frac{6 n_3^{o4} \beta_T^2 \omega_o^6 n_j (1+k_D^2/q^2)}{n_o n_3^o c^4 \omega_p^2 (1+2k_D^2/q^2)} \, |\bar{a}_j^* . \bar{Q}|^2 \quad (\mathrm{cm}^2 \ \mathrm{cm}^{-3} \ \mathrm{sr}^{-1}) \quad (5.38)$$

and $$\eta_j(\theta) = \sigma_j \frac{V}{L^2} \qquad (\mathrm{sr}^{-1}). \qquad (5.39)$$

(d) Transformation of Plasma Waves in The Active Solar Corona

As the amplified plasma wave generated by an electron stream propagates away from the source region in the outward direction, its phase velocity decreases rapidly (see Fig.5.1) and collective wave motion becomes completely disorganized. However, because of non-linear effects, the plasma wave will transfer part of its energy to the electromagnetic radiation which may eventually be observed on the Earth.

In most cases, in the high frequency region, the frequencies of the transformed waves in the o-mode and the x-mode are of the same

order of that of the plasma wave while the refractive index for the plasma wave greatly exceeds those for the o-mode and x-mode waves. Thus, the three vectors $\bar{k}$, $\bar{k}_o$ and $\bar{q}$ can satisfy the equality (5.18) only if the directions of $\bar{k}$ and $\bar{q}$ represent nearly "head-on" collisions (Tidman, Birmingham and Stainer, 1966). According to Fig. 5.4, this implies that $\tilde{\phi} = 180^o$ and $\tilde{\theta} \geq \pi/2$ while $\theta_o \leq \pi/2$, where $\tilde{\theta}$ and $\tilde{\phi}$ are the wave-normal angle and azimuthal angle of the fluctuation vector $\bar{q}$. For simplicity, we assume that both $\bar{k}_o$ and $\bar{q}$ lie on the x-z plane* (so that $\tilde{\phi}$ can be 180^o or 0^o) and let $q \simeq k_o$ in $|\bar{a}_j^* . \bar{Q}|^2$, then, for coherent scattering,

$$|\bar{a}_j^* . \bar{Q}|^2 = A^2 K_j^2 S^2 / (4\pi)^4 (\xi^2 - 1)^2 \xi^2, \qquad (5.40)$$

---

* Strictly speaking, for θ_o different from 0^o (or 180^o) appreciably, we should consider the cases for arbitrary azimuthal angle $\tilde{\phi}$. However, for $\tilde{\phi} \neq 0^o$, 180^o, the mathematics involved in the theory of transformation of plasma waves into electromagnetic waves by thermal fluctuations in a magnetoactive plasma is extremely complicated. Since the Cerenkov plasma waves excited by an electron stream maximize at $\theta_o \simeq 0^o$ and the scattering of plasma waves with $\theta_o \simeq 0^o$ is independent of the choice of $\tilde{\phi}$ (or ψ), the results obtained under the present assumption will give the main characteristics of the electromagnetic radiation arising from the transformation of Cerenkov plasma waves excited by an electron stream.

$$S = A^2X_o\tilde{F}/(\xi^2-1)(\xi_o^2-1) - 3n_3^{o2}\beta_T^2\xi_o(1-U)M_o,$$

$$M_o = \varepsilon_2\sin\theta_o(1/\xi - \alpha_x) - \alpha_z\cos\theta_o(1-1/\xi^2),$$

$$X_o = \varepsilon_2\sin\theta_o\left[\frac{1}{\xi_o} + \frac{1}{\xi} - \alpha_x\left(1 - \frac{1}{\xi\xi_o}\right)\right] - \alpha_z\cos\theta_o\left(1- \frac{1}{\xi_o^2}\right)\left(1- \frac{1}{\xi^2}\right),$$

$$U = (\xi_o+\tilde{\xi})/\xi + A[F_o/(\xi_o^2-1) + \tilde{F}/(\tilde{\xi}^2-1)]/\xi ,$$

$$F_o = \xi_o[\varepsilon_1\sin\theta_o\sin\tilde{\theta} + (1-1/\xi_o^2)\cos\theta_o\cos\tilde{\theta}],$$

$$\tilde{F} = \tilde{\xi}[\varepsilon_1\sin\theta_o\sin\tilde{\theta} + (1 - 1/\tilde{\xi}^2)\cos\theta_o\cos\tilde{\theta}] ,$$

$$\xi = \omega/\omega_H,\ \tilde{\xi} = \tilde{\omega}/\omega_H,\ \xi_o = \omega_o/\omega_H .$$

$\varepsilon_1 = \pm 1$ and $\varepsilon_2 = \cos\psi$, where ψ is the azimuthal angle of the wave vector $\bar{k}$ and under the present assumption, ψ is either 0^o or 180^o. Since $\bar{k}_o$ lies on the x-z plane (with positive x-axis), the sign of ε_1 is then determined by the sign of the quantity $I = \varepsilon_2 k\sin\theta - k_o\sin\theta_o$. Substituting (5.40) in (5.34) and (5.35), we have the coefficient of transformation of the plasma wave by combination scattering

$$\eta_j(\theta) = \frac{K_j^2 n_j \tilde{n}_3^2 \xi^4 \tilde{\xi}^2 \omega_H^4 S^2 V[\delta(\tilde{\omega}-\omega_s)+\delta(\tilde{\omega}+\omega_s)]}{3(4\pi)^2 n_3^o n_o AK(\xi^2-1)^2 c^4 L^2} \quad (sr^{-1}), \qquad (5.41)$$

where K is defined in (2.27). The frequency ω_s and $\tilde{\theta}$ satisfy the longitudinal plasma wave dispersion equation $Re\varepsilon_{11}(\tilde{\theta},\omega_s) = 0$.

For given wave vectors $\tilde{q},\bar{k}_o$ and wave frequencies $\tilde{\omega}$ and ω_o, the wave-normal angle θ and the wave frequency ω of the transformed wave can be determined by solving the equations (5.18) and the dispersion equation for the transformed wave simultaneously,

$$\omega = \omega_o + \tilde{\omega},$$

$$k^2 = \frac{\omega^2 n^2}{c^2} = k_o^2 + q^2 + 2k_o q(\cos\theta_o\cos\tilde{\theta}+\varepsilon_1\sin^2\theta_o\sin\tilde{\theta}), \quad (5.42)$$

and $$A_o n^4 + B_o n^2 + C_o = 0. \quad (5.43)$$

When the terms proportional to kv_T/ω in (5.23) are discarded, we have

$$A_o = \varepsilon_{xx}\sin^2\theta + \varepsilon_{zz}\cos^2\theta ,$$

$$B_o = -[(\varepsilon_{xx}^2 - \varepsilon_{xy}^2)\sin^2\theta + \varepsilon_{xx}\varepsilon_{yy}(1+\cos^2\theta)], \quad (5.44)$$

$$C_o = \varepsilon_{zz}(\varepsilon_{xx}^2 - \varepsilon_{xy}^2).$$

The solution for $\cos\theta$ is then given by

$$\cos\theta = \pm\left[\frac{(\varepsilon_{xx}^2-\varepsilon_{xy}^2+\varepsilon_{xx}\varepsilon_{zz})G-\varepsilon_{zz}(\varepsilon_{xx}^2-\varepsilon_{xy}^2)-G^2\varepsilon_{xx}}{(\varepsilon_{zz}-\varepsilon_{xx})G^2+G(\varepsilon_{xx}^2-\varepsilon_{xy}^2-\varepsilon_{xx}\varepsilon_{zz})}\right]^{\frac{1}{2}} \quad (5.45)$$

with $$G = \frac{1}{\omega^2}[\omega_c^2 n_3^o \mp \tilde{\omega}^2 n_3^2 + 2n_3 n_3^o \omega_o\tilde{\omega}(\cos\theta_o\cos\tilde{\theta}+\varepsilon_1\sin\theta_o\sin\tilde{\theta})].$$

From (5.45), we see that transformation is possible if $|\cos\theta| \leq 1$. Since the two unkowns ω and θ have to satisfy three equations, (5.42) and (5.43) may not yield the required solutions for θ and ω. Furthermore, even (5.42) and (5.43) do give real solutions for ω and θ, we still require that $1 \geq n_j(\omega,\theta) > 0$. Therefore, the incident plasma wave cannot be transformed into electromagnetic wave with arbitrary wave-normal angle and arbitrary wave frequency by combination scattering. The sign of $\cos\theta$ must follow the sign of the quantity $k_o\cos\theta_o + q\cos\tilde{\theta}$. In practice, we assign the wave frequency ω and the wave-normal angle θ of the transformed wave and look for the approximate solutions for the wave frequency $\tilde{\omega}$ and the wave vector $\bar{q}$ satisfying the equations (5.18) as well as $\mathrm{Re}\,\varepsilon_{\parallel}(\bar{q},\tilde{\omega}) = 0$.

As an example, the approximate solutions for θ and ω (normalized by gyrofrequency) of the transformed wave in the o-mode and the x-mode for $A = 4.5$ and $\cos\psi = 1$ are shown in Fig. 5.5. The incident plasma wave is the Cerenkov plasma wave generated by a helical electron stream with $\beta_{\parallel} = 0.1$. Therefore, the wave-normal angle θ_o and the corresponding wave frequency ξ_o are related by the Cerenkov condition $n_3^o\beta_{\parallel}\cos\theta_o = 1$. It is easily seen that the transformed waves in the x-mode and in the o-mode are emitted at a similar frequency in the same direction.

The solutions for ξ and θ in Fig. 5.5 are used to compute the efficiency of transformation. If the linear size of the scattering volume is $L \simeq 10^9$ cm, which is a typical value for the solar corona, $f_H = 56$ MHz and the corresponding electron density $n_o = 1.24\times10^4 f_H^2 A \simeq 1.75\times10^8$ cm^{-3}, the coefficient of transformation by combination scattering is illustrated in Fig. 5.6 as a function of wave-normal angle θ. From this figure, we find that the transformed wave in the o-mode is strongly emitted in the direction transverse to the static magnetic field line while the transformed radiation in the x-mode emitted in the direction $\theta \simeq 120^o$, 60^o is of greater intensity (for $\theta_o \leq 10^o$). For $\theta_o \leq 10^o$, the maximum efficiency of transformation of the Cerenkov plasma wave into the o-mode wave is about a few times higher than that into the x-mode wave.

In the case of transformation of longitudinal plasma waves into electromagnetic waves by incoherent scattering, we assume $q \simeq k_o$ in $|\bar{a}_j^* \cdot \bar{Q}|^2$ again. Then, from (5.39), the transformation coefficient reads

$$\eta_j(\theta) = \frac{3K_j^2 n_j n_3 c^3 \beta_T^2 \xi_o^6 A \omega_H^4 (1+k_D^2/q^2) L M_o^2 Y^2}{8\pi^2 n_o c^4 (\xi_o^2-1)^2 (1+2k_D^2/q^2)} \quad (sr^{-1}), \qquad (5.46)$$

where $Y = \frac{A}{(\xi_o^2-1)} [\, \varepsilon_1 \sin\theta_o \sin\tilde{\theta} + (1-1/\xi_o^2)\cos\theta_o \cos\tilde{\theta}]$

and M_o is defined in (5.40).

The transformed wave frequency can be approximated by $\omega = \omega_o + \tilde{\omega} \simeq \omega_o$ (for $\omega_o >> \tilde{\omega}$). For given $\bar{k}$ and $\bar{k}_o$, the magnitude of the vector $\bar{q}$ and the angle $\tilde{\theta}$ of the fluctuation can be determined by (5.18),

$$q^2 = k^2 + k_o^2 - 2kk_o \cos(\hat{\bar{k}\bar{\kappa}}_o),$$

$$\cos\tilde{\theta} = (k\cos\theta - k_o\cos\theta_o)/q,$$

where $\hat{\bar{k}\bar{k}}_o$ is the angle between $\bar{k}$ and $\bar{k}_o$.

In the absence of static magnetic field, the plasma becomes isotropic, and the refractive indices n_3^o (plasma wave) and n (transverse wave) are related by

$$3\, n_3^{o2}\beta_T^2 = 1 - \omega_p^2/\omega_o^2 \simeq n^2(\omega) .$$

If the electromagnetic wave is of the form $\exp(i\bar{k}.\bar{r}-i\omega t)$ and $\bar{k} = (k\sin\theta, 0, k\cos\theta)$, where θ is the angle between the z-axis and wave vector $\bar{k}$, the polarization vector $\bar{a}$ is represented by

$$\bar{a} = \frac{1}{\sqrt{2}}\{\mp i\cos\theta,\ 1,\ \pm i\sin\theta\}.$$

For $k_o >> k$, $q >> k$, then $k_o \simeq q$ and the terms Y and M_o in (5.46) are approximated by

$$Y = \frac{\omega_p^2}{\omega^2} \ , \quad M_o \simeq \pm(\sin\theta_o\cos\theta - \cos\theta_o\sin\theta) = \pm\sin\phi \ ,$$

where ϕ is the angle between $\bar{k}$ and $\bar{k}_o$. Then (5.46) can be written as

$$\eta(\theta) \simeq \frac{n^4\omega_p^4(1+k_D^2/q^2)L\sin^2\phi}{6\pi^2\sqrt{3}\beta_T(1+2k_D^2/q^2)n_o c} \quad (sr^{-1}). \tag{5.47}$$

Taking $\theta_o = 0^o$, and carrying out the integration over the whole space, we have

$$\eta = 2\int \eta(\theta)d\Omega = \frac{2\times 2\times 4\pi e^2 n_o n^4(1+k_D^2/q^2)L}{3\sqrt{3}\, m_o^2 n_o v_T(1+2k_D^2/q^2)} .$$

The factor 2 arises from the fact that in an isotropic plasma, the plasma wave can be transformed into two oppositely circularly polarized waves equally. Since $q < k_D$, the transformation coefficient can be further simplified as

$$\eta = \frac{2n^4}{\sqrt{3}}\left(\frac{4\pi e^4 n_o L}{3m_o^2 v_T c^3}\right) , \tag{5.48}$$

which differs from that obtained by Ginzburg and Zheleznyakov (1958) by a factor $2n^4/\sqrt{3}$. If $n \simeq 1$, then $\eta \simeq \frac{4}{3}(4\pi e^4 n_o L/3m_o^2 v_T c^3)$. This small discrepancy is due to different methods of solving the problem.

In Fig. 5.6(c), the coefficient of transformation of the plasma wave into an o-mode wave (5.46) with the same set of parameters corresponding to Fig. 5.5 is illustrated. We note that transformation of the plasma wave at the frequency $\omega_o \simeq \omega_p$ into an x-mode wave is impossible since the transformed wave frequency given by equality (5.18), $\omega \simeq \omega_o \simeq \omega_p$, is less

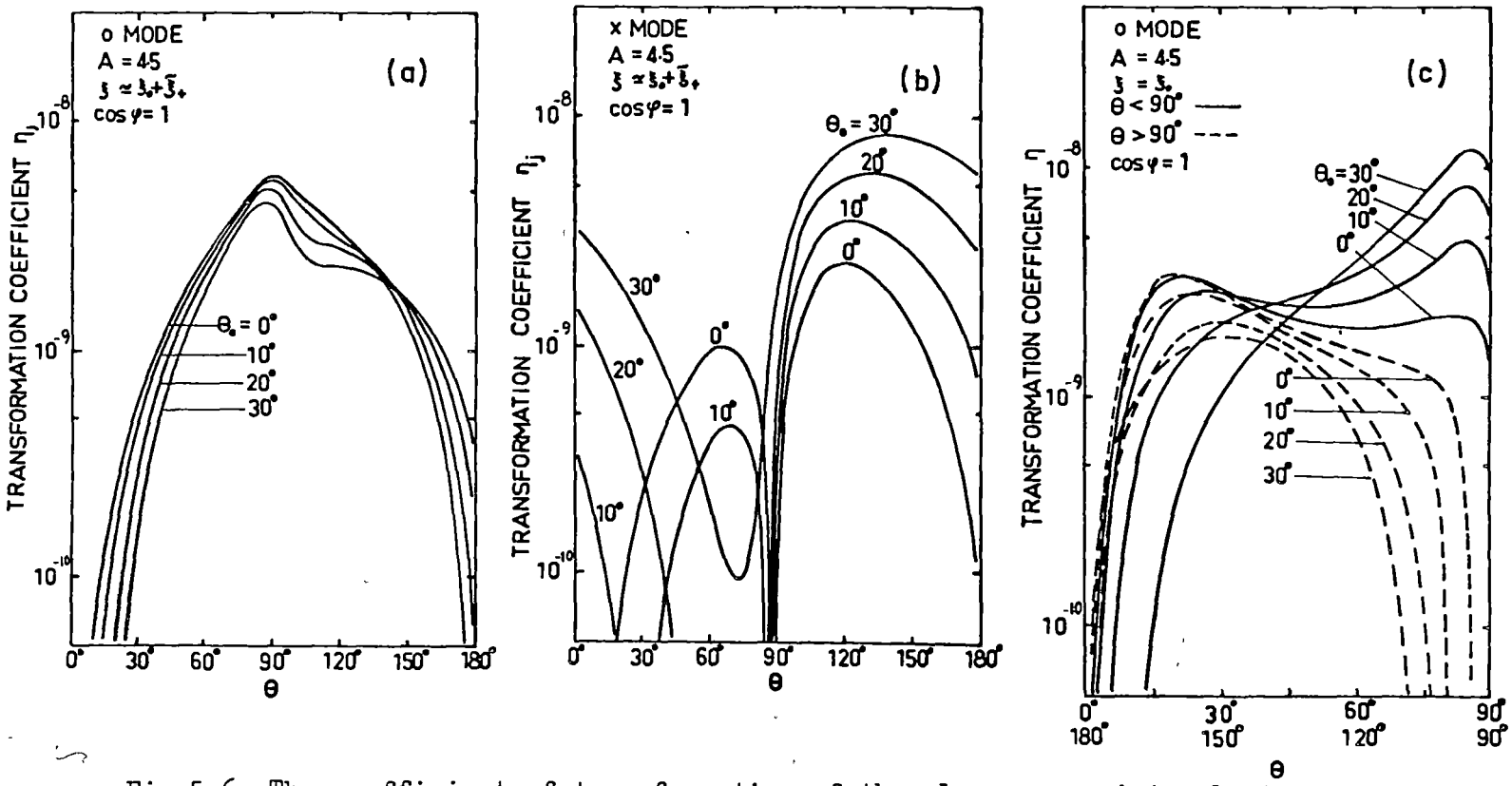

Fig.5.6 The coefficient of transformation of the plasma wave into electromagnetic wave in the

(a) o-mode by combination scattering

(b) x-mode by combination scattering

(c) o-mode by incoherent scattering

is illustrated as a function of wave-normal angle of the transformed wave θ for A = 4.5, $\beta_T = 10^{-2}$, L = 10^9 cm, $n_o = 1.75 \times 10^8$ cm^{-3} and cosφ = 1.

than the minimum frequency of the x-mode wave, $\omega_x = 2\pi f_x$. From Fig. 5.6 (a,b) and (c), it is found that the efficiency of transformation of the Cerenkov plasma wave (with $\theta_o = 0^o$ and $\omega_o \simeq \omega_p$), excited by the electron stream moving with $\beta_{||} \simeq 0.1$, into the o-mode wave by incoherent scattering is similar to that by combination scattering.

(e) Discussion

We have used the hydrodynamic equations to formulate the coefficients of transformation of incident plasma waves into electromagnetic waves by scattering on the coherent and incoherent thermal fluctuations. The electron density fluctuation spectrum (5.15) and the system of hydrodynamic equations are valid only when the weakly damped conditions (2.1), (2.2) are met. From the expressions (5.41) and (5.46), it can be seen that when absorption of the plasma wave is weak, the efficiency of transformation of the plasma wave into electromagnetic waves by electron density fluctuations is also low.

However, under the weakly damped conditions, Cerenkov plasma waves can easily be excited by a stream of electrons with energy of a few tens of keV. The intensity of the coherent Cerenkov plasma wave emitted in the direction along the magnetic field is stronger than the electromagnetic radiation in other modes emitted by the same electron stream (Chapter II and Chapter VIII). Thus, converting small

fraction of the strong Cerenkov plasma waves will result in the emission of electromagnetic radiation in the x-mode and the o-mode of appreciably intensity. The possibility of observing such converted electromagnetic radiation depends not only on the intensity of the coherent Cerenkov plasma wave but also on the possibilities of escaping the two normal waves from the solar corona. Moreover, the spectral characteristics of such radio emission from the solar corona will be determined by the properties of the radiating electron stream and the coronal plasma together with the source position. In the next chapter, we shall consider these problems in detail.

CHAPTER VI

THEORY OF POLARIZED SOLAR TYPE III BURST AND U BURST EMISSIONS

A. Introduction

The type III solar radio bursts are characterized by a short duration about 1 to 10 sec and a rapid frequency drift with time from high to low frequencies. They regularly occur in groups, typically about ten bursts per group in time by about 10 sec. The highest frequency of most type III bursts or U bursts observed does not exceed 600 MHz, but it seems that there is no lower limit for these bursts and they have been observed at 1 MHz and 30 kHz by the Venus 2 space probe (Slysh, 1967). A statistical study on the starting frequency of type III bursts (Malville, 1961) gives the maxima at 100 MHz and 200 MHz, the second being probably due to the harmonic (Fig. 6.2(a)). When both the fundamental and second harmonic are observed, the harmonic is emitted nearer the centre of the Sun (Smerd et al., 1962).

The type III bursts were first thought to be unpolarized. However, Komesaroff (1958) reported that some of the type III bursts observed (about 50%) were strongly circularly polarized. Akabane and Cohen (1961) observed that type III bursts were weakly linearly , or highly elliptically polarized. The type III bursts observed by Bhonsle and McNarry (1964) also exhibit

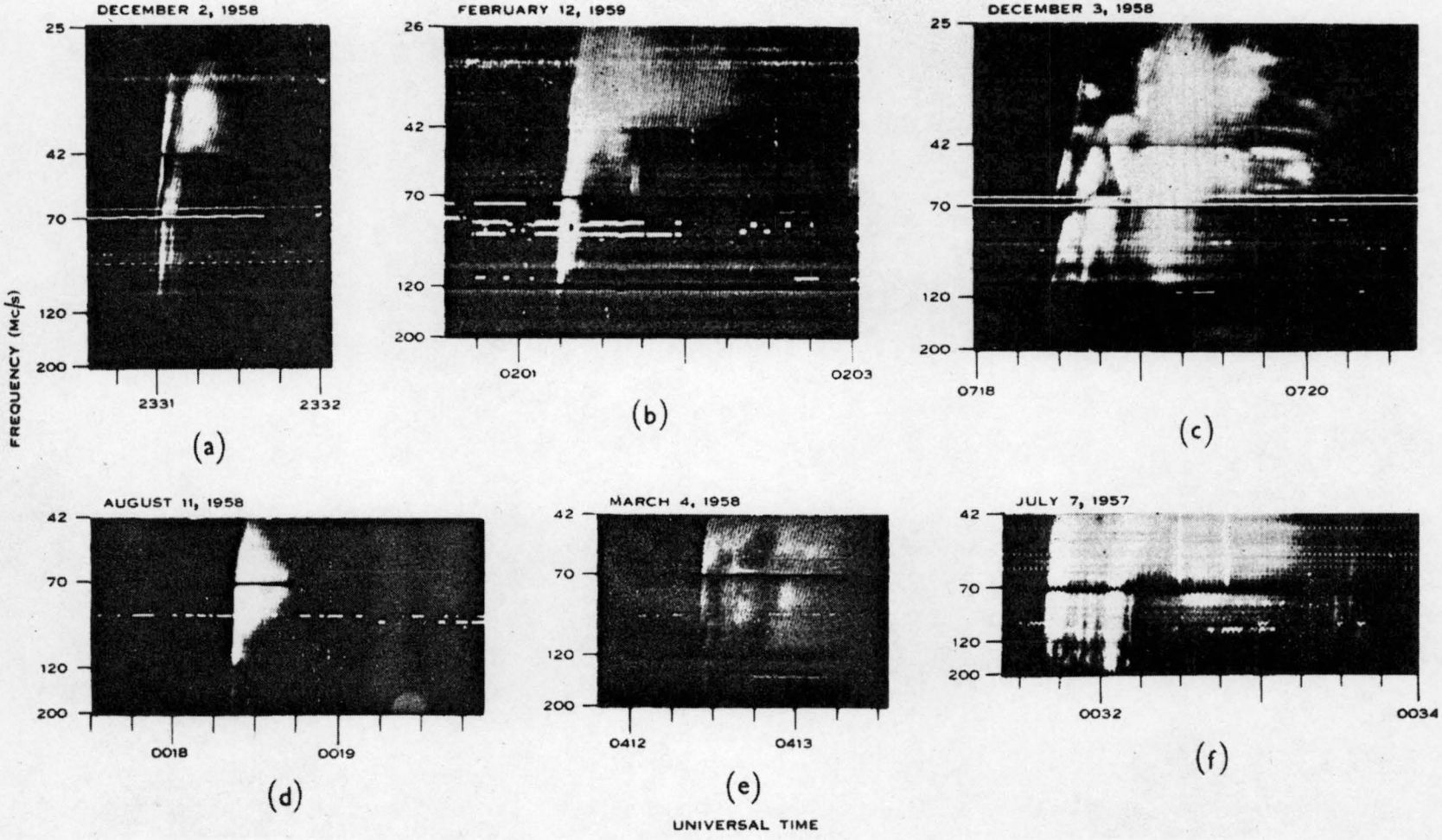

Fig. 6.1 Examples of type III bursts followed by pronounced type V emission (after Wild, Sheridan, and Neylan 1959).

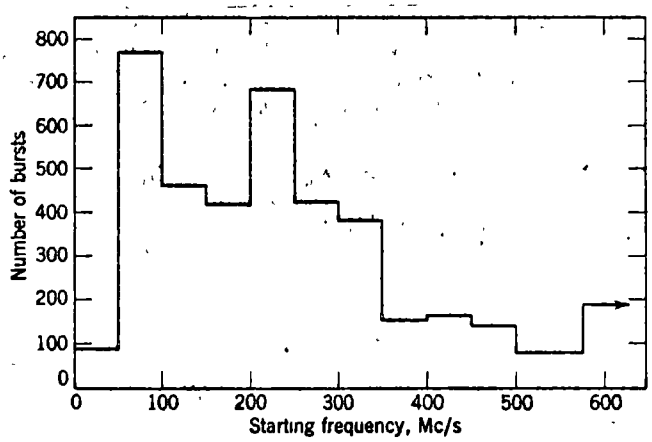

Fig. 6·2(a) Distribution of starting frequencies of type III bursts in the 25 to 580 Mc/sec range (after Malville 1961).

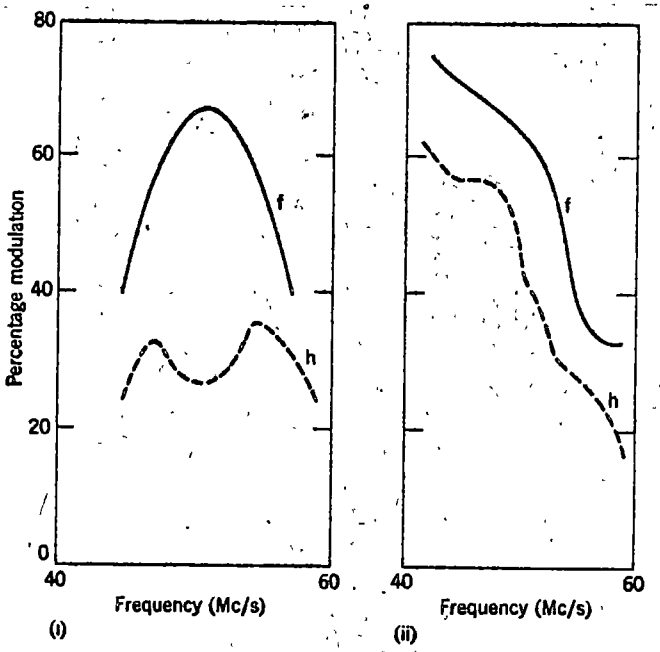

Fig. 6·2 (b) Degree of modulation as a function of frequency for the two polarized harmonic type III bursts (after Komesaroff 1958).

similar polarization characteristics. In general, for bursts showing harmonic structure, the fundamental appears to be more strongly polarized than the second harmonic with the left-handed sense of polarization more frequent than the right-handed sense of polarization (Komesaroff, 1958) (Fig. 6.2(b)). If it is assumed the sense of polarization depends on the polarity of the magnetic field associated with the source of radiation, the bursts showing left-handed sense of polarization should be associated with the north-polarity of the magnetic field of the leading sunspot. Such polarization is identified as the ordinary mode in the magneto-ionic theory. Most of the bursts have mean values of the degree of polarization about 5% to 40% (Gopala Rao, 1965).

Maxwell and Swarup (1958) first observed that inverted-U bursts also appear in the type III burst spectrum (Fig. 6.1 (c)). The U bursts are characterized by a rapid decrease in frequency followed by an increase with a duration of a few seconds (~ 8 sec.). In general, U bursts are rich in harmonics (Haddock, 1958).

The type III bursts are the most common of the metre-wavelength bursts and normally occur during the active period of the flare explosion. Studies of the characteristics of the type III burst emission event have been carried out both experimentally and theoretically by many authors since the first discovery of the type III bursts. Here we have outlined

only a few distinct characteristics of the type III bursts. A detailed description of the type III burst and its related U burst emission event is given in the reviews by Wild, Smerd and Weiss (1963) and by Maxwell (1963) and in the monograph by Kundu (1965).

Wild (1950) first suggested that the type III burst emission is the result of excitation of plasma oscillations by disturbances moving outward through the corona at velocities of about 0.2c to 0.8c. Ginzburg and Zheleznyakov (1958) interpretated the type III burst as the consequence of radio emission arising from transformation of Cerenkov plasma waves excited by electron streams moving in the isotropic solar corona. Smerd, Wild and Sheridan (1962) further developed Ginzburg and Zheleznyakov's theory and many characteristics of the type III bursts have been accounted for quantitatively.

All the interpretations of the type III burst emission given in the above mentioned references are based on the isotropic solar corona model and the appearance of the strong circular polarization of the type III bursts and U bursts has not been fully explained. Because of the presence of the sunspot magnetic field, it is more realistic to assume a magnetoactive coronal streamer model for the interpretation of the radio emissions originating from the lower layer of the active solar corona. Indeed, it is difficult to explain the polarization characteristics of the type III bursts if the

sunspot magnetic field is disregarded. Komesaroff (1958) suggested that the polarization of the type III bursts arises in the emission process. Fomichev and Chertok (1968) argued that the polarization of the harmonic type III bursts is caused only by the conditions for escape and propagation of radio emissions from the magnetoactive solar coronal active region.

We believe, however, that the effect of the sunspot magnetic field should be taken into account in the generation as well as the propagation of electromagnetic waves in the solar active coronal region. In the present chapter, the results of the theoretical investigations into the generation and transformation of the Cerenkov plasma waves in a magnetoactive plasma in Chapter II and Chapter V are used to examine the radio emissions expected from the solar corona with particular reference to the polarized type III bursts and the U bursts.

B. Radiation of Plasma Waves by An Electron Stream Moving in The Coronal Streamer

It is generally accepted that electron streams ejected from the flare region during the flare phase of the explosion of a solar flare are responsible for the emission of type III bursts and U bursts. We assume that such an electron stream can travel along the sunspot magnetic field line either following a rectilinear trajectory or a helical line with normalized translational speed $\beta_{\parallel} \simeq 0.1$ to 0.6.

The position measurement of the type III burst emission source height leads to the conclusion that the disturbances travel outwards along a coronal streamer where the electron density is about five to ten times higher than the background corona (cf. Section A of Chapter IV). Therefore, we assume the coronal streamer models given by Fig. 4.5(b) as the regions where the type III bursts and U bursts are emitted. For these coronal streamer models, while the plasma frequency f_p ranges from 100 to 50 MHz, the corresponding value of A along the strongest sunspot field line increases from unity to fifteen.

In a magnetoactive plasma, when the gyrofrequency is comparable to the plasma frequency, the weakly damped plasma wave can propagate in two different frequency ranges:

$$(1)\quad f \simeq f_- < f_H \text{ and } (2)\quad f \simeq f_+ > f_H \qquad (6.1)$$

where $f_\pm$ are the plasma resonance frequencies given by (2.5). It is easy to see that when $\theta \simeq 0$, $f_- \simeq f_p$ for $A < 1$ and $f_+ \simeq f_p$ for $A > 1$. For a given wave-normal angle, the phase velocity of the weakly damped plasma wave in the frequency range (1) of (6.1) decreases with the increase of the value of A. This is demonstrated in Fig. 6.3 where $\beta_T = 10^{-2}$, $\theta = 5^\circ$ and A = 0.2, 0.6, 2,4.5,6. Therefore, when A tends to be large, the weakly damped plasma wave occurs only in the frequency range (2) of (6.1) and $f_+ \to f_p$ for all wave-normal angles.

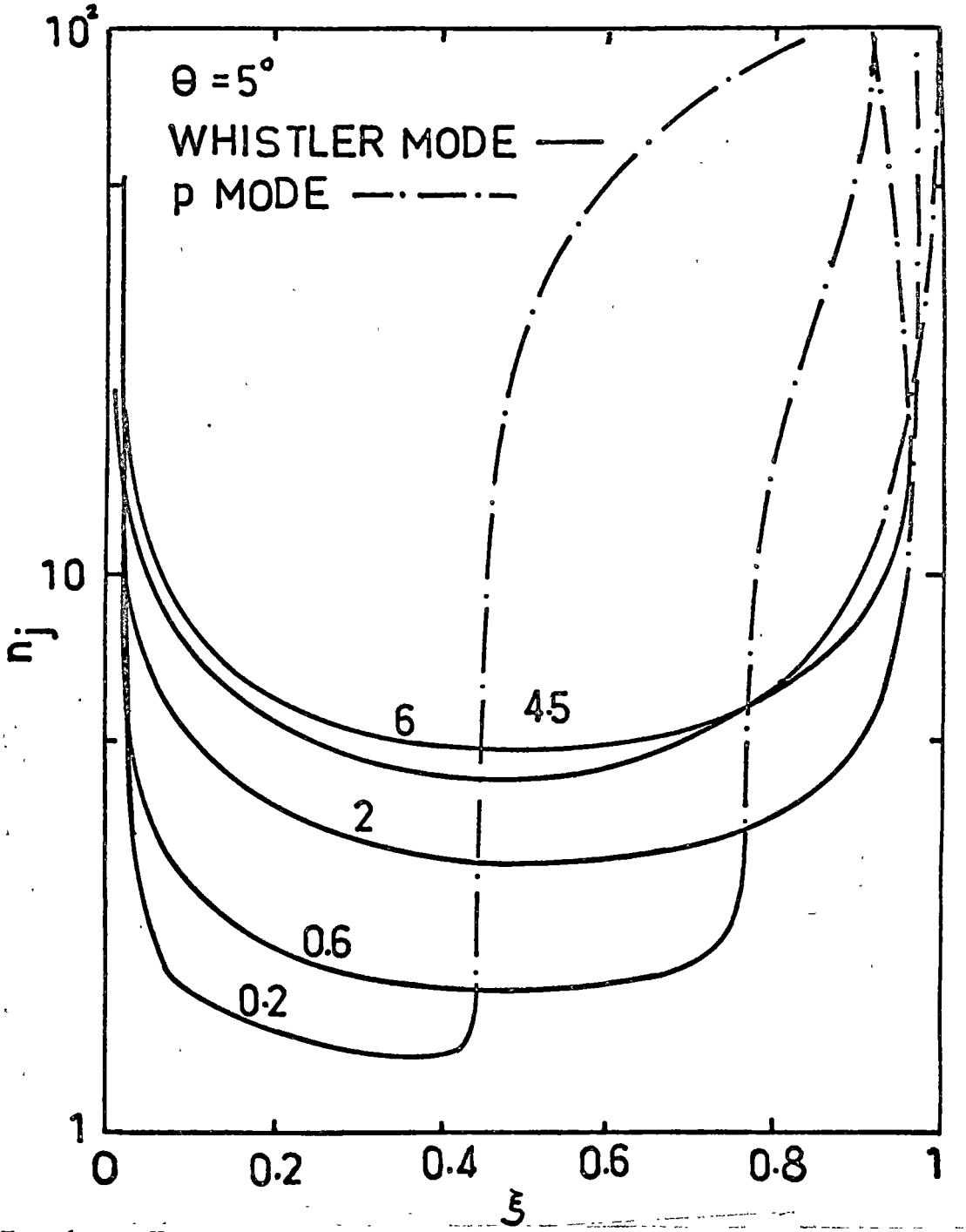

Fig.6.3 - Variation of refractive index n_j for the plasma mode (j = 3, dashed-dotted lines) and the whistler mode (j = 2, solid lines) with normalized frequency ξ for $\theta = 5^\circ$ and A = 0.2, 0.6, 2, 4.5, 6.

The features of the coherent radiation of weakly damped plasma waves in the frequency ranges (6.1) by an electron stream with small momentum spread and moving in a magnetoactive plasma have been studied in Chapter II. Fig. 6.4(a) and 6.4(b) illustrate the dependence of the intensity of the Cerenkov plasma wave emitted by a single electron and the rate of growth $\left| \mathrm{Im} \frac{\delta}{\omega_H} \right|$ of the Cerenkov plasma wave in the stream-plasma system with respect to the wave-normal angle θ_o ($\beta_{||} = 0.3$, $\beta_{\perp} = 0.2, 0.3$, $f_H = 50$ MHz, $A = 4.5$ and $\sigma = 10^{-4}$). The normalized wave frequency $\xi_o = f_o/f_H$ of the Cerenkov plasma wave emitted in the direction $\theta_o \simeq 0$ at which the intensity of the Cerenkov plasma wave maximizes can be written as

$$\xi_o \simeq A^{\frac{1}{2}}\left(1 + \frac{3\beta_T^2}{2\beta_{||}^2}\right) . \qquad (6.2)$$

For $\beta_{||} >> \beta_T$, we have $\xi_o \simeq A^{\frac{1}{2}}$.

C. The Wave Frequency of The Radio Emission Arising From Transformation of The Cerenkov Plasma Wave by The Thermal Fluctuations in The Solar Corona

If the generation of coherent Cerenkov plasma waves by an electron stream is the cause of the solar radio emission observed on the Earth, it is necessary that the plasma waves be transformed into electromagnetic waves through combination

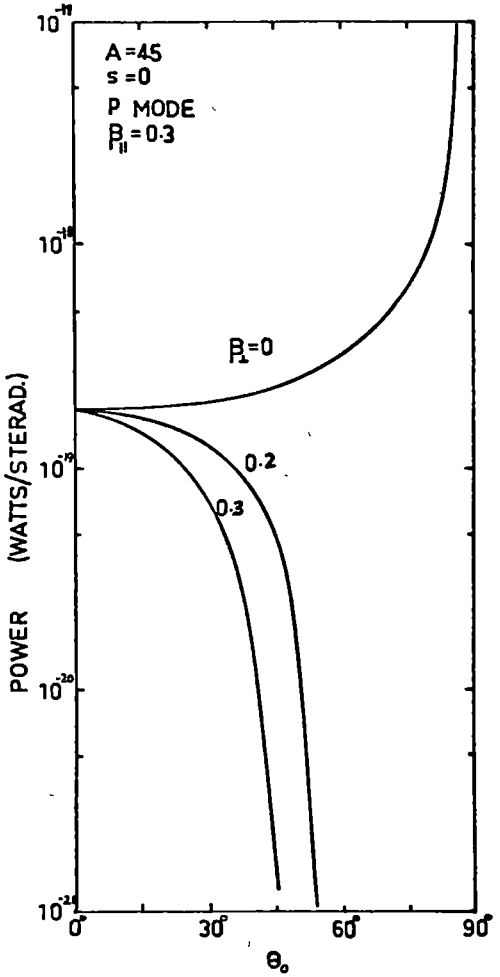

Fig.6.4(a)- Angular Cerenkov plasma wave power spectra radiated by a single electron for normalized frequency $\xi > 1$ and $\beta_{||} = 0.3, \beta_\perp = 0.0.2, 0.3$, $f_H = 50$ MHz, A = 4.5, and $\beta_T = 10^{-2}$.

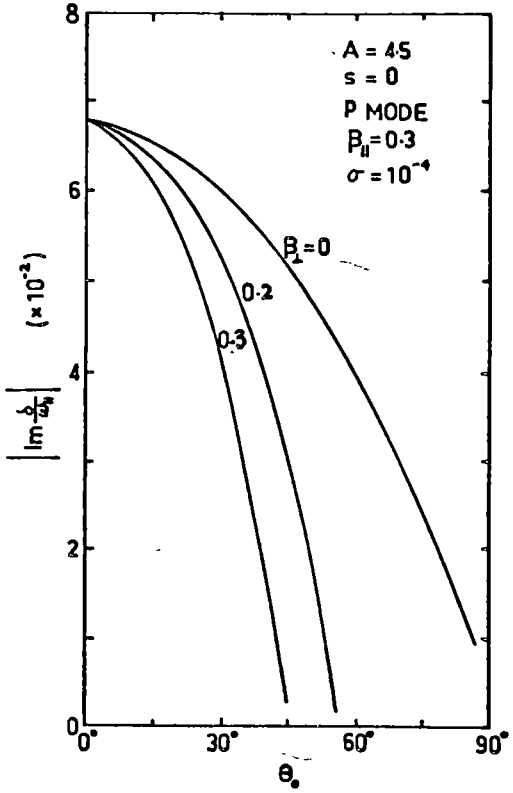

Fig.6.4(b)- The dependence of the rate of growth of the Cerenkov plasma wave with normalized frequency $\xi > 1$ on wave-normal angle θ_o for $\beta_{||} = 0.3$, $\beta_\perp = 0, 0.2, 0.3$, A = 4.5, $\beta_T = 10^{-2}$, and $\sigma = 10^{-4}$.

scattering or incoherent scattering by the thermal fluctuations (Chapter V, Section D).

The wave frequency and the wave vector of the transformed electromagnetic wave are restricted by the equality (5.18). As a result of transformation of the Cerenkov plasma wave with the frequency (6.2) by the thermal fluctuations, the frequencies of the electromagnetic waves in the x-mode and the o-mode will be

$$\omega \simeq \omega_o + \tilde{\omega}_{\pm}, \quad \omega \simeq \omega_o, \tag{6.3}$$

$$\text{i.e.} \quad \xi \simeq \xi_o + \tilde{\xi}_{\pm}, \quad \xi \simeq \xi_o.$$

Transformation of the Cerenkov plasma waves into electromagnetic waves would hence occur if $f \gtrsim f_p, f_x$, where f_x is given by (5.1). The phase velocity of the coherent fluctuation responsible for the transformation process in general is proportional to the phase velocity of the Cerenkov plasma wave and hence to $\beta_{//}$. In Fig. 6.5, we demonstrate the dependence of the combination frequencies of the transformed electromagnetic waves, the Cerenkov plasma wave frequency and the minimum x-mode wave frequency f_x on the value of A for $\beta_{||} = 0.3$, $\beta_T = 10^{-2}$, $\theta_o \simeq 0$ and $\theta \simeq 90^o$. It can be observed that

(1) The Cerenkov plasma wave can only be transformed into the o-mode wave with small frequency change by incoherent

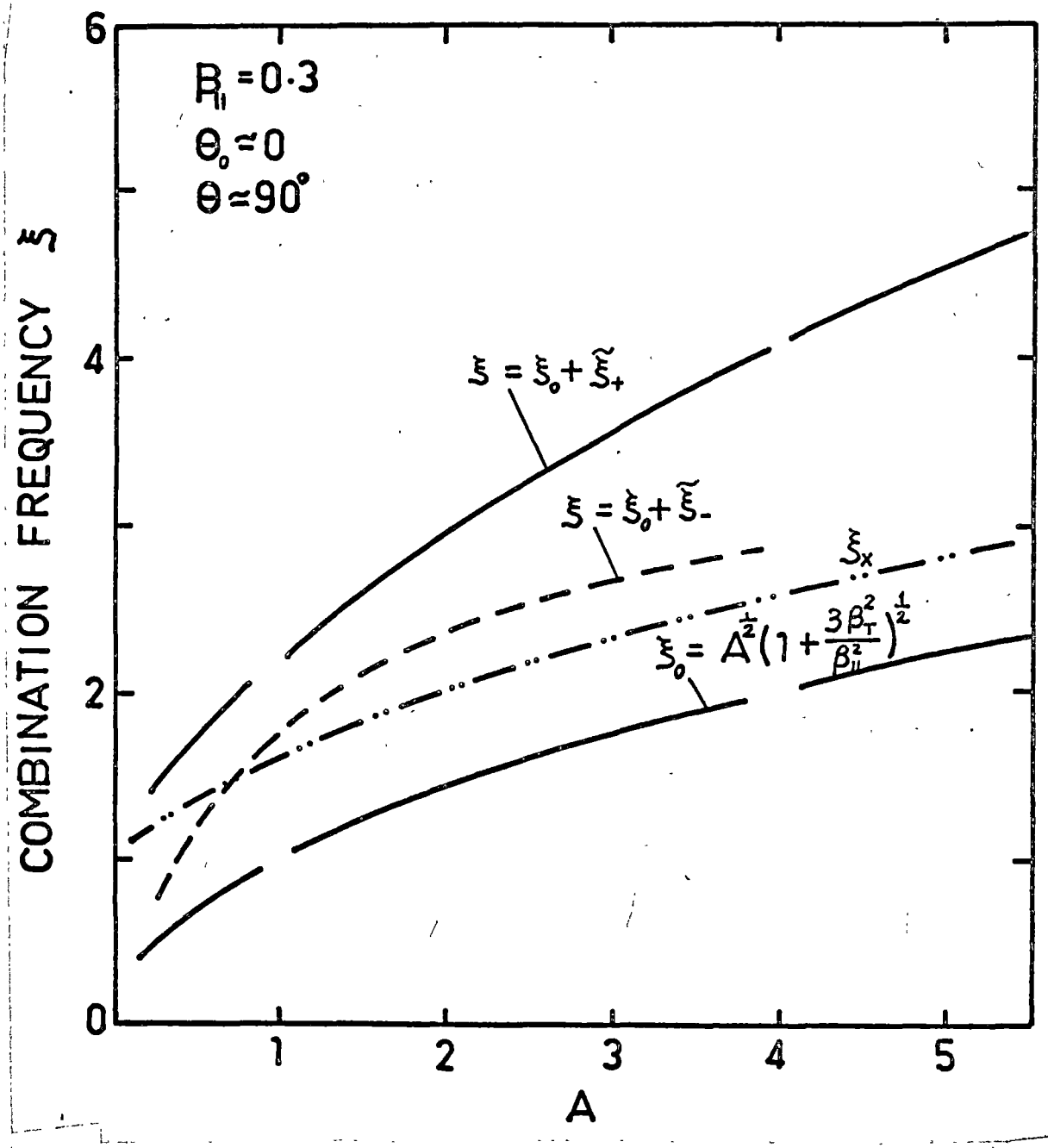

Fig.6.5 - The dependence of the normalized combination frequencies ξ, the normalized minimum frequency for x-mode wave ξ_x and the normalized Cerenkov plasma wave frequency ξ_0 on the value A for $\beta_{11} = 0.3$, $\theta_0 \simeq 0$, $\theta \simeq 90°$ and $\beta_T = 10^{-2}$.

scattering process for all values of A.

(2) The Cerenkov plasma wave can also be transformed into the o-mode and x-mode waves at the normalized wave frequency $\xi \simeq \xi_o + \tilde{\xi}_+$ through combination scattering. It has been shown in Chapter V, (Fig. 5.5), that for a given θ, the combination frequencies of the o-mode and x-mode waves are almost identical. However, transformation of the Cerenkov plasma wave into the x-mode electromagnetic wave at the frequency $\xi \simeq \xi_o + \tilde{\xi}_-$ occurs only when A becomes greater than 0.5 at least.

(3) The possibility of transformation of Cerenkov plasma waves into electromagnetic waves at the frequency $\xi \simeq \xi_o + \tilde{\xi}_-$ by combination scattering process depends on $\beta_{//}$. The phase velocity of the coherent fluctuation at the frequency $\tilde{\xi}_-$ and taking part in the transformation process is similar to that of the Cerenkov plasma wave and hence to $\beta_{//}$. When A is large, the coherent fluctuation at the frequency in the region (1) of (6.1) can propagate only with very small phase velocity (see Fig. 6.3). Hence, when A and $\beta_{//}$ are greater than certain values, transformation of the Cerenkov plasma wave excited by the electron stream into electromagnetic waves at the frequency $\xi \simeq \xi_o + \tilde{\xi}_-$ may not be possible. In fact, as A is sufficiently large, the weakly damped coherent fluctuations occur at the frequency $f \simeq \tilde{f}_+$ for all directions and combination scattering of the

Cerenkov plasma wave will give rise to electromagnetic waves at the frequency $\xi \simeq \xi_o + \tilde{\xi}_+ \simeq 2\xi_o$ only. From these arguments, we can conclude that

(a) When A is not large (less than 4, say), the Cerenkov plasma waves excited by mildly relativistic electrons can be transformed into electromagnetic waves at the frequencies $f \simeq 2f_p$, f_p, $f_p + \tilde{f}_-$.

(b) When A is large, f can only be near the first and second harmonics of the plasma frequency.

D. Resonance Absorption and Escape of Transformed Electromagnetic Radiations From The Active Solar Corona

As is well known from the principle of detail balancing, each emission process is associated with a damping process. It has been shown that the absorption coefficient for the electromagnetic radiation in a Maxwellian isothermal plasma is always positive, for any possible emitting process, i.e. damping of the electromagnetic waves (Smerd, 1963). Therefore, in addition to the collisional damping associated with the bremsstrahlung, the electromagnetic wave with the frequency ω and wave vector $\bar{k}$ passing through a Maxwellian magnetoactive plasma will be damped by the resonant electrons which are capable of extracting energy from the wave. The absorptions of this type are the inverse of the Cerenkov and cyclotron emission processes and generally known as the

resonance absorptions. Without solving the actual dispersion equation, Shafranov (1967) showed that the absorption of electromagnetic waves in a plasma is associated with the anti-hermitian part of the dielectric tensor which is proportional to $\exp\left[\frac{-(\omega-s\omega_H)^2}{2n_j^2\beta_T^2\omega^2\cos^2\theta}\right]$. Hence the resonance absorptions will occur in peaks around $\omega = s\omega_H$, $s = 0,1,2,3,\ldots$ For $s = 0$, the resonance absorption corresponds to the Cerenkov emission from the plasma. As regards the problem of emergence of electromagnetic radiation from the solar corona, the Cerenkov absorption is not of great importance. For $s = 1,2,3,\ldots$, the resonance absorption is the inverse process of the cyclotron radiation. It has been shown by Ginzburg (1964, p.417) that in the solar corona the cyclotron resonance absorption must be taken into account only for $f = sf_H$, $s = 1,2,3$.

A complete theory of cyclotron resonance absorption is given by Gershman (1960). In Gershman's theory, the electromagnetic wave propagating in the magnetoactive plasma is described by the form $\exp(i\tilde{k}z - i\omega t)$, where z is the path length in the direction of propagation (i.e. wave vector direction) and $\tilde{k} = k + iq$, k being the wave number and q the absorption coefficient. The damping factor due to absorption is then written as $\exp(-qz)$. Starting with the general

dispersion equation which is obtained by solving a linearized kinetic equation for the electrons and the self-consistent field equations simultaneously, and investigating the absorption in the frequency region $\omega \simeq s\omega_H$, Gershman obtained the expressions for the first three harmonic specific resonance absorption coefficients for $\theta \neq 0, \pi/2$ as

$$(q/k)_{s=1} = \left(\frac{2}{\pi}\right)^{\frac{1}{2}} \frac{\beta_T \cos\theta / n_j X}{(2X-2-\sin^2\theta+2n_j^2\sin^2\theta)} \left\{\left[1-(1-\frac{7}{4}\sin^2\theta)X\right]n_j^4 \right.$$

$$- \left[2+X\left(\frac{7}{4}\sin^2\theta-\frac{5}{2}\right) + \frac{1}{4}X^2(2\cos 2\theta-\tan^2\theta)\right] n_j^2$$

$$\left. + \left[1-\frac{3}{2}X+\frac{1}{2}X^2(1-\tan^2\theta) + \frac{1}{4}X^3\tan^2\theta\right]\right\}, \qquad (6.4)$$

$$(q/k)_{s=2} = \left(\frac{\pi}{8}\right)^{\frac{1}{2}} \frac{X\beta_T n_j \sin^2\theta}{\cos\theta} B(Y=\tfrac{1}{2}) \exp\left[\frac{-(1-2Y)^2}{2\beta_T^2 n_j^2 \cos^2\theta}\right], \qquad (6.5)$$

$$(q/k)_{s=3} = \frac{27}{8}\left(\frac{\pi}{8}\right)^{\frac{1}{2}} \frac{X\beta_T^3 n_j^3 \sin^4\theta}{\cos\theta} B(Y=\tfrac{1}{3}) \exp\left[\frac{-(1-3Y)^2}{2\beta_T^2 n_j^2 \cos^2\theta}\right], \qquad (6.6)$$

where $B(Y) = \left(\frac{Y^2-1}{Y^2 n_j^2}\right)\left\{\tfrac{1}{2}n_j^4\sin^2\theta + \left[X(\tfrac{1}{2}+\tfrac{1}{2}\cos^2\theta + \frac{\sin^2\theta}{1+Y}\right)\right.$

$$\left. - (1+\tfrac{1}{2}\sin^2\theta)\right]n_j^2 + \left[(1-X)\left(1-\frac{X}{1+Y}\right)\right]\right\}$$

$$\times \left[2(1-Y^2-X+Y^2X\cos^2\theta)n_j^2-2(1-X)^2-(1+\cos^2\theta)Y^2X+2Y^2\right]^{-1} ,$$

$j = 1,2.$

For $\omega \simeq 2\omega_H, 3\omega_H$, we must substitute $Y = \frac{1}{2}, \frac{1}{3}$ in (6.5) and (6.6) respectively. The expression (6.4) is valid only for the inner region of the line Y=1 while (6.5) and (6.6) for both the inner and the outer regions.

The actual resonance absorption on passing through the layer $\omega = s\omega_H$ (s = 1,2,3) depends on the effective thickness of the layer which increases with the decrease of the wave-normal angle. According to Ginzburg and Zheleznyakov (1959), the effective thickness is given by

$$L_j = L_H\left(\frac{2\pi}{3}\right)^{\frac{1}{2}} n_j \beta_T \left|\cos\theta\right| , \qquad (6.7)$$

where L_H is the characteristic length of the magnetic field of the sunspot (in centimetres). Zheleznyakov (1962) defined the characteristic length of the magnetic field as $L_H = H_o/\mathrm{grad}H_o$, H_o being the magnetic field intensity. Then, the power loss on passing through the resonance absorption layer (in decibels) will be

$$l_j = 8.68qL_j, \quad (j = 1,2) . \qquad (6.8)$$

For the outer layer of the coronal streamer, we can assume $L_H \simeq 10^9 - 10^{10}$ cm and $\beta_T = 10^{-2}$. The power losses

for the two characteristic waves at the frequency f = 100 MHz on passing through the first three harmonic absorption layers are illustrated in Fig. 6.6 for various wave-normal angles. The first harmonic resonance absorption for the extraordinary wave (z-mode and x-mode) is not shown since the z-mode wave cannot escape through the layer X = 1 - Y in the solar corona even if it can survive after passing through the level Y = 1. The x-mode wave able to escape from the solar corona always propagates in the layer above the level Y = 1. From these diagrams, it can be seen that the power loss for the x-mode wave is at least two orders of magnitude higher than that for the o-mode wave. Thus, we can conclude that for wave-normal angles not too close to zero and for typical active solar corona conditions, the first two harmonic resonance absorption levels are opaque to both the x-mode and the o-mode waves while the third harmonic resonance absorption layer is partially transparent to the o-mode wave but remains opaque to the x-mode wave except when $X = f_p^2/f^2 \ll 1$ and grad H_o is very large at the layer $\omega = 3\omega_H$.

We assume that the electron stream travels along the strongest spot field line which extends to the outer layer of the solar corona ($\rho \gtrsim 1.5$, say) with $\beta_{\parallel} \simeq 0.3$ and generates coherent Cerenkov plasma waves. The sunspot magnetic field intensity not only decreases with the increase of the height above the photosphere but also decreases in the normal

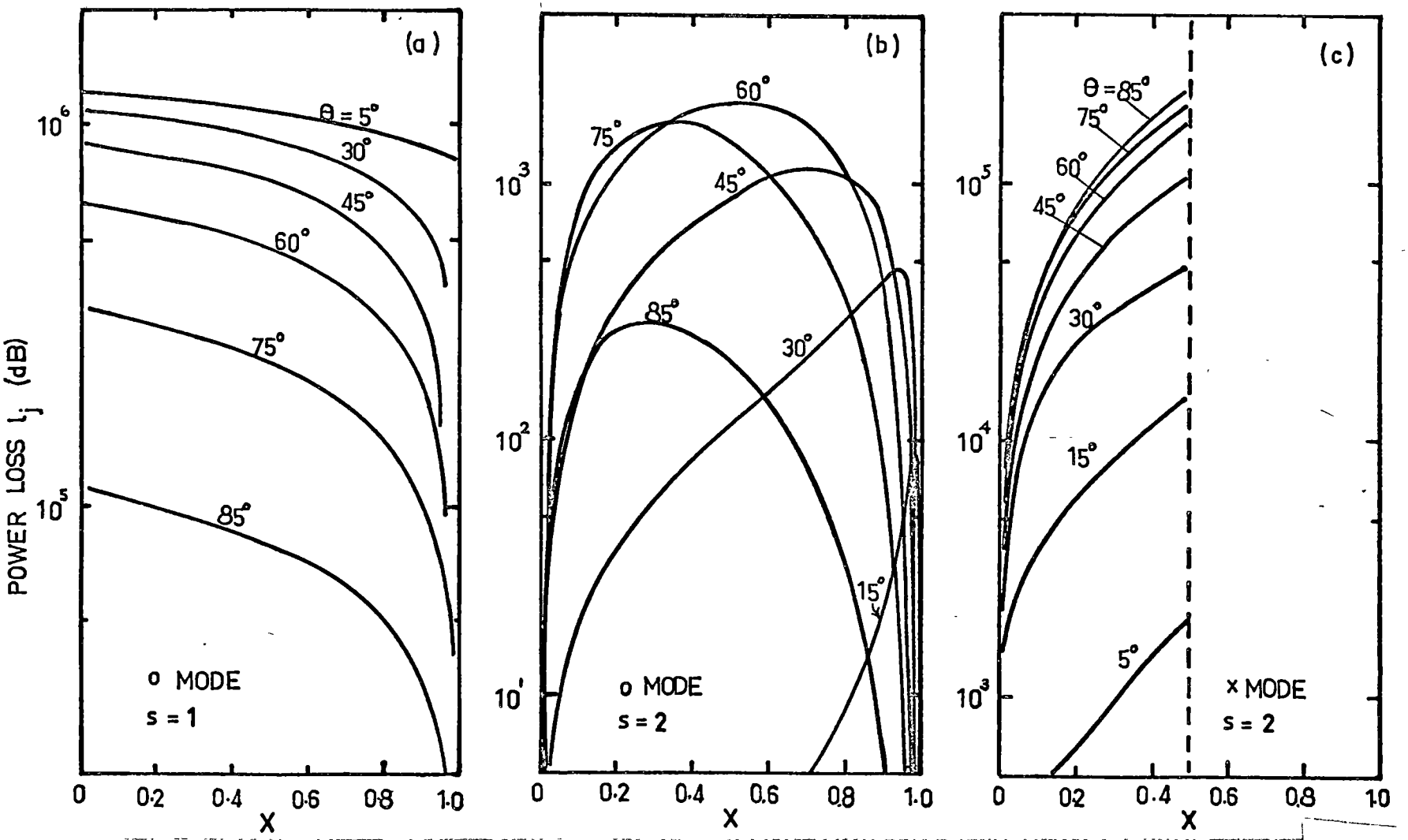

Fig.6.6 - Variation of power loss (dB) on passing through the layer $f = sf_H$ with $X = \omega_p^2/\omega^2$, taking the characteristic length of the sunspot magnetic field $L_H = 10^9$ cm and $\beta_T = 10^{-2}$, for frequency f = 100 MHz and various values of wave-normal angle θ, and for (a) s = 1, o-mode wave; (b) s = 2, o-mode wave; (c) s = 2, x-mode wave.

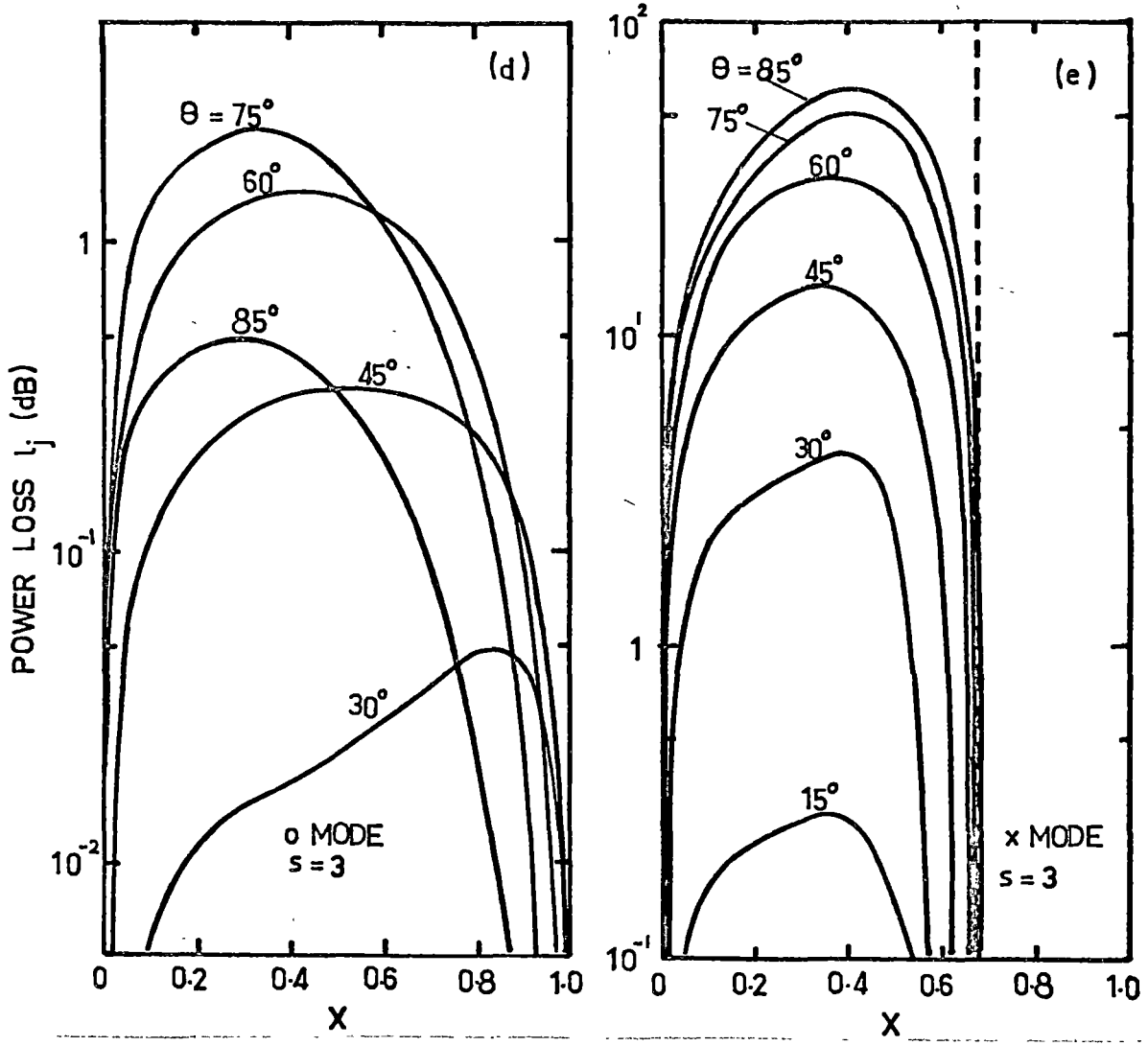

Fig.6.6 - Variation of power loss (dB) on passing through the layer $f = sf_H$ with $X = \omega_p^2/\omega^2$, taking the characteristic length of the sunspot magnetic field $L_H = 10^9$ cm and $\beta_T = 10^{-2}$, for frequency f = 100 MHz and various values of wave-normal angle θ, and for (d) s = 3, o-mode wave; (e) s = 3, x-mode wave.

direction from the strongest field line. Thus, any electromagnetic radiation leaving the radiation source will encounter regions where the wave frequency is equal to the harmonic of the local gyrofrequency i.e. s = 1,2,3,...(cf. Fig. 16 of Fung and Yip, 1966).

The possibility of observing solar radio emissions resulting from the transformation of Cerenkov plasma waves requires not only the possibility of transformation as discussed in Section C but also that the transformed wave frequency be at least greater than the second harmonic of the gyrofrequency at the source region. Referring to Fig. 6.5, we note firstly that observation of the o-mode electromagnetic radiation at the frequency $\xi \simeq \xi_o$ arising from incoherent scattering of the Cerenkov plasma waves is impossible unless the source is situated in a region where A > 4. Secondly, if A < 1 in the source region, any transformed electromagnetic radiation will be unable to escape from the solar corona. Thirdly only part of the transformed o-mode electromagnetic radiation at the frequencies $\xi \simeq \xi_o + \tilde{\xi}_{\pm}$ generated in the source medium with A lying between 1 and 2 will be able to escape from the solar corona. When A > 3 in the source region, the transformed o-mode and x-mode waves at the frequency $\xi \simeq \xi_o + \tilde{\xi}_{\pm}$ can arrive at the Earth without being heavily attenuated since the resonance absorption of electromagnetic radiation at the layers $\omega \simeq s\omega_H$ with $s \geq 4$

is insignificant.

Now, if we assume that at a certain wave-normal angle θ, the efficiencies of transformation of Cerenkov plasma waves excited by an electron stream into electromagnetic waves at the frequencies f_p, $f_p + \tilde{f}_-$ and $f_p + \tilde{f}_+$ are similar, then it can be predicted that

(a) An electron stream may produce a pair of radio bursts with instantaneous frequency separation about $\tilde{f}_+ - \tilde{f}_-$ when it passes through the layers where $1 < A < 4$ (We shall refer this region as region I later).

(b) A pair of radio bursts of similar intensities and with frequency ratio 1:2 generated by the electron stream moving in the layer where $A \geq 4$ (region II) could be seen on the Earth.

The value of A along the strongest sunspot magnetic field line increases with the height above the sunspot group, therefore, the electromagnetic radiation arising from transformation of the Cerenkov plasma waves through scattering processes will not be observed on the Earth until the electron stream arrives at the layers where $A \geq 1$. This restricts the highest possible observed frequency of the type III and U bursts. From the model given by Fig. 4.5(b), we can find that the upper cut-off frequency of type III bursts would not exceed 700 MHz. This predicted upper cut-off frequency of type III burst agrees with the observational data

fairly well (Malville, 1961). However, if explosion of the solar flare takes place in the transitional region between the chromosphere and the base of the solar corona ($\rho \leq 1.04$) where the electron density is much higher than that predicted by (4.1), the electromagnetic radiation at the frequency $\sim 2f_p$ (about 1,000 MHz to 2,000 MHz) can leave the solar corona and the type III bursts may occasionally be observed in the centimetre wavelength region (Hughes and Harkness, 1963). Moreover, the absence of distinct lower cut-off frequency of the type III bursts can also be realized.

E. Efficiency of Transformation of Cerenkov Plasma Waves into Electromagnetic Waves by Thermal Fluctuations

In order to predict the observed spectral characteristics of the plasma radiation, we need to investigate the efficiencies of transformation of coherent Cerenkov plasma waves into electromagnetic waves at different frequencies and in different directions.

In the coronal streamer, at the height from about 0.5 to 1 solar radius above the photosphere, we can take $\beta_T = 10^{-2}$, linear size of the scattering volume $L \simeq 10^9 - 10^{10}$ cm and $f_H \simeq 50$ MHz - 5 MHz. The coefficients of transformation of the Cerenkov plasma waves excited by electron streams moving with $\beta_{\parallel} \simeq 0.3$ into electromagnetic waves by means of combination and incoherent scatterings (expressions (5.41) and (5.46)), are

shown as functions of the transformed waves' wave-normal angle θ in Fig. 6.7. The quantity A is assumed to be 4.5 (i.e. region II). The small peaks of the coefficients have been smoothed out by taking the mean values of $\eta_j(\theta)$ (the dotted curves and the dashed-dotted curves).

It is found that the intensity of the transformed waves in the x-mode and the o-mode is distributed with axial symmetry about the scattering centre. For $\theta = 0$, from (5.41) and and (5.46), we can see that the polar diagrams of the transformed waves at the frequencies ~ f_p and ~$2f_p$ are completely symmetrical about the z-axis (i.e. the sunspot magnetic field line). For small values of θ, the intensity of the o-mode transformed wave at frequency ~ $2f_p$ will be greatest within a solid cone with axis almost transverse to the static magnetic field and with a half apex angle ~ 30^o. However, the corresponding x-mode transformed wave intensity maximizes in the direction $\theta \sim 60^o$ and 125^o. On the other hand, most of the energy of the o-mode transformed wave of frequency ~ f_p is emitted in the directions around $\theta \simeq 15^o$, 170^o.

For a given wave-normal angle, the power of the combination radiation

$$P_{2f_p}(\theta) \propto P_c(\theta_o) \; [\, \eta_1(\theta) + \eta_2(\theta)] \qquad (6.9)$$

where $P_c(\theta_o)$ is the power of the Cerenkov plasma wave excited

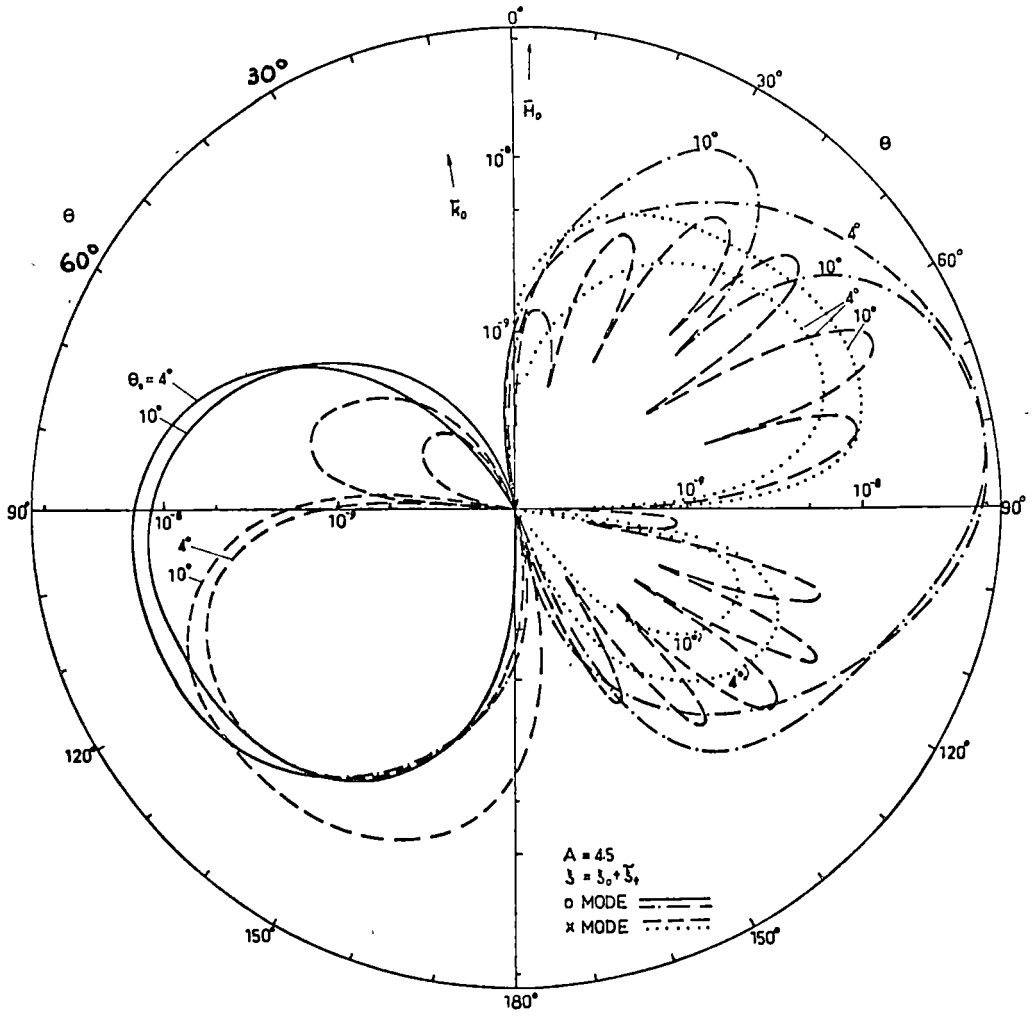

Fig.6.7(a) Variation of the coefficient of transformation of the Cerenkov plasma wave into x-mode wave (dashed lines and dotted lines) and o-mode wave (solid lines and dashed-dotted lines) at the normalized frequency $\xi \simeq \xi_0 + \tilde{\xi}_+$ by combination scattering with wave-normal angle θ for $A = 4.5$, $\beta_{ii} = 0.3$ and $\theta_0 = 4°, 10°$, $L = 4 \times 10^9$ cm and $f_H = 50$ MHz.

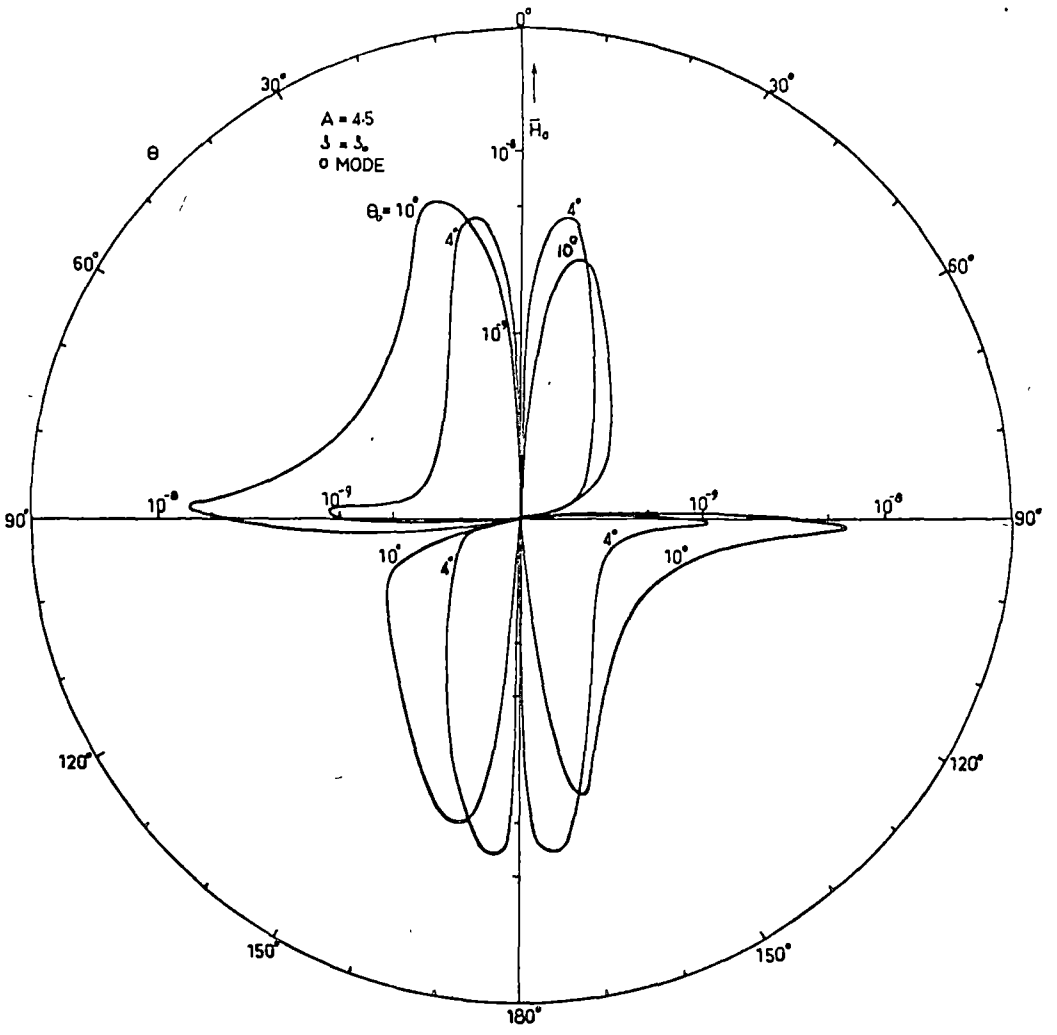

Fig.6.7(b) Variation of the coefficient of transformation of the Cerenkov plasma wave into o-mode wave by incoherent scattering with wave-normal angle θ for A = 4.5, $\beta_{\parallel}$ = 0.3, θ_o = 4°, 10°, L = 4×10^9 cm and f_H = 50 MHz.

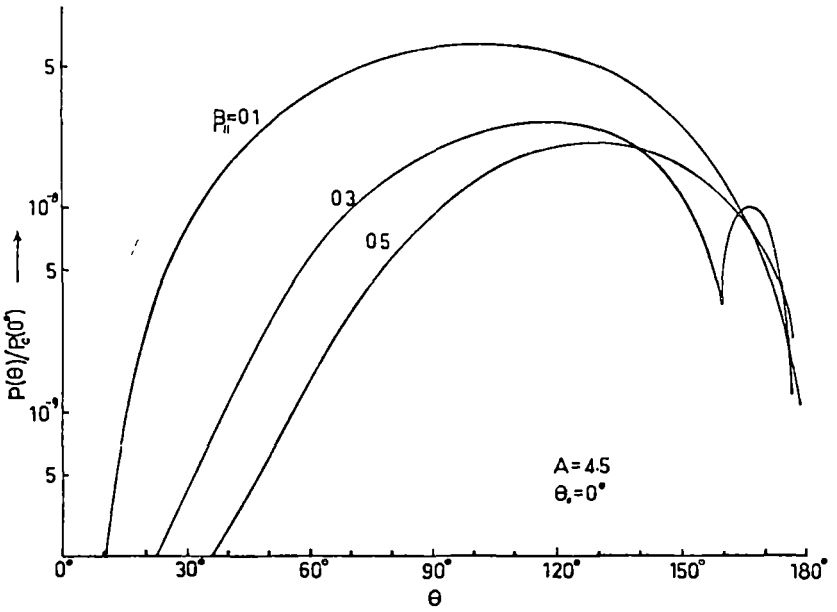

Fig.6.8(a)- Variation of P_{2f_p}/P_c with wave-normal angle θ for A = 4.5, f_H = 50 MHz, L = 4×10^9 cm, $\beta_\perp$ =0.3, $\beta_{\parallel}$ = 0.1,0.3,0.5.

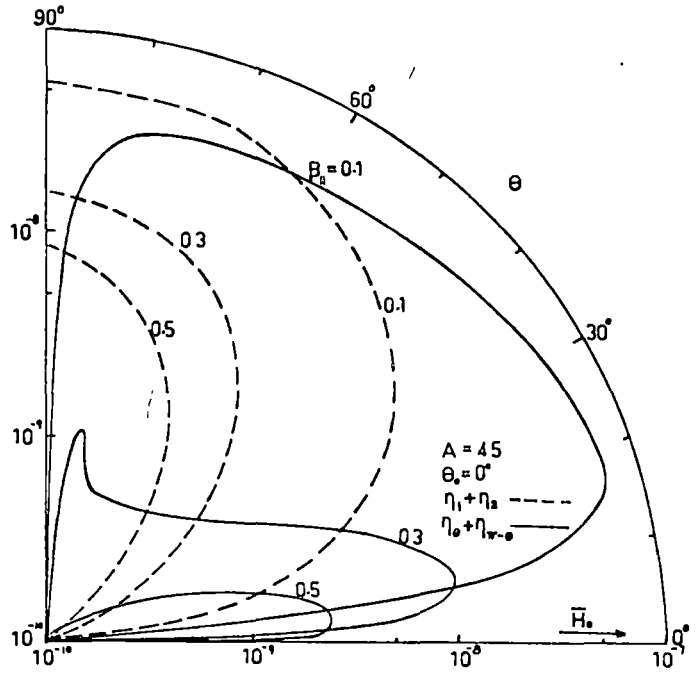

Fig.6.8(b)- Variation of P_{2f_p}/P_c and P_{f_p}/P_c with wave-normal angle θ for A = 4.5, f_H = 50 MHz, $\beta_\perp$ = 0.3, $\beta_{\parallel}$ = 0.1,0.3,0.5, L = 4×10^9 cm. θ is the angle between the wave vector and the magnetic field vector of a sunspot with the north polarity.

by the electron stream in the direction θ_o. Taking $\theta_o = 0$, $A = 4.5$, $f_H = 50$ MHz, $\cos\psi = 1$ and $\beta_{||} = 0.1, 0.3, 0.5$, the dependence of the quantity P_{2f_p}/P_c on the wave-normal angle θ is present in Fig. 6.8(a). As the speed of the electron translational motion increases, the combination radiation tends to maximize in the backward direction with respect to the guiding centre motion. The o-mode electromagnetic radiation with frequency slightly higher than the plasma frequency and emitted in the direction towards the Sun will be reflected immediately on leaving the scattering volume.

If we assume that after reflection, such an o-mode wave, initially emitted in the direction $\pi-\theta$, will follow a phase path similar to that of o-mode wave emitted in the direction θ ($\theta \leq \pi/2$), then we have

$$P_{f_p}(\theta) \propto P_c(\theta_o)[\eta(\pi-\theta) + \eta(\theta)] , \qquad (6.10)$$

where $\eta(\pi-\theta)$, $\eta(\theta)$ are given by (5.46). Corresponding to Fig. 6.8(a), we show the variations of the quantities P_{2f_p}/P_c and P_{f_p}/P_c as functions of θ ($\theta \leq \pi/2$) in Fig. 6.8(b). In any direction θ ($\theta \leq \pi/2$), radio emissions with frequency ratio $\sim$ 1:2 and intensity ratio

$$R = P_{f_p}/P_{2f_p} = \frac{\eta(\theta) + \eta(\pi-\theta)}{\eta_1(\theta) + \eta_2(\theta)} \qquad (6.11)$$

will emerge from the scattering volume simultaneously. From

Fig. 6.8, we also see that for $\beta_{11} \gtrsim 0.2$, the power P_{f_p} predominates for $\theta \leq 35^{o}$. For other directions, $P_{2f_p} > P_{f_p}$. Moreover, the reflection of the backward emission at the frequency $\sim 2f_p$ will lead to the increase of the number of the observed second harmonic components. The type III bursts and U bursts might hence be expected to have strong second harmonic components more frequently.

About 60% of the type III bursts and some of the U bursts observed show harmonic structure. The emission of harmonic pairs of the type III bursts or U bursts is attributed to the transformation of the Cerenkov plasma waves by incoherent and coherent thermal fluctuations. Since the polar diagrams of the electromagnetic radiations arising from incoherent scattering and combination scattering of the Cerenkov plasma waves differ from each other, the fundamental and the second harmonic components will be of comparable intensity on leaving the source region only in the direction for which R is close to unity. If we neglect the effect of the differential refraction of the ray paths of waves at different frequencies in the solar corona, electromagnetic radiations emitted in this direction would arrive at the Earth concurrently and appear as a harmonic pair of radio bursts with similar intensities in the dynamic spectrum. However, transformed electromagnetic radiation at these frequencies emitted in the direction for

which R differs from unity greatly, would not form a harmonic pair of radio bursts in the dynamic spectrum, since in this case the intensities of the two components will be substantially different.

Assuming the sunspot magnetic field line be quasi-radial, we can estimate the dependence of the probability of observing harmonic pairs of type III (or U) bursts on the source latitude. Let us define the quantity H as

$$H = (1 - R)/(1 + R) \qquad (6.12)$$

where R is given by (6.11). H is the measure of the intensity ratio of the fundamental to the second harmonic emissions. When $H < 0$, the fundamental component predominates while $H > 0$, the intensity of the second harmonic emission is greater. That is harmonic pairs of transformed electromagnetic radiations will be emitted in those directions for which $H \simeq 0$. According to Fig. 6.8, we plot H as a function of emission wave-normal angle θ in Fig. 6.9(c). Under the present assumptions, the wave-normal angle θ in Fig. 6.9(c) can be regarded as the source latitude. Thus, it is expected that most of the harmonic pairs of the type III (or U)bursts will originate from sources situated at latitudes from 40° to 75°. Assuming the coronal streamer electron density models Fig. 4.5(b), we show the estimated disk positions of the sources of the harmonic

pairs of the type III bursts at the frequency 60 MHz (i.e. f_p = 60 MHz) in Fig. 6.9(a). It is expected that the fundamental harmonic components will be found in the position closer to the central part of the disk while the second harmonic in the positions near or above the solar limb. Comparing Fig. 6.9(a) with Fig. 6.9(b), we find that the disk distribution of harmonic pairs of the type III bursts predicted by the present theory agrees well with the observational data obtained by Wild et al. (1959). In fact, from the polar diagrams of the electromagnetic radiations arising from scattering of the Cerenkov plasma wave (Fig. 6.7), we can realize that for a limb source the electromagnetic radiation at the frequency ~ $2f_p$ will dominate when $\beta_{||} \geq 0.2$. Therefore no harmonic pairs will come from a limb source. We should remark that Fig. 6.9(a) and Fig. 6.9(c) are only rough theoretical estimations of the disk distribution of the harmonic pairs of the type III bursts since the differential refraction of the ray paths of the first and second harmonics, the reflection of the backward emission of the second harmonic and the actual curvature of the sunspot magnetic field line have been neglected.

When reflection of the backward second harmonic is taken into account, it is possible for the second harmonic backward emission to follow a ray path similar to that of the fundamental and if the two components are initially similar in intensity, they can form a harmonic pair in the dynamic spectrum.

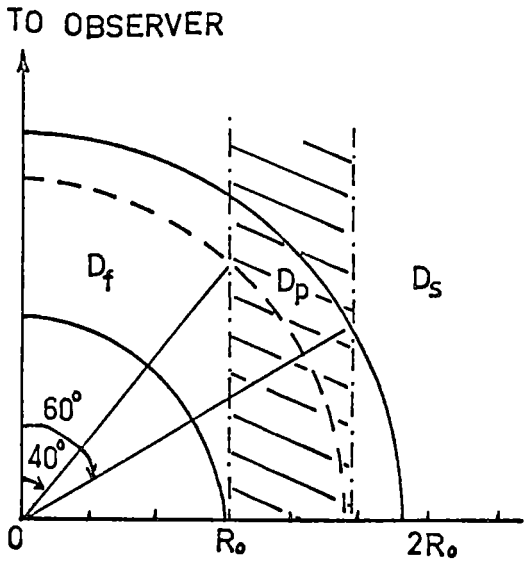

Fig.6.9(a) Theoretical disk positions of type III burst sources: (a)fundamental harmonic (60 MHz), D_f;
(b)harmonic pair, D_p;
(c)second harmonic, D_s.
The solid and dashed levels are the 60 MHz plasma level of the coronal streamers with electron density distributions given by 10xB.A. model and 5xB.A. model respectively.

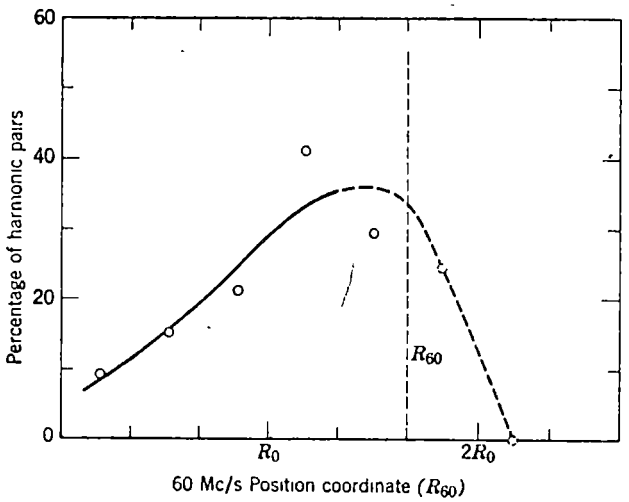

Fig. 6.9(b) Distribution with 60 Mc/sec position on the disk of the percentage of type III bursts showing recognizable harmonics (after Wild, Sheridan, and Neylan 1959).

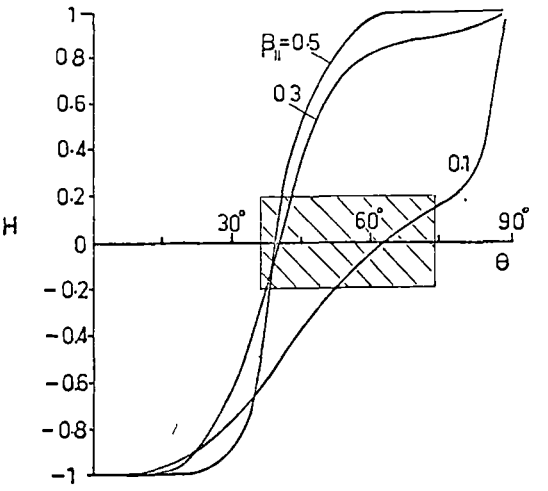

Fig.6.9(c)- Variation of H with wave-normal angle θ for $\beta_{\perp}$= 0.3, β_{II}= 0.1,0.3,0.5. The shaded region is the range of wave-normal angles θ ~~ab~~ which the harmonic pairs of the radio bursts would be emitted. The other parameters are equivalent to those used in Fig.6.8 .

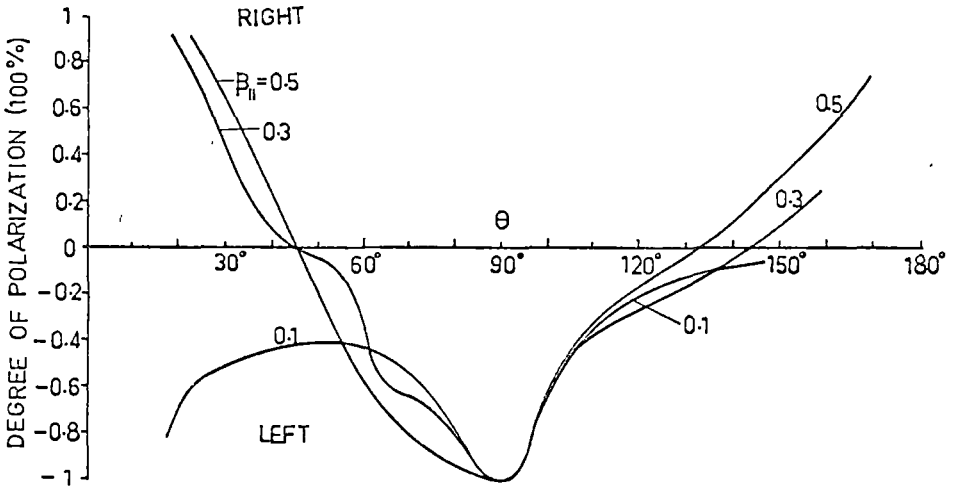

Fig.6.10 - The dependence of the degree of polarization of the radio emission at the second harmonic plasma frequency on wave-normal angle θ with parameters equivalent to those used in Fig.6.8. . Referring to the north polarity of the leading sunspot, the left-handed polarization corresponds to the polarization of the ordinary wave in the magneto-ionic theory.

In this case, it is expected the second harmonic would appear a few seconds later than the appearance of the fundamental harmonic. The observational data do indicate that in some of the harmonic pairs, the second harmonic is delayed with respect to the fundamental by 1.5 to 5 seconds (Kundu, 1965). However, because the source of type III bursts is in the coronal streamer where the electron density at least a few times higher than the background corona, it is difficult to predict the reflection height as well as the ray trajectory of the second harmonic backward emission.

F. Polarization of The Electromagnetic Radiation Arising From Transformation of Cerenkov Plasma Waves by Thermal Fluctuations of Electron Density

Having studied the polar diagrams of the transformed electromagnetic radiations at the first and the second harmonics of the plasma frequency,we can predict the polarization characteristics of the polarized type III bursts and U bursts. For wave-normal angles not close to zero or $\pi/2$, the electromagnetic waves in the x-mode and o-mode are elliptically polarized. The axial ratio of the polarization ellipse depends on the quantity $\xi(\xi^2-A)^{-1}$ which, for a given frequency, decreases to very small values with the increasing distance from the Sun (Piddington and Minnett, 1951). The polarization of the electromagnetic radiation emitted from a source in the

solar corona will change continuously on propagating outward through the corona until the polarization limiting region* is reached, where the polarization of the radiation is fixed. Thus, from the discussion in Section C(a), the fundamental harmonic component of type III bursts (or U bursts) is strongly polarized in the left-handed sense. On the other hand, the transformed electromagnetic radiations with frequency ~ $2f_p$ and in the o-mode and the x-mode can be emitted in a given direction. Then, the degree of polarization of the second harmonic component of type III (or U) bursts will be

$$\rho_{2f_p}(\theta) = \frac{\eta_1(\theta) - \eta_2(\theta)}{\eta_1(\theta) + \eta_2(\theta)} \qquad (6.13)$$

We adopt the convention that for $\theta \leq \pi/2$, when ρ_{2f_p} is negative the second harmonic is polarized in the left-handed sense with respect to the direction of the magnetic field (i.e. the sense of polarization of the o-mode wave). Taking the wave-normal angle of the Cerenkov plasma wave $\theta_o = 0$, $\beta_{\parallel} = 0.1, 0.3,$

---

* The polarization limiting region is the region beyond which the magneto-ionic parameters (X,Y) have very small values that the state of polarization is no longer affected by the change in the direction of the magnetic field.

0.5 and $\cos\psi = 1$, we show the variation of the degree of polarization of the second harmonic component as a function of wave-normal angle θ in Fig. 6.10.

From Fig. 6.10 and Fig. 6.7, we find that the majority of the second harmonic component of type III bursts will be left-handed polarized with a low degree of polarization. Because the main power of the second harmonic component is emitted at large wave-normal angles, it is possible that some electromagnetic radiation at the frequency $f \simeq 2f_p$ passes through the polarization limiting region where the bipolar sunspot field is opposite to that in the source region. Then, referring to the leading sunspot magnetic field polarity, the sense of polarization of the second harmonic component reverses on passing through the polarization limiting region (see Fig. 6.12) and a fraction of the type III bursts will be right-handed polarized (Komesaroff, 1958; Bhonsle and McNarry, 1964). From Fig. 6.10, for θ not close to $\pi/2$, the degree of polarization of the second harmonic component does not exceed 60%

Since the electron density and the magnetic field intensity in the solar corona decreases with the distance from the Sun, electromagnetic waves generated in the active solar corona will propagate outward through the corona satisfying the quasi-longitudinal propagation condition in all directions except at the point where $\theta \simeq \pi/2$. For a bipolar sunspot magnetic field configuration, the electromagnetic

wave, after passing through the quasi-longitudinal propagation region, would subsequently traverse through the quasi-transverse propagation region where the interaction between normal waves occurs (cf. Fig. 6.12). From the discussion in Section C of Chapter V, if a left-handed polarized electromagnetic radiation penetrates into the QT region, an electromagnetic radiation consisting of a circularly polarized component and a linearly polarized component, whose degrees of polarization are given by (5.10) and (5.11) respectively, will leave the solar corona.

Taking f_p = 30 MHz and $L_H = 5\times10^9$ cm, f_H = 1 MHz and 2.5 MHz in the QT region, the dependence of the degree of linear polarization and degree of circular polarization of the emerging radiation on wave frequency f are shown in Fig. 6.11 where f_t is the transition frequency characterizing the QT region. According to Cohen (1960), a left-handed circularly polarized radiation with the frequency $f > f_t$ will maintain its original sense of polarization on passing through the QT region. On the other hand, if $f < f_t$, only weak coupling occurs in QT region and the sense of polarization will change since the direction of the magnetic field with respect to the direction of wave propagation has reversed. Now if the left-handed and right-handed polarized electromagnetic raidations with intensities proportional to $\eta_2 P_c$ and $\eta_1 P_c$ respectively penetrate into the QT region, the degree of

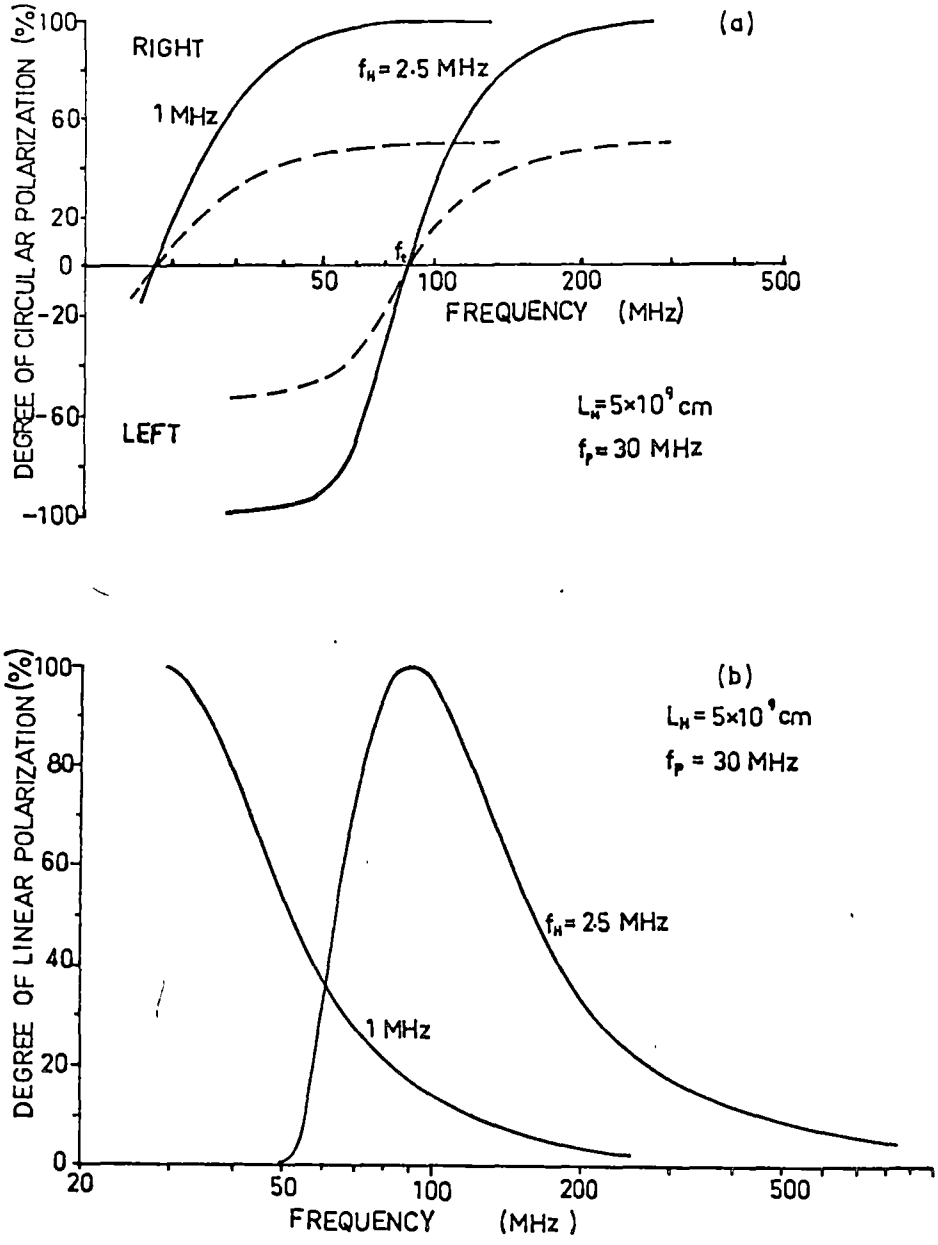

Fig.6.11 - The dependence of
(a) the degree of circular polarization,
(b) the degree of linear polarization
of the electromagnetic wave emerging from the quasi-transverse propagation region (QT region) on the wave frequency f, assuming $L_H = 5\times10^9$ cm, f_p = 30 MHz and f_H = 1, 2.5 MHz in the QT region.

circular polarization of the electromagnetic radiation emerging from the interaction region is given by

$$\lambda = \frac{\eta_1 - \eta_2}{\eta_1 + \eta_2} (1 - 2e^{-2\delta_o}) = - \rho_{2f_p} \rho_{cir} . \quad (6.14)$$

where ρ_{2f_p} is given by (6.13). For ρ_{2f_p} = -50% (left-handed polarized), the observed degree of polarization of the second harmonic component is plotted against the wave frequency in Fig. 6.11($\hat{b}$) (dashed curves). Therefore, on passing through the QT region, the degree of polarization of the second harmonic component would be reduced and the sense of polarization with respect to the direction of the magnetic field in the source region will not change if $f > f_t$.

The second harmonic component emitted at $\theta \simeq \pi/2$ is linearly polarized. Assuming a quasi-radial sunspot magnetic field line, radiation emitted at $\theta \simeq \pi/2$ will be observed to originate from a limb source in which case it is likely that it will pass through the polarization limiting region at right angles to the sunspot magnetic field. The characteristic polarization of such radiation is linear. However, owing to the depolarization through Faraday rotation, the observed second harmonic component originating from a limb source would be observed as weakly polarized or even unpolarized radio signal (Fokker, 1964). The linearly polarized component arising from interaction in QT region will also be depolarized in this manner.

In concluding this section, we summarize the discussion in the following points:

(a) Electromagnetic radiation strongly polarized in the left-hand sense and at the fundamental plasma frequency is expected to be emitted from a central source.

(b) Most of the weakly polarized or unpolarized electromagnetic radiation at the second harmonic plasma frequency will be observed to originate from sources lying at high latitudes.

(c) Whenever both the fundamental and second harmonic components are observed, the fundamental harmonic component will be more strongly polarized than the second harmonic component.

(d) The sense of polarization can be left-handed or right-handed.

These points are illustrated in the schematic drawing in Fig. 6.12 where the size of the coronal streamer is based on the model suggested by Morimoto (1963).

We have discussed the polarization characteristics of the electromagnetic radiations arising from transformation of the Cerenkov plasma wave emitted in the direction $\theta_o = 0$. From Fig. 6.7, it is not difficult to see that for small θ_o (but not equal to zero), the polarization characteristics of the transformed electromagnetic radiation remain similar to those for $\theta_o = 0$. These polarization properties of the

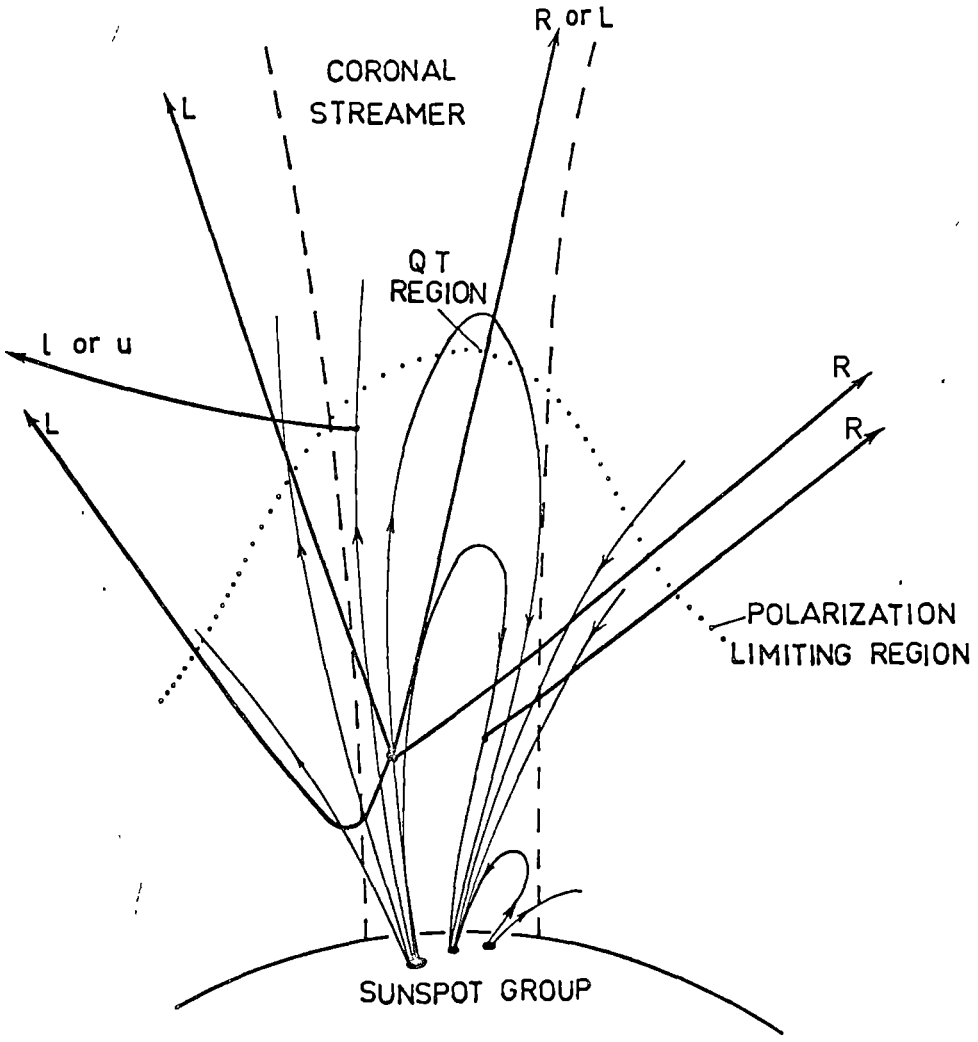

Fig.6.12 - Schematic drawing illustrating the left-handed (L), right-handed (R), random (u) and linear (l) polarized electromagnetic radiations would arise from the magnetoactive coronal streamer. The polarization limiting region is represented by the dotted line.

transformed radiations, in general, agree well with the observed polarization characteristics of the type III and U bursts (Komesaroff, 1958; Bhonsle and McNarry, 1964; Gopala Rao, 1965; Fomichev and Chertok, 1968).

G. Conclusion

The solar type III burst and U burst emissions have been recognized as the consequence of the excitation of longitudinal plasma waves by electron steams moving in the solar corona (Wild, 1950; Ginzburg and Zheleznyakov, 1958; Wild et al., 1959; De Jager, 1960; Smerd et al., 1962; etc.). A comprehensive review on the theories of type III and U burst emissions based on the isotropic corona model is given by Kundu (1965). In the present chapter, we have explained some of the features of the type III and U bursts, which had not been considered in detail previously, taking into account the effect of the coronal magnetic field.

So far, interpretations of the type III burst emission have been based on the linear theory of stream-plasma instability which is valid only for small perturbations of the distribution function of the stream electrons. But the strong resonance interaction between the growing plasma wave and the stream electrons leads to the formation of a plateau on the distribution function for the stream-plasma system and subsequent coherent generation of Cerenkov plasma waves will no

longer be possible (see Section D of Chapter III). If the Cerenkov plasma waves emitted by an individual stream electron remain in the stream-plasma system for an appreciable time interval and grow continuously, then the energy of the stream will be depleted quickly and the electron stream will be unable to escape beyond the base of the solar corona.

Thus, if the interpretation of the type III burst emission on the basis of linear kinetic theory is valid, the low cut-off frequency (i.e. very large source height) and the duration of the type III and type U bursts imply that there is a process for stabilizing the electron stream faster than the plateau formation. At present, such a process is not clear. Kaplan and Tsytovich (1968) showed that non-linear transfer of the plasma wave across the spectrum with a characteristic time much shorter than the plateau formation time is a possible mechanism for cutting off the continuous resonance interaction between the growing plasma wave and the stream electrons. According to this reference, in the case of excitation of plasma waves by electron streams, the plateau formation time τ_p is of the order of $1/\sigma\omega_p$ while the characteristic time for the non-linear transfer across the spectrum τ_n will be given by $v_T^i/\sigma\omega_p v$, where v is the velocity of the stream electron. Assuming that these characteristic times are also applicable to the case of excitation of plasma waves by electron streams in a magnetoactive plasma and $\sigma = 10^{-5}$,

$f_p \simeq 100$ MHz, $\beta_{\parallel} \simeq 0.2$, $\beta_T \simeq 10^{-2}$, we find $\tau_n \simeq 2\times10^{-5}$ sec and $\tau_p \simeq 10^{-3}$ sec. Thus, the plasma wave emitted by the individual electrons will grow at the linear growth rate in the stream-plasma system only within the time interval of the order of 10^{-5} sec during the onset of the excitation process.

Alternatively, it has been proposed that type III burst emission is the consequence of the enhanced bremsstrahlung in the medium comprising the thermal ambient plasma and a system of energetic electrons (Bekefi, 1966). However, a detailed and quantitative study of the type III burst emission based on this proposal has not been attempted and the interpretation of the type III burst emission on the basis of linear theory of radiative instability in the stream-plasma system provides a satisfactory approximation.

CHAPTER VII

THE ORIGIN OF DRIFT PAIR BURST AND HOOK BURST EMISSIONS FROM THE SOLAR CORONA

A. Introduction

The low frequency drift pair emission is a rarely occurring phenomenon which since its first discovery by Roberts (1958), was not reported again for about ten years. Maxwell pointed out that the drift pairs were only rarely seen on the Harvard spectral record (Maxwell, 1963). However, Ellis and McCulloch (1967) and Ellis (1969) recently reported that a large number of the drift pairs had been observed during the period 1966 to 1967. In addition to the drift pairs, hook bursts associated with drift pairs have also been discovered in spectral records in the frequency range from 28 MHz to 40 MHz (Ellis, 1969) (Fig. 7.1 (C)).

The drift pair is characterized by pair of traces starting almost at the same frequency but separated by a time about 1.5 to 2 sec in the dynamic spectrum (Fig. 7.1(A) and 7.1 (B)). Roberts (1958) and Zheleznyakov (1965) interpreted the drift pair as the consequence of the excitation of plasma waves by some distrubances travelling in the isotropic regular solar corona. The second trace is assumed to be the echo of the first, reflected at a lower level in the solar corona. Kundu (1965) and Zheleznyakov (1965) suggested that the

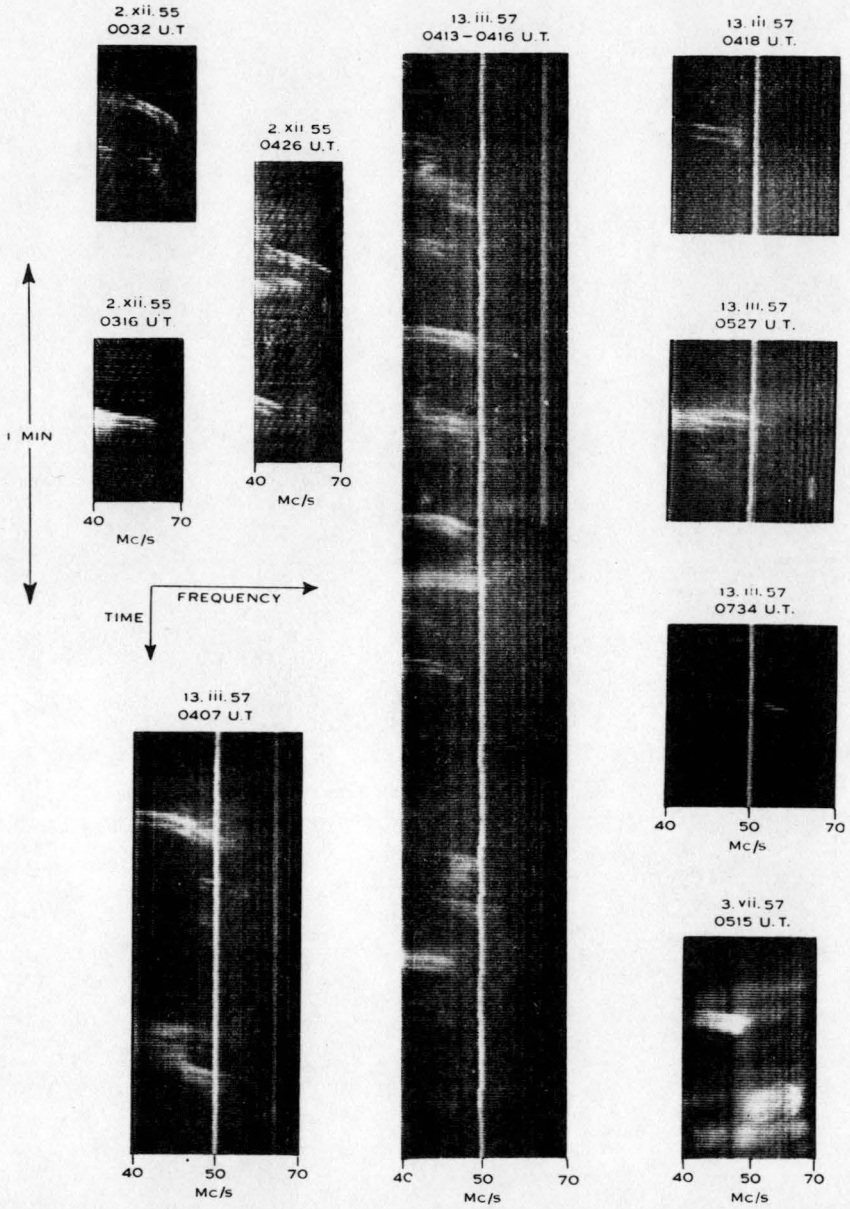

Reproductions of spectrum records showing double bursts with positive frequency drift (reverse drift pairs). Vertical features in these records are due to interfering signals or are instrumental and should be disregarded. The diagonal lines in the records of December 2, 1955 are produced by interference modulated at 100 c/s. (Roberts, 1958)

Fig. 7·1 A

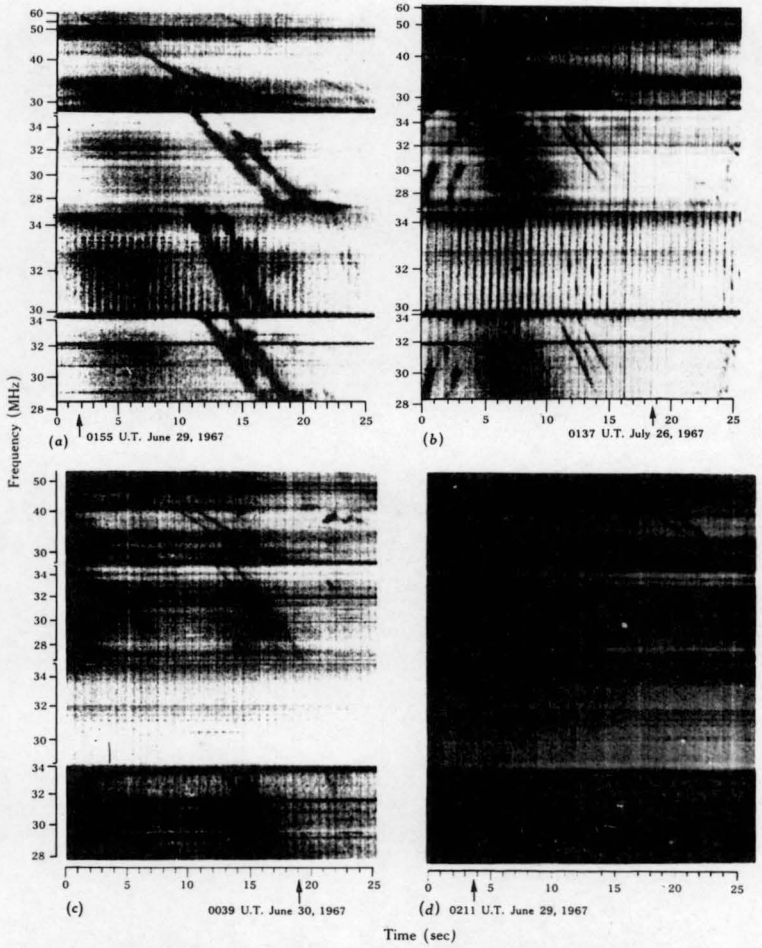

Fig. 7.1B Records of drift pairs: (*a*) drift pair with breaks in the two traces near 30 MHz showing a frequency shift in the second trace with respect to the first; (*b*) and (*c*) drift pairs with weak midpoint traces; (*d*) drift pair extending upwards in frequency to 60 MHz and showing an absence of a subharmonic trace near 30 MHz. A second drift pair on (*d*) also shows a weak midpoint trace.
(Ellis, 1969)

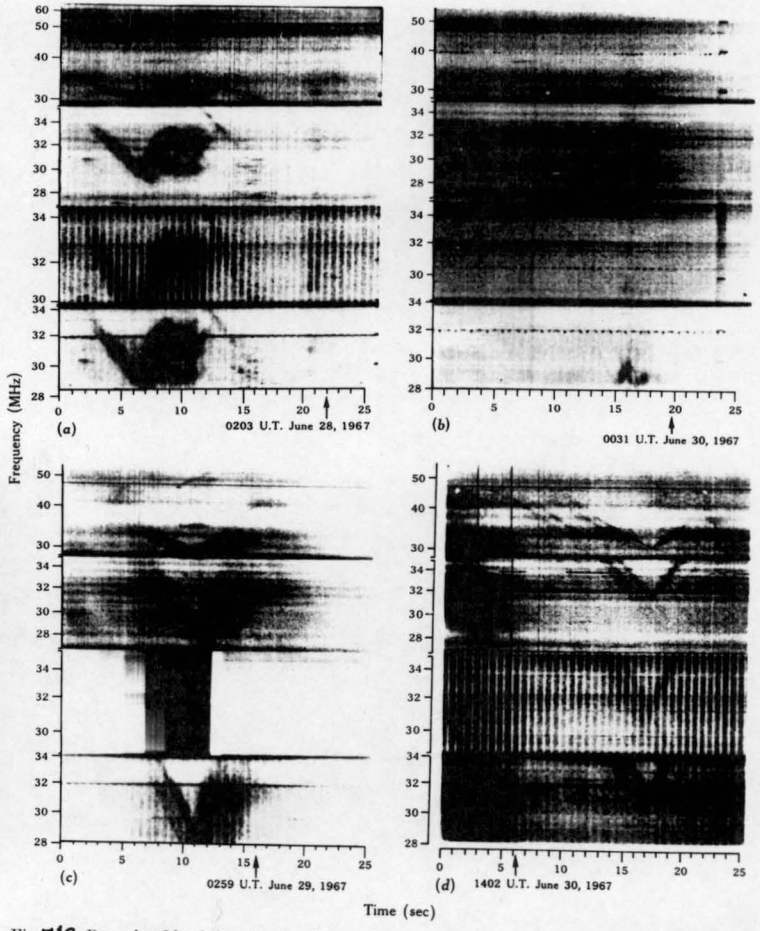

Fig. 7.1C Records of hook bursts. In (*b*) a weak drift pair apparently led to a double burst in which the second component did not appear as an echo of the first.
(Ellis, 1969)

particle streams, under favourable circumstance, excite plasma oscillations responsible for the drift pairs.

Although Roberts' theory qualitatively can explain several features of the bursts, quantitative agreement requires certain assumptions which so far have not been justified theoretically. At the same time, certain important spectral characteristics, particularly those pointed out by Ellis (1969), remain unexplained.

At present, there is no definite optical observational data of sunspot magnetic field intensity at the coronal height, particularly at the altitude about one solar radius above the photosphere. However, various theories of radio bursts emitted from the active solar corona suggest that there would be sunspot magnetic field of intensity about a few gauss at the altitude one solar radius above the sunspot group (see Fig. 4.2). Then, if one assumes the regular corona, the gyrofrequency at this altitude will be comparable with the plasma frequency and the effect of the magnetic field on the propagation and generation of electromagnetic waves can no longer be neglected. In fact, as we shall see later, some characteristics of the drift pair burst emission event cannot be well explained without the magnetic field taken into account. The hook bursts, which have spectral characteristics similar to those of the drift pairs and will probably be generated by the same process, indicate that the

exciting disturbances are guided by a bipolar sunspot magnetic field line of force. Therefore, in the present chapter, we shall consider the drift pair as the consequence of radiation of plasma waves by electron streams in the magnetoactive coronal plasma.

As we have seen in Chapter VI, the spectral characteristics of the plasma radiation depend on the nature of the ambient plasma as well as the character of the radiating electron stream. If both the type III burst emission and the drift pair burst emission are considered as the consequence of the excitation of plasma waves by electron streams in the solar corona, then the distinct spectral appearances of these two burst emissions reveal that the type III bursts and drift pair bursts are emitted by electron streams of different characters and under different corona conditions. Moreover, the fact that while type III bursts are the most common metre wavelength burst emission, that the drift pair burst emission is only a rarely occurring event clearly indicates that the electron streams responsible for these two emissions are of different origins. Therefore, in this chapter, we assume an active solar corona model and other parameters appropriate to the emission of the drift pair burst and hook burst in the solar corona to study the characteristics of the plasma radiation and hence discuss the possible origin of the energetic electrons responsible for the drift pair burst emission.

B. Observation Data (Roberts, 1958; Ellis, 1969)

(i) Frequency Range - Drift pairs and Hook bursts are low frequency events; most frequently appearing in the frequency range from 40 MHz extending to 25 MHz (Fig. 7.2(a)). In general, the frequency range of a single burst is only a few MHz to ten MHz. But some bursts can extend from 30 MHz to 60 MHz (Fig. 7.1 (8)).

(ii) Frequency Separation and Time Delay - The bursts are mostly double; the first element is followed about 1.5 to 2 sec later by a similar second element. The starting and terminating frequencies of the two elements are mostly the same (Fig. 7.2(b)). In some examples in which the beginning and the end of the traces are observed, the second trace was found to start and to terminate at slightly higher frequencies than the first trace (Fig. 7.1(B),b). In a few cases, the two elements start (or finish) at a similar time but at different frequencies; the starting (or finishing) frequency separation being 2 MHz to 4 MHz.

(iii) Frequency Drift Rate - The frequency-time slope of the drift pair observed by Roberts in the frequency range 50 MHz to 40 MHz was about 2 MHz per sec to 8 MHz per sec and was positive. The majority of the drift pairs observed by Ellis (1969) had a negative frequency drift at a low rate, about 1 MHz to 2 MHz per sec. The drift rate of the associated type III burst found in the drift pairs spectral

record is much higher than that of the drift pair (about 10 MHz/sec) (Fig. 7.2(c)).

(iv) Bandwidth - The instantaneous frequency bandwidth is only a fraction of a MHz and narrower than that of the type III burst. The histogram of the bandwidth of the drift pairs measured by Ellis shows that a large majority of drift pairs have bandwidths about 0.3 to 0.6 MHz (Fig. 7.2(d)).

(v) Burst Duration - The duration of each element can extend from a few seconds to ten seconds.

(vi) Intensity - The measured flux densities in one plane of polarization range from 5×10^{-21} W $m^{-2}Hz^{-1}$ up to 5×10^{-20} W $m^{-2}Hz^{-1}$. The two elements of a pair are similar in intensity.

(vii) Polarization - The drift pairs were found to be not significantly polarized.

(viii) Association with other types of Bursts - There is a tendency for the drift pairs to occur in noise storms which last for hours or days. In some cases, the drift pair occurs in the type III burst. The intensity of the associated type III burst is lower and diffuse. Recent observation showed that on some occasions split pair bursts occur during the period of drift pair emission activity. Besides these, no other type activities have been found related to drift pairs.

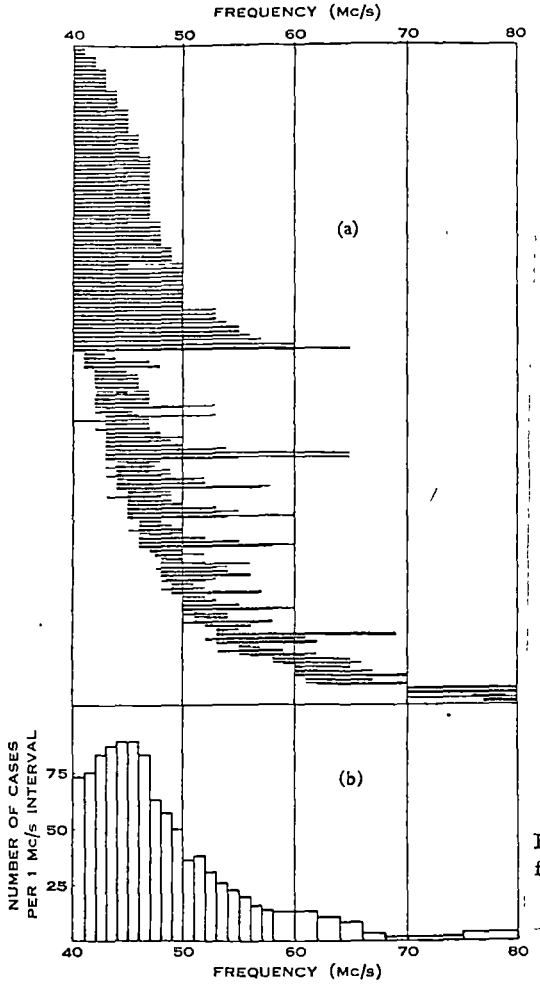

Fig. 7·2(a) To illustrate the range of frequencies covered by the reverse pairs. (*a*) Each reverse pair is represented by a pair of contiguous lines which show the frequency extent of the two elements of the burst. (*b*) Histogram showing the prevalence of bursts at different frequencies.
(Roberts, 1958)

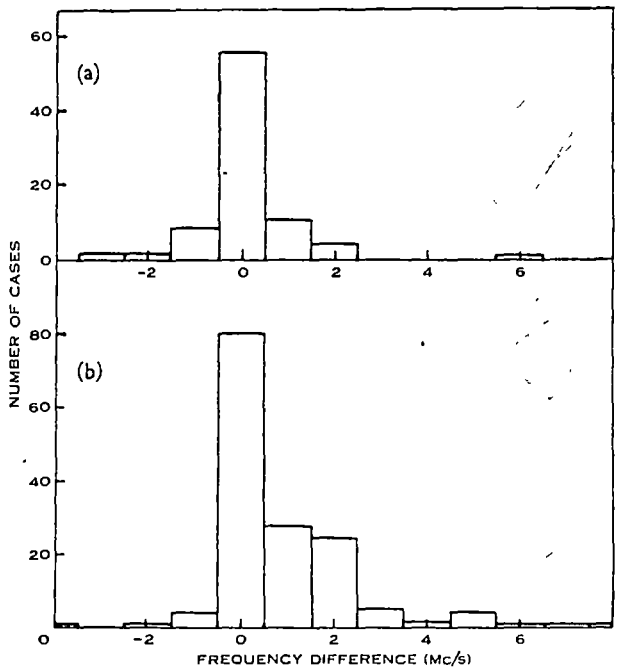

Fig. 7·2(b) Histograms showing the difference in (*a*) the starting frequency, and (*b*) the finishing frequency of the two elements of the observed reverse pairs. (Roberts, 1958)

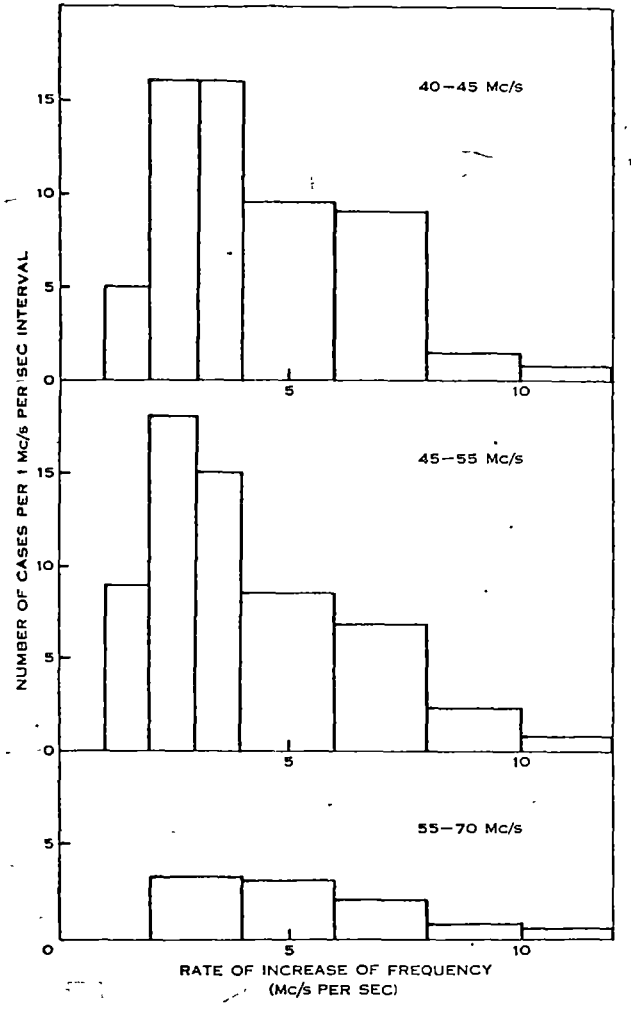

Fig. 7·2 c The rate of frequency drift in the reverse pairs.
(Roberts, 1958)

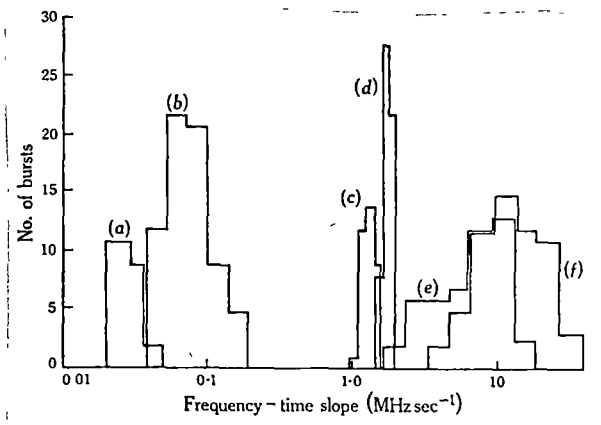

Fig. 7·2 C Distribution of frequency–time slopes for
(*a*) type II bursts,
(*b*) split pair bursts,
(*c*) drift pair bursts,
(*d*) fast drift storm bursts,
(*e*) type III bursts, and
(*f*) chains of split pair bursts.
(Ellis, 1969)

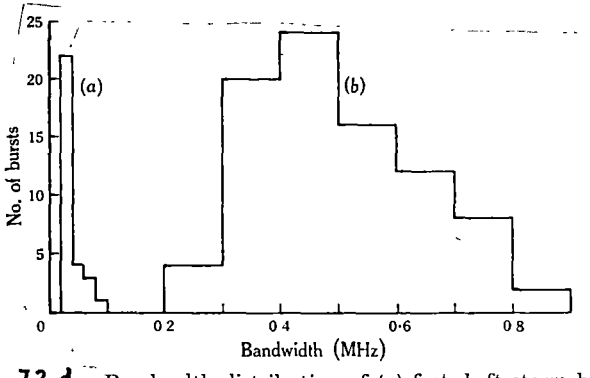

Fig. 7·2 d –Bandwidth distribution of (*a*) fast drift storm bursts and (*b*) drift pairs.
(Ellis, 1969)

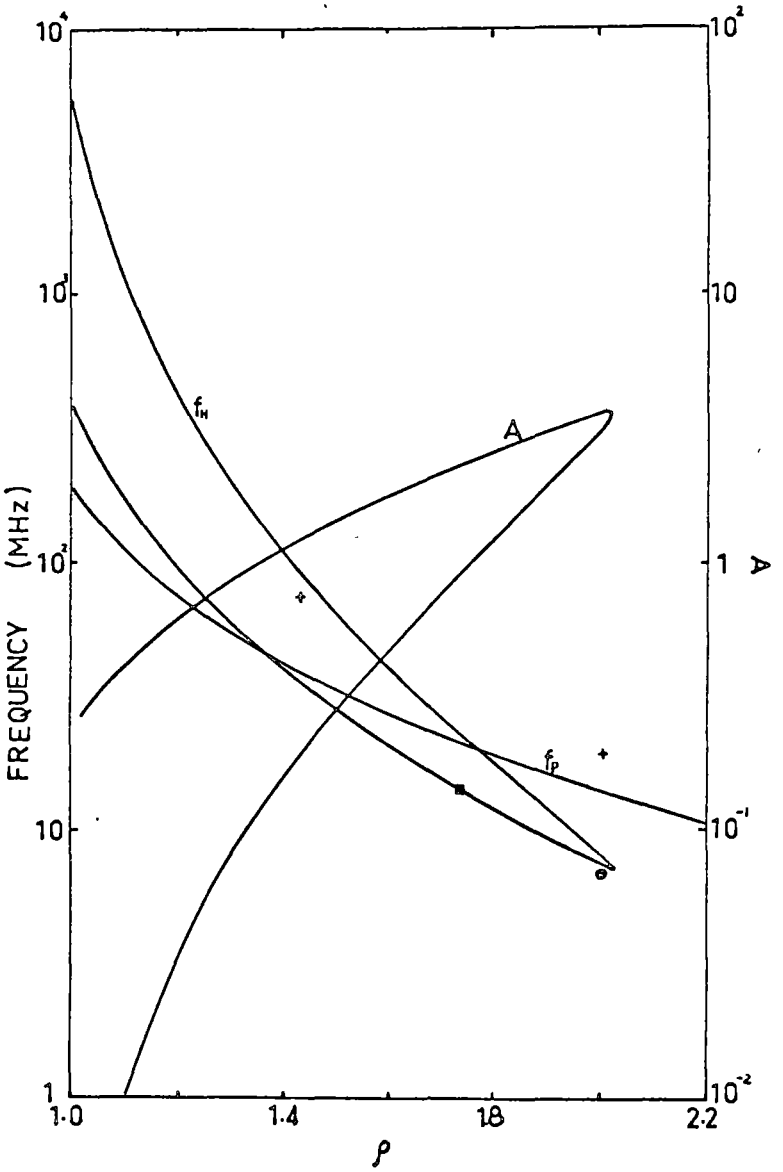

Fig.7.3 - Variation of the plasma frequency f_p (using the Baumbach-Allen model), gyrofrequency f_H and A along the strongest field line of a bipolar spot group specified by H_s = 2000 G. The magnetic field intensity in the solar corona (in term of gyrofrequency) inferred from theories of type II and type III radio bursts:
■ Morimoto (1963); ● Hatanaka (1966); + Tidman et al. (1966).

The hook bursts have a bandwidths and a drift rates similar to those of the drift pairs. The leading trace drifts downward to the turning point frequency and then drifts upward immediately to the starting frequency again. Thus the spectral appearance of the hook burst is analogous to the VLF hook occurring in the Earth's magnetosphere (Fig. 7.1 (C)).

C. Model of The Solar Corona

The drift pair burst consists of a pair of smooth continuous traces. If the second trace is considered as the echo of the radio emission from the corona, the solar corona must be in a fairly stationary and regular condition. Hence, we assume during the period of drift pair burst emission the electron density distribution along the solar corona is given by Baumbach-Allen's model (4.1). We further assume that two narrow magnetic flux tubes emerging from the leading and the following sunspots connect together forming an arch in the solar corona. The central field line of the magnetic flux tube is assumed to be of greatest intensity. With these assumptions, we propose a model of the active solar corona during the drift pair burst emission period as shown in Fig. 7.3 where the electron density and the intensity of the magnetic field along the strongest bipolar field line (in terms of plasma frequency and gyrofrequency respectively) are plotted against the radial distance from the centre of the Sun.

Similarly, a unipolar sunspot magnetic field configuration given by Fig. 4.5(a) is also assumed. From these models, the quantity A never exceeds four for $\rho \leq 2.0$.

D. Radiation of Plasma Waves by an Electron Stream moving in the Solar Corona

Now we assume an electron stream with small dispersion in momentum components moves along the strongest sunspot magnetic field line and generates coherent Cerenkov plasma waves. The kinetic energy of the radiating electron is taken to be of the order of ten keV. During the initial stage of the excitation process, the angular power spectrum of the weakly damped Cerenkov plasma waves emitted by a single electron and the rate of growth $\left| \text{Im} \frac{\delta}{\omega_H} \right|$ for the Cerenkov plasma wave in the stream-plasma system are given by (2.13) and (2.28) respectively and illustrated as functions of the wave-normal angle for $\xi > 1$ and $\xi < 1$ in Fig. 7.4(a),(b), where $\beta_\perp = 0, 0.2$, $\beta_{||} = 0.1, 0.2, 0.3$, $A = 2$, $\beta_T = 10^{-2}$, $\sigma = 10^{-4}$ and $f_H = 10$ MHz. Taking the interaction time $t = 2.1 \times 10^{-5}$ sec* and $\sigma = 10^{-5}$, we show the variation of the power gain (in decibels) with the normalized wave frequency in Fig. 7.4(c) for the weakly damped

---

* We assume that the interaction time is approximately equal to the characteristic time for non-linear transfer of the plasma wave across the spectrum (see Section G (10)).

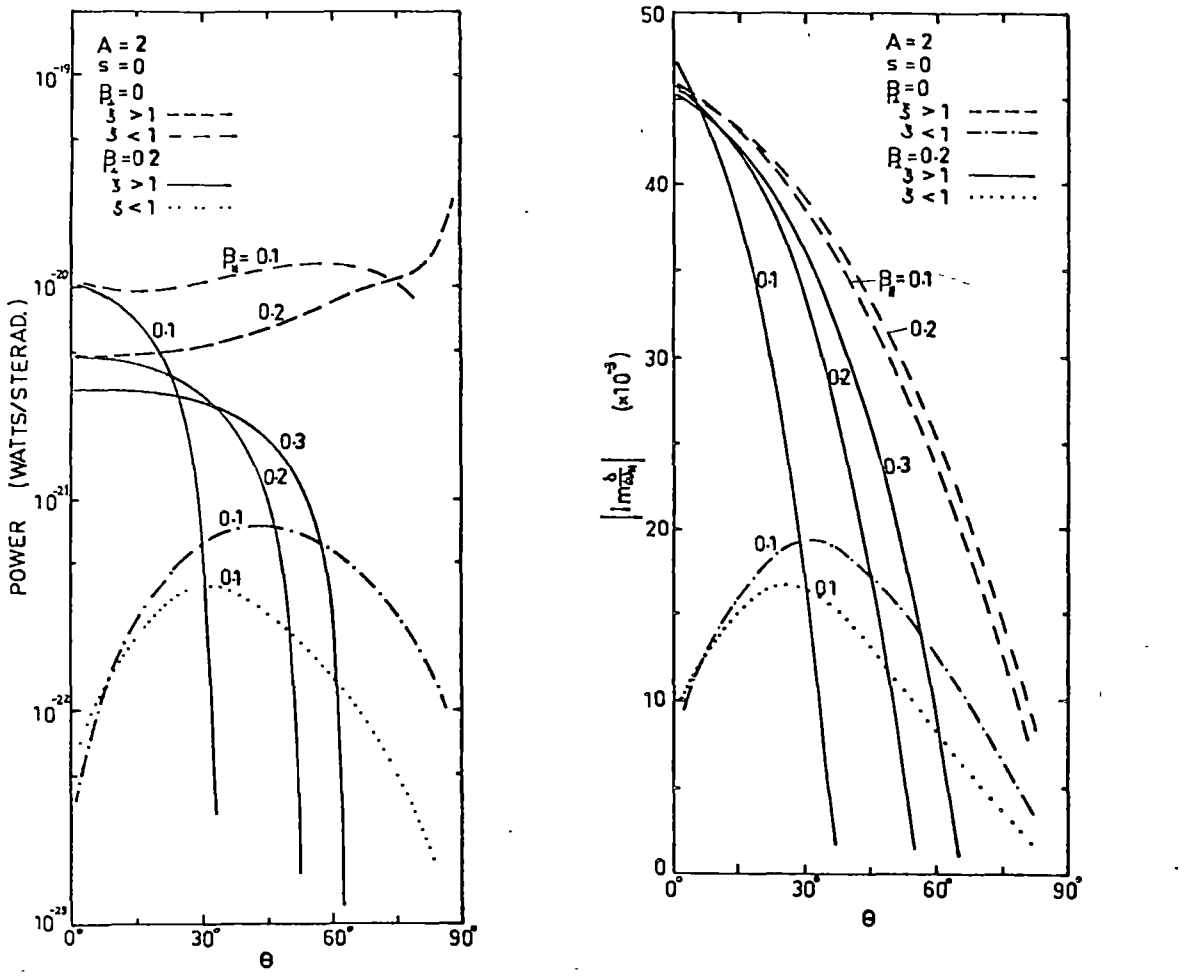

Fig.7.4 - (a) The angular Cerenkov plasma wave power spectra radiated by a single electron;
(b) The growth rate $\left|\mathrm{Im}\frac{\delta}{\omega_H}\right|$ as a function of wave-normal angle θ;
for f = 10 MHz, $\beta_T = 10^{-2}$, A = 2, $\sigma = 10^{-4}$, $\beta_\parallel$ = 0.1, 0.2, 0.3, $\beta_\perp$ = 0 (dashed curve for $\xi > 1$ and dashed-dotted curve for $\xi < 1$) and $\beta_\perp$ = 0.2 (solid curve for $\xi > 1$ and dotted curve for $\xi < 1$).

Cerenkov plasma waves. The intensity of the coherent Cerenkov plasma wave is beamed in the direction along the magnetic field line and at the frequency near the plasma frequency no matter whether $A < 1$ or $A > 1$ (see Fig. 2.6 also). The broadness of the cone of emission and the frequency bandwidth of the coherent Cerenkov plasma wave are inversely proportional to the electron pitch angle.

E. Transformation of Plasma Waves in A Magnetoactive Plasma

According to the discussion given in Section B of Chapter V, it is not difficult to see that the radio bursts consisting of pair of traces, starting at similar frequencies but separated by a time of the order of a second, cannot be due to the transformation of plasma waves by wave-mode coupling. Only the transformation of plasma waves by scattering on small-scale thermal fluctuations in the solar corona should be considered.

The Cerenkov plasma wave can be transformed into electromagnetic waves at the frequencies $f \simeq f_p$ and $f \simeq f_o + \tilde{f}_{\pm}$ (where f_o is the Cerenkov plasma wave frequency and $\tilde{f}_{\pm}$ are the plasma resonance frequencies) by means of incoherent scattering and combination scattering respectively. However, if the solar corona models Fig. 7.3 and Fig. 4.5(a) (for $\rho \leq 2.0$) are assumed as the regions where the drift pair burst emissions occur, the harmonic resonance absorptions at the layers

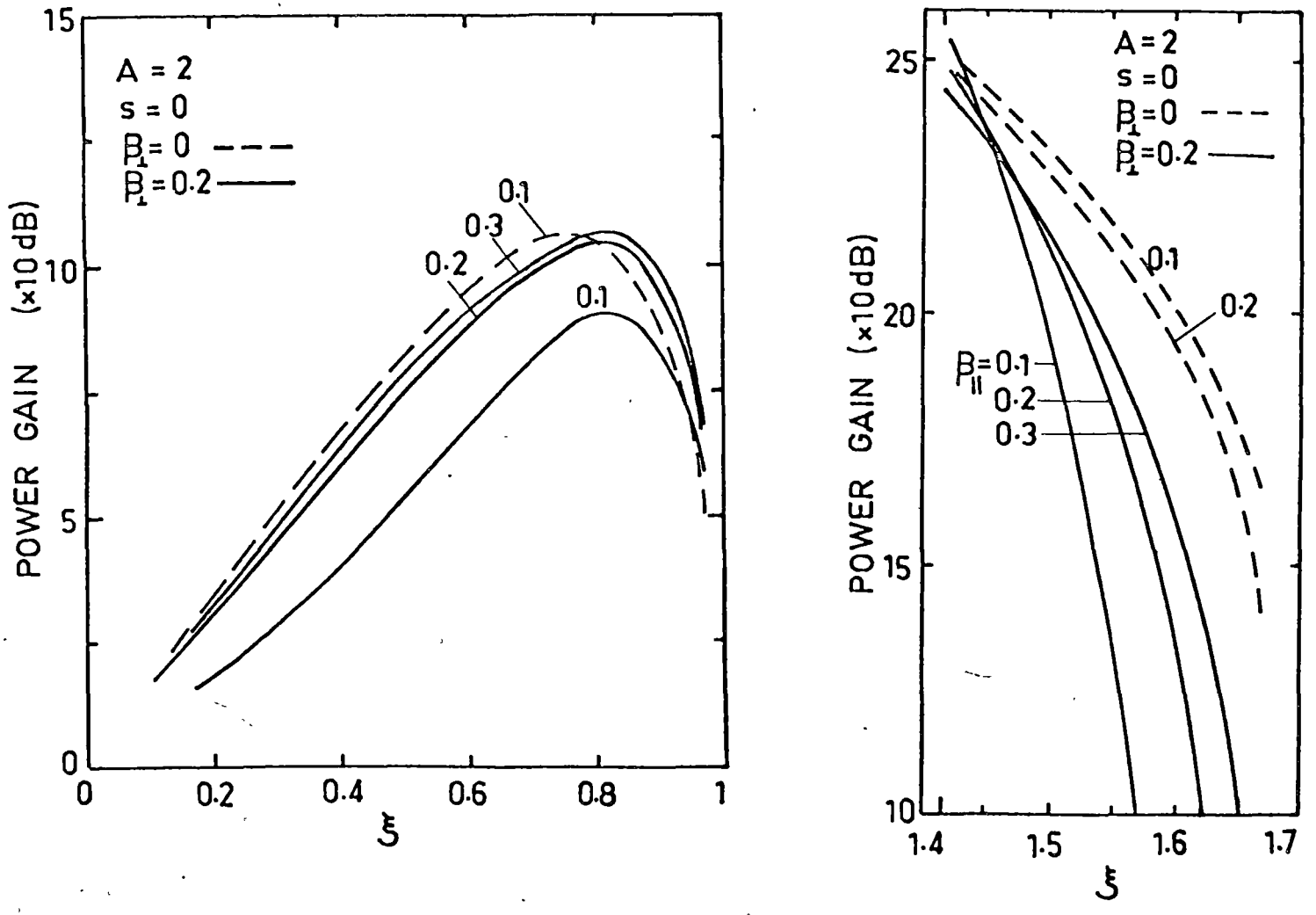

Fig.7.4(c)- Power gain versus wave normalized frequency ξ for f_H= 10 MHz, $\beta_T = 10^{-2}$, $\sigma = 10^{-5}$, interaction time t = 2.1×10^{-5} sec, s = 0, A = 2, $\beta_\parallel$= 0.1, 0.2, 0.3, $\beta_\perp$= 0 (dashed curve) and $\beta_\perp$= 0.2 (solid curve).

$f = sf_H$ ($s = 1,2,3$) prevent the transformed electromagnetic radiation at the frequency $f \simeq f_p$ escaping from the solar corona (cf. Chapter VI(D) and Fig. 6.5). Hence we confine ourselves to the consideration of transformation of Cerenkov plasma waves by combination scattering only.

The normalized combination frequency arising from scattering of the Cerenkov plasma wave emitted in the direction $\theta_o \simeq 0$ is given by

$$\xi = \tilde{\xi}_o + \tilde{\xi}_{\pm} \simeq A^{\frac{1}{2}}(1 + 3\beta_T^2/\beta_{||}^2)^{\frac{1}{2}} + \tilde{\xi}_{\pm} \quad . \tag{7.1}$$

So the combination frequency depends not only on the electron translational speed but also on the mean thermal speed of the plasma electrons. This is demonstrated in Fig. 7.5 in which $A = 2$, $\beta_T = \sqrt{3}x10^{-2}$, and the normalized combination frequency $\xi = \xi_o + \tilde{\xi}_+$ of the o-mode wave is plotted as a function of wave-normal angle θ for the ratio $r = \beta_T/\beta_{||} = 0.0865, 0.1732, 0.22$. We find that when r is large, (i.e. $\beta_{||}$ is small), the combination radiation is emitted at slightly higher frequencies in the backward direction than in the forward direction with respect to the electron guiding centre's motion.

Furthermore, we note that the Cerenkov plasma wave emitted at a single frequency f_o and at the wave-normal angle θ_o will be transformed into the x-mode and the o-mode waves at similar combination frequencies in various directions

(see Fig. 5.5). As a result, the observed frequency bandwidth of the combination radiation generated at a point in the solar corona depends on the bandwidth of the Cerenkov plasma wave spectrum excited by the electron stream.

We have mentioned in Chapter VI that in a magnetoactive plasma the Cerenkov plasma waves can be transformed into electromagnetic waves at the frequencies $f \simeq f_o + \tilde{f}_+$ and $f \simeq f_o + \tilde{f}_-$ concurrently when the scattering medium is characterized by a value of A less than four. Hence, it is expected that two pairs of normal traces, having starting frequencies $f_o + \tilde{f}_+$ and $f_o + \tilde{f}_-$ respectively, would appear in the dynamic spectrum simultaneously. However, so far such double pairs of bursts were not observed. We require to investigate the efficiencies of transformation of the Cerenkov plasma waves into electromagnetic waves at these frequencies so that we can determine which of the two pairs of bursts will correspond to the observed drift pair burst and hence to evaluate the delay time between the two elements of a pair.

For A = 2, f_H = 10 MHz , linear size of the scattering volume L = 10^9cm, $\beta_T = 10^{-2}$, $\beta_{||} = 0.1$ and for $\theta_o = 0^o$, 10^o, 20^o, cos $\psi = \pm 1$, the variations of the coefficients of transformation of the Cerenkov plasma waves into electromagnetic waves in the x-mode and the o-mode at frequencies $f \simeq f_o + \tilde{f}_\pm$

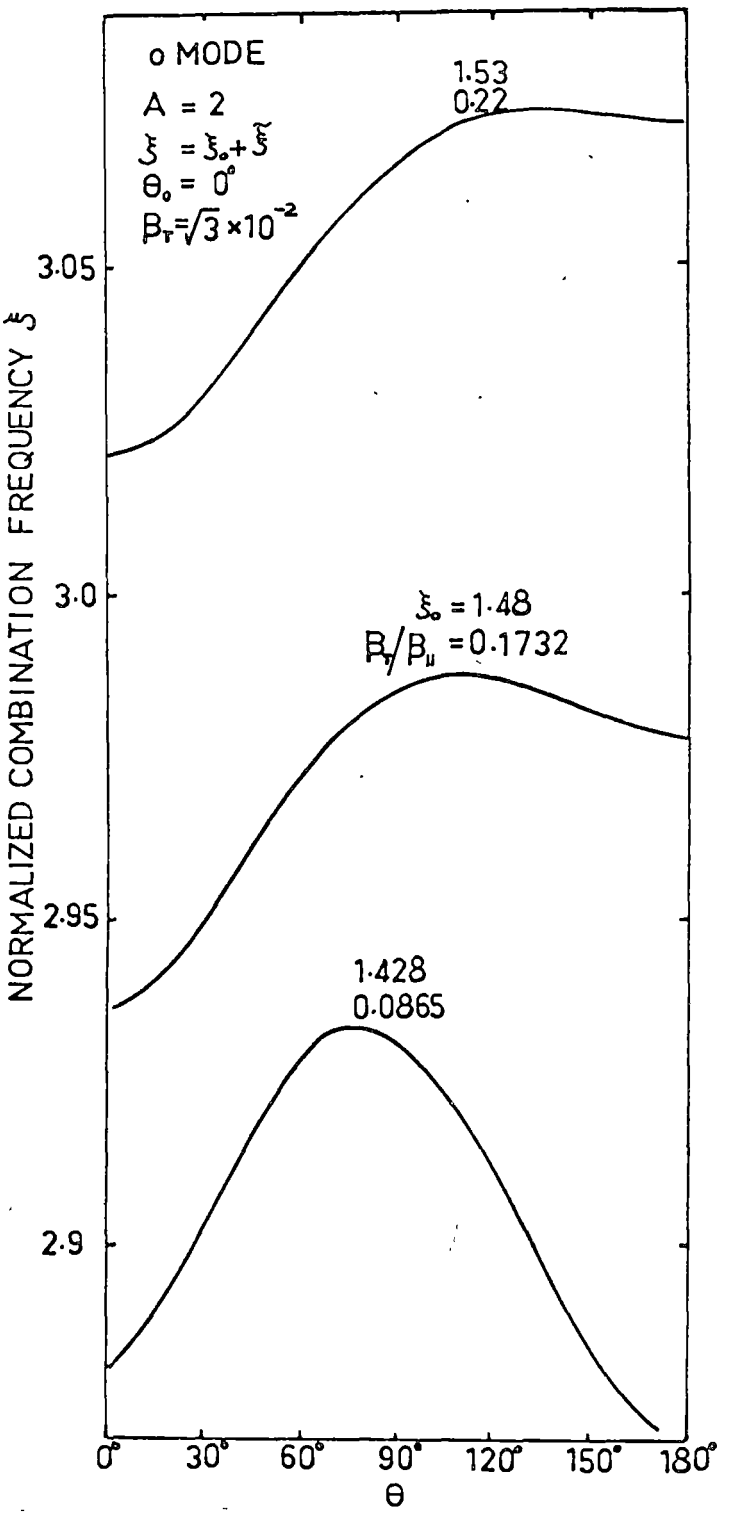

Fig.7.5 - The dependence of the normalized combination frequency $\xi \simeq \xi_0 + \tilde{\xi}_+$ on wave-normal angle θ of the combination radiation in the o-mode for A = 2, the ratio $r = \beta_T/\beta_{II} = 0.22, 0.1732, 0.0865$ and $\beta_T = \sqrt{3} \times 10^{-2}$. ξ_0 is the normalized frequency of the Cerenkov plasma wave emitted at the wave-normal angle $\theta_0 = 0$ by electron stream moving with β_{II}.

by combination scattering on fluctuations of electron density (expression (5.41)) with wave-normal angle θ are shown in Fig. 7.6(a) - (c). Fig. 7.6(d) illustrates the effect of the thermal motion of the plasma electron on the polar diagram of the combination radiation.

Before we examine the characteristics of the curves in Fig. 7.6, we should recall that the Cerenkov plasma wave emitted in the direction close to the static magnetic field line carries most of the energy emitted by the electron stream (Fig. 7.4). Then the combination radiations arising from transformation of the Cerenkov plasma wave with wave-normal angle lying within the range from 0^{o} to 10^{o} have greatest intensity. Now, from Fig. 7.6, we can realize that

(1) Even in the presence of the static magnetic field in the plasma, the combination radiation is also mainly emitted at the frequency $f \simeq 2f_p$ since the intensity of the combination radiation at the frequency $f \simeq f_o + \tilde{f}_-$ is very small in comparison with that at the second harmonic of the plasma frequency. When $\beta_{//}$ is small, the frequency of the combination radiation emitted in the backward hemisphere with respect to the electron guiding centre motion is slightly higher than that in the forward hemisphere (Fig. 7.5).

(2) In general, the flux density of the combination radiation in the o-mode is stronger than that in the x-mode.

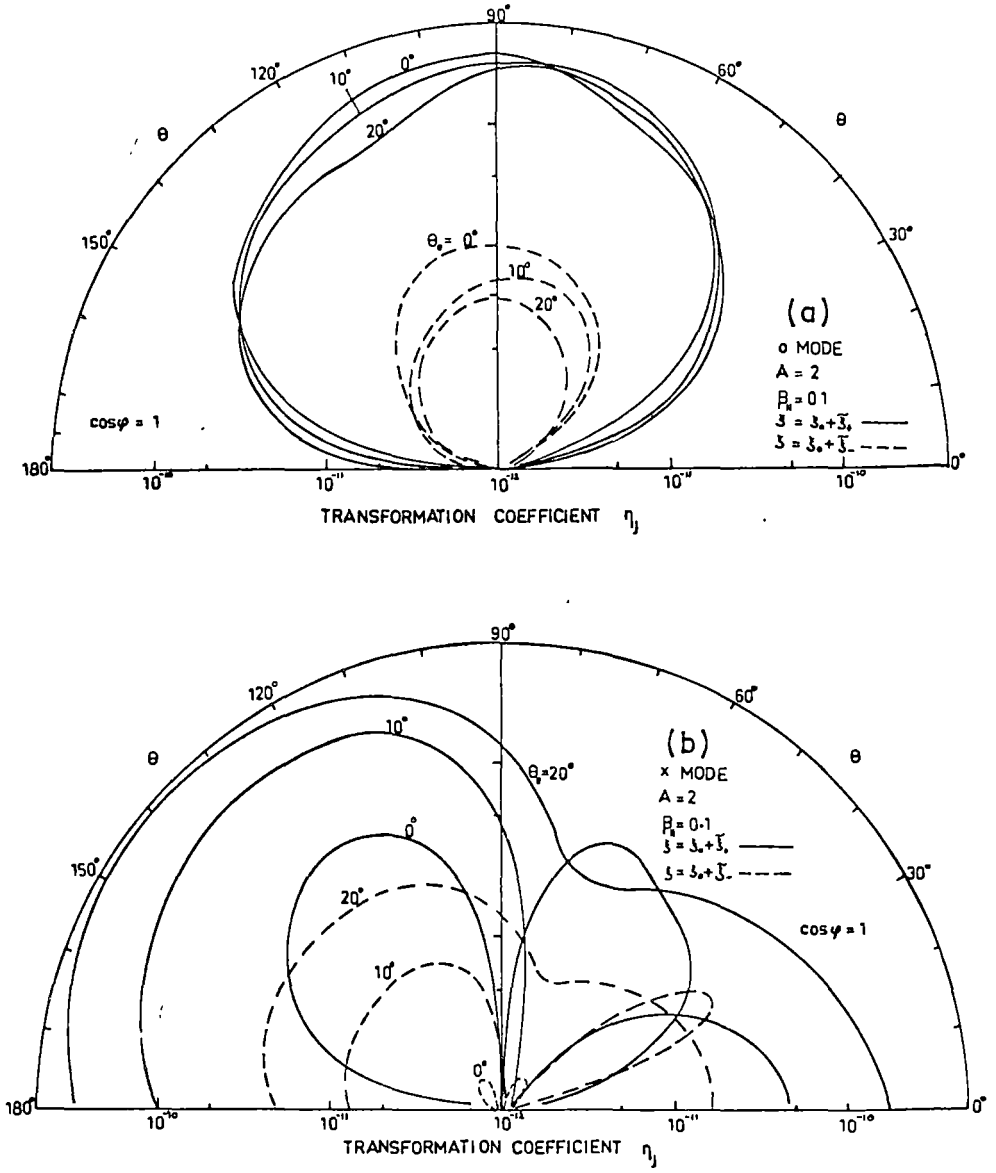

Fig.7.6 - Coefficient of transformation of the Cerenkov plasma wave into electromagnetic waves with normalized frequency ξ by combination scattering as a function of wave-normal θ of the combination radiation for f_H = 10 MHz, linear size of the scattering volume L = 10^9 cm, $\beta_T = 10^{-2}$, A = 2 and for

(a) o-mode, $\cos\varphi = 1$, solid line for $\xi \simeq \xi_o + \tilde{\xi}_+$ and dashed line for $\xi \simeq \xi_o + \tilde{\xi}_-$;

(b) x-mode, $\cos\varphi = 1$, solid line for $\xi \simeq \xi_o + \tilde{\xi}_+$ and dashed line for $\xi \simeq \xi_o + \tilde{\xi}_-$.

The number on each curve is the wave-normal angle θ_o of the Cerenkov plasma wave excited by electron stream with $\beta_{\parallel} = 0.1$.

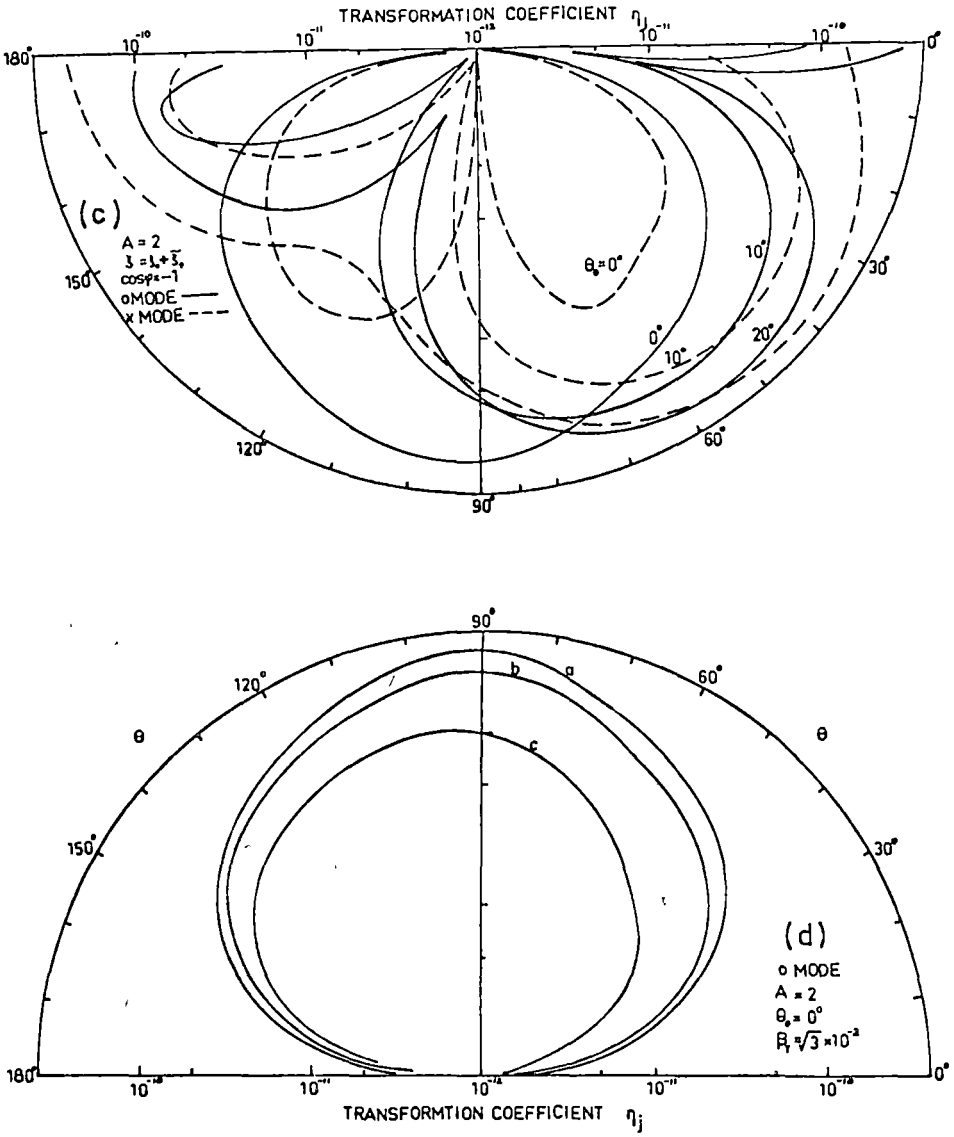

Fig.7.6 - Coefficient of transformation of the Cerenkov plasma wave into electromagnetic waves with normalized frequency ξ by combination scattering as a function of wave-normal angle θ of the combination radiation for $f_H = 10$ MHz, linear size of the scattering volume $L = 10^9$ cm, $\beta_T = 10^{-2}$, A = 2 and for

(c) o-mode (solid line) and x-mode (dashed line) at the normalized frequency $\xi \approx \xi_0 + \tilde{\xi}_+$ and $\cos\varphi = -1$: (The number on each curve is the wave-normal angle θ_0 of the Cerenkov plasma wave excited by electron stream with $\beta_{II} = 0.1$.)

(d) o-mode, $\theta_0 = 0$, $\beta_T = \sqrt{3} \times 10^{-2}$, $\xi \approx \xi_0 + \tilde{\xi}_+$ and for $\cos\varphi = 1$, a. $r = \beta_T/\beta_{II} = 0.22$; b. $r = 0.1732$; c. $r = 0.0865$.

(3) The frequency bandwidth as well as the emission cone of the combination radiation is broader when the electron pitch angle is small. The axis of the cone of emission of the combination radiation in the o-mode is transverse to the static magnetic field.

F. Propagation of The Electromagnetic Radiation in The Solar Corona

In the presence of the static magnetic field in the plasma, the extraordinary and ordinary wave packets propagate along the paths different from their phase paths and with different group velocities. Moreover, for normal penetration, the x-mode and the o-mode waves will be reflected at the layers where $X = 1 - Y$ and $X = 1$ respectively. However, as the magnetic field intensity is very weak, with $f_p >> f_H$ (or $A >> 1$), the x-mode and the o-mode waves are both reflected from the level $X = 1$ and the wave groups of both modes propagate along their phase paths. Since we assume only a narrow magnetic flux tube can extend from the umbra of the sunspot at the photosphere to the outer layers of the solar corona, reflection of the x-mode and the o-mode waves would take place in the region where the effect of the magnetic field can be neglected. Hence, in general, omission of the sunspot magnetic field would not lead to significant error in the estimations of the ray path and the wave group travelling

time. In this section we shall consider the ray paths, wave group travelling times and collisional absorptions of the cc ɔination radiations at the frequency $f \simeq 2f_p$ in the isotropic solar corona.

a. Ray Paths of The Combination Radiations in the Solar Corona

According to Jaeger and Westfold (1950), the Snell's law for a ray propagating in the spherically symmetrical isotropic coronal plasma is written as

$$n \rho \sin i = a = \text{constant}, \qquad (7.2)$$

where i is the incident angle, i.e. angle between the ray direction and the radial line (Fig. 7.7) and defined in the range $0 \leq i \leq \pi/2$, $n(\rho)$ is the refractive index for the wave at a point at a distance ρ(in units of solar radius) from the centre of the Sun and given by

$$n^2(\rho) = 1 - 8.1\times10^3 \ (1.55\rho^{-6} + 2.99\rho^{-16})/f^2, \ (f \text{ in MHz}). \qquad (7.3)$$

The constant parameter a in (7.2) specifies the separation between the ray path and the Sun-Earth line at infinite distance. A ray of frequency f emitted in the direction towards the Sun from a source will be reflected at a lower layer where the incident angle i becomes 90^o. From (7.2)

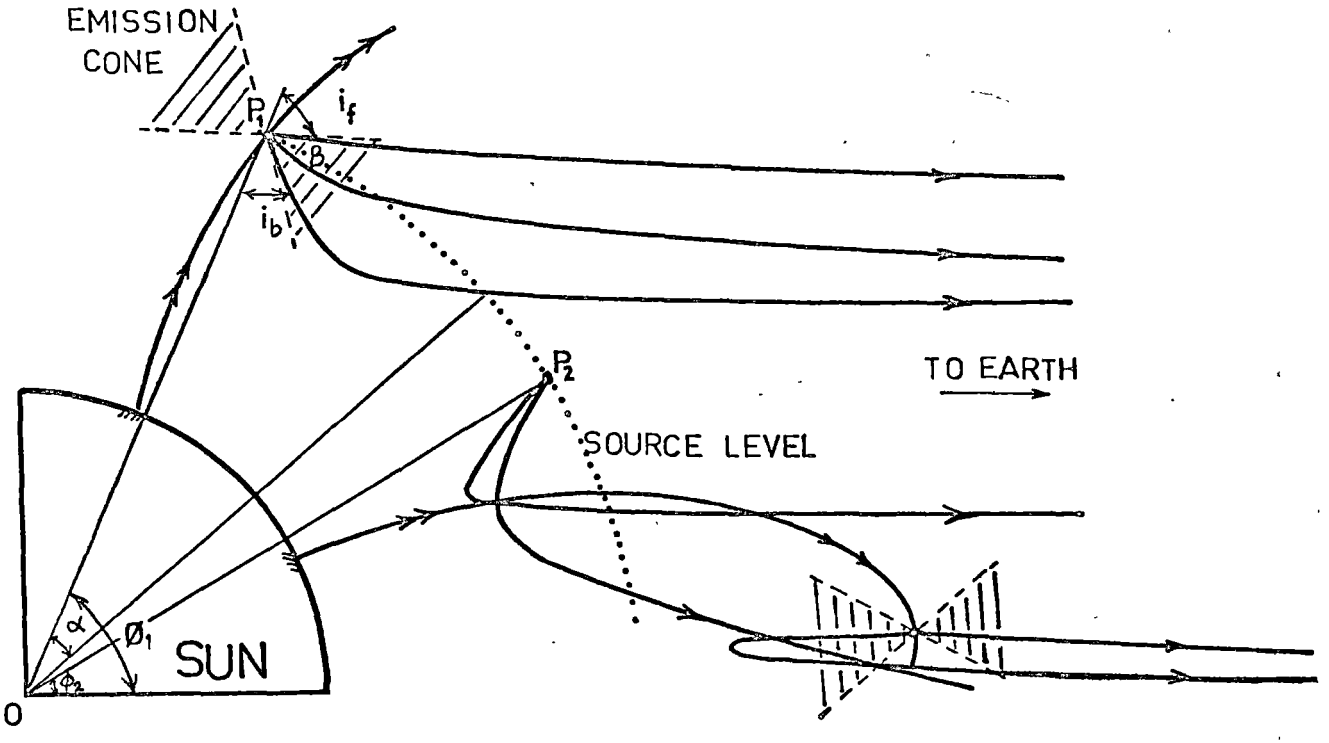

Fig.7.7 - Forward and backward ray paths in the regular solar corona for radiations with frequency f = 30 MHz and emitted at the points P_1 and P_2. The wave frequency f is assumed to be about double the local plasma frequency at the point P_1 (or P_2). The forward and backward rays emitted from a central source are also illustrated.

and (7.3), if ρ_s is the position of a source on the radial line, the reflection height ρ_o will be given by the root of the equation,

$$\rho^2 \left[1 - 8.1\text{x}10^3(1.55\rho^{-6}+2.99\rho^{-16})/f^2\right] - a^2 = 0, \quad (7.4)$$

with $a = n(\rho_s)\rho_s \sin i_s$, i_s being the incident angle at the source level. The angle subtended at the centre of the Sun by the ray path below the source level α, (which we shall call the central angle), is given by

$$\alpha = 2a \int_{\rho_o}^{\rho_s} \frac{d\rho}{\rho(n^2\rho^2-a^2)^{\frac{1}{2}}} \quad . \quad (7.5)$$

Any backward ray ($i_s \neq 0$) will subtend a non-zero central angle at the centre of the Sun while the forward ray will never cross the source level again after being emitted. When the refraction effect is omitted, the incident angles of the backward ray and the forward ray at the source level i_b, i_f, the central angle α and the source latitude ϕ are related by

$$i_b + \alpha = \phi \simeq i_f \quad . \quad (7.6)$$

Correspondingly, the constant parameters for the forward and the backward rays emitted from the same source at the position (ρ_s,ϕ) will be

$$a = n(\rho_s)\ \rho_s \sin\phi \qquad \text{(forward)},$$
$$b = n(\rho_s)\ \rho_s \sin i_b \qquad \text{(backward)}. \tag{7.7}$$

Assuming $f = 2.1\ f_p$, we show the variations of the reflection height ρ_o, constant parameters a,b, central angle α and the incident angle of the backward ray i_b with the source latitude for f = 30 MHz and 51 MHz in Fig. 7.8 and Fig. 7.9. In the limiting source latitude ϕ_m, the forward and the backward rays are identical. The central angle reaches its maximum α_m at $\phi \simeq 70^\circ (i_b \simeq 45^\circ)$ and then decreases quickly to zero at the limiting source latitude. In Fig. 7.9, the absolute angular separation between the forward and the backward rays at the source position, β, is defined by

$$\beta = \cos^{-1} \left| \cos \bar{\kappa}_f \hat{\bar{\kappa}}_b \right| ,$$

where $\bar{\kappa}_f$ and $\bar{\kappa}_b$ are the unit vectors along the forward and the backward rays and $\bar{\kappa}_f \hat{\bar{\kappa}}_b$ is the angle between $\bar{\kappa}_f$ and $\bar{\kappa}_b$.

So far we have neglected the refraction of the forward ray paths. The refraction of the ray path is insignificant for a central ray but becomes noticable for a ray emitted from a limb source (see expression (7.2)).

b. Convergence of Rays emitted from A Single Source

In order that both the forward and the backward radiations can be seen on the Earth, the backward radiation

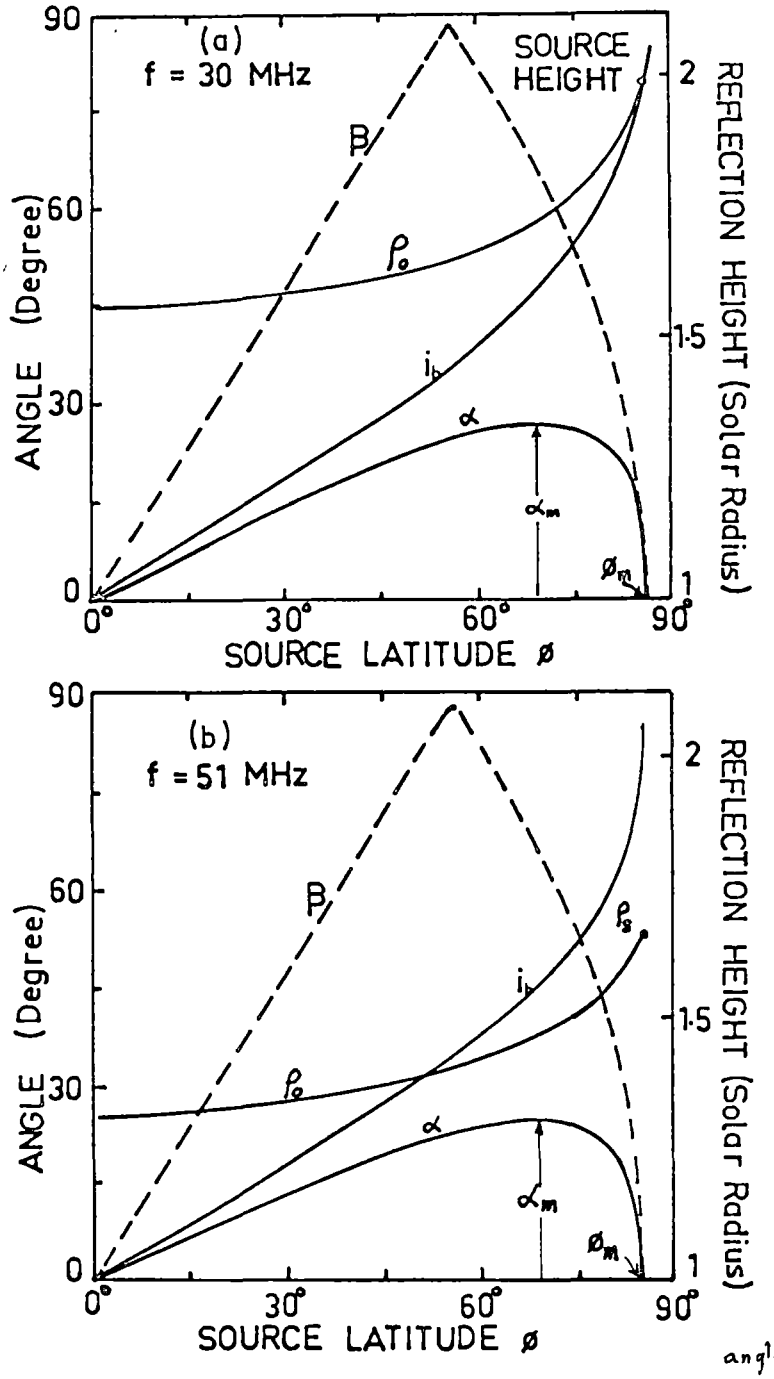

angle

Fig.7.8 - Variation of the initial incident of the backward ray i_b, reflection height ρ_o, central angle α and the absolute initial angular separation between the forward and the backward rays β with source latitude ϕ in a Baumbach-Allen model corona for (a) f = 30 MHz; (b) f = 51 MHz.

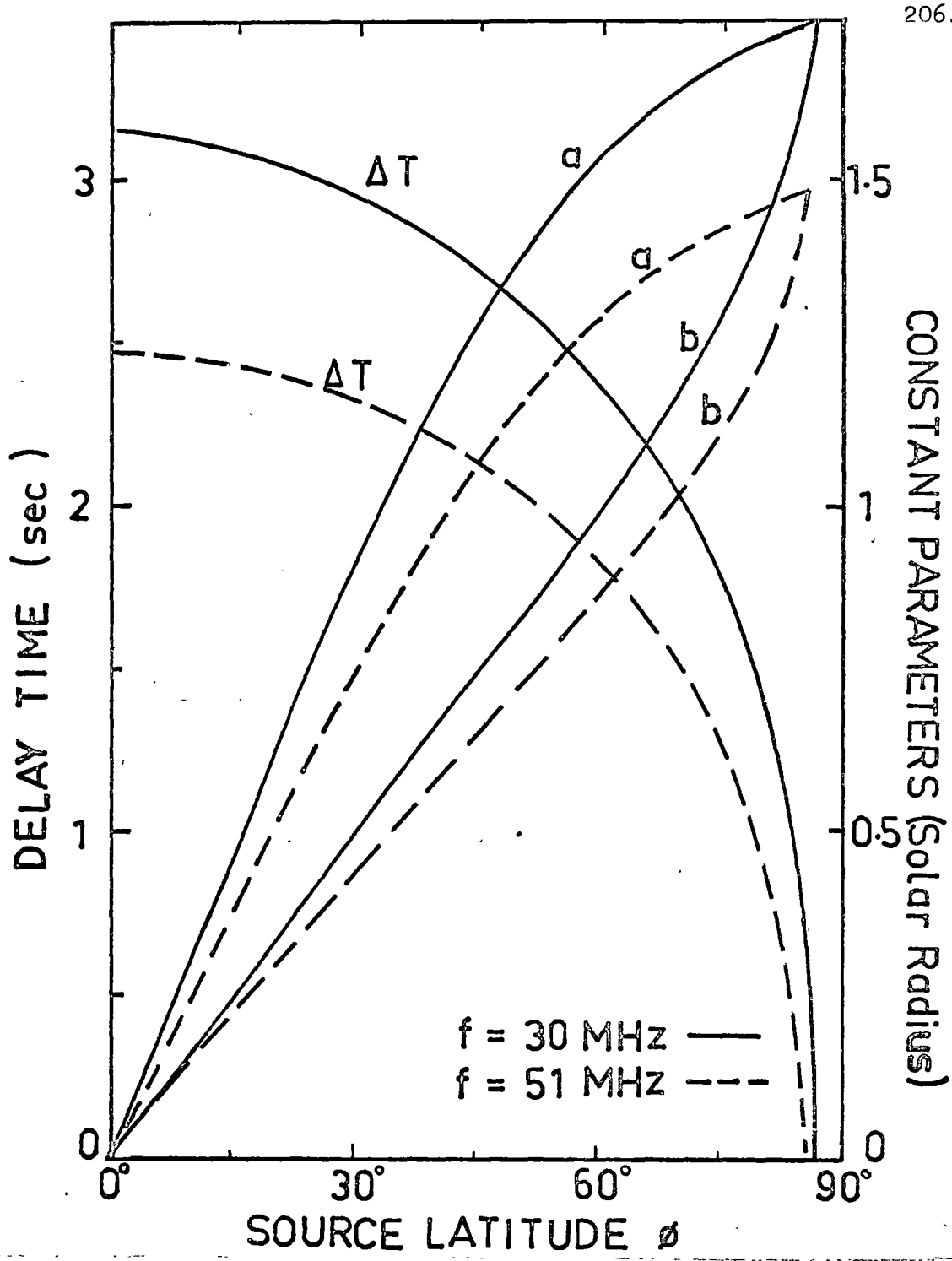

Fig.7.9 - Wave group delay time between the forward and backward combination radiations versus source latitude ø for frequencies 30 MHz (solid line) and 51 MHz (dashed line). The constant parameters (in units of solar radius) a,b for the forward and backward rays are also plotted as functions of source latitude.

must be emitted in a particular direction depending on the source latitude such that its ray path meets the forward ray at the Earth. Owing to the refraction, the actual incident angle of the forward ray i_f has to be slightly greater than the source latitude given by (7.6).

While the ray paths of the forward radiations emitted from a single source will never cross each other, the ray paths of the backward radiations at the same frequency will cross each other either above or below the source level after they have been reflected from a lower level. From Fig. 7.8, we can see that two backward rays will cross each other above the source level when the source latitude is large (Fig. 7.7). Due to the differential refraction of the ray paths with different initial incident angles, two backward rays would meet at very large distance from the Sun.

c. Wave Group Travelling Time

In order to investigate the possible time delay between the forward and the backward radiations emitted from a single source and the time delay between the radiations at different frequencies emitted at different layers, we have to calculate the time taken for the wave packet to travel from the source to the observer. For an isotropic coronal plasma, the time taken by a wave packet to travel along the trajectory is

$$t_g = \int \frac{ds}{v_g} ,$$

where $v_g = cn$ is the wave group velocity. Making use of the relation

$$\frac{ds}{d\rho} = n\rho/(n^2\rho^2 - a^2)^{\frac{1}{2}} \quad ,$$

the wave group travelling time can be expressed as an integral of a function of the distance from the centre of the Sun,

$$t_g = 2.316 \int_{\rho_s}^{\rho} \frac{\rho d\rho}{(n^2\rho^2 - a^2)^{\frac{1}{2}}} \quad \text{(sec)}. \qquad (7.8)$$

The delay time between the forward and the backward combination radiations at the frequency $f \simeq 2.1\ f_p$ and emitted from a source at the poisition (ρ_s, ϕ) will be

$$\Delta T \simeq 2.316 \left[2 \int_{\rho_o}^{\rho_s} \frac{\rho d\rho}{(n^2\rho^2 - b^2)^{\frac{1}{2}}} + \int_{\rho_s}^{\rho_E} \frac{\rho d\rho}{(n^2\rho^2 - b^2)^{\frac{1}{2}}} - \int_{\rho_s}^{\rho_E} \frac{\rho d\rho}{(n^2\rho^2 - a^2)^{\frac{1}{2}}} \right] \text{(sec)}. \qquad (7.9)$$

Here, a,b are the constant parameters for the forward and the backward rays and determined by (7.7) and ρ_E is the Sun-Earth distance. The variation of the time delay between the two rays with the source latitude is shown in Fig. 7.9 for f = 30 MHz and 51 MHz. The time delay decreases with increasing source latitude because the paths of the two rays tend to be identical as the source latitude increases. Indeed, that the backward radiation arrives at the Earth a

few seconds later than the forward radiation is mainly due to the fact that the backward radiation has to travel an excessive path below the source level with small group velocity. For $i_b > 45^o$, ΔT decreases rapidly with increasing i_b (Fig. 7.9 and Fig. 7.8). Thus if two backward rays meet at the Earth, the time delay between them would be significant owing to the difference in their excessive path lengths below the source level. For example, two backward rays and a forward ray at the frequency f = 30 MHz emitted at incident angles 40^o, 75^o and 68^o respectively (Fig. 7.7) would arrive at the Earth with time delays about 0.9 sec and 1 sec between them. The dependence of the time delay between the forward and the backward rays on the wave frequency for various latitudes is shown in Fig. 7.12.

Combination radiations at different frequencies emitted in the forward direction simultaneously from different source levels will also have time delay due to different lengths of their ray paths. If two sources situated at ρ_1 and ρ_2 ($\rho_2 > \rho_1$) emit combination radiations at the frequencies f_1 and f_2 ($f_2 < f_1$) respectively, the wave group delay time between the two forward rays will be

$$\Delta t_g = t_{g_2} - t_{g_1} = 2.316\left[\int_{\rho_2}^{\rho_E} \frac{\rho d\rho}{(n^2\rho^2 - a_2^2)^{\frac{1}{2}}} - \int_{\rho_1}^{\rho_E} \frac{\rho d\rho}{(n^2\rho^2 - a_1^2)^{\frac{1}{2}}}\right] \text{(sec)}, \quad (7.10)$$

where a_1, a_2 are constant parameters for the two forward parallel rays. Since the combination frequency is a continuous function of ρ, for small $|\Delta f| = |f_2 - f_1|$, Δt_g can be approximated by

$$\Delta t_g = \Delta f \left(\frac{\partial t_g}{\partial f} \right)_{f=\bar{f}} , \qquad (7.11)$$

where $\bar{f} = \frac{1}{2}(f_2 + f_1)$ and $\frac{\partial t_g}{\partial f}$ (sec per MHz) is the slope of the curve t_g vs f (expression (7.8)). The dependence of $\frac{\partial t_g}{\partial f}$ on frequency f is shown in Fig. 7.10 for various source latitudes. We find that the value of $\frac{\partial t_g}{\partial f}$ depends slightly on the source latitude. The average of $\frac{\partial t_g}{\partial f}$ is also plotted as a function of frequency in Fig. 7.10 for the source latitudes ranging from 50° to 80° (the solid curve). The positive $\frac{\partial t_g}{\partial f}$ means that as the combination radiations at the frequencies $f_1, f_2 (f_1 > f_2)$ are emitted at different layers in the solar corona simultaneously, the higher frequency is emitted at deeper layer and arrives at the Earth later. We shall make use of this figure in the evaluation of theoretical dynamic spectra of the drift pair burst and the hook burst in section H.

d. Absorption of Electromagnetic Radiation in The Solar Corona

The high frequency electromagnetic waves passing through a warm magnetoactive plasma will be damped by the collision

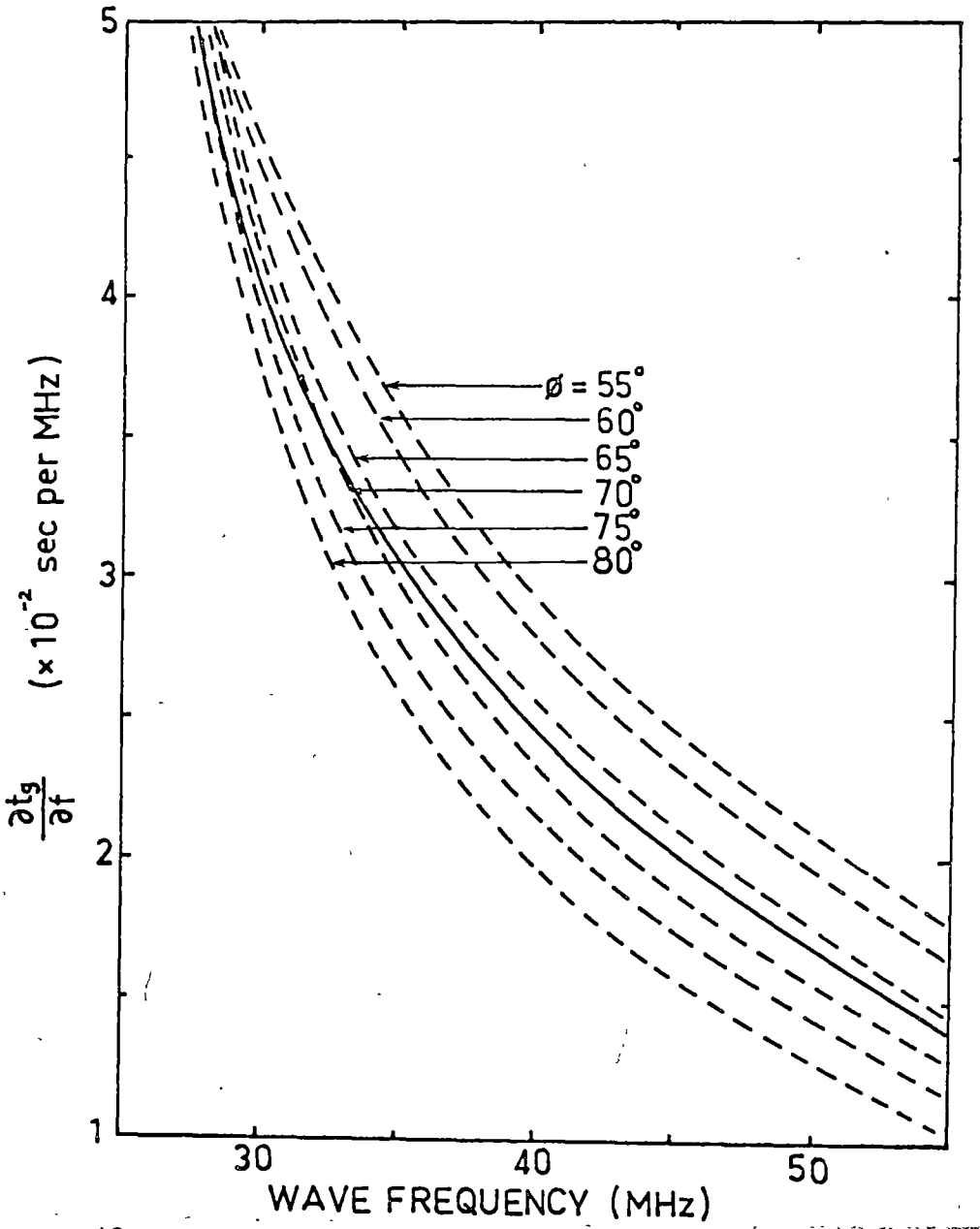

Fig.7.10 - The dependence of the rate of change of the wave group travelling time with frequency on the wave frequency for source latitude $\phi = 55°, 60°, 65°, 70°, 75°, 80°$. The mean value is represented by the solid curve.

process and the harmonic resonance process. Owing to the low collision frequency in the solar corona, collision absorption becomes significant only in the layers where the wave frequency is close to the plasma frequency and would be important for the backward combination radiation. Hence only the collision absorption and the third harmonic resonance absorption need to be considered.

Taking $L_H = 4 \times 10^9$ cm and $T = 1.5 \times 10^6$ ^oK, we show the power losses of the x-mode and the o-mode waves on passing through the layer $f = 3f_H$ as functions of X $(=f_p^2/f^2)$ in Fig. 7.11 (a) for $f = 35$ MHz and $\theta = 5^o$, 15^o, 45^o, 60^o, 75^o, 85^o. Only the o-mode wave can survive after passing through the layer $f = 3f_H$.

The combination radiation at the frequency about twice the plasma frequency and able to escape from the solar corona has to suffer further absorption along the wave group trajectory due to the electron-ion collision. If the effect of the sunspot magnetic field is neglected, the integrated collision absorption along the path s of the radiation is (Wild et al., 1963):

$$\tau = \int \kappa \, ds \qquad (7.12)$$

and the damping factor is $\exp(-\tau)$, where the collision absorption coefficient $\kappa = \nu(1 - n^2)/cn$. For the solar corona

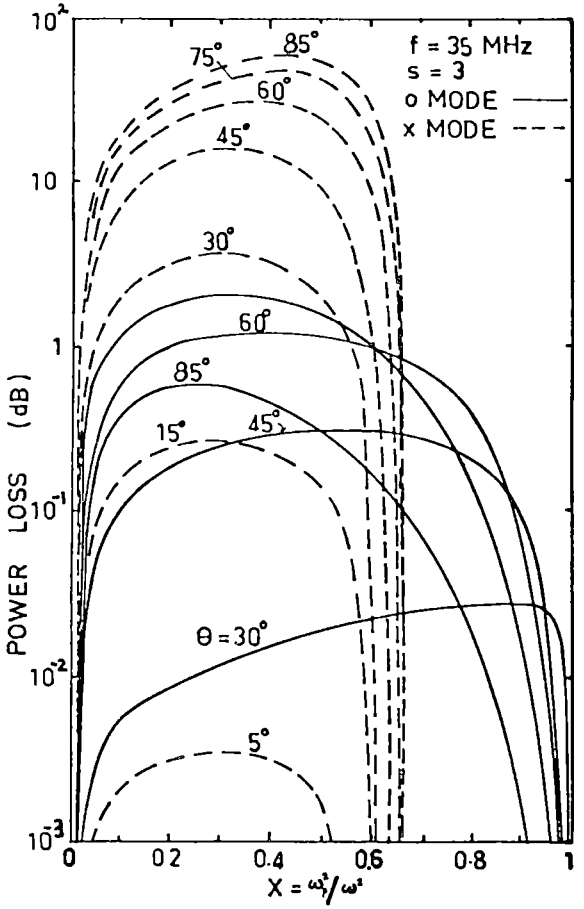

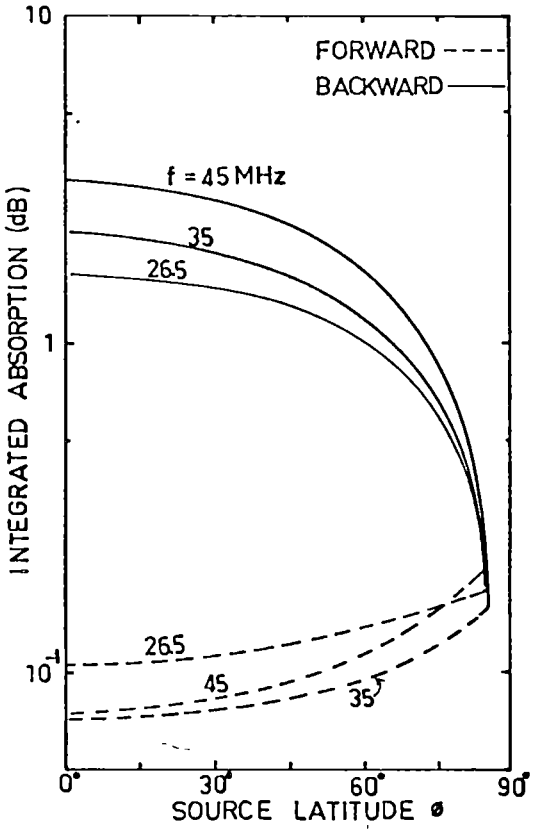

Fig.7.11 - (a) Power loss due to the third harmonic resonance absorption as a function of $X = \omega_p^2/\omega^2$ for the o-mode and the x-mode waves at the frequency f = 35 MHz and wave-normal angles $\theta = 5°, 15°, 30°, 45°, 60°, 75°, 85°$.

(b) Power loss due to collision absorption in the forward and backward rays as a function of source latitude in the solar corona for frequencies f = 45, 35, 26.5 MHz.

ν is given by (5.7). Then the integrated absorptions along the forward and the backward rays are specified by

$$\tau = 2.316 \times \frac{50}{T^{3/2}} \int_{\rho_s}^{\rho_E} \frac{n_o(1-n^2)\rho}{(n^2\rho^2-a^2)^{\frac{1}{2}}}\, d\rho \ , \tag{7.13}$$

$$\text{and } \tau = 2.316 \times \frac{50}{T^{3/2}} \left[2\int_{\rho_o}^{\rho_s} \frac{n_o(1-n^2)\rho}{(n^2\rho^2-b^2)^{\frac{1}{2}}}\, d\rho + \int_{\rho_s}^{\rho_E} \frac{n_o(1-n^2)\rho}{(n^2\rho^2-b^2)^{\frac{1}{2}}}\, d\rho \right]$$

respectively. Here, n_o is the electron number density given by (4.1) and a,b are the constant parameters defined by (7.7).

The variations of the integrated collision absorption (in decibels) for the forward ray and the backward ray with the source latitude are shown in Fig. 7.11 (b). The collision absorption will be comparable with the third harmonic resonance absorption only for the backward ray. The collision absorption for the backward combination radiation decreases as the source is displayed from the centre of the disk. Whether the third harmonic resonance process or the collision process plays the major role in the absorption of the backward combination radiation depends on the temperature of the coronal plasma and the effective thickness of the third harmonic resonance absorption layer. The backward combination radiation would suffer more absorption than the forward radiation at the same frequency due to excessive collision absorption.

However, when the third harmonic resonance absorption predominates, the observed intensity of the forward radiation would be equal to or less than that of the backward radiation if the effective thickness of the third harmonic absorption layer for the forward ray is greater than that for the backward ray.

G. Interpretation

Having studied the generation and the propagation of the combination radiations in the magnetoactive coronal plasma, we shall interpret the characteristics of the drift pair burst and the hook burst emission event. First of all, we assume that the drift pair and the hook burst emissions are produced by electron streams gyrating along the sunspot magnetic field configurations. The electrons each having energy of the order of ten keV are assumed to be accelerated in the solar corona during the period of the emission of the drift pair burst. The interaction of the stream electrons with the background coronal plasma results in the production of a strong coherent Cerenkov plasma wave which in turn interacts with the small-scale thermal fluctuations of electron density in the solar corona and gives rise to the combination radiation at the frequency $f \simeq 2f_p$. The combination radiation under suitable condition can escape from the solar corona and will be observed as a drift pair or a hook burst.

(1) Frequency Range

Because of the harmonic resonance absorption, the source of the drift pair burst must lie on the layer where $A \geq 1$ (Chapter VI, Section D). With the model of the active solar corona given in Fig. 7.3, the maximum frequency of the combination radiation observed on the Earth would not exceed 90 MHz. Along the bipolar sunspot magnetic field line, the largest value of A does not exceed four, hence in general, the electromagnetic radiation at the frequency $f \simeq f_p$ arising from incoherent scattering of the Cerenkov plasma wave is unable to leak away from the solar corona due to second harmonic resonance absorption. Pairs of bursts having frequency ratio 1:2 are hence not observed.

(2) Preferential Source Position

The double bursts with almost the same starting frequency are attributed to the combination radiations at similar frequencies emitted in the forward and the backward directions from a single source at the same instant but arriving at the Earth at different times. A pair of bursts can be observed to have similar intensities only when both the forward and the backward radiations are emitted in the directions within the cone of emission (Section E (3)). That is the absolute angular separation between the two rays at the source position must be smaller than the apex angle of the emission cone. Since the main power of the combination

radiation will be confined within a solid cone with an apex angle about 60° to 80° (Fig. 7.6), from Fig. 7.8, we find the preferential source latitude would be $\phi \geq 60^{\circ}$. In fact, the forward and the backward radiations of similar intensities can also be emitted from a central source provided that the sunspot magnetic field line is almost parallel the surface of the Sun (see Fig. 7.7). However, in this case, the bursts are expected to show no frequency-time drift (at the most, only very slightly drift) and short duration. Thus the central area of the disk is not the preferential position for drift pair emission.

(3) Time Delay

According to Fig. 7.12, in the frequency range 40 MHz to 25 MHz and for source latitudes $\phi \geq 60^{\circ}$, the backward combination radiation will arrive at the Earth about 1.5 to 2.2 sec later than the corresponding forward combination radiation. A pair of bursts with frequencies ranging from f_1 to f_2 ave radiated by a source moving from the position $P_1(\rho_1,\phi_1)$ to $P_2(\rho_2,\phi_2)$. If there is no change in the source latitude along the entire source trajectory (i.e. $\phi_1 = \phi_2$), the time delay between the forward and the backward combination emissions will increase with decreasing frequency (the dotted curves in Fig. 7.12). On the other hand, when the source latitude as well as source height change continuously along the source trajectory, the time delay would be constant or

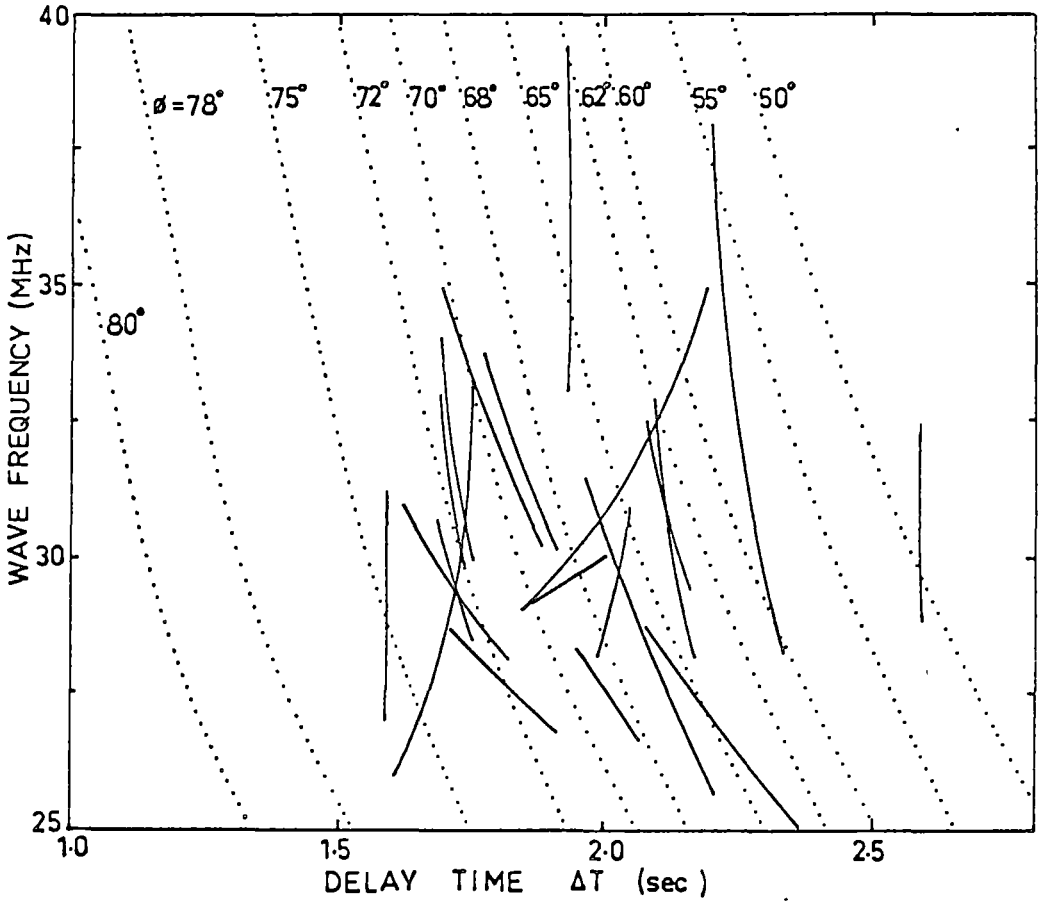

Fig.7.12 - Dependence of the wave group delay time between the forward and the backward rays on frequency for various source latitudes (dotted curves). The solid bars are the actual observation results obtained by Ellis (1969).

even increase with the frequency. The variation of the delay time with the frequency for various observed drift pairs measured by Ellis (1969) are re-plotted in Fig. 7.12 (thick solid bars). The sources were found to be situated at the latitudies ranging from 55^{o} to 75^{o}. Many burst sources showed no changes in the source latitude along their trajectories while a few had non-radial motion.

(4) Rate of Frequency Drift

The drift rate of the bursts arising from combination scattering of the Cerenkov plasma waves excited by an electron stream depends on the radial velocity component of the electron and radial electron density gradient along the solar corona. For the same electron energy, the drift rate of the burst emitted by a linear stream travelling radially is greater than that emitted by a helical stream gyrating along a curved sunspot magnetic field line. The type III bursts are attributed to the radiation of Cerenkov plasma waves by streams of electrons with energy from 10 to 100 keV ejected almost radially from the flare region (Wild et al., 1963; Stewart, 1965). As we interpret the drift pair as the result of radiation of Cerenkov plasma waves by a helical stream of electrons with energy about 10 keV and gyrating along a curved sunspot magnetic field line, the drift rate of the drift pair is lower than that of the associated type III burst appearing in the same spectral record. The theoretical dynamic spectrum given in

Section H shows that electrons having guiding centre velocity about 0.1c can generate a drift pair with the frequency drift rate about 2 MHz per sec in the frequency range 40 to 28 MHz. The variation of the frequency drift rate along an element of a pair arises from the changes of the electron pitch angle, the radial electron density gradient along the solar corona and also the curvature of the sunspot magnetic field line. The slight difference in the frequency-time slopes of the first and the second elements of a pair is probably due to the variation of the time delay with wave frequency as discussed in (3).

If all the major combination radiations emitted by an electron stream, moving from one point on the leading spot field line to another point on the following spot field line, can reach the Earth, the frequency of the burst observed will first decrease to the minimum value and then increase again with time. Such a continuous emission appears as a hook shape burst in the spectral record. Owing to the different curvatures and different magnetic field intensity gradients along the leading and the following spot field lines, the magnitudes as well as the senses of the frequency-time slopes of the upward and downward traces differ from each other.

(5) The Difference in The Starting Frequency and The Finishing Frequency

It is shown in Fig. 7.5 that when the electron guiding

centre velocity is small, the combination frequency emitted in the backward hemisphere with respect to the guiding centre motion is slightly higher than that in the forward hemisphere. Assuming $\beta_{||} \simeq 0.1$ and $\beta_T = 0.22\,\beta_{||}$, we find the normalized combination frequencies emitted in the directions $\theta = 125^o$ and 70^o are 3.074 and 3.054 respectively. If the actual starting frequency of the burst is about 35 MHz, the actual difference in the forward and the backward emission frequencies will be ~ 0.24 MHz. This explains the fact that the second element of a negative drift pair starts and terminates at slightly higher frequencies than the first element. The separation between the starting frequencies of the two elements of a pair by several MHz cannot be interpreted as the result of combination radiations at the frequencies $f \simeq f_o + \tilde{f}_+$ and $f \simeq f_o + \tilde{f}_-$ from a single source simultaneously because the intensity of the latter is not comparable to the former (Fig. 7.6). This can be due to the fact that a pair of bursts of similar intensities emitted from a single source will not be seen until the electron stream arrives at the suitable position such that both the observed forward and backward rays are emitted in the directions within the cone of emission of the combination radiation (Fig. 7.7). In other words, the separation between two bursts is a time delay and not a frequency separation.

(6) Bandwidth

The bandwidth of the observed combination radiation is

mainly determined by the frequency bandwidth of the Cerenkov plasma wave spectrum and the radial extent of the electron stream. The frequency bandwidth of the coherent Cerenkov plasma wave spectrum excited by an electron stream is inversely proportional to the electron pitch angle (Section D and Fig. 7.4 (c)). Moreover, an electron stream gyrating along a curved spot field line will have a radial extent smaller than that of a linear stream moving along the radial line of the Sun. Consequently, the observed bandwidth of the drift pair is narrower than that of the type III burst. In fact, the broadness of the apparent bandwidth of the type III burst is also due to its high drift-rate.

(7) The Mid-point Burst

The mid-point burst appearing in the drift pair burst and the drift pair followed (or preceded) by a hook burst are of the same character (Fig. 7.1(B),(C)) and expected to arise by the same cause. We note that the three bursts have the same frequency-time slope and bandwidth. They either start or finish at almost the same frequency and appear to have been generated by the identical exciting agents through the same process under the same condition . This would occur when two identical electron streams pass through the same position consecutively and generate combination radiations. However, in this case, two identical pairs of bursts are expected to

be observed more frequently. Therefore, the three elements of a triple burst are likely to be caused by the same electron stream. Since the time interval between the first and the third elements of a triple burst is similar to the characteristic time interval between the two elements of a normal pair (see Fig. 7.1 (C)), the mid-point burst can be attributed to the backward combination radiation emitted at an incident angle larger than that for the third element (see Fig. 7.7).

According to the discussion in Section F (b), two backward rays emitted from a source situated at a large latitude would meet at the Earth, particularly when there is a slight deviation of the spherical symmetry of the radial electron density distribution at one of the reflection layers. Of course, convergence of two backward rays at the Earth is possible only for a very particular range of source latitude and hence the mid-point burst mid-way between the two normal traces occurs only occasionally. In view of the facts that the preferential drift pair source position and the characteristic time interval between the two elements of a pair are also in favour of large source latitude ((2) and (3) of this section), we suggest that convergence of two backward rays and a forward ray at the Earth is a plausible explanation for the appearance of a triple burst.

(8) The Duration of Drift Pair Burst

The duration of the drift pair is as long as that of the type

III burst. We assume that a cut-off mechanism such as that suggested by Kaplan and Tsytovich (1968) exists and causes the radiating electron stream to retain its identity for a few or ten seconds.

(9) Polarization

It has been shown in Chapter VI that the polarization of the combination radiation at $f \simeq 2f_p$ emitted from a source situated at a large latitude is insignificant.

(10) Intensity

Let us assume that electrons having $\beta_{||} \simeq 0.1$ in a volume of $10^8 \times 10^{18}$ cm^3 radiate a particular frequency, 30 MHz, say. If n_o' is the electron density of the stream, then the maximum power of the Cerenkov plasma wave emitted by these electrons coherently is about 10^5 $n_o'G$ W/sr, where G is the power gain factor in the stream-plasma system. The theoretical flux density received on the Earth would then be $1.5 \times 10^{-25} n_o' G\eta$ W $m^{-2}Hz^{-1}$, where η is the coefficient of transformation (per steradian). Assuming the electron density of the ambient plasma in the drift pair source is $3 \times 10^6 cm^{-3}$, $\sigma = 10^{-5}$ gives $n_o' = 3 \times 10$ cm^{-3}. Then if the coefficient of transformation due to combination scattering is $\eta \simeq 10^{-10}$ (per steradian) the theoretical flux density would be $4.5 \times 10^{-34} G$ W $m^{-2}Hz^{-1}$. In order to attain the maximum observed flux density (about 5×10^{-20} W $m^{-2}Hz^{-1}$), we need a power gain $G \simeq 10^{14}$ (i.e. 140 dB). From

Fig. 7.4(c), the interaction time needed is less than 1.5×10^{-5} sec (The characteristic time for non-linear transfer of the plasma wave across the spectrum is ~ 1.6×10^{-5} sec).

The first and the second elements of a pair correspond to combination radiations emitted in different wave-normal directions and their intensities would be different from each other. Collision absorption for the backward ray and the third harmonic resonance absorption are the other factors causing the variation of the intensities of the two elements (Section F (d)).

H. Theoretical Dynamic Spectra

The drift pairs and hook bursts can be well accounted for as the consequence of the Cerenkov radiation of plasma waves by electron streams gyrating along the sunspot magnetic field lines. It is expected that the theoretical dynamic spectra, which are calculated on the basis of the present theory, should well agree with those observed. Here we calculate the theoretical dynamic spectra by assuming that the magnetic field intensity along the length of the segment of the stream, which radiates a particular frequency, is constant so that the characteristics of this bunch of electrons may be described in terms of a single electron.

Suppose an electron travels from a point S_o to a point S_1 along the sunspot magnetic field line and causes combination

radiation at the frequencies from f_o to f. The total time delay between these two frequencies will be

$$t = t_e + \Delta t_g \ , \qquad (7.14)$$

where t_e is the electron travelling time from S_o to a point S_1 and Δt_g is the wave group delay time given by (7.10).

Taking into account of conservation of electron's magnetic moment, the variation of the electron guiding centre velocity is given by

$$\beta_{\|} = \beta(1 - \sin^2\phi_o \frac{fH}{f_{H_o}})^{\frac{1}{2}} \ , \qquad (7.15)$$

where ϕ_o and f_{H_o} are the initial pitch angle and gyrofrequency of the electron at the initial point S_o respectively. The normalized velocity β of the electron is assumed to be constant. The travelling time for the electron from S_o to S_1 along a dipole field line is then

$$t_e = \frac{1}{c} \int_{S_o}^{S_1} \frac{ds}{\beta_{\|}} = 2.316 \int_{\ell_o}^{\ell} \frac{r_o \cos\ell (1+3\sin^2\ell)^{\frac{1}{2}} d\ell}{\beta[1-g(1+3\sin^2\ell)^{\frac{1}{2}}/\cos^6\ell]} \, d\ell \qquad (7.16)$$

where $g = \frac{r_e^3}{r_o^3} \frac{\sin^2\phi_o}{(1+3\sin^2\ell_o)^{\frac{1}{2}}}$ with $r_e = r_o\cos^2\ell_o$ (in units of solar radius) and r_o is defined in (4.4). ℓ and ℓ_o are the latitudes of the points S_1 and S_o with respect to the centre of the

dipole.

The combination frequencies emitted from these points, according to the discussion in section E, can be approximated as

$$f_o \simeq 2.05 f_p(\rho_{so})(1 + 3\beta_T^2/\beta_{||}^2)^{\frac{1}{2}} , \qquad (7.17)$$

$$f \simeq 2.05 f_p(\rho_{s1})(1 + 3\beta_T^2/\beta_{||}^2)^{\frac{1}{2}} ,$$

where $f_p(\rho_s) = 90\times(1.55\rho_s^{-6} + 2.99\rho_s^{-16})^{\frac{1}{2}}$ MHz. The radial distance from the centre of the Sun ρ and the dipole latitude ℓ are related through the equation (4.5). If $\Delta f = |f - f_o|$ is small, the wave group delay time Δt_g can be estimated with the help of the solid curve in Fig. 7.10. Then we can evaluate the total delay time between f_o and f in the frequency-time plane.

The second element of a pair can also be plotted by assuming that the time delay between the direct and reflected rays is about 1.7 sec and the combination frequency emitted in the backward hemisphere with respect to the electron guiding centre motion is slightly higher than that emitted in the forward hemisphere. In the case that two reflected rays meet at the Earth, a mid-point burst separated from the first element of a normal pair by a time about 0.9 sec also appears (see section F (c)).

The theoretical dynamic spectra of the drift pair bursts and hook bursts radiated by streams of electrons with energy

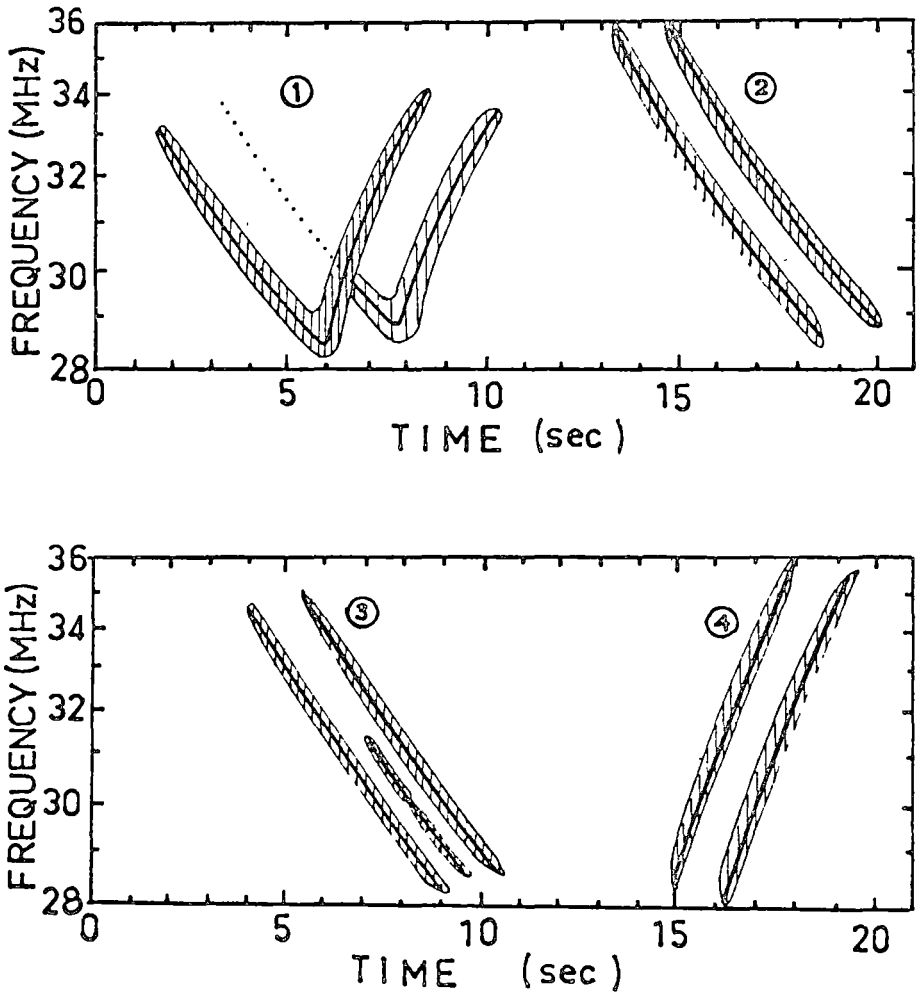

Fig.7.13(a)- The theoretical dynamic spectra of drift pair bursts and hook bursts radiated by electron streams moving along the bipolar spot field line.

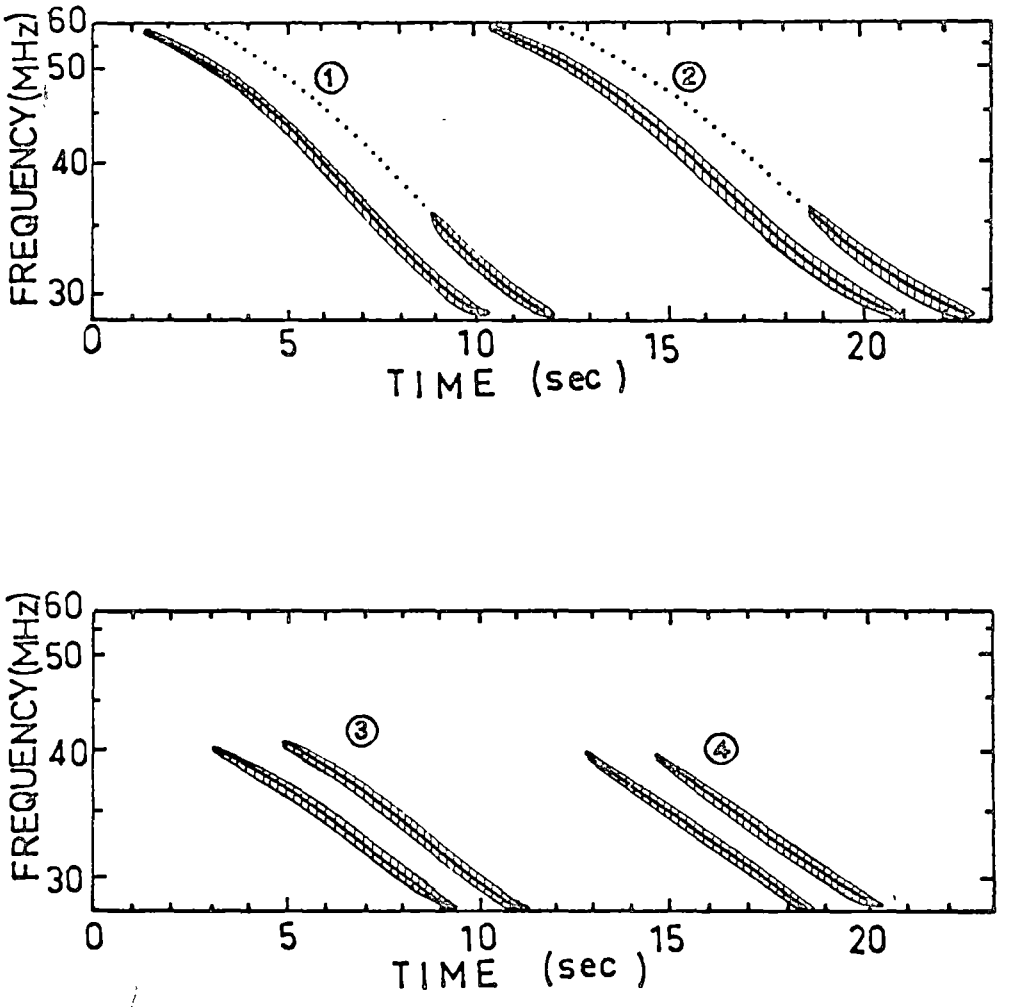

Fig.7.13(b)- The theoretical dynamic spectra of drift pair bursts radiated by electron streams moving along unipolar spot field line.

about ten keV are shown in Fig. 7.13. Table 7.1 and Table 7.2 show the significant numbers used in deriving the corresponding theoretical dynamic spectra in Fig. 7.13. Those backward rays reaching the Earth but not carrying sufficient observable intensity are represented by dotted traces. The average ~~value of the~~ drift rates of these calculated spectra range from 3 MHz per sec to 1 MHz per sec in the frequency range from 50 MHz to 28 MHz. The drift rate of the burst depends on the initial source position, initial electron pitch angle and the electron energy. The good agreement of the theoretical dynamic spectra with those observed suggests that the electron responsible for the drift pair emission has an energy of the order of ten keV and a pitch angle mostly greater than 45^{o}.

I. Conclusion

Using the theory of Cerenkov radiation of plasma waves by electron streams gyrating along sunspot magnetic field lines, most of the important characteristics of the drift pair and hook burst emissions can be explained if we assume the intensity of sunspot magnetic field slowly decreases with increasing altitude from the photosphere. The magnitude of the sunspot magnetic field intensity at $\rho=2$ is assumed to be 2 or 3 gauss. Although there are no optical observational data supporting such assumptions, theories of solar type II and

Table 7.1 (Bipolar Sunspot Field Model)

Burst	β	ρ_s	$\beta_{\|\|}$	ϕ	f MHz	Δt_g $\times 10^{-2}$ sec	t_e sec	$\Delta\dot{\nu}$ sec	Mean Drift Rate
①	0.2	1.937	0.07375	68.4°	32.60	0	0	0	
		1.949	0.08497	65.0°	31.75	-3.90	0.649	0.6100	
		1.966	0.09610	61.3°	30.81	-3.50	0.844	1.4190	
		1.977	0.10250	59.2°	39.20	-2.35	0.507	1.9025	-1.1 MHz -sec^{-1}
		1.987	0.10800	57.4°	29.80	-1.65	0.475	2.3610	
		1.996	0.11280	55.7°	29.55	-2.31	0.450	2.7880	
		2.008	0.11880	53.6°	28.75	-2.20	0.640	3.4060	
		2.015	0.12210	52.4°	28.40	-1.59	0.387	3.7770	
		1.991	0.11670	54.3°	29.44	4.60	0.485	4.2080	
		1.967	0.11070	56.4°	30.60	4.70	0.438	4.6930	
		1.943	0.10390	58.8°	31.80	4.45	0.563	5.3050	2.18 MHz -sec^{-1}
		1.920	0.09600	61.4°	33.00	6.80	0.551	5.8930	
		1.896	0.08685	64.2°	34.40	4.00	0.600	6.5330	
③	0.2	1.916	0.5200	75.0°	34.40	0	0	0	
		1.924	0.06040	72.5°	33.80	-4.84	0.462	0.4130	
		1.937	0.07375	68.6°	32.60	-4.02	0.766	1.1380	
		1.949	0.08410	65.0°	31.75	-2.98	0.649	1.7580	
		1.966	0.09610	61.3°	30.81	-3.48	0.844	2.5670	-1.22 MHz -sec^{-1}
		1.977	0.10250	59.2°	30.21	-2.37	0.507	3.0500	
		1.987	0.10800	57.4°	29.80	-1.62	0.475	3.5100	
		1.996	0.11280	56.0°	29.25	-2.30	0.450	3.9360	
		2.008	0.11880	53.4°	28.75	-2.18	0.640	4.5540	
		2.015	0.12210	52.4°	28.40	-1.58	0.407	4.9200	

Table 7.2 (Unipolar Sunspot Field Model)

Burst	β	ρ_s	$\beta_{\|\|}$	ϕ	f MHz	Δt_g $\times 10^{-2}$ sec	t_e sec	ΔT sec	Mean Drift Rate
①	0.18	1.590	0.0405	77.0°	58.00	0	0	0	
		1.651	0.0750	65.0°	51.48	-9.10	2.097	2.006	
		1.699	0.0976	58.0°	46.62	-7.10	1.330	3.265	
		1.749	0.1130	51.0°	42.54	-8.36	1.117	4.300	
		1.800	0.1240	46.5°	38.92	-8.50	1.012	5.230	3.58
		1.852	0.1330	42.5°	35.68	-9.00	0.966	6.100	MHz-sec^{-1}
		1.906	0.1400	38.6°	32.68	-9.30	0.913	6.920	
		1.961	0.1460	36.0°	29.98	-9.25	0.902	7.730	
		2.017	0.1510	33.4°	27.53	-1.10	0.890	8.520	
③	0.18	1.800	0.0405	77.0°	40.00	0	0	0	
		1.852	0.0721	66.4°	36.20	10.60	2.368	2.262	
		1.906	0.0936	58.6°	32.89	10.90	1.517	3.670	2.14
		1.961	0.1086	53.0°	30.08	11.10	1.268	4.827	MHz-sec^{-1}
		2.017	0.1199	48.5°	27.58	15.60	1.152	5.823	

type III bursts proposed by various authors do suggest the existence of magnetic field of the intensity about a few gauss at the altitude $\rho=2$ (Morimoto, 1963; Newkirk, 1967) (see Fig. 7.3 and Fig. 4.2).

The very sharp turning point of a hook burst reveals that the sunspot magnetic field lines, emerging from the leading spot and the following spot radially, are joined acutely at the altitude about one solar radius above the photosphere. This agrees with the optical observational fact that the sunspot field lines coming from the umbral area incline to the radial line at small angles and the pair of spots are separated by a small distance on the photosphere (cf. Section B of Chapter IV).

The most significant characteristic of the drift pair is the constancy of the delay time between the two elements of a pair over a long period of time. The average delay times observed by Roberts (1958) and by Ellis (1969) are almost identical ($\sim$ 1.7 sec) although the recent observation was carried out about ten years after the first observation. Any mechanism responsible for the drift pair emission has to generate electromagnetic radiations at similar frequencies in the forward and backward directions; the backward emission would arrive at the Earth after reflection at the layer lower than the source level. Then, the high degree of similarity of the spectral appearance of the two elements of a pair and

the constancy of the delay time suggest that during the period of the drift pair emission, the electrons were distributed along the solar corona in the most regular form. Hence we infer that during the period of drift pair emission, a coronal streamer with electron density a few times higher than that of the background corona does not exist above the sunspot group or does not extend to the height about 0.5 solar radius above the photosphere. In fact, the characteristic delay time and the other spectral features of the drift pair can only be explained satisfactorily by the theory of Cerenkov excitation of plasma waves by electron streams if we assume a regular corona. In view of the facts that the drift pair bursts are associated with flares of lesser importance and occur solely during fairly quiet period of solar activity, a regular solar corona with spherically symmetrical distribution of electron density is not improbable.

The type III bursts whose rates of drift are higher than those of drift pairs are also considered to be the result of excitation of coherent Cerenkov plasma waves by electron streams. The smallness of the drift rate of the drift pair can be due to electron streams with either large pitch angles or small energy. In Fig. 7.14, the frequency drift rate of the combination radiation emitted by a linear electron stream moving radially along the regular solar corona is plotted against the wave frequency for various electron velocities.

It is clear that for drift rates as low as 1.2 MHz per sec at the frequency 35 MHz, the velocity of a radially moving stream must be less than 0.1c, that is less than the velocity limit for electrons travelling through the solar corona (0.2c) (De Jager, 1960). Moreover, from the discussion given in Section G (6), the narrow bandwidth of the drift pair, compared with that of the type III burst, suggests that the electron stream responsible for the emission of drift pair follows a helical trajectory along the sunspot field line rather than a radial trajectory. The theoretical dynamic spectrum of the drift pair with negative drift rate about 1.4 MHz per sec radiated by a helical stream of electrons of energy about ten keV requires that the initial electron pitch angle is at least greater than 45^{o}.

It is believed that energetic electrons with energy up to 100 keV in the solar corona can be produced in the flare region by a mechanism such as that proposed by Sweet (1958) and Gold and Hoyle (1959), and ejected upward along lines of force on the neutral planes between two magnetic fields of opposite polarity. The excitation of plasma waves by these electrons results in the type III burst emission. Alternatively, through the Fermi-like process (Wentzel, 1963; Schatzman, 1963), electrons can also be accelerated to higher energy by the magnetohydrodynamic shock wave front ahead of

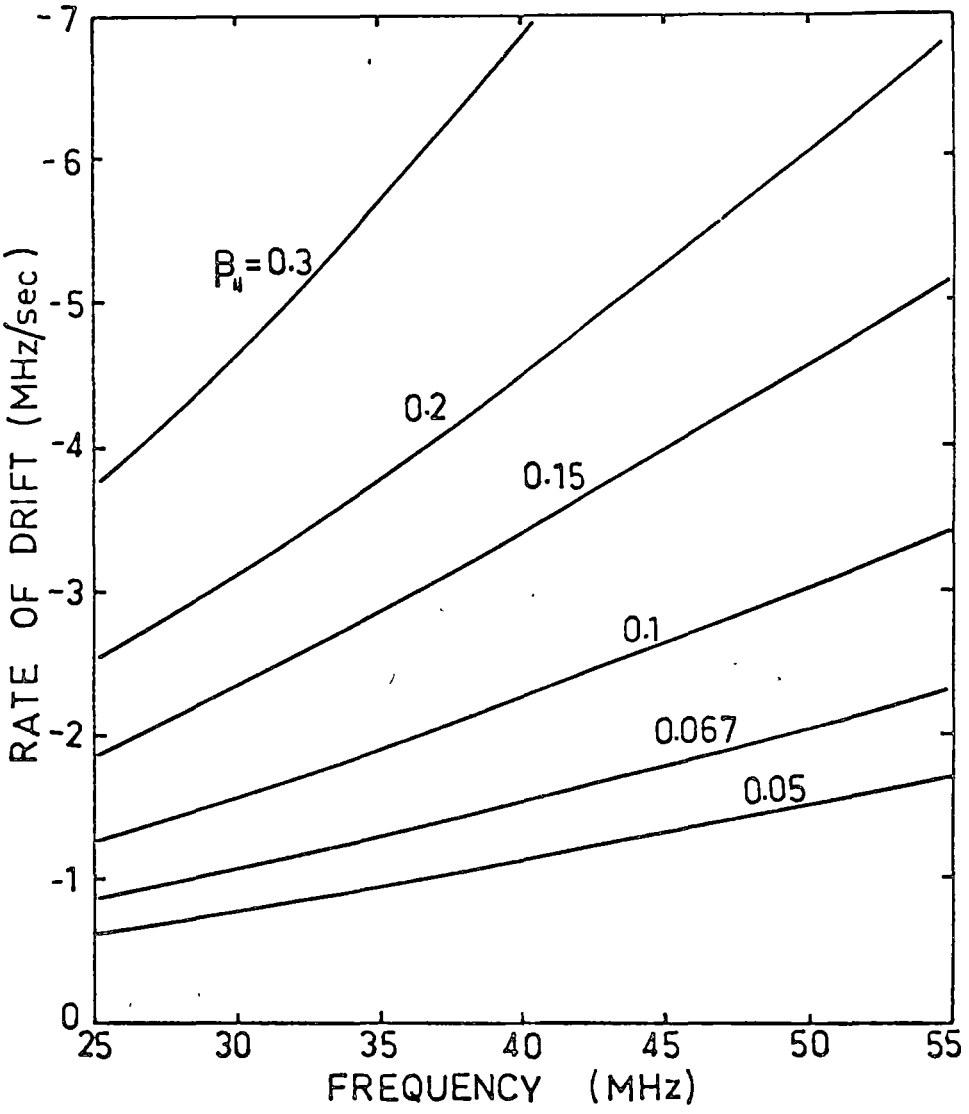

Fig.7.14 - The rate of frequency drift of the combination radiation burst expected for electron stream moving through a Baumbach-Allen model corona at constant radial speed $\beta_{\parallel}$ = 0.3,0.2,0.15,0.1,0.067,0.05 as a function of wave frequency.

the plasma cloud which is ejected upward from the flare region*. Those electrons with large pitch angles found in the outer layers of the solar corona are likely to be produced by the latter mechanism. The process of acceleration of electrons in a shock front proposed by Schatzman (1963) is derived from both the Fermi and the betatron mechanisms and is able to accelerate a small proportion of electrons to high velocity. A particle crossing the magnetohydrodynamic shock front perpendicularly will be accelerated. However, the acceleration can take place only when the electron density is smaller than a certain limit which depends on the temperature, the magnetic field and the shock strength. Moreover, a shock front is not formed in front of the gas cloud when the motion of the gas is mostly along the lines of force of the magnetic field. Thus the preferential region for acceleration is where the magnetic field lines of force are perpendicular to or incline at very large angles to the direction of the gas motion. Then, the accelerated electrons will be ejected from the shock front and trapped in the near-by strongest sunspot magnetic field line with large initial pitch angles.

If the acceleration takes place in the region where the value of A is larger than unity, the accelerated electrons

---

* The possibility that the shock wave front originating from the Sun would cause geomagnetic disturbance depends on the geometry.

forming a stream with small momentum spread would produce combination radiations at the frequency about double the plasma frequency in the forward and the backward directions with respect to the electron guiding centre motion. These combination radiations will finally be observed as a drift pair or a hook burst on the Earth (Fig. 7.15). However, because of the small electron energy and large pitch angle, the peak power of the cyclotron radiation in the x-mode and the o-mode emitted by the same electron stream will be small, and in any case it will be unable to escape from the solar corona owing to the second harmonic resonance absorption (cf. Chapter VIII). The spectral characteristics of the drift pair burst and hook burst have already been explained in the previous section.

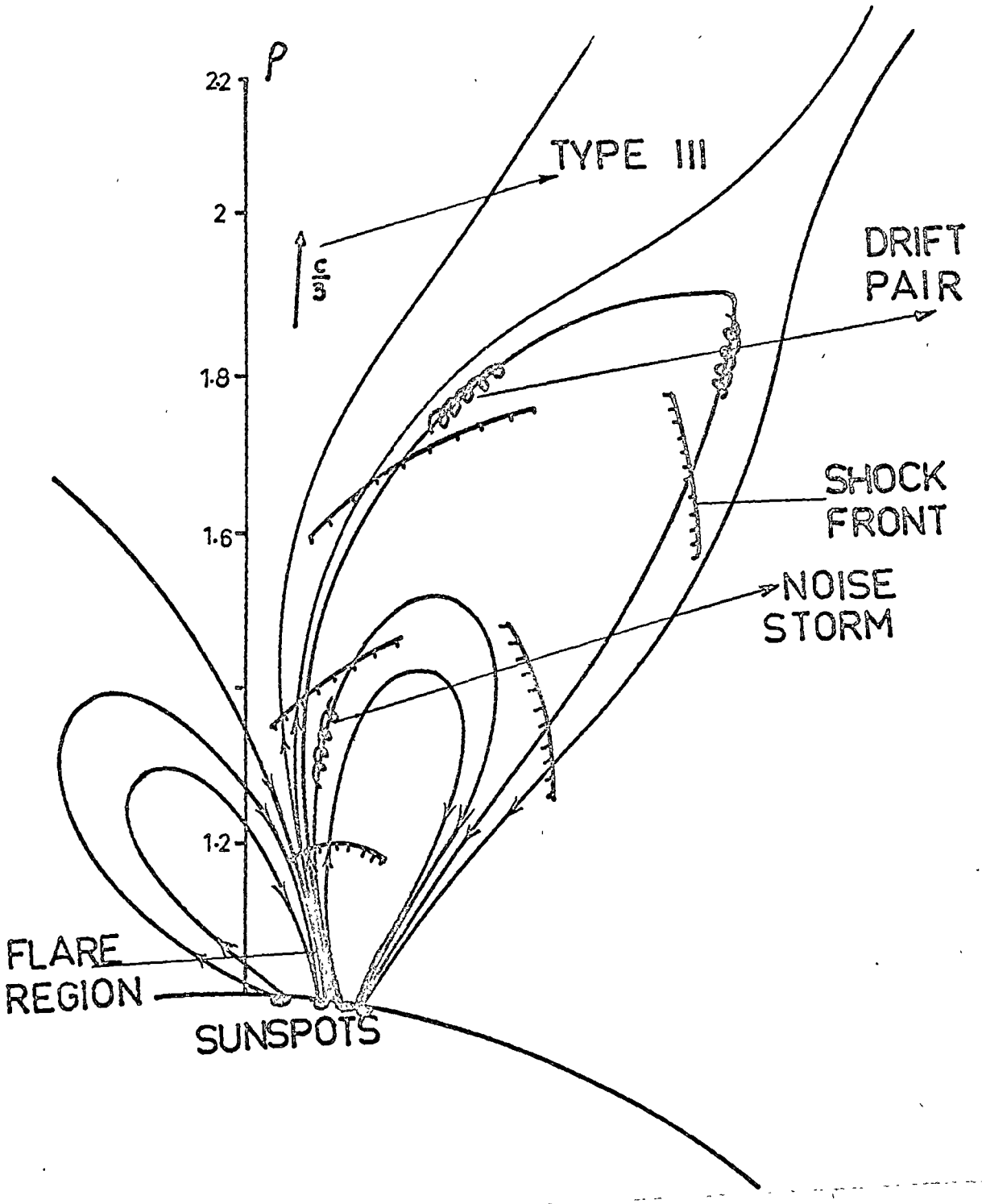

Fig.7.15 - Schematic drawing of the solar drift pair and hook burst emission event.

CHAPTER VIII

A THEORY OF SOLAR TYPE IV EMISSION AT CENTIMETRE AND DECIMETRE WAVELENGTHS

A. Introduction

Immediately after the occurrence of large flares, long periods of enhanced continuum radiation superimposed with fast-drift bursts may be observed. Such emission occurs in a frequency range from a few hundred to several thousand megahertz and lasts for a period of a few tens of minutes or hours. Usually, it is associated with the type IV bursts at metre wavelengths (designated as type IVm), which possess similar spectral characteristics. Therefore this enhanced continuum emission superimposed with variabilities at centimetre and decimetre wavelengths is regarded as the first phase of the whole type IV emission and is designated as type IVA by Kundu (1965), or type IV μ(microwave type IV) by Wild et al. (1963), or type IV group A and group A-B by Takakura and Kai (1961), while type IVm bursts are regarded as the second and the third phase emissions. Here, Kundu's nomenclature is used (see Fig. 1.1). Dynamic spectrum and single frequency observations in various frequency ranges have been reported by Haddock (1959), Takakura (1960a, 1963), Kundu (1961). Pick (1961), Young et al. (1961) and Thompson and Maxwell (1962). From all the observational

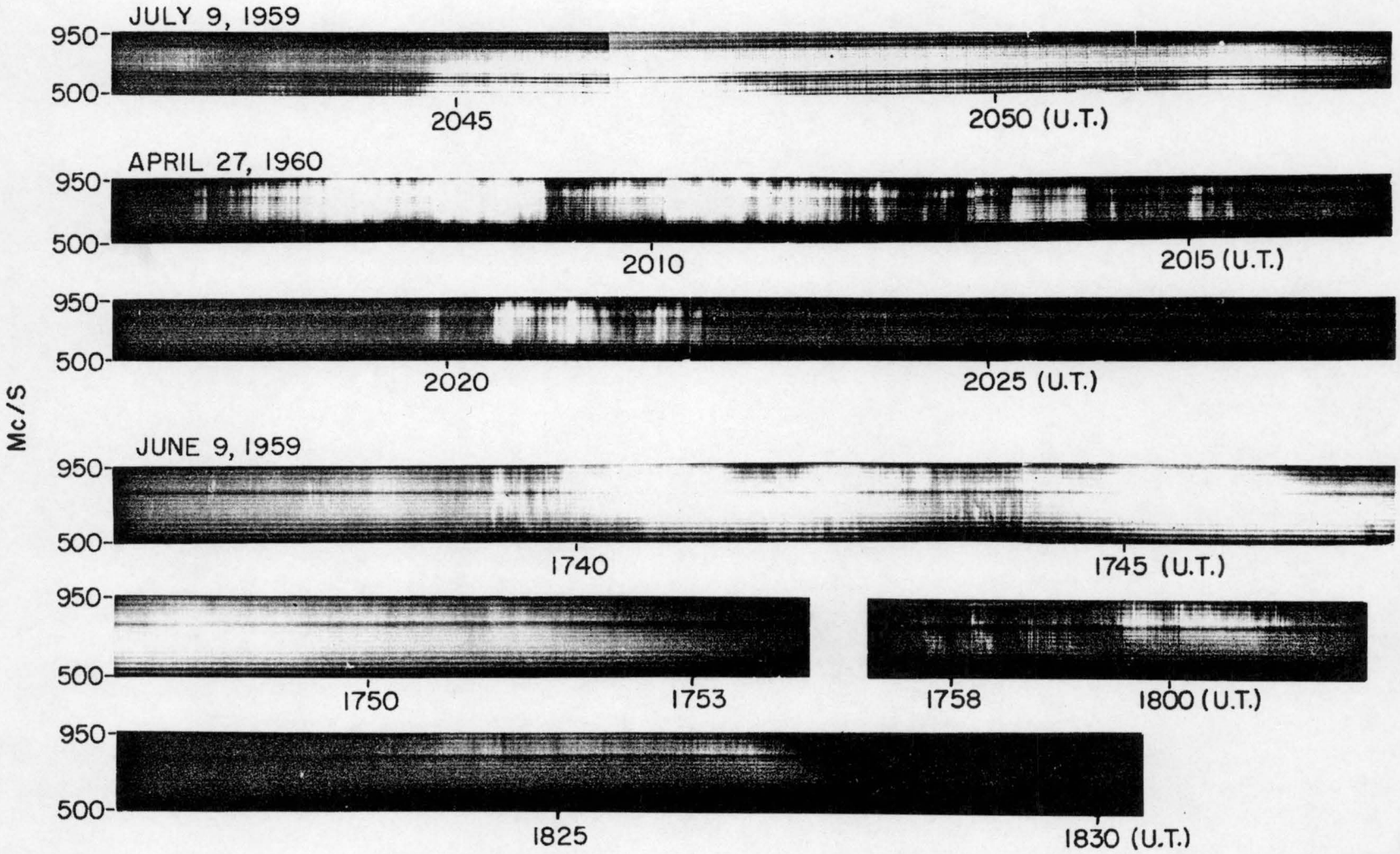

Fig.8.1 – Dynamic spectrum records of 500–1000 Mc/s continuum bursts associated with meter-λ type IV radiation. The dcm-λ continuum radiation is smooth continuum having fine structures superimposed on it (After Kundu and Spencer 1963).

records, the spectral features and the source characteristics of type IVA emission can be summarized as follows.

(i) Frequency Range

Type IVA continuum occurs from frequencies higher than 10,000 MHz and extends down to 200 MHz. The frequencies of the fast-drift elements that are superimposed on the background continuum mostly lie within the range 300-1,000 MHz (decimetre wavelength region) (Kundu, 1965) (Fig. 8.1).

(ii) Intensity

The intensity varies from a barely detectable value of about 5×10^{-22} W $m^{-2} Hz^{-1}$ to greater than 10^{-18} W $m^{-2} Hz^{-1}$ (Fig. 8.2(A)). For great bursts (associated with type IVm bursts), the decimetre wavelength burst intensity is usually less than that of the centimetre or metre wavelength bursts. The intensity of the fast-drift burst is high and can reach 10^{-18} W $m^{-2} Hz^{-1}$. There is some tendency for the intensity to decrease with the frequency (Kundu, 1965)(Fig. 8.2(A)).

(iii) Bandwidth

The continuum in centimetre and decimetre wavelength regions extends over hundreds of megahertz. Dynamic spectra (Kundu et al., 1961; Thompson and Maxwell, 1962) indicate that type IVA emission consists of groups of very broad band bursts, which occur in rapid sequence and which may be superimposed upon each other or may merge together to form a continuum. The bandwidth of decimetre wavelength emission is

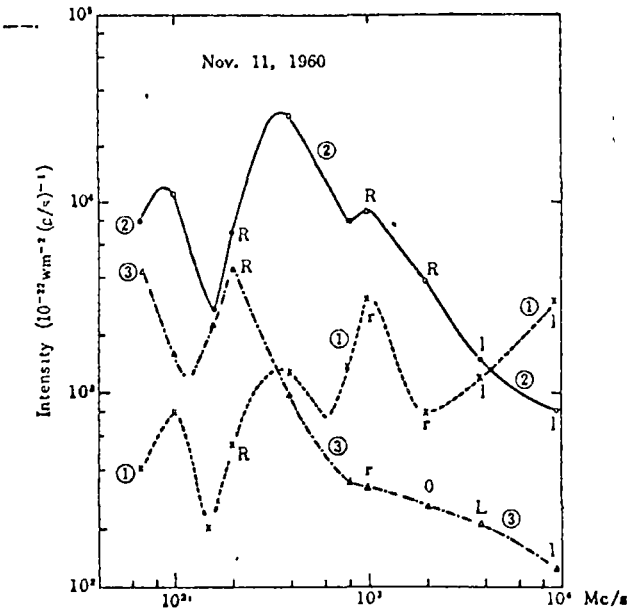

FIG. 8.2(A) Intensity spectra of type IV burst on Nov. 11, 1960
1) 0334 UT, 2) 0430 UT, 3) 0500 UT.
l: left-handed polarization, polarization degree<50%.
L: left-handed polarization, polarization degree>50%.
r: righ-handed polarization, polarization degree<50%.
R: righ-handed polarization, polarization degree>50%.
O: unpolarized.

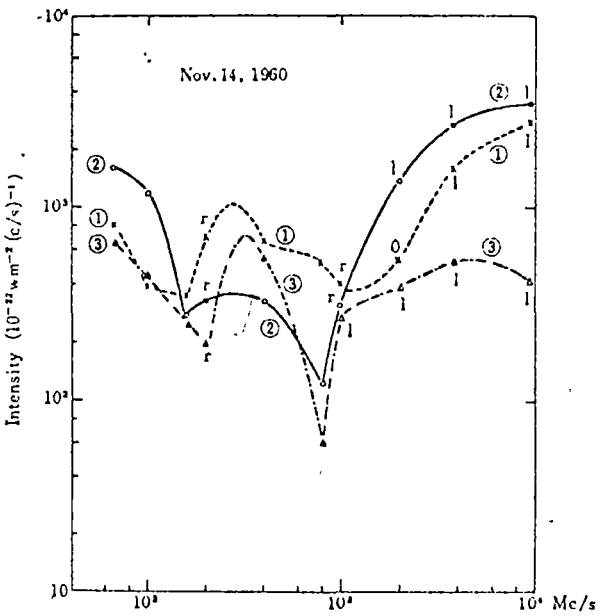

FIG. 8.2(A) Nov. 14, 1960 1) 0340 UT, 2) 0400 UT, 3) 0420 UT. Swept-frequency record of this burst is shown in a previous paper (Takakura 1963)

narrower than that of centimetre wavelength emission. The drifting elements in the decimetre wavelength region have bandwidths as narrow as 10 MHz.

(iv) Variabilities

The dynamic spectra of the long duration centimetre wavelength bursts show a broad band smooth continuum and lack complexity, while in the decimetre wavelength region the smooth continuum has very short duration drift bursts superimposed on it.

(v) Frequency Drift

Only a few decimetre wavelength continuum bursts show a steady and slow drift from high frequencies towards lower frequencies. The drift rate is roughly estimated to be 200 MHz/hr. (Takakura, 1963). The drift bursts on the other hand may have a frequency drift greater than 2,000 MHz/sec. Both senses of drift are observed (Young et al., 1961; Kundu and Spencer, 1963) (Fig. 8.2(B)).

(vi) Duration

Thompson and Maxwell (1962) reported that typical durations of the event are 5 - 40 min in the centimetre wavelength region and 5 - 120 min in the decimetre wavelength region. Individual fast-drift bursts have durations of the order of half a second.

(vii) Polarization

The centimetre and decimetre wavelength continuum

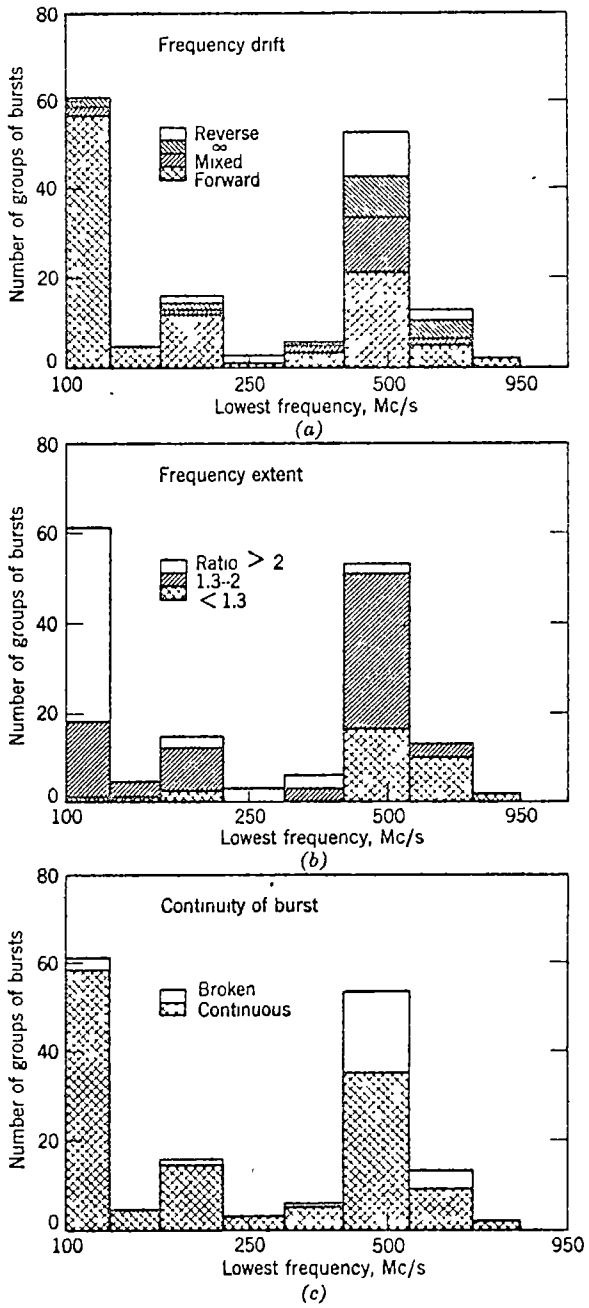

Fig. 8.2(8) The histograms show the number of groups of bursts observed over a period of one year (May 1959 to April 1960) with low frequency limits in each of eight frequency intervals selected to approximate a logarithmic frequency scale. The shading of the histograms indicates the separation of each class according to (*a*) sense of frequency drift, (*b*) frequency extent of the group measured as a ratio of the highest to lowest frequency of the group, and (*c*) continuity of the burst across its frequency extent (after Kundu, et al., 1961).

bursts are partially circularly polarized and the sense of polarization may change between 2,000 and 4,000 MHz. If the leading sunspot is taken to have north polarity, then at high frequencies the polarization is in the extraordinary mode but changes to the ordinary mode at decimetre wavelengths. The degree of polarization increases towards lower frequencies (Takakura, 1963; Kundu, 1965) (Fig. 8.2(A), (C)).

(viii) Position and Movement of the Sources

At all frequencies ranging from 9,400 to 340 MHz the source is situated less than 40,000 km above the photosphere. Significant movement of the type IVA source has not been observed (Kundu, 1959; Kundu and Firor, 1961) (Fig. 8.2(C)).

(ix) Association with Flares

The type IVA burst emissions are strongly associated with solar flares. The percentage of solar flares that are associated with type IV bursts at centimetre wavelengths increases with flare importance (reaching nearly 100% for flares of importance 3). The association of flares with decimetre wavelength bursts is not so strong (for flares of importance 2 and 3 the association is about 25% and 85% at 545 MHz, as compared with about 40% and 100% at 3,000 MHz). A flare has a greater probability of being associated with a type IV burst if the flare area covers the umbra of the active region where the flare originates (Fig. 8.2 (E)). The time of start of type IVA bursts appears to coincide with the

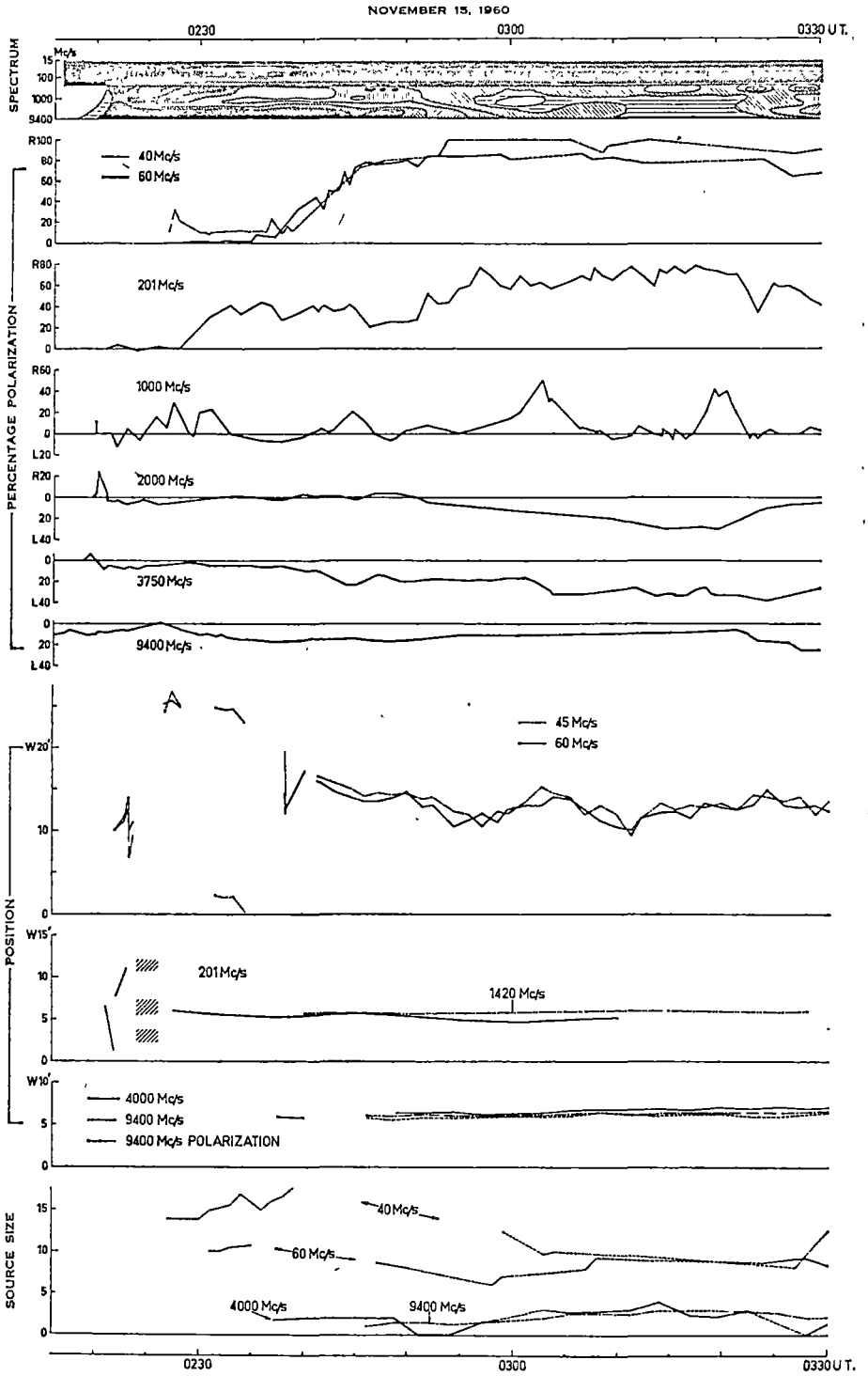

Fig. 8.2 (c) Source characteristics of the type IV event of November 15, 1960, as compiled by Suzuki and by Weiss (1963b). The spectrum above 200 Mc/sec is obtained synthetically from several single frequency observations. Note the initial development of circular polarization on 50 to 60 Mc/sec and its reversal of sense between 1000 and 2000 Mc/sec.

explosive phase rather than with the commencement of the associated flares. In nearly all observable cases there are groups of type III bursts almost in coincidence with the explosive phase of the flare (Fig. 8.2(D)). Sometimes, for a flare of great importance, the type III bursts are followed by type II and type IVm bursts. The flares associated with type IV without type II bursts are of less importance than those associated with type IV-type II bursts (Kundu, 1965). When the associated flares are of great importance ($2, 2^+$, and 3), the decimetre wavelength and centimetre wavelength continua start more or less simultaneously and often reach peak intensities at about equal times. Further, their source characteristics are very similar. Both the centimetre and decimetre wavelength bursts reach their maximum intensities before the flare maximum.

(x) Association with Metre Wavelength Bursts

Type IVA bursts can occur with or without type II bursts at metre wavelengths. In the frequency range 250-580 MHz, type IV emission (decimetre wavelength) in most cases occurs a few minutes earlier than the associated type II bursts, but at frequencies less than 250 MHz, type IV emission (metre wavelength) follows the occurrence of type II (Fig. 8.2(F)). The centimetre wavelength bursts associated with type IV-type II events have stronger intensity and the importance of the associated flares is also greater (Kundu, 1965, p.406). The short duration decimetre wavelength

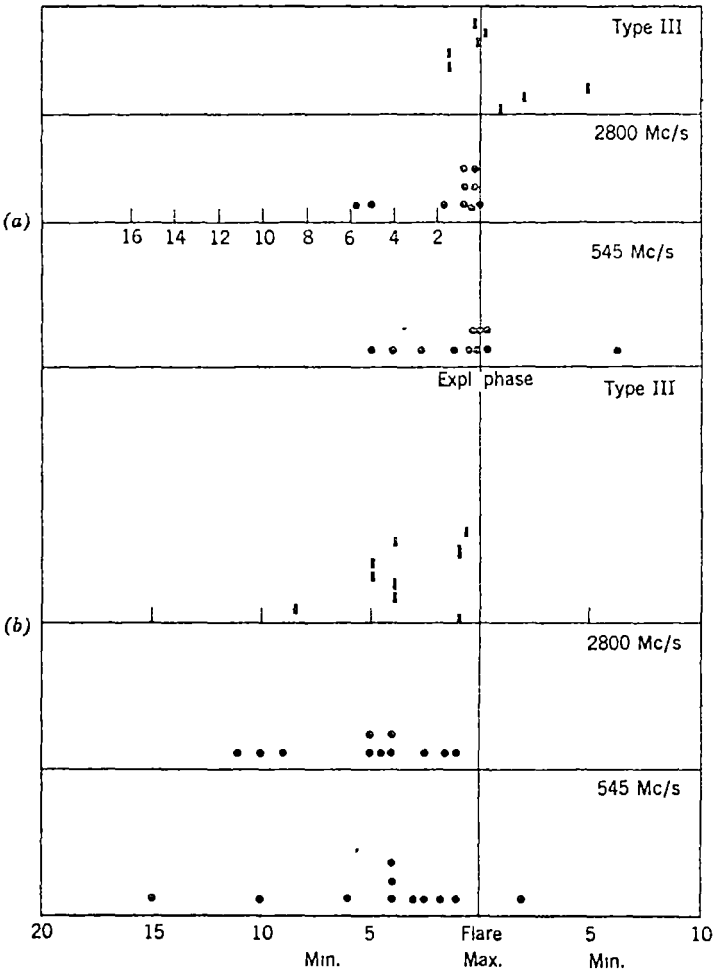

Fig. 8.2(D) Distribution of start of 545 Mc/sec, 2800 Mc/sec, and meter-wavelength type III bursts with respect to the (*a*) explosive phase, (*b*) maxima of the associated flares. (After Kundu, 1965)

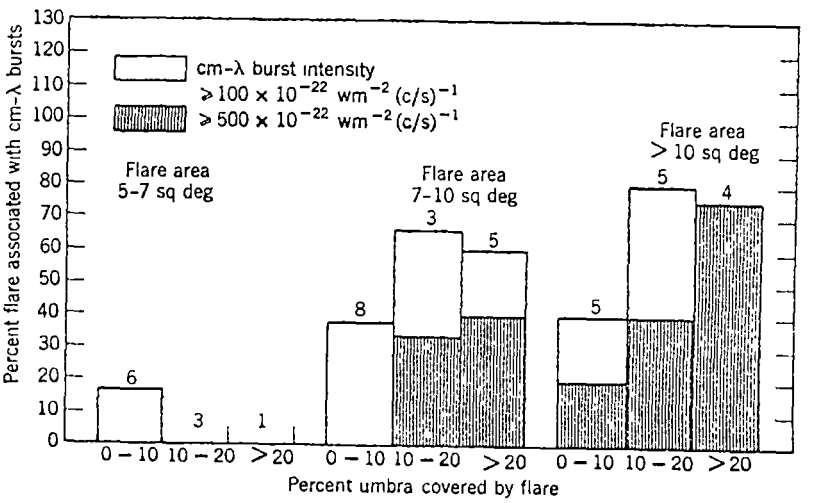

Fig. 8.2(E) Percentage of flares of different areas associated with centimeter-wavelength bursts as a function of the percentage of the umbra covered by the associated flare (after Malville and Smith 1963)

continuum bursts, sometimes with fine structure bursts superimposed on it, are in most cases associated with a group of type III bursts.

(xi) Directivity and Angular Size

Type IVA bursts at centimetre wavelengths do not exhibit any directivity, but at decimetre wavelengths they show slight directivity towards the centre of the Sun (Takakura, 1963) (Fig. 8.2(H)). The diameter of the source is 2-4 min of arc (Wild et al., 1963), which is less than that of a type I noise storm (Fig. 8.2(C)).

Type IV emission at metre wavelengths was first discovered by Boischot (1957) and was interpreted as a consequence of incoherent synchrotron radiation from electrons of energy of a few million electron-volts gyrating in the sunspot magnetic field (Boischot and Denisse, 1957). Takakura (1960b, 1960c) and Takakura and Kai (1961) used the synchrotron radiation theory to explain the whole type IV event in different phases and at different wavelengths. In order to explain the reverse of sense of polarization, without taking account of differential harmonic resonance absorption, Takakura (1962) suggested that the centimetre wavelength type IV was associated with synchrotron radiation from electrons with energy of the order of a few hundred keV accumulated above the leading spot while the decimetre wavelength type IV source was above the following spot. The

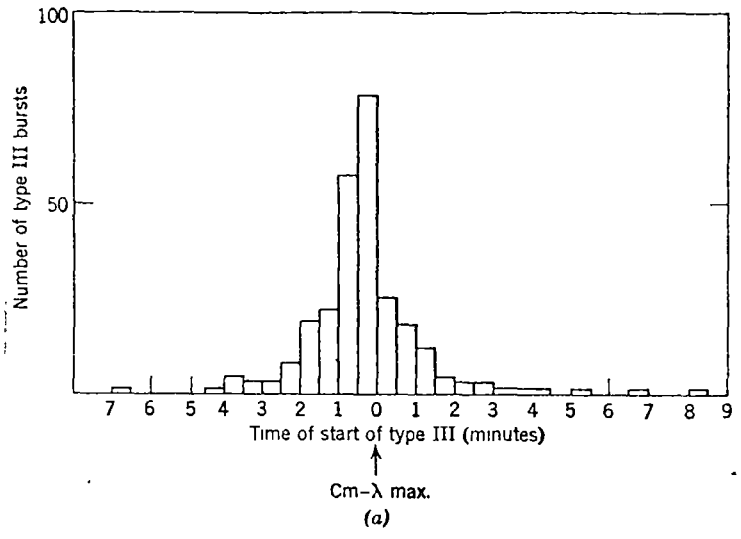

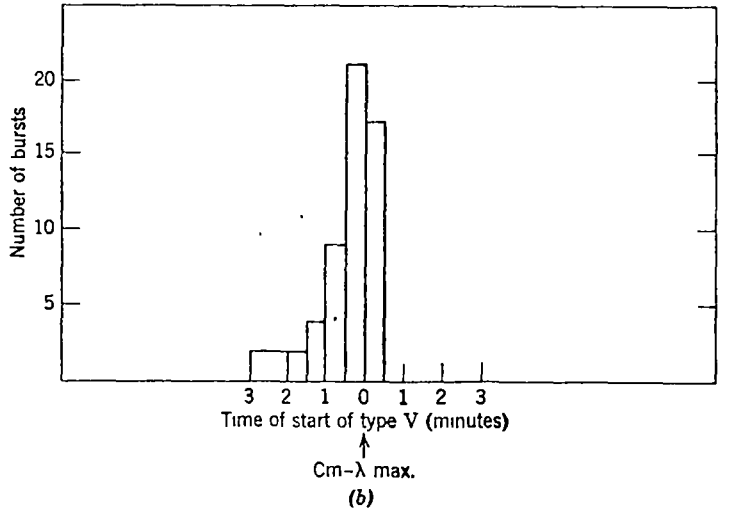

Fig. 8.2(F) Distributions of time of start of (*a*) type III bursts, (*b*) type V bursts, and (*c*) type II bursts, relative to centimeter-wavelength maximum (after Kundu 1962a).

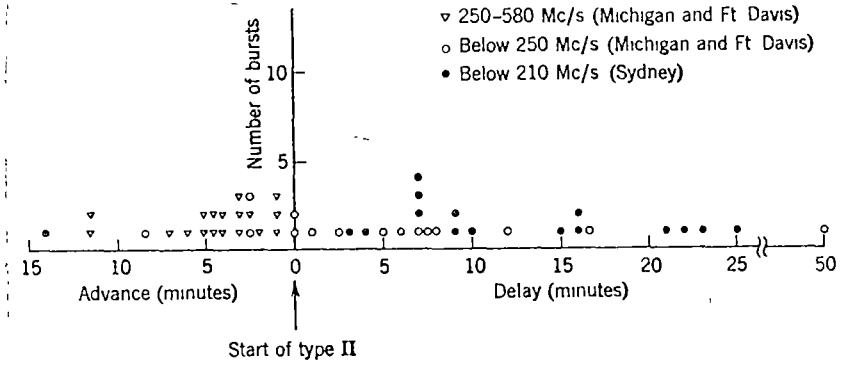

Fig. 8.2(G) Distribution of the starting times of type IV bursts in two frequency ranges—250 to 580 Mc/sec and 100 to 250 Mc/sec—relative to associated type II bursts (after Kundu 1962b).

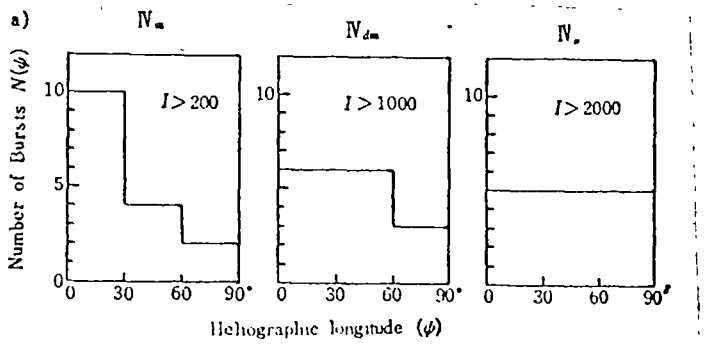

FIG. 8.2(H) Center to limb variation in the *number* of each component of type IV bursts with intensities greater than a given value shown in the diagram. (After Takakura, 1963).

type IVA bursts at centimetre and decimetre wavelengths are considered to have separate sources. Kundu (1965, p.441) pointed out that the narrow bandwidth of decimetre wavelength bursts cannot be explained as synchrotron radiation; radiation from plasma waves may be a possible mechanism. The drift bursts that are superimposed on the smooth continuum are considered as plasma radiation induced by passage of disturbances travelling outward through the solar corona with speed ~ ½c (Young et al., 1961).

It was suggested by Kai (1964) that the type IVA continuum bursts in both centimetre and decimetre wavelength regions may be the consequence of gyro-synchrotron radiation by energetic electrons moving along a quasi-circular orbit in the sunspot magnetic field configurations. The energy of radiating electrons responsible for the centimetre and decimetre wavelength components are of the order of 100 keV and of 10 keV respectively. Hence, using the general expressions of emissivity and absorption coefficient for gyro-synchrotron radiation in the tenuous plasma ($f_p << f$) obtained by Kawabata (1964), Kai showed that the polarization character and high intensity of the type IVA continuum burst emission may be accounted for by the theory of gyro-synchrotron emission if the self-absorption as well as cyclotron resonance absorption due to the thermal plasma electrons are taken into account. It was believed that the high intensity decimetre

wavelength component was associated with the low harmonic cyclotron resonance absorption. Kawabata's general expressions of the emissivity and the absorption coefficient were derived on the assumption that the refractive index for the gyro-synchrotron radiation is unity. This assumption is valid only if we assume that in the type IVA source region, the local gyrofrequency is much greater than the local plasma frequency (i.e. $A \ll 1$) such that the frequency of the low harmonic gyro-synchrotron radiation by weakly or mildly relativistic electrons satisfies the inequality $f \gg f_p$. Alternatively, one may assume that the energy of the radiating electrons is highly relativistic such that the maximum gyro-synchrotron radiation occurs at very high harmonics.

However, interpretation of the type IVA emission based on either assumption will meet severe difficulties. Since under these assumptions, the plasma becomes so tenuous to the gyro-synchrotron radiation that the lower harmonic cyclotron resonance absorptions are ineffective for electromagnetic waves in both x- and o-modes (see Fig. 6.6, Chapter VI), the polarization of the type IVA continuum burst emission at both decimetre and centimetre wavelengths is expected to be extraordinary mode. We shall see later in this chapter that the refractive index associated with the maximum cyclotron radiation emitted by electrons with energy in the

range from a few ten to hundred keV departs from unity significantly. Moreover, in general, it is more realistic to assume a helical trajectory for the radiating electron rather than a quasi-circular orbit. The Cerenkov plasma radiation can be the origin of the drifting elements superimposed on the continuum burst but obviously cannot be considered to be responsible for the wide bandwidth continuum since electromagnetic radiations at different frequencies in a very wide frequency range cannot be emitted simultaneously from a narrow emission layer in the solar corona by means of Cerenkov plasma radiation process (cf. Chapter VI and Chapter VII). Therefore, it is the purpose of this chapter, by adopting the generally accepted model for the evolution of the flare phenomena (Kundu, 1965, p. 594), to examine the possibility that the cyclotron radiation from a helical electron stream moving in the lower solar corona is the origin of the type IVA burst emission.

B. Model of The Type IVA Emission Source Region

The observed type IVA emission sources rarely extends beyond the altitude about 0.06 solar radius above the photosphere. Optical observational data indicate that in the transition region between the chromosphere and the base of the solar corona, the electron density and the electron density gradient are greater than those predicted by the

coronal streamer model (several to ten times the Baumbach-Allen formula). Ivanov-Kholodnyi and Nikol'skii (1962), from a detailed analysis of observational data, obtained the distribution of electron density with height in the active and undisturbed regions of the solar atmosphere (see Section A, Chapter IV). Using their observation results, the plasma frequency along the active corona from $\rho = 1.005$ to 1.043 is plotted in Fig. 8.3. The curve is smoothly continued by employing the 5×Baumbach-Allen formula.

Since only a small number of the sunspot magnetic field lines normal to the photosphere in the umbral area of a sunspot can stretch to the outer layers of the solar corona forming a narrow magnetic flux tube, many sunspot field lines inclining to the radial line of the Sun at an angle at the photosphere will not extend to great height but curve quickly down to the photosphere forming small loops of bipolar sunspot magnetic field lines in the most inner layers of the solar atmosphere. Taking the maximum field intensity of the leading spot to be H_s = 3,000 gauss, we set up the model for the sunspot magnetic field intensity as shown in Fig. 8.3. If the type IVA emission whose frequencies range from 500 to 10,000 MHz is the result of cyclotron radiation from electron streams gyrating along sunspot magnetic field lines, the region of emission will be less than 40,000 km above the photosphere. Within the type IVA emission source region, the

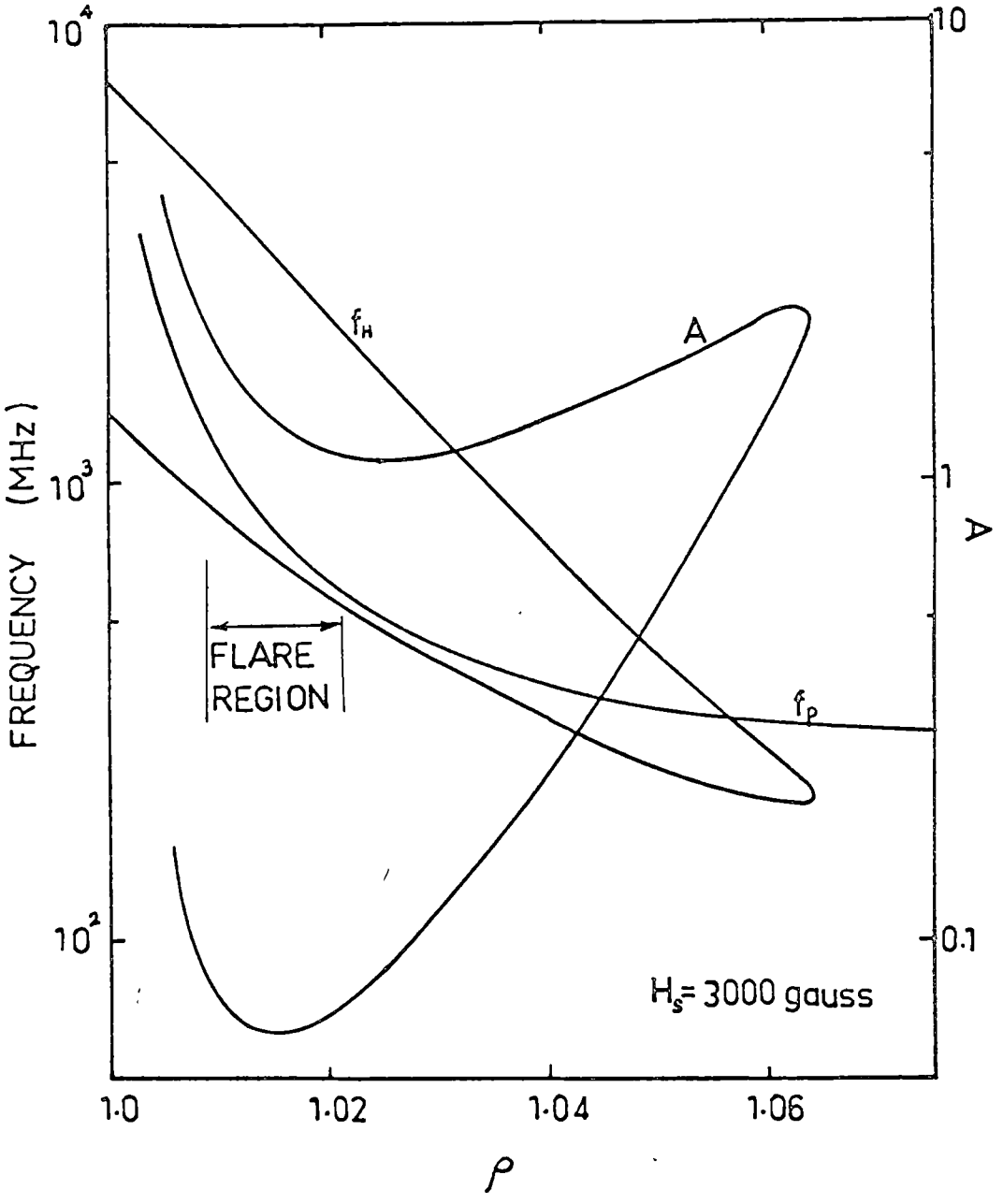

Fig.8.3 - Variation of the plasma frequency f_p (using the Ivanov-Kholodnyi and Nikol'skii model and the 5xBaumbach-Allen model), gyrofrequency f_H and A along the strongest field line of a bipolar sunspot pair specified by H_s = 3000 G.

quantity A varies from a very small value to about several.

C. Radiation From Electron Streams In Sunspot Magnetic Field

During the occurrence of a very large flare, electrons with energy 10-100 keV (occasionally more) in the form of electron streams are expelled from the flare region (De Jager, 1960). Most of these electron streams will be trapped in the neighbouring strong sunspot magnetic field and will interact with the ambient plasma. Harmonic cyclotron radiations in the ordinary and extraordinary modes from stream electrons will grow as they propagate through the stream-plasma system. Using the model indicated in Section B for the type IVA emission source medium, we shall study the characteristics of forward normal cyclotron radiation from streams of electrons with energy in the range from a few ten to two hundred keV for different electron pitch angles $\emptyset$. In considering generation of coherent cyclotron radiation in the x-mode and the o-mode by electron streams, we can assume the coronal plasma is cold and collisionless.

(a) Radiation Frequency

A single electron spiralling along a magnetic field line of force radiates electromagnetic waves at different frequencies and in different modes in different directions.

The relation between the normalized radiation frequency ξ and the wave-normal angle θ is given by the emission equation:

$$\xi = s\gamma/(1 - n_j\beta_{\parallel}\cos\theta), \qquad (8.1)$$

where n_j is the refractive index for the ordinary wave (j=2) or the extraordinary wave (j=1) in the ambient plasma. For a cold and collisionless magnetoactive plasma

$$n_{1,2}^2 = 1 - \frac{2A(\xi^2-A)}{2\xi^2(\xi^2-A)-\xi^2\sin^2\theta \mp \sqrt{\xi^4\sin^4\theta+4\xi^2(\xi^2-A)^2\cos^2\theta}}. \qquad (8.2)$$

In order to find the normalized radiation frequency in a particular direction with respect to the magnetic field, equations(8.1) and (8.2) must be solved simultaneously by the algebraic or graphical method (Ellis, 1964). The curves of refractive index n_j against normalized frequency ξ for various values of θ and $s > 0$ (normal cyclotron radiation) from (8.1) and (8.2) are plotted in Fig. 8.4. Fig. 8.5 shows the simultaneous solutions for ξ and θ of (8.1) and (8.2).

From Fig. 8.5, we find that there are two types of simultaneous solutions for ξ and θ:

(1) the double-frequency solution, i.e. to each wave-normal angle there corresponds two normalized frequencies;

(2) the single-frequency solution, i.e. only one

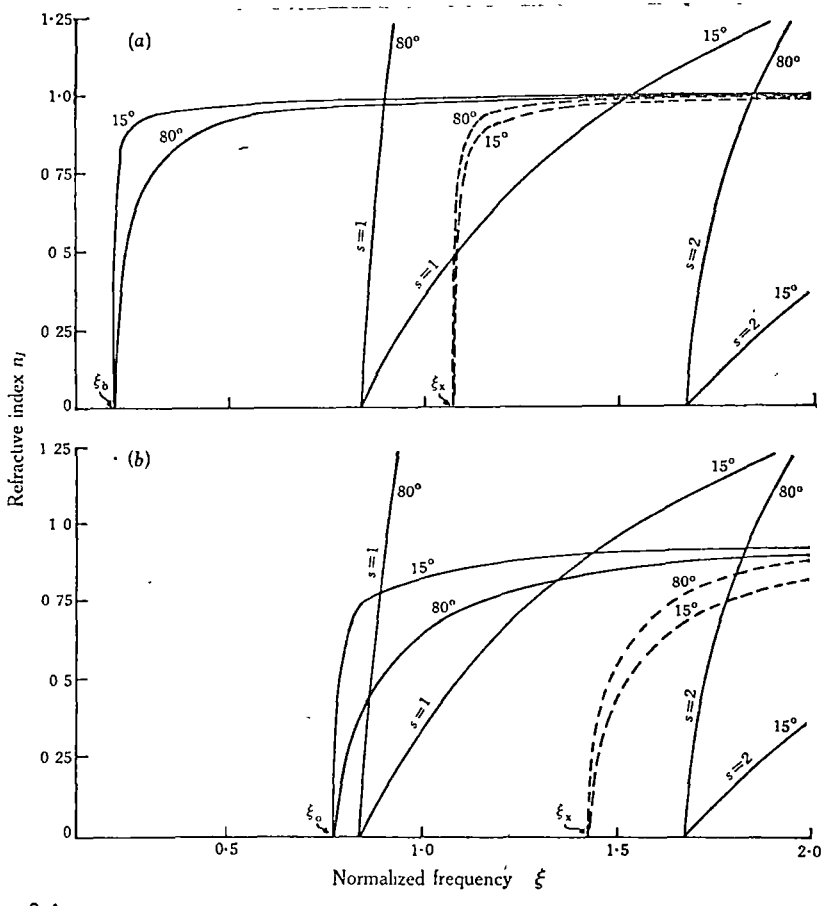

Fig 8·4 Refractive index n_f for the o-mode (full lines) and x-mode (dashed lines) against the normalized wave frequency ξ for (*a*) $A = 0{\cdot}04$, (*b*) $A = 0{\cdot}6$, and $\theta = 15°$ and 80°. The emission equation is also plotted for the first two harmonics $s = 1$, 2 as a function of ξ for electron energy $E = 100$ keV and electron pitch angle $\phi = 30°$.

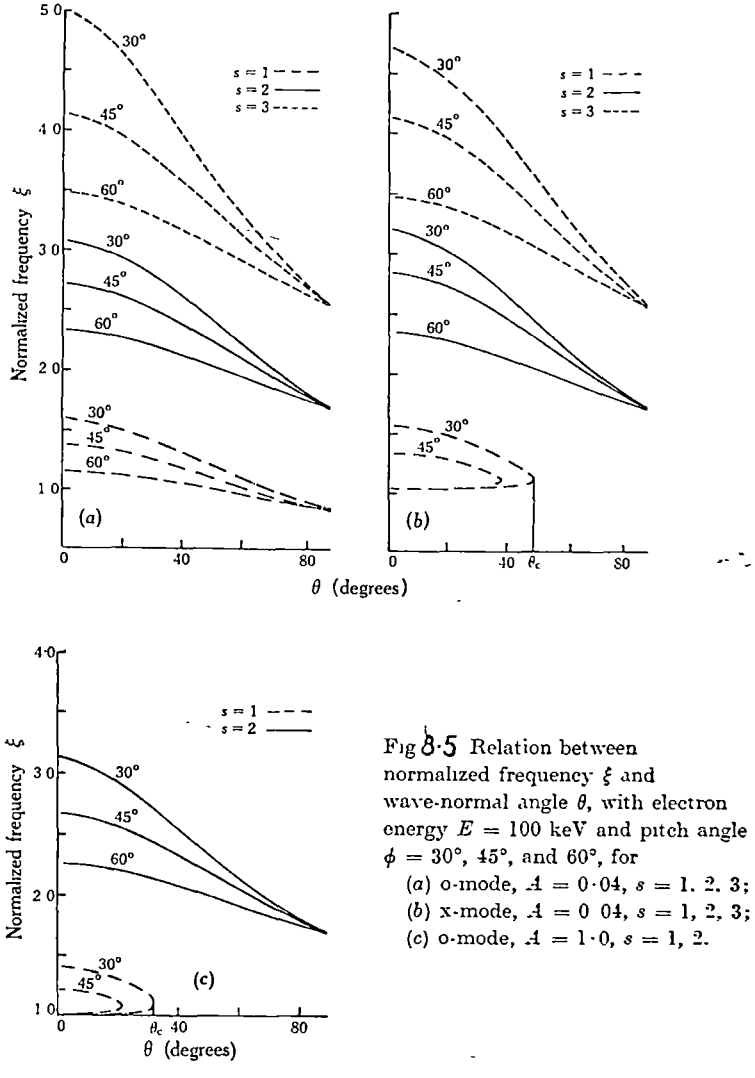

Fig 8·5 Relation between normalized frequency ξ and wave-normal angle θ, with electron energy $E = 100$ keV and pitch angle $\phi = 30°$, 45°, and 60°, for
(*a*) o-mode, $A = 0{\cdot}04$, $s = 1, 2, 3$;
(*b*) x-mode, $A = 0{\cdot}04$, $s = 1, 2, 3$;
(*c*) o-mode, $A = 1{\cdot}0$, $s = 1, 2$.

normalized frequency corresponds to one wave-normal angle.

The double-frequency solution is possible when

$$s\gamma < \xi_o = A^{\frac{1}{2}} \quad \text{(o-mode)}, \tag{8.3}$$

or $$s\gamma < \xi_x = \tfrac{1}{2}[1+(1+4A)^{\frac{1}{2}}] \quad \text{(x-mode)}.$$

Whenever conditions (8.3) are satisfied, the radiation is emitted within a cone with an apex angle $2\theta_c$ and the magnetic field line as axis. The angle θ_c is the angle beyond which there is no radiation at all and is termed the cut-off angle. For conditions other than (8.3) we have a single-frequency solution only. We note that in certain cases, e.g. for a very large electron pitch angle or ξ_o(or ξ_x) >> $s\gamma$, there is no simultaneous solution of any type for ξ and θ. For both o-mode and x-mode, the range of the radiation frequency is wider for smaller electron pitch angles.

(b) Power Spectra radiated by a Single Electron

Corresponding to the values of normalized frequency ξ and wave-normal angle θ obtained by solving equations (8.1) and (8.2) simultaneously, the radiation power by a single electron within unit solid angle can be computed by using the equation (Liemohn, 1965):

$$P(\theta) = e^2\omega^2 n_j K_j^2 [-\beta_\perp J_s'(a)+(\alpha_y s\beta_\perp/a+\alpha_z\beta_{||})J_s(a)]^2(1+\frac{\omega}{n_j}\frac{\partial n_j}{\partial\omega})/$$

$$2\pi c \left|1 - \beta_{||} n_j \cos\theta(1 + \frac{\omega}{n_j}\frac{\partial n_j}{\partial\omega})\right| , \qquad (8.4)$$

where $\alpha_y = \alpha_\theta'\cos\theta + \alpha_k'\sin\theta$, $\alpha_z = \alpha_k'\cos\theta - \alpha_\theta'\sin\theta$,

$$K_j = (1 + \alpha_\theta'^2)^{-\frac{1}{2}} ,$$

$$\alpha_\theta' = -\cos\theta/[\xi^2+A(n_j^2 - 1)^{-1}] \ , \ \alpha_k' = -\xi\sin\theta(n_j^2-1)/(A-\xi^2),$$

J_s and J_s' are the Bessel function and its derivative with respect to the argument $a = \beta_\perp\xi\sin\theta n_j/\gamma$, and n_j is the refractive index given by (8.2). Here the wave is assumed to be in the form $\exp(-i\bar{k}.\bar{r}+i\omega t)$ with wave vector $\bar{k}$ lying on the y-z plane in a Cartesian coordinate system. For electron energy E = 50, 100, 200 keV, A = 0.04, 1, s=1,2,3 and electron pitch angle $\phi = 60^\circ$, 45°, 30°, the power spectra radiated by a single electron in the o-mode and the x-mode are presented in Fig. 8.6. From these spectra, the following points are noted:

(1) For the double-frequency solution, the radiation power peaks sharply at wave-normal angles near θ_c.

(2) For the single-frequency solution and s = 2,3, the o-mode power reaches a maximum at wave-normal angles ranging from 50° to 70°, while for the x-mode the emission

cone is very broad.

(3) For the single-frequency solution, radiation power for both the o-mode and the x-mode is inversely proportional to the harmonic number.

(4) For the same set of values of A, s, $\emptyset$ and E, the peak power in the x-mode radiated by a single electron is about one order of magnitude higher than that in the o-mode. However, this difference tends to decrease as the electron energy increases (Fig. 8.6(d)).

(5) When the electron energy increases, radiation power in both modes tends to maximize in the direction of the electron velocity vector (Fig. 8.6(d) and (e)).

(c) Excitation of Cyclotron Radiation in the Stream-plasma System

It is known that electromagnetic waves emitted from gyrating electrons can be amplified in a stream-plasma system if the distribution of the stream electrons has a narrow momentum spread. Using the classical kinetic approach, the radiative instability problem of a helical stream-plasma system for the most general cases has been studied in Chapter III. Assuming no dispersion of electron momentum components, it is found that the rate of growth of the electromagnetic wave in a helical stream-plasma system $|\mathrm{Im}\delta|$ is given by

$$\left| \mathrm{Im} \frac{\delta}{\omega_H} \right| = \frac{\sqrt{3}}{2} \xi \left| M_p^{\frac{1}{3}} - N_p^{\frac{1}{3}} \right|, \qquad (8.5)$$

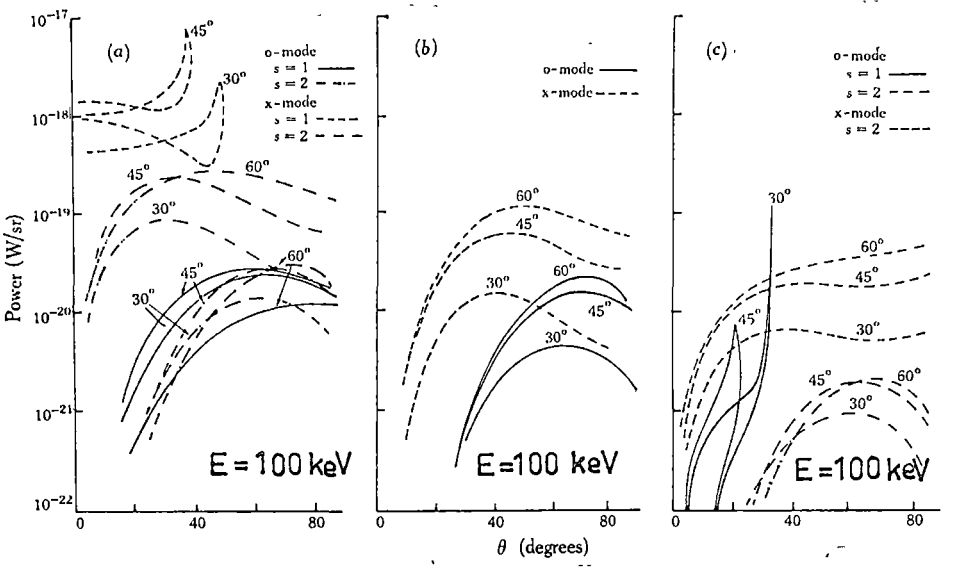

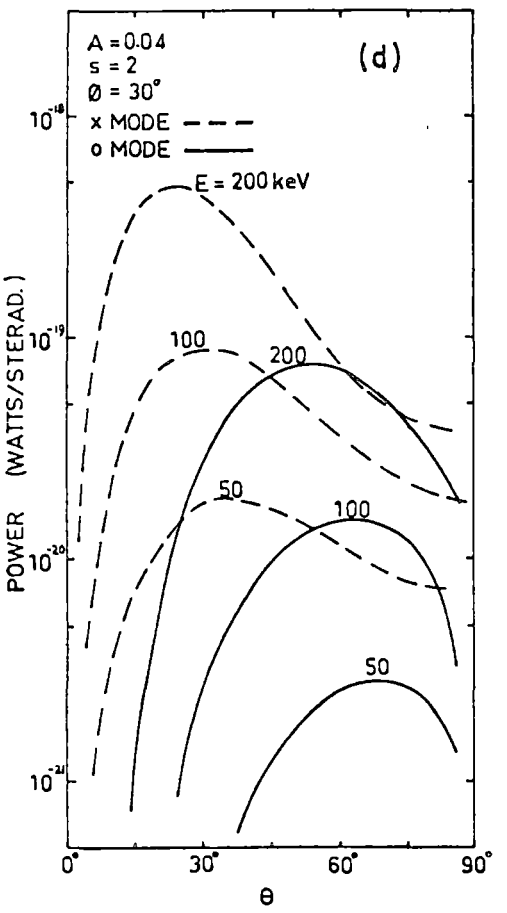

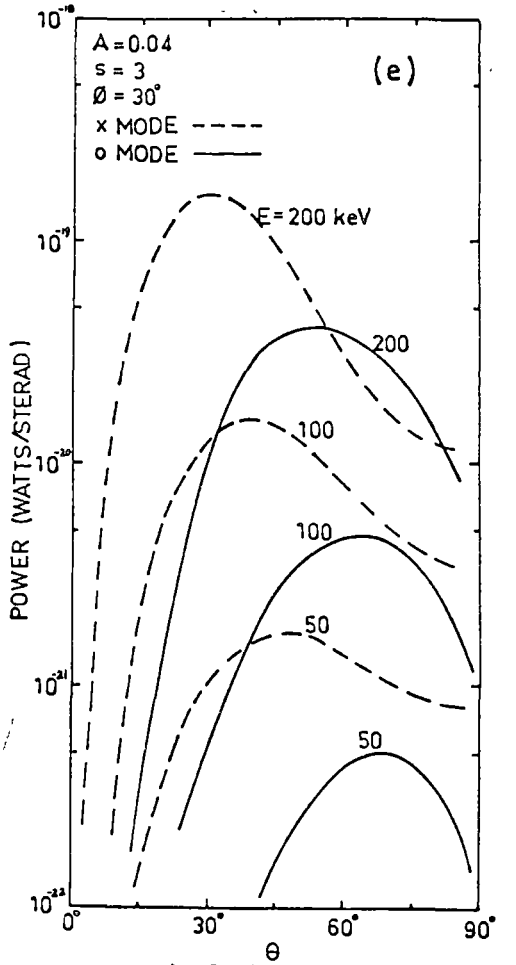

Fig.8.6 - Power spectra radiated by a single electron with energy E = 50,100,200 keV and pitch angle $\emptyset$ = 30°,45°,60°, for o-mode and x-mode, various values of s and

(a) A = 0.04, f_H = 1000 MHz;
(b) A = 0.04, f_H = 1000 MHz, s=3;
(c) A = 1, f_H = 300 MHz;
(d) A = 0.04, f_H = 1000 MHz;
(e) A = 0.04, f_H = 1000 MHz.

where M_p and N_p are defined in (3.9) (Chapter III).

Taking $\sigma = 10^{-6}$ and various values of the other parameters, the rates of growth of cyclotron radiation power in the o-mode and the x-mode are illustrated in Fig. 8.7, Fig. 8.8 and Fig. 8.9. The normalized frequency ξ and the wave-normal angle θ of the cyclotron radiation satisfy the emission equation (8.1). These graphs indicate:

(1) With the same values of f_H, s and σ, radiation power in the x-mode grows with time at a rate similar to that for the o-mode radiation power when A is small, but as A increases the growth rate for the o-mode power exceeds that for the x-mode power (Fig. 8.7 and Fig. 8.9).

(2) For the single-frequency solution and for both modes, the growth rate maximizes at the wave-normal angle θ in the range from 50° to 70° when the electron pitch angle $\phi \leq 30^\circ$ and $s > 1$. However, the rates of growth for the second and the third harmonic radiations in both modes tend to maximize in the direction transverse to the static magnetic field line as ϕ increases (Fig. 8.7(a)-(f)).

(3) In the case of a single-frequency solution for the x-mode and the o-mode, the growth rate for the third harmonic radiation does not exceed that for the second harmonic radiation if $\phi < 30^\circ$ and $E < 100$ keV. But the third harmonic radiation would grow more rapidly than the corresponding second harmonic radiation when the stream electrons have either pitch

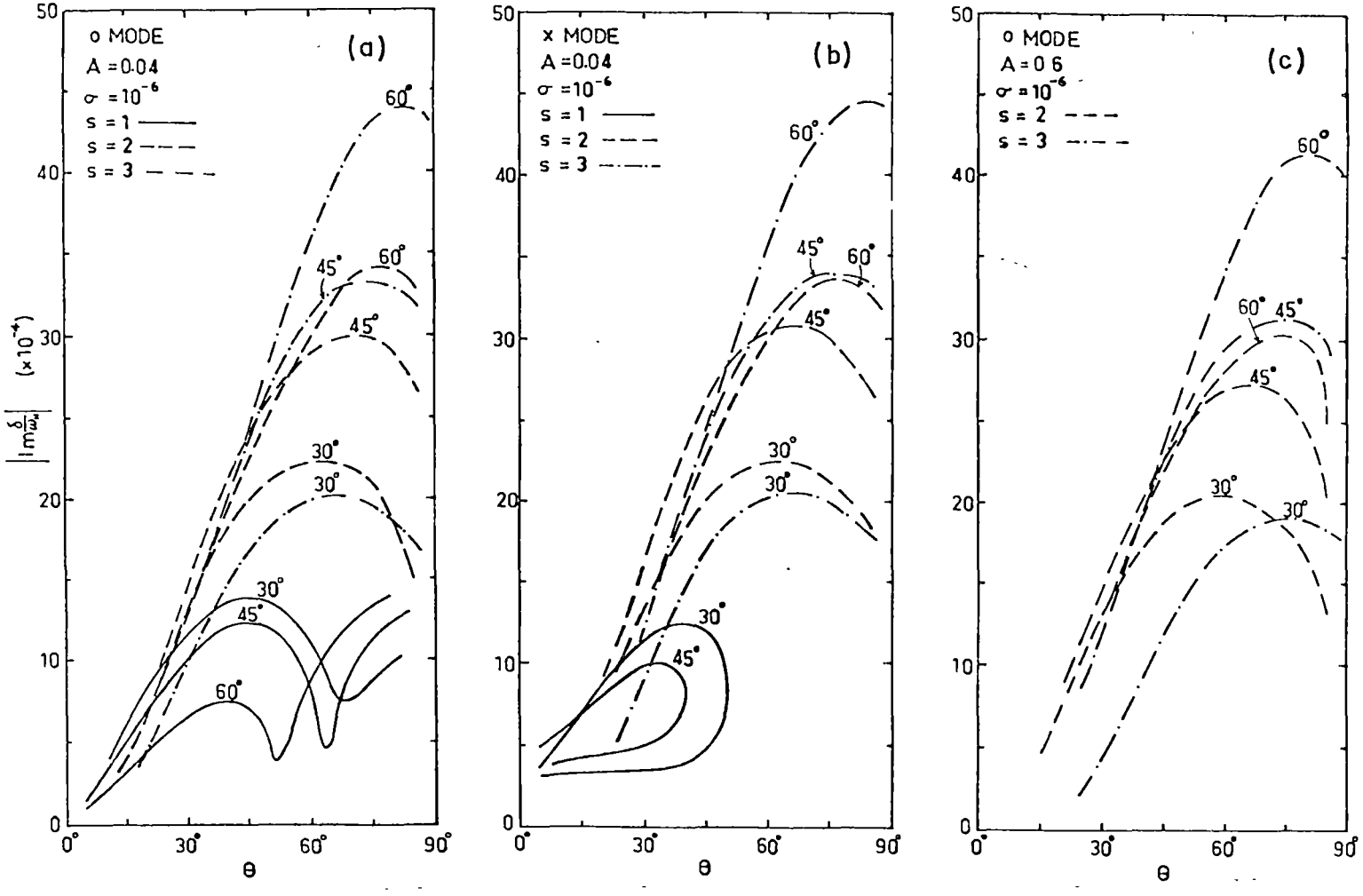

Fig. 8.7 -The dependence of the growth rate $\left|\frac{\text{Im}\,\delta}{\omega_H}\right|$ on wave-normal angle θ, with $\sigma = 10^{-6}$, $E = 100$ keV, and $\phi = 30°$, 45°, and 60°, for

(*a*) o-mode, $A = 0{\cdot}04$, $f_H = 1000$ MHz, $s = 1, 2, 3$;

(*b*) x-mode, $A = 0{\cdot}04$, $f_H = 1000$ MHz, $s = 1, 2, 3$;

(*c*) o-mode, $A = 0\ 6$, $f_H = 600$ MHz, $s = 2, 3$;

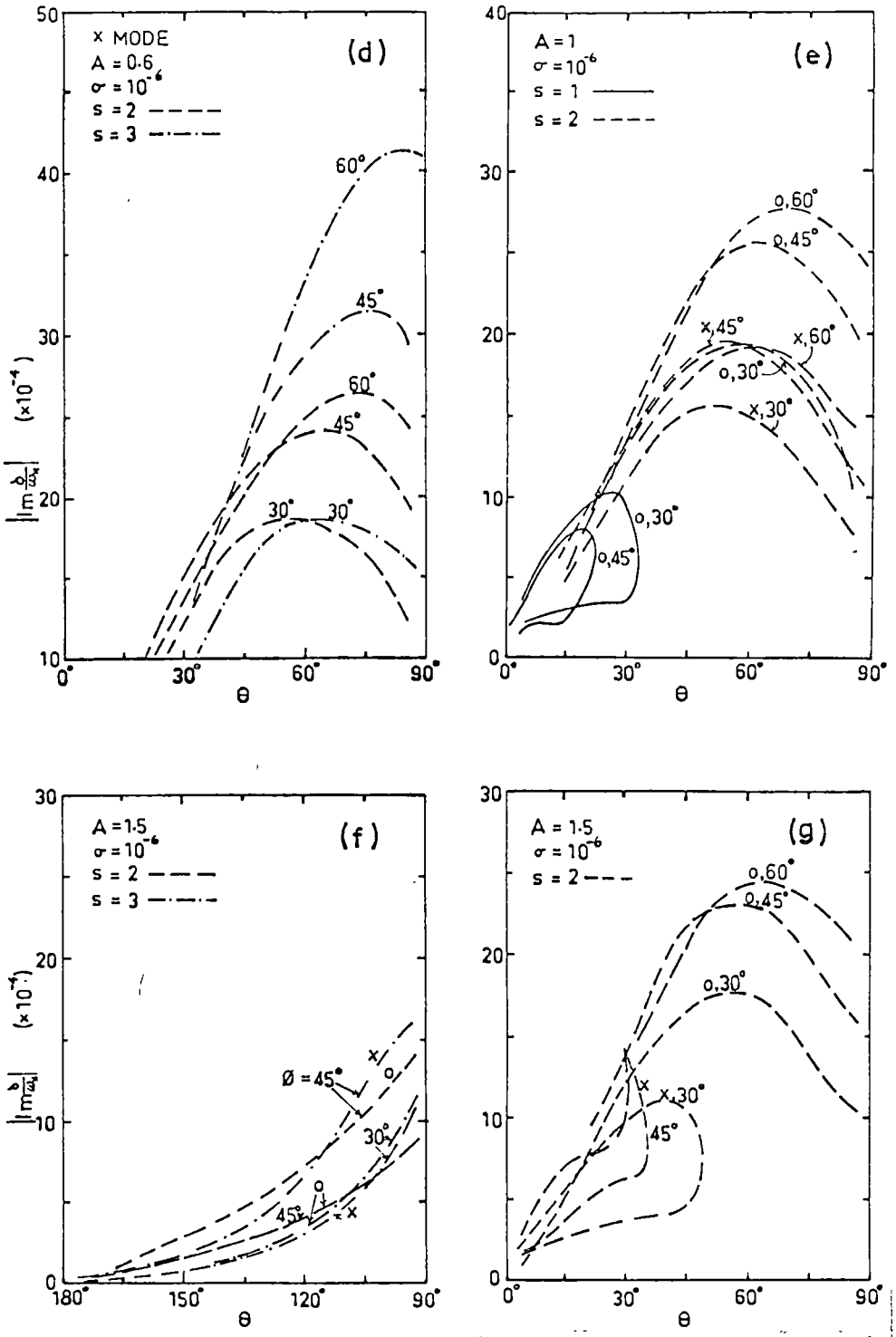

Fig. 8.7 The dependence of the growth rate $\left|\frac{\mathrm{Im}\,\delta}{\omega_H}\right|$ on wave-normal angle θ, with $\sigma = 10^{-6}$, $E = 100$ keV, and $\phi = 30°$, 45°, and 60°, for

(*d*) x-mode, $A = 0{\cdot}6$, $f_H = 600$ MHz, $s = 2, 3$;

(*e*) o-mode and x-mode, $A = 1{\cdot}0$, $f_H = 300$ MHz, $s = 1, 2$;

(*f*) o-mode and x-mode, $A = 1{\cdot}5$, $f_H = 300$ MHz, $s = 2, 3$;

(*g*) o-mode and x-mode, $A = 1{\cdot}5$, $f_H = 300$ MHz, $s = 2$.

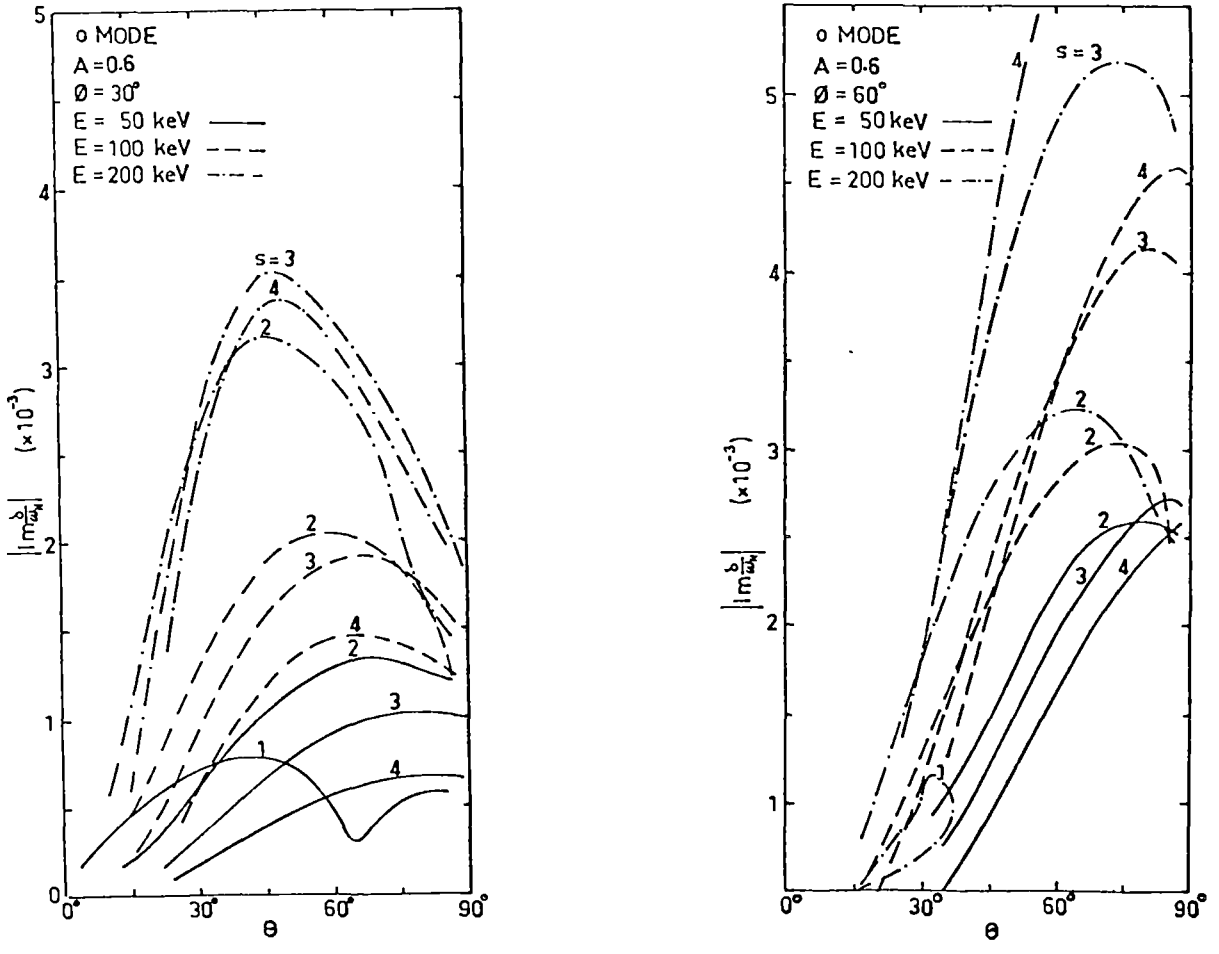

Fig.8.8 - The dependence of the growth rate $\left|\mathrm{Im}\frac{\delta}{\omega_H}\right|$ on wave-normal angle θ for o-mode wave and for $\sigma = 10^{-6}$, A = 0.6, s = 1,2,3, E = 50,100,200 keV, and (a) $\phi = 30°$; (b) $\phi = 60°$.

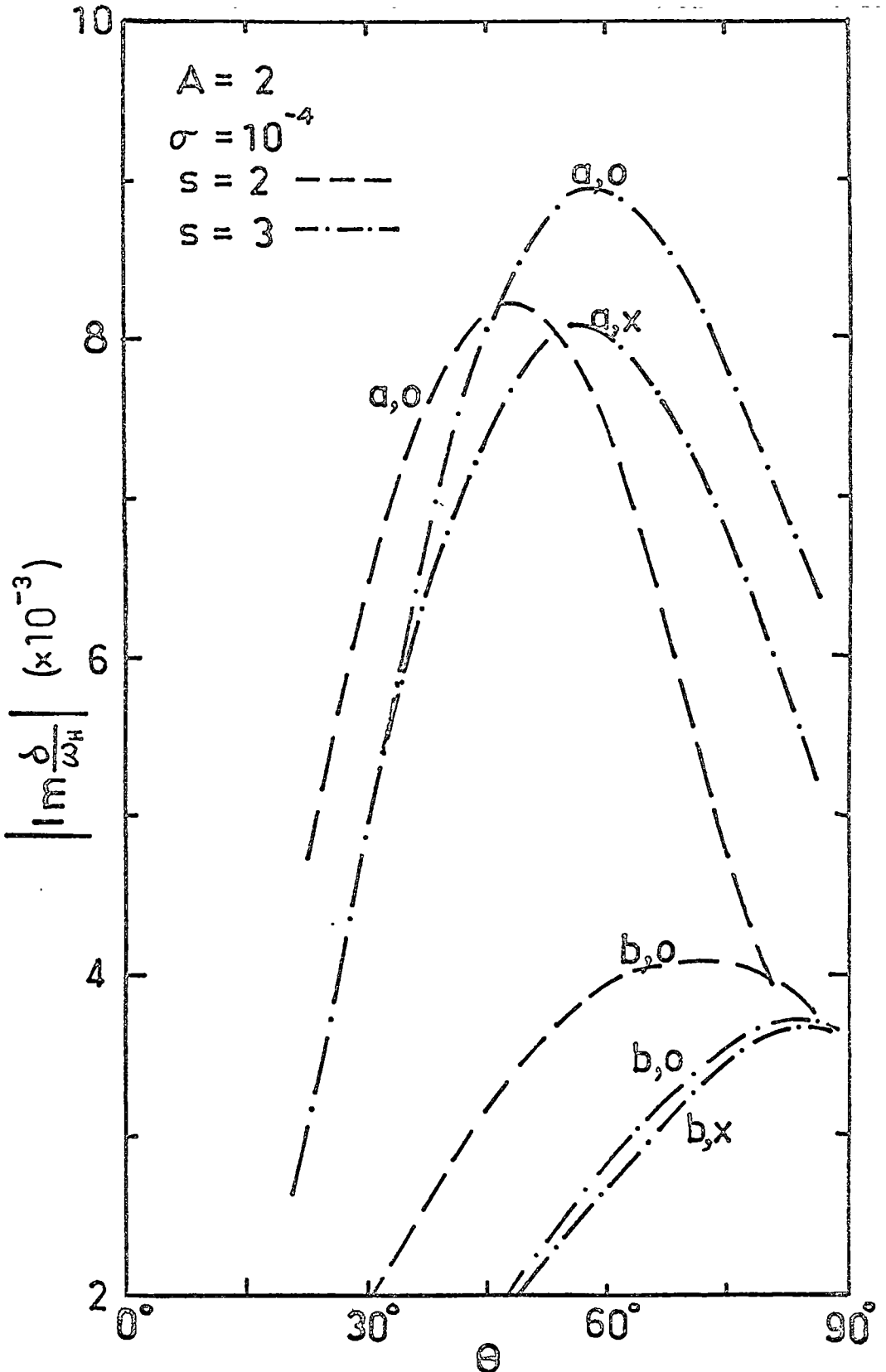

Fig.8.9 - The dependence of the growth rate $\left|\mathrm{Im}\frac{\delta}{\omega_H}\right|$ on wave-normal angle θ for x-mode and o-mode, A = 2, $\sigma = 10^{-4}$, s = 2,3, and for (a) E = 115 keV, ϕ = 31°; (b) E = 20.5 keV, ϕ = 45°.

angle $\emptyset > 30^{o}$ or electron energy E > 100 keV (Fig. 8.7 (a) - (c); Fig. 8.8 (a) - (b)). For higher electron energy, the maximum coherent cyclotron radiation occurs at higher harmonics of the Doppler-shifted gyrofrequency (Fig. 8.8 and Fig. 8.9).

(4) For a given harmonic number, the cyclotron radiation in the subluminous mode (i.e. x-mode and o-mode) emitted in the forward direction with respect to the electron guiding centre motion will grow more rapidly than that emitted in the backward direction (Fig. 8.7 (f) and (g)).

(5) As the electron energy tends to be highly relativistic, the coherent cyclotron radiation tends to maximize in the direction of the instantaneous electron velocity vector (Fig. 8.8).

(6) In Fig. 8.10, the rates of growth for the cyclotron radiation in the x-mode and the o-mode in the stream-plasma system are shown as functions of normalized emission frequency for A = 0.04, 1.5, $\sigma=10^{-6}$, E=50,100,200 keV, s=2,3, $\emptyset = 30^{o},45^{o},60^{o}$ and for wave-normal angle $\theta \leq 90^{o}$. The corresponding rate of growth for the Cerenkov radiation in the plasma mode is also illustrated as a function of normalized combination frequency $\xi \simeq 2\xi_{ch}$, ξ_{ch} being the normalized Cerenkov plasma wave frequency (dash-dotted lines). Firstly we observe that the frequency bandwidth of the coherent cyclotron radiation in the forward subluminous mode increases with

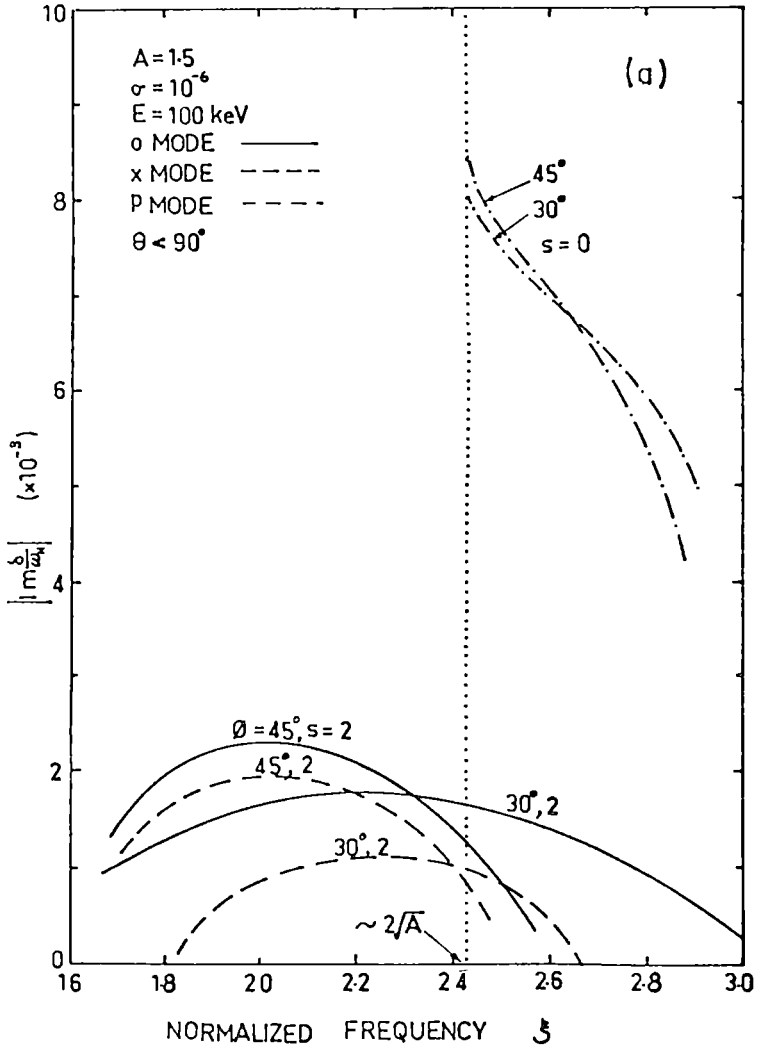

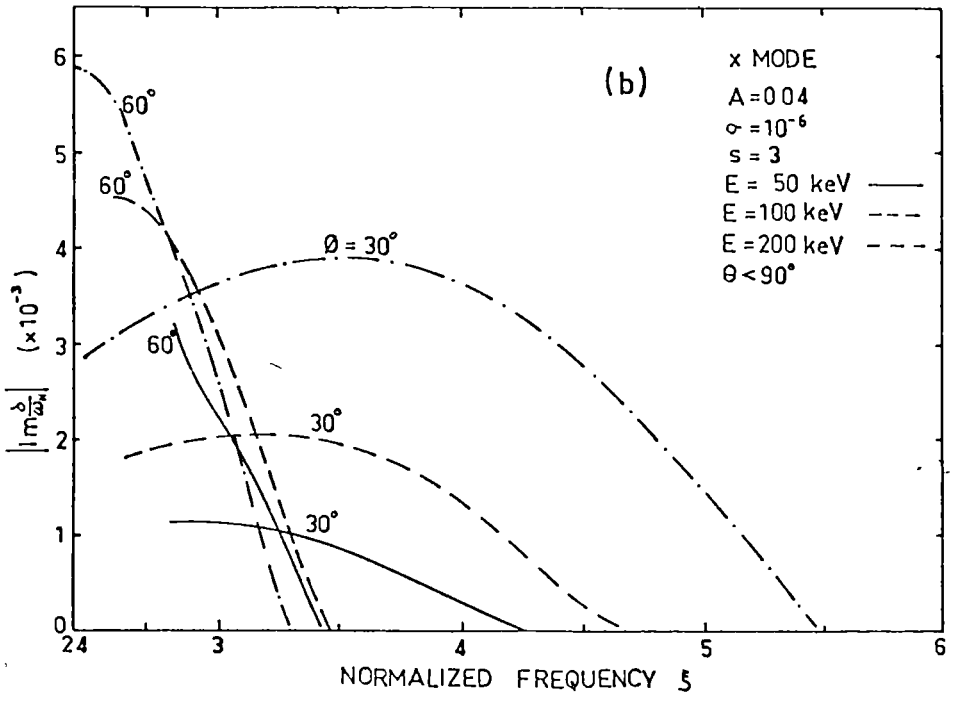

Fig.8.10- Variation of growth rate $\left|\mathrm{Im}\frac{\delta}{\omega_H}\right|$ with normalize wave frequency ξ for wave-normal angle $\theta \leq 90^\circ$, $\sigma = 10^{-6}$ and for

(a) x- ,o- and n- modes, A=1.5, E = 100 keV, $\phi = 30^\circ, 45^\circ$, s = 0,2, $\beta_T = 10^{-2}$;

(b) x-mode, A = 0.04, E = 50,100,200 keV, $\phi = 30^\circ, 60^\circ$, s = 3.

decreasing electron pitch angle. Secondly, the maximum coherent cyclotron radiation would be emitted at the frequency lower than the third harmonic of the gyrofrequency only when the electron energy is less than 100 keV and when electron pitch angle is greater than 60^{o}.

(7) Finally, comparing Fig. 8.7 with Fig. 8.6, we find that in general the cyclotron radiation grows most rapidly in the direction close to the direction in which the maximum single electron cyclotron radiation power is emitted. Therefore, when the electron energy is less than 100 keV, the main coherent cyclotron radiation power in both modes is emitted at the second harmonic Doppler-shifted gyrofrequency and within a cone whose axis is along the wave-normal direction $\theta \simeq 65^{o}$. The ratio of the x-mode power to the o-mode power (denoted by r) does not exceed ten. According to the discussion given in (1), the ratio r will decrease with increasing value of A. Hence, we conclude that the x-mode radiation power will predominate when either A is small or the electron energy is large.

D. Resonance Absorption at The First Three Harmonic Layers

Since the radiating electron stream is assumed to move along the strongest sunspot magnetic field line, the cyclotron radiation at the s-th harmonic of the Doppler-shifted gyrofrequency will encounter the harmonic resonance

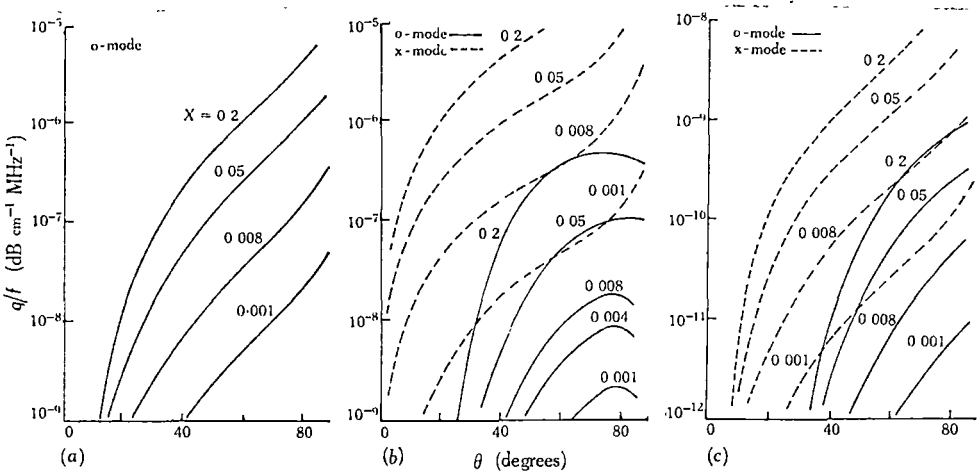

Fig 8.11 Variation of harmonic resonance absorption coefficient (q/f) for o-mode and x-mode with wave-normal angle θ for various values of X, $\beta_T = 10^{-2}$, and (*a*) $s = 1$, (*b*) $s = 2$, and (*c*) $s = 3$.

TABLE 8·1

POWER LOST AND TRANSMITTED BY O-WAVES AND X-WAVES OF VARIOUS FREQUENCIES ON PASSING THROUGH THE FIRST THREE HARMONIC RESONANCE ABSORPTION LAYERS

f (MHz)	s	X	Power Loss (dB) l_2	l_1	R_j $j=2$	$j=1$	S $r=8$	$r=5$	P (%) $r=8$	$r=5$
6000	1	0·0045	1·04(3)*	/ —	1(−104)	—				
	2		1·87(2)	8(3)	2(−19)	1(−800)				
	3		2·34(−1)	5·6	9·5(−1)	2·76(−1)	2·32	1·45	40	18·4
5000	1	0·0064	1·29(3)	—	1(−129)	—				
	2		2·55(2)	9·9(3)	3·12(−26)	1(−990)				
	3		2·85(−1)	6	9·36(−1)	2·5(−1)	2·13	1·34	36·2	14·5
3500	1	0·0079	1·1(3)	—	1(−110)	—				
	2		2·52(2)	8·5(3)	6·3(−26)	1(−850)				
	3		2·3(−1)	7·35	9·5(−1)	1·84(−1)	1·55	0·87	21·6	−7·0
3000	1	0·018	1·98(3)	—	1(−198)	—				
	2		4·15(2)	1·62(4)	3·16(−42)	1(−1620)				
	3		5·04(−1)	9·9	8·9(−1)	1·02(−1)	0·92	0·57	−4·15	−27·4
2000	1	0·04	3·12(3)	—	1(−312)	—				
	2		6(2)	2·64(4)	1(−60)	1(−2640)				
	3		7·8(−1)	1·56(1)	8 35(−1)	2·75(−2)	0·264	0·16	−58·1	−72·5
1000	1	0·16	6·6(3)	—	1(−660)	—				
	2		2·4(3)	6(4)	1(−240)	1(−6000)				
	3		1·5	2·52(1)	7(−1)	3(−3)	0·0344	0·022	−93	−95·5

* Each number in parentheses is the common logarithm of the multiplier; 1·04(3) means $1{\cdot}04 \times 10^3$.

absorption layers $f = (s+n)f_H (n = 1,2,3,..)$ on leaving the radiation source. The efficiency of the s-th harmonic resonance absorption is specified by the coefficient

$$q = (q/k)_s n_j \omega/c \quad \text{(per unit phase path length)}, \quad (8.6)$$

where for $s = 1,2,3, (q/k)_s$ is given by (6.5) and (6.6). The dependence of the resonance absorption coefficient (q/f) on wave-normal angle θ for electromagnetic waves in both modes is shown in Fig. 8.11 for $\beta_T = 10^{-2}$, $s = 1,2,3$ and for various values of X. For all values of X, the resonance absorption is comparatively small when the wave-normal angle θ is less than 30°. For the same harmonic number s but higher wave frequency, resonance absorption will take place at a layer with stronger magnetic field and hence stronger is the resonance absorption. However, in this case, X becomes much smaller for the cyclotron radiation at higher frequencies if the electron density gradient is much less than the magnetic field intensity gradient. As a result, the resonance absorption for the same harmonic number s decreases with increasing frequency.

The power loss on passing through the resonance absorption layer given by (6.8) can be obtained by multiplying the value of (q/f) given in Fig. 8.11 by the effective thickness of the layer and the wave frequency. For the lower active

solar corona $\beta_T \simeq 10^{-2}$ and $L_H = 10^9$ cm, the effective thickness of the resonance absorption layer $L \simeq 6\times10^6$ cm if $\theta \simeq 65^o$ and $n_j \simeq 1$. Since the electron density gradient in the solar corona is much smaller than the magnetic field intensity gradient, the plasma frequencies in the first three resonance absorption layers for wave frequencies 6,000 - 1,000 MHz are similar. Thus, for simplicity, we take $f_p \simeq 400$ MHz (see Fig. 8.3) and compute the power loss l_j (in decibels) for the extraordinary and ordinary waves at frequencies 6,000, 5,000, 3,500, 3,000, 2,000 and 1,000 MHz on passing through the first three harmonic resonance absorption layers (Table 8.1). If I_{jo} and I_j are the powers of the jth normal wave before and after passing through the s-th harmonic resonance absorption layer respectively, the fraction of power emerging from this layer is

$$R_j = I_j/I_{jo} = 10^{-l_j/10} \quad . \qquad (8.7)$$

The values of R_j are shown in Table 8.1. For all cases, l_2 is less than l_1 and hence R_2 is greater than R_1. We note that for frequencies 6000 - 1000 MHz in the lower solar corona the first two harmonic resonance absorption layers are opaque to both extraordinary and ordinary waves. Although the third harmonic resonance absorption for the extraordinary wave is larger than that for the ordinary wave, for a sufficiently

small value of X (i.e. for a sufficiently high frequency or a very low electron density) there is an appreciable fraction of extraordinary radiation power emerging from the layer $f \simeq 3f_H$ which is transparent to the ordinary wave. As the X value increases gradually, the radiation power in the x-mode is cut off and only the o-mode wave will carry significant power on leaving the layer $f \simeq 3f_H$.

E. Escape of Cyclotron Radiation from The Lower Solar Corona

After studying the characteristics of forward normal cyclotron radiation in both modes from electron streams and the propagation of electromagnetic waves in the solar corona, we can predict the mode and the degree of polarization of the emission observed on the Earth.

Assuming a spherically symmetrical electron density distribution for the solar atmosphere (Fig. 8.3) and neglecting the effect of the sunspot magnetic field, we find that the true escape level for both modes at a particular frequency is higher than the plasma level X = 1 at the limb (Jaeger and Westfold, 1950), and so radiation emitted from a limb source may not be able to escape from the solar corona. This is demonstrated in Fig. 8.12 for waves at the frequencies 400 and 800 MHz. It can be seen that sources of lower frequency emissions will mostly concentrate in the central area of the solar disk.

Owing to the strong resonance absorption at the layer $f \simeq 2f_H$, we can assume that the type IVA emissions are emitted from a layer above the second harmonic resonance absorption level. Taking into account the characteristics of the coherent cyclotron radiation mentioned in Section C and the effect of differential resonance absorptions for the x-mode and the o-mode waves in the solar corona, it can be found that the x-mode waves emitted by electron streams would be of observable intensity after escape from the solar corona in the following circumstances.

(a) The x-mode radio emission observed on the Earth is the second harmonic cyclotron radiation emitted by a stream of electrons of energy less than 100 keV and with small pitch angle (less than 30^o, say). The source must be situated at a layer where A is very small such that $f >> f_p$ at the third harmonic resonance absorption layer.

(b) The observed x-mode radiation corresponds to the third (or fourth) harmonic normal cyclotron radiation in the x-mode from a stream of electrons having energy higher than 100 keV and with electron pitch angle either smaller or greater than 30^o. Again, the value A at the source region should be small. For if A is not very small in the source region, then the maximum third harmonic cyclotron radiation in the x-mode is emitted at frequencies less than $3f_H$ by electron streams with large pitch angle and the third harmonic resonance

absorption layer will prevent the x-mode radiation from escaping. Moreover, the rate of growth for the normal cyclotron radiation in the o-mode exceeds that for the x-mode when A is greater than unity (Fig. 8.7(e) and (g); Fig. 8.9).

(c) The observed x-mode radiation may also be attributed to the fourth harmonic normal cyclotron radiation by streams of electrons with energy less than 100 keV but with pitch angle as large as 60^{o}, since in this case the rate of growth for the fourth harmonic is comparable to that for the second harmonic (see Fig. 8.8 (b)), and the fourth harmonic resonance absorption is insignificant.

Thus, observability of the normal cyclotron radiation in the x-mode generated by the electron stream moving in the solar corona depends on the characteristics of the magneto-active coronal plasma and the nature of the electron stream.

The source position and the source size of the observed type IVA emission reveal that the emission source covers only very small radial distance and can emit a very wide range of frequencies within a narrow wave-normal angle interval $\Delta\theta$. Referring to Fig. 8.5 and Fig. 8.10, this suggests that the pitch angle of the stream electrons responsible for the type IVA emission is small (less than 30^{o}, say). It is hence inadequate to interpret that the observed x-mode radiation at centimetre wavelengths is emitted from a source under the condition (c).

With small electron pitch angle but with energy greater than 100 keV, the third and the fourth harmonic cyclotron radiations in the x-mode are of greatest intensity and will travel away from the solar corona without being absorbed significantly. From Fig. 8.3 and Fig. 8.5, we see that if the source is situated within the flare region, the actual frequencies of the third or fourth harmonic normal cyclotron radiation in the x-mode range from 15,000 MHz to 7,000 MHz. It is clear that these radiations will form the part of type IVA continuum emission at centimetre wavelengths. For s=3 (or 4), the normal cyclotron radiation power in the x-mode emitted by a single electron is about one order of magnitude higher than the corresponding radiation power in the o-mode. Then, if $A \ll 1$ in the source region, the continuum emission at high frequencies is expected to be fairly strongly polarized in the right-handed sense, referring to the magnetic polarity of the leading sunspot in the northern hemisphere. However, the type IVA burst emission originates from a source lying in the transition region between the chromosphere and the base of the solar corona where the magnetic field configuration of a bipolar sunspot group is extremely complicated. The random orientations of the sunspot magnetic field lines of force in this region may destroy completely or partly the polarization of the radiation emitted from this region. Here we should mention that according to Kundu's nomenclature, only

those intense centimetre wavelength outbursts but not the weak emission of thermal origin are regarded as a component of type IVA burst emission. The observed centimetre wavelength component of the type IVA burst emission may consist of a part of the random polarized bremsstrahlung. As a result, only weakly right-handed polarized type IV radio bursts at centimetre wavelengths are observed.

We now compare the second harmonic radiation power in the x-mode escaping from the corona with that in the o-mode. As we have shown that the intensity of the x-mode cyclotron radiation is greater than that of the o-mode particularly when A is small. However, the predominant cyclotron radiation observed on the Earth will not be in the x-mode unless the value of X at the layer $f \simeq 3f_H$ in the solar corona is small enough such that the third harmonic resonance absorption is not very effective. Taking f_p = 400 MHz, $L_H \simeq 10^9$ cm, $\beta_T = 10^{-2}$, $\theta \simeq 65^o$ and r = 5, where r is the ratio of the x-mode power to the o-mode power before passing through the layer $f \simeq 3f_H$ (Section C (c), point (7)), the ratio S of the x-mode power to the o-mode power leaving this layer is greater than unity when the frequency f is greater than 3,000 MHz. This is illustrated in Table 8.1. For the emission at decimetre wavelengths ($f \lesssim 3{,}000$ MHz) emitted from a source with larger A value, only the o-mode is

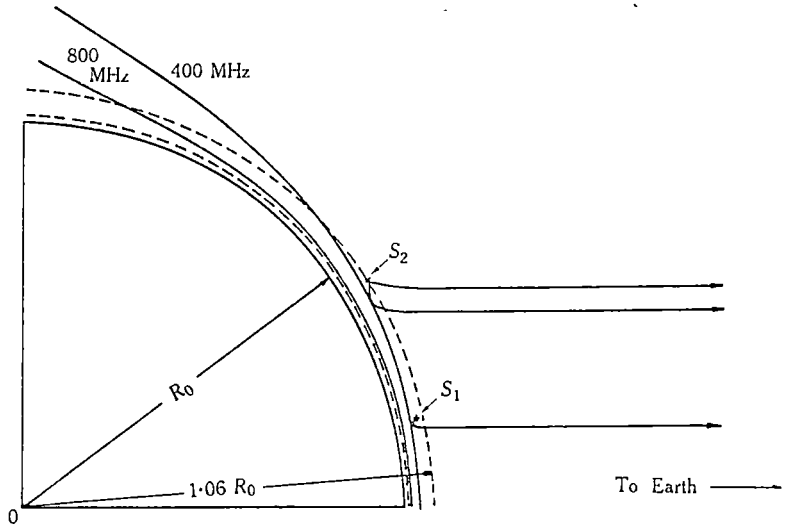

Fig. 8·12 Escape levels in the active corona for waves of frequencies 400 and 800 MHz. The electron density distribution model given in Figure 1 is used. The layer between the dashed lines specifies the type IVA source region.

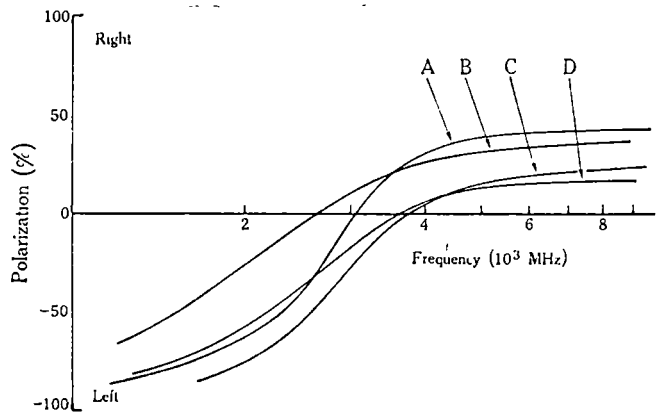

Fig. 8·13 Variation of degree of polarization with wave frequency taking $\theta = 65°$, $\beta_T = 10^{-2}$, and

curve A: $f_p = 400$ MHz, $L_H = 10^9$ cm, $r = 8$;
curve B: $f_p = 450$ MHz, $L_H = 5 \times 10^8$ cm, $r = 5$,
curve C: $f_p = 400$ MHz, $L_H = 10^9$ cm, $r = 5$;
curve D: $f_p = 450$ MHz, $L_H = 7{\cdot}5 \times 10^8$ cm, $r = 5$.

observed on the Earth, firstly because the growth rate for the o-mode exceeds that for the x-mode (Section C (c), point (1)) and secondly because of the increase in the value of X, the effect of the third harmonic resonance absorption becomes great enough to prevent the x-mode wave escaping from the solar corona. This explains why the type IVA bursts are polarized in the o-mode at decimetre wavelengths but in the x-mode at the centimetre wavelengths (leading-spot hypothesis).

In general, cyclotron radiations in both modes emitted by spiralling electron streams are elliptically polarized but owing to the propagation effect, the high frequency radiation in either modes becomes circularly polarized except at $\theta \simeq 90^{o}$ in the boundary region (Piddington and Minnett, 1951). For two independent beams of radiation polarized in opposite senses, the observed degree of circular polarization of the resultant radiation is defined by

$$P = (I^{e} - I^{o})/(I^{e} + I^{o}) = (S-1)/(S+1), \quad (8.8)$$

where I^{e} and I^{o} are the intensities of the x-mode and the o-mode waves escaping from the solar corona respectively and $S = I^{e}/I^{o}$. Following the hypothesis put forward by Weiss (1963b), in the northern hemisphere left-handed polarization corresponds to emission in the ordinary mode if we assume that the sense of polarization is determined by the magnetic polarity of the leading spot. Thus the resultant

radiation is left-handed polarized when P is negative and is right-handed polarized when P is positive. From (8.7), we have

$$S = r \times 10^{(l_2 - l_1)/10} . \qquad (8.9)$$

The sign of P changes at S=1, that is, when the condition

$$\log_{10} r = (l_1 - l_2)/10 \qquad (8.10)$$

is satisfied. For the second harmonic forward emission, l_1 and l_2 are the power losses in decibels due to absorption at $f \simeq 3f_H$ and $r < 10$. In other words, for a given value of r (> 1) and under typical active corona conditions, there exists a frequency such that (8.10) holds. We call this frequency the transition frequency f_t.

It has been shown in Section C that the greatest second harmonic radiation intensities in the x-mode and in the o-mode occur at similar wave-normal angles $\theta \simeq 65^\circ$ and at similar frequencies. Thus the radiations in both modes will travel outward along nearly identical paths. Again taking $\theta = 65^\circ$, $\beta_T = 10^{-2}$ and $f_p \simeq 400$-450 MHz, and with the help of Fig. 8.9 and equation (8.8), we can calculate the degree of polarization of the resultant radiation at various frequencies (Table 8.1). The dependence of the degree of polarization on frequency is illustrated in Fig. 8.13. Under certain active corona conditions, two points can be

observed from Fig. 8.13: (1) forward normal cyclotron radiation from electron streams changes the sense of polarization at some frequency between 2,000 and 4,000 MHz owing to the differential resonance absorption effect; (2) the degree of polarization is stronger in the decimetre wavelength region than in the centimetre wavelength region. These properties are completely in agreement with the observational data (Tanaka and Kakinuma, 1959; Kundu, 1965, p.248).

F. The Drift Bursts superimposed upon the Continuum Burst at Decimetre Wavelengths

So far we have only considered coherent generation of normal cyclotron radiation in the x-mode and the o-mode by an electron stream (or electron bunch) with narrow momentum spread in a cold and collisionless magnetoactive plasma. However, when the thermal motion of the plasma electrons is taken into account, the weakly damped plasma waves at frequencies near the plasma resonance frequencies can also be excited by the same electron stream. It has been found that the weakly damped plasma wave is strongly emitted in the direction of the electron guiding centre motion and at frequencies close to the plasma frequency by the electron stream through the Cerenkov process (Chapter II). Part of the Cerenkov plasma wave energy can be converted into electromagnetic radiations by the small-scale thermal fluctuations

existing in the solar corona (Chapter V and Chapter VI). In general, owing to resonance absorption, the electromagnetic radiation arising from transformation of Cerenkov plasma waves can be observed on the Earth provided that the emission source lies at the layer where the value of A is greater than unity. Referring to Fig. 8.3, within the type IVA burst emission source region, A does not exceed three and only the combination radiation at the normalized frequency $\xi \simeq \xi_{ch} + \tilde{\xi}_{+}$ can escape from the solar corona. Although the rate of growth for the Cerenkov plasma wave is much greater than that for the second harmonic (or third harmonic) cyclotron radiation (Fig. 8.10(a)), only a small fraction of the Cerenkov plasma wave energy can be transformed into the electromagnetic radiation by the coherent thermal fluctuations. As a result, only the combination radiation at the normalized frequency $\xi \simeq 2\sqrt{A}$ would be observable on the Earth. The polar diagram shows that the combination radiation at normalized frequency $\xi \simeq 2\sqrt{A}$ is confined within a cone whose axis is almost transverse to the static magnetic field and whose half-apex angle is about 30^{o} to 40^{o}. If the intensity of the combination radiation at the normalized frequency $\xi \simeq 2A^{\frac{1}{2}}$ exceeds that of the second harmonic normal cyclotron radiation appreciably, the combination radiation would appear in the dynamic spectrum as narrow bandwidth fast drifting bursts superimposed on the

broad band continuum at the decimetre wavelengths. Taking into account the escape condition for the combination radiation at the normalized frequency $\xi \simeq 2A^{\frac{1}{2}}$, it can be seen that the drift bursts occur only in the decimetre wavelength region (cf. Chapter VI, Section D).

The low drift rate of the intermediate drift burst compared with the fast drift burst is probably due to the non-radial trajectory of the electron guiding centre motion. It is possible that during the early stage of the explosion of a large solar flare, a number of electron bunches (or streams) are ejected from the flare region simultaneously and trapped in the near-by bipolar sunspot field configurations. The Cerenkov radiation in the plasma mode can be generated by these electron bunches concurrently and eventually observed on the Earth as a wide bandwidth continuum emission superimposed with variabilities at the decimetre wavelengths. The complexity of the dynamic spectra of the type IVA bursts at the decimetre wavelengths reveals the complication of the magnetic field configurations of a bipolar sunspot group and the intensiveness of the explosion of a large solar flare.

G. Interpretation of the Type IVA Burst Emission

The type IVA emission at centimetre and decimetre wavelengths is the first phase of the whole type IV event.

It starts simultaneously with the explosive phase of a flare that is of importance 2 to 3^+ and usually covers a large fraction of the umbral area of the sunspot group (Kundu, 1965, p.423). During the occurrence of the flare phenomenon, electrons with energy up to 100 keV or more are ejected from the flare region in various directions in the form of electron steeams (De Jager, 1960). Those ejected in the forward direction radially will travel in the neutral plane or along the sunspot magnetic field line and will cause type III bursts by plasma radiation (Chapter VI). Most of these electron streams (or bunches) are trapped in the neighbouring stronger sunspot magnetic field configuration forming helical streams with narrow momentum spread. They emit electromagnetic waves at different frequencies in both x-mode and o-mode by cyclotron mechanism, giving rise to type IVA bursts (Fig. 8.14(a)). For certain large flares, such as those associated with the type IV phenomena, fragments of plasma clouds with hydromagnetic shock wave front are expelled intermittently. Each plasma cloud with the shock front ahead moves through the active solar corona with a speed ~ 1,000 km/sec. Arriving at some region where the electron density is sufficiently low ($f \simeq 100$ MHz), the shock front excites the longitudinal oscillation, which in turn is converted into transverse electromagnetic radiation by incoherent scattering and combination scattering, and is finally observed

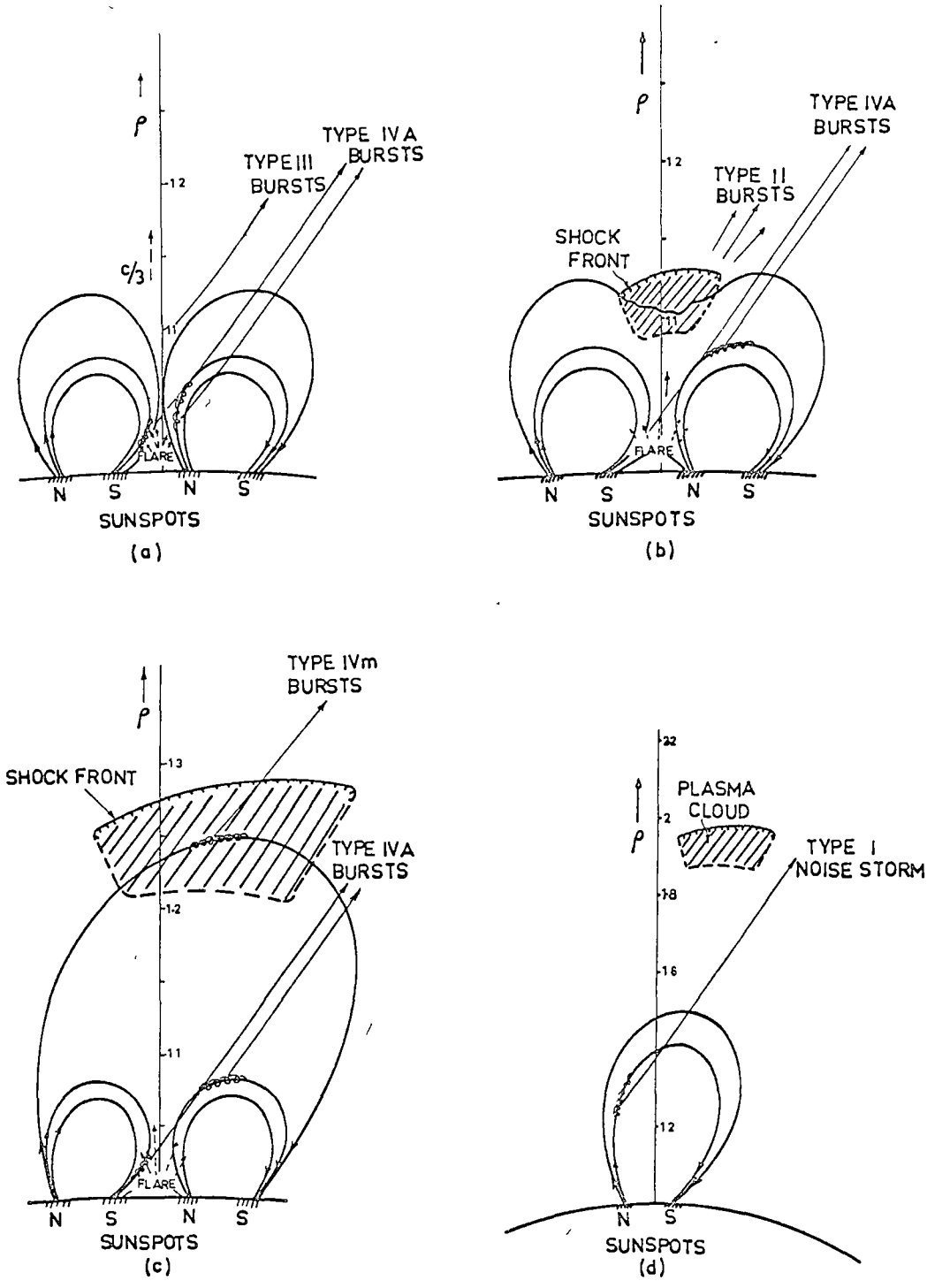

Fig.8.14 - Schematic diagrams of the solar flare phenomenon and its associated radio emissions.

as type II bursts (Fig. 8.14(b)). Therefore the type IVA burst emission occurs several minutes earlier than the type II burst emission (Section A(x)).

The outermost field lines of the two bipolar pairs are highly disturbed by the plasma and merge together forming a single loop of a magnetic field line of force (Fig. 8.14(b)). Meanwhile, due to the high conductivity of the plasma cloud, this newly formed field line is frozen in and brought to a level as high as a few solar radii above the photosphere by the moving plasma cloud (Fig. 8.14(c)). Some more energetic electrons inside this cloud are accelerated to intermediated relativistic energies by a Fermi-like mechanism and gyrate along the frozen-in field line; radiation from these accelerated electrons is responsible for the type IVm emission (McLean, 1959; see also the discussion in Chapter IX Section D). At a later stage, this stretched field line remains in a steady position and eventually the type IVm emission may develop into a type I noise storm (Fig. 8.14 (d)).

The importance of a flare may be regarded as a rough measurement of the speed and quantity of plasma clouds ejected from the flare region. For a flare of lesser importance, the speed of the plasma cloud would be so low that no shock front would be formed or that the associated shock front would not be strong enough to excite a type II

burst. Hence type IVA bursts associated with a less important flare could occur without type II and type IVm bursts. On the other hand, type IVm bursts would always associated with type IVA and type II bursts. This is consistent with the observational data.

The quantitative studies of the generation of electromagnetic waves by electron streams and the conditions for escape of the cyclotron radiation from the active solar corona in previous sections lead to the following conclusion. The centimetre wavelength component of the type IVA continuum burst emission is attributed to the third and the fourth harmonic cyclotron radiations by streams of electrons with energy about 100 keV spiralling along the spot field lines in a layer where $A \ll 1$ (Section E (b)). The second harmonic cyclotron radiation in the o-mode and the Cerenkov plasma radiation at the frequency $f \simeq 2f_p$ emitted by streams of low energy electrons (about ten to several ten keV) are associated with the continuum bursts superimposed with fast drifting elements at decimetre wavelengths. Then type IVA bursts can be explained as follows.

(a) Frequency Range and Frequency Drift

Assuming the model for the lower active corona as shown in Fig. 8.3, the lowest emission frequency of the broad band second harmonic radiation can range from 10,000 to 500 MHz.

The low frequency cutoff is either due to the limit of the intensity of the bipolar field line or to A being greater than four. For intense narrow bandwidth emission, A must be greater than unity and the drift bursts are expected to occur in the frequency range from 500 to 2,000 MHz. Therefore the variabilities occur only in the decimetre wavelength region.

Due to the large gradients of electron density distribution in the transition region, the combination radiation caused by the mildly relativistic electron stream can drift through a wide range of frequencies within a very short time interval. For electron stream with $\beta_{\parallel} \simeq 0.2$ travelling from $\rho = 1.01$ to $\rho = 1.06$ radially, the drift rate of the combination radiation in the frequency range 500 - 2,000 MHz will vary from 5×10^{2} to 5×10^{3} MHz per sec. Since the decimetre wavelength burst emission sources showed only slight directivity towards the centre of the solar disk, electron streams responsible for the emission of drift bursts at decimetre wavelengths would travel along a non-radial trajectory so that drifting bursts can also be emitted from a source near the disk centre (cf. Fig. 7.7 and Chapter VII section G(2)). Hence the observed drift rates will be much smaller than those estimated above. The extremely slow drift occurring in a few decimetre wavelength continuum

bursts is probably due to the decrease of magnetic field intensity in the source (Takakura, 1963). This is supported by the optical observation that a decrease in the magnetic field gradient and sometimes in the magnetic field energy occurs during a flare (Severnyi, 1966).

(b) Duration and Bandwidth

Whenever the single-frequency solution condition is satisfied for the generating process, the second harmonic emissions in both modes have a broad bandwidth and a wide cone of emission. Many such broad band emissions from the low level of the active corona will superimpose upon each other to form a long-lived broad band continuum in the centimetre and decimetre wavelength regions. For the same electron energy, pitch angle and the value of A, the actual half-power bandwidth is proportional to the local gyrofrequency and hence the centimetre wavelength bursts have broader bandwidth. The narrow bandwidth combination radiation at decimetre wavelengths are grouped together and superimposed on the background continuum, appearing as the fine structures or patchiness in the dynamic spectrum. The complexity of the spectral appearance of the type IVA bursts at decimetre wavelengths has been explained in Section F.

The electron streams trapped in the sunspot magnetic field configuration can remain there for a certain time but the narrow momentum spread cannot last for a period as long

as one hour owing to diffusion of velocity of the stream electrons. Thus the long duration of type IVA burst emission should be attributed to the continuous expulsion of energetic electrons from the flare region. The long duration observed in the decimetre wavelength region may be the result of high frequency extensions of type IVm emission (Smerd, 1964).

(c) Polarization

The change in polarization modes of type IVA bursts is due to differential harmonic resonance absorption. This has been discussed in detail in Section E. It should be mentioned that the transition frequency depends on the lower corona conditions, i.e. electron density and magnetic field intensity gradient.

(d) Angular Size and Directivity

Michard (1963) indicated thatthe probability of a flare with type IV bursts or a polar blackout increases as the distance between spots decreases. Also the type IVA bursts are emitted at a low altitude in the corona. Hence the diameter of a type IVA emission source is comparatively small.

Since the decimetre wavelength continuum bursts are considered to be associated with the second harmonic cyclotron radiation in the o-mode emitted from a layer where $A > 1$ ($A=3$, say) the frequencies associated with the second harmonic cyclotron radiation of greatest intensity $\xi_m \gtrsim 2$ are close to

the local plasma frequency, i.e. $\xi_m \simeq \sqrt{A}$. The second harmonic cyclotron radiation in the o-mode emitted from a limb source may not be observed (Section E). On the other hand, the emission frequencies of the third (or fourth) harmonic forward cyclotron radiation in the o-mode and the x-mode emitted by electrons with energy ~ 100 keV greatly exceed the local plasma frequency when A is very small ($A \ll 1$, say). Consequently, only the decimetre wavelength continuum bursts would show slight directivity towards the centre of the solar disk.

(e) Intensity

The second harmonic cyclotron radiation in both modes suffers significant third harmonic resonance absorption on propagating outwards through the solar corona. That is, the intensity of the type IVA bursts at decimetre wavelengths will be normally less than that at centimetre wavelengths (Kundu, 1965, p.245).

H. Conclusion

Adopting the current model for the solar flare evolution, type IVA emission is well accounted for by the Doppler-shifted cyclotron radiation theory. In spite of their distinct source characteristics, the type IVA and type IVm bursts can result from the explosion of the same large flare above a complex sunspot group. Radio and optical

observations during previous solar cycles lead to the conclusion that there are two phases of fast electrons created during a flare period (Wild et al., 1963): (1) a succession of bursts of electrons (~ 100 keV) produced by conversion of magnetic energy into kinetic energy owing to plasma instability in the magnetic neutral region, and (2) thermal electrons accelerated to higher energies by the magnetohydrodynamic shock wave front through a Fermi process. The second phase is initiated by the first and occurs only in large flares associated with type IV phenomena. During the occurrence of a very large flare, the electrons of the first phase released from the flare region cause type III, V and IVA burst emissions; while those of the second phase arising from the ejection of a plasma cloud radiate type IVm bursts*, and the associated magnetohydrodynamic shock wave front excites type II emission. All these nonthermal radio emissions are associated with the same large flare and appear consecutively.

A satisfactory interpretation of the type IVA burst emission event as the consequence of normal cyclotron radiation and Cerenkov plasma radiation by electron streams moving in the solar corona requires the following assumptions:

(1) The plasma frequency is much smaller than the gyrofrequency in most part of the type IVA burst emission

---

* A discussion on the origins of the type V and type IVm burst emissions is given in Chapter IX.

source region (i.e. A << 1).

(2) The pitch angle of the radiating electron is less than 30°. The energy of the radiating electron ranges from a few tens of keV to slightly higher than 100 keV.

Optical observations show that the intensity of the sunspot magnetic field at the photosphere can reach as high as 4,000 gauss (Bray and Loughhead, 1964) and decreases with increasing height above the photosphere quickly in the chromosphere and at the base of the solar corona; in term of frequency, the gyrofrequency over a large sunspot would cross below the plasma frequency near 200 to 300 MHz (Wild et al., 1963). The sunspot magnetic field intensity decreases slowly at greater heights and some of the field lines can extend to the height about one solar radius above the photosphere (Severnyi, 1966). Thus, the model for the type IVA emission source given in Fig. 8.3 and the assumption (1) are appropriate to these optical observational data.

The time of start of the type IV bursts at the centimetre and decimetre wavelengths has been found to be co-incident with the explosive phase of a solar flare and almost co-incident with a group of type III bursts (see Fig. 8.2 (D)). We believe that the streams or bunches of electrons responsible for the type III and type IVA burst emissions are produced in the same manner during the period

of the explosion of a large solar flare in the transition region. The streams or bunches of electrons accelerated in the neutral plane between two spot fields of opposite polarity would be trapped in the near-by strong bipolar spot field configuration or along the neutral plane. Thus, it seems likely that the electron streams produced in this manner would be trapped in the field configuration with small pitch angle. In fact, Stewart (1965), using the type III burst data, showed that the electron stream travelled through the solar corona with fairly constant speed ~ 0.2c - 0.6c (average ~ $\frac{1}{3}$ c) and pointed out that the electron streams were rarely ejected at angles larger than 30^{o} to the radial direction. So the assumption (2) is also realistic.

With the limited optical and other radio observational data associated with the explosion of a solar flare, the type IV burst emission at centimetre and decimetre wavelengths can be explained as the consequence of the excitation of cyclotron radiation in the subluminous mode and the Cerenkov radiation in the plasma mode by electron streams in the active solar corona. Interpretation of the type IVA burst emission event on the basis of this theory can lead to the understanding of the physical condition of the base of the active solar corona.

CHAPTER IX

SYNCHROTRON RADIATION AND SOLAR CONTINUUM RADIO EMISSIONS

A. Introduction

So far we have considered the generation of electromagnetic radiation by mildly relativistic electrons moving in the solar corona. However, relativistic electrons with energies up to about 8 MeV were observed at the Earth (Cline and McDonald, 1968a). These relativistic electrons, either accelerated near the flare regions or accelerated at the outer layers of the solar corona, will give rise to the synchrotron radiation which would eventually be observed as a wide bandwidth smooth continuum.

In using the theory of synchrotron radiation in the interpretation of radio emissions from the solar corona, the effects of the medium on the radiation process, namely the reabsorption and Razin effect, have to be taken into account. Previous theories of the solar radio emissions on the basis of incoherent synchrotron radiation in the vacuum, in general, are not satisfactory. In the present chapter, we study the synchrotron radiation from an ensemble of monoenergetic relativistic electrons. The possibility of the synchrotron radiation as the source of some wide bandwidth solar radio emissions is discussed.

In deriving the theory of synchrotron radiation in this chapter, we make the following assumptions:

1. The ambient plasma is cold and collisionless.

2. The distribution function for the relativistic electrons is stationary and uniform, i.e. $f_o(p)$ (or $f_o(E)$) is a function of electron's momentum (or electron's energy) only.

3. The number density of the radiating electrons is much smaller than that of the ambient plasma, so that the refractive index for the wave remains unchanged in the presence of the radiating electrons and the electrons radiate independently of one another.

B. Incoherent Synchrotron Radiation from A System of Relativistic Electrons

Let us assume the electromagnetic wave emitted by an electron varies as $\exp(-i\bar{k}.\bar{r}+i\omega t)$, where the wave vector $\bar{k}$ lies on the y-z plane of a Cartesian co-ordinate system (Fig. 9.1). For sufficiently high frequencies such that $\xi^2 >> 1$ and $\xi^2 >> A$, the magnetoactive plasma tends to be isotropic and the transverse electromagnetic wave propagates with the phase velocity $v_p = c/n$, where

$$n^2 = 1 - A/\xi^2 \quad , \tag{9.1}$$

and the wave group velocity is given by $v_p v_g = c^2$.

In this case, the single electron emissivity tensor

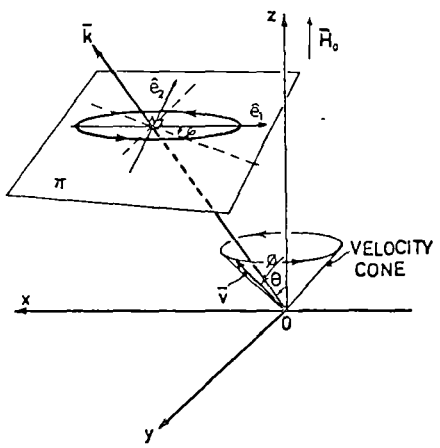

Fig.9.1. Coordinate system for the synchrotron radiation.

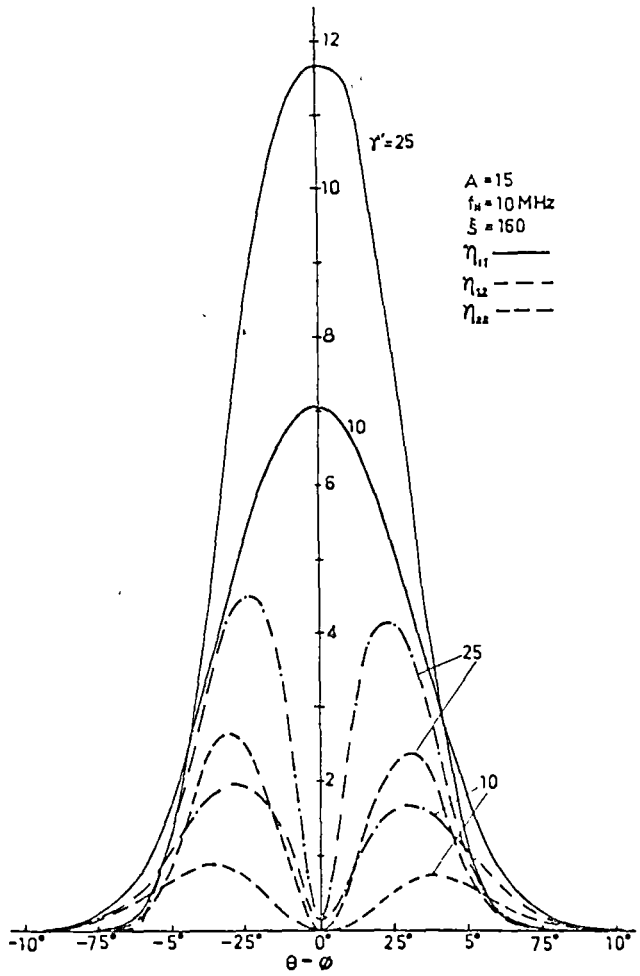

Fig.9.2. Dependence of the magnitudes of the emissivity tensor components $\eta_{ij}(\bar{v})$ (in units of 10^{-30} W/sr-Hz) on wave-normal angle for A = 15, f_H = 10 MHz, normalized frequency ξ = 160, γ' = 10, 25 and electron pitch angle $\phi = 60^{\circ}$.

for the synchrotron radiation will be (Appendix C)

$$\eta_{ij}(\bar{p}) = \sum_{s=1}^{\infty} \frac{e^2\omega^2 n}{2\pi c} \begin{pmatrix} \beta_\perp^2 J_s'^2 & -i\beta_\perp J_s J_s' \left(\frac{\cos\theta - n\beta_{//}}{n\sin\theta}\right) \\ i\beta_\perp J_s J_s' \left(\frac{\cos\theta - n\beta_{//}}{n\sin\theta}\right) & J_s^2 \left(\frac{\cos\theta - n\beta_{//}}{n\sin\theta}\right)^2 \end{pmatrix}$$

$$\times \delta\left(\omega - k_{//} v_{//} - \frac{s\omega_H}{\gamma'}\right) , \qquad (9.2)$$

where $\gamma' = (1 - \beta_\perp^2 - \beta_{//}^2)^{-\frac{1}{2}}$ is the Lorentz factor. J_s and J_s' are the Bessel function of s-th order and its first derivative with respect to the argument $X = \gamma' k_\perp v_\perp / \omega_H$. The trace of $\eta_{ij}(\bar{p})$ is the mean spontaneous radiation power emitted by a single electron at the frequency ω per unit frequency interval per unit solid angle at any direction, i.e.

$$\eta(\bar{p}) = Sp\left[\eta_{ij}(\bar{p})\right] = \eta_{11} + \eta_{22} = \eta^\perp + \eta^{//} ,$$

$$= \frac{e^2\omega^2 n}{2\pi c} \sum_{s=1}^{\infty} \left[\beta_\perp^2 J_s'^2 + \left(\frac{\cos\theta - n\beta_{//}}{n\sin\theta}\right)^2 J_s^2\right] \delta\left(\omega - k_{//} v_{//} - \frac{s\omega_H}{\gamma'}\right) \quad (W\ sr^{-1} sec^{-1}) \qquad (9.3)$$

η_{11} and η_{22} are the spontaneous radiation power with the two principal polarization directions $\hat{e}_1$ and $\hat{e}_2$ (Fig. 9.1).

In Fig. 9.2, the quantities η_{11}, η_{22} and $|\eta_{12}|$ are plotted as a function of wave-normal angle for $\phi = 60^\circ$, $\gamma' = 10$, 25 (electron energy $E \simeq 4.5$, 12 MeV respectively), $A = 15$, $f_H = 10$ MHz and normalized frequency $\xi = 160$ (the

frequency where $\eta(\bar{p})$ exhibits its maximum). It is clear that η_{11} makes the main contribution to $\eta(\bar{p})$ and $|\eta_{12}|, \eta_{22}$ will be comparable with η_{11} only in the wave-normal direction where $|\theta - \phi|$ becomes large ($\geq 4^{o}$, say). Since the angular distributions of η_{11} and η_{22} are symmetrical about the velocity vector, from Fig. 9.2, we infer that for a single relativistic electron, linearly polarized radiation will be emitted in the direction $\theta = \phi$ where the synchrotron radiation is of greatest intensity and elliptically polarized radiations of equal intensity but with opposite sense of polarization are emitted in the direction for which $|\theta - \phi|$ is greater than a few degrees (Ginzburg and Syrovat-skii, 1966; Takakura, 1967).

Considering synchrotron radiation from a system of electrons, one defines the volume emissivity as the power generated by unit volume of medium per unit frequency interval $d\omega$ per steradian flowing in the direction of the ray. Accordingly, for a system of electrons with stationary, homogeneous isotropic momentum distribution function $f_{o}(p)$, the volume emissivity is

$$j(\bar{p}) = Sp[j_{ij}(\bar{p})] ,$$

where

$$j_{ij}(\bar{p}) = \int \eta_{ij}(\bar{p}) f_{o}(p) d\bar{p} \qquad (9.4)$$

and $\eta_{ij}(\bar{p})$ is given by (9.2). The element of the momentum space $d\bar{p}$ can be written as

$$d\bar{p} = \frac{E^2}{c^3} \sin\phi d\phi dE d\psi \ , \qquad (9.5)$$

where, for highly relativistic electrons, $E = pc$ and ψ is the azimuthal angle of the electron momentum vector. $f_o(p)$ satisfies the normalization condition $\int f_o(p)d\bar{p} = N_o'$, N_o' being the number density of the radiating electrons. Then (9.4) is expressible as

$$j_{ij}(\bar{p}) = \frac{1}{4\pi} \int_o^\infty f_o(E)dE 2\pi \int_o^\pi \eta_{ij}(\bar{p})\sin\phi d\phi, \qquad (9.6)$$

where the momentum distribution function has been replaced by the energy spectrum $f_o(E)$ through the relation $f_o(p)4\pi p^2 dp = f_o(E)dE$. When the energy spread of a group of electrons is sufficiently small, the energy distribution function $f_o(E)$ can be approximated by a monoenergetic energy spectrum,

$$f_o(E) = N_o'\delta(E - E_o), \qquad (9.7)$$

where $\delta(E - E_o)$ is the Dirac delta function. The energy spectrum has a narrow width around the maximum energy E_o.

Recalling that the intensity of synchrotron radiation emitted by a single electron is sharply peaked in the direction of the electron velocity vector (i.e. $\theta \simeq \phi$), it is possible

to assume that $2\pi\sin\phi d\phi \simeq 2\pi\sin\phi d\psi$ in (9.6) (where $\psi = \phi - \theta$). That is, in a given direction, only those electrons having pitch angles $\phi \simeq \theta$ will make major contribution to the volume emissivity. With this fact taken into account, it has been shown that (Sazonov and Tsytovich, 1968; Ginzburg et al., 1968):

$$2\pi \int_0^{\pi} \frac{n^2\omega^2\gamma'}{\omega_H} \beta_\perp^2 J_s'^2 \sin\phi d\phi = \frac{1}{\sqrt{3}} \xi\omega_H \zeta F^{\perp}(z),$$

$$2\pi \int_0^{\pi} \frac{n^2\omega^2\gamma'}{\omega_H} \left(\frac{\cos\theta - n\beta_{//}}{n\sin\theta}\right)^2 J_s^2 \sin\phi d\phi = \frac{1}{\sqrt{3}} \xi\omega_H \zeta F^{//}(z), \qquad (9.8)$$

$$2\pi \int_0^{\pi} \frac{n^2\omega^2\gamma'}{\omega_H} \beta_\perp \left(\frac{\cos\theta - n\beta_{//}}{n\sin\theta}\right) J_s J_s' \sin\phi d\phi = \frac{2}{\sqrt{3}} \frac{\omega_H}{\gamma'} \cos\theta F^{\perp//}(z),$$

where $z = 2\gamma'\xi\zeta^{3/2}/3\sin\theta$,

$$F^{\perp,//}(z) = \int_z^{\infty} K_{5/3}(\eta)d\eta \pm K_{2/3}(z), \qquad (9.9)$$

$$F^{\perp//}(z) = zK_{1/3}(z) + \int_z^{\infty} K_{1/3}(\eta)d\eta = zK_{1/3}(z) + 2K_{2/3}(z) - \int_z^{\infty} K_{5/3}(\eta)d\eta,$$

$$\zeta = \frac{1}{\gamma'^2} + \frac{A}{\xi^2},$$

and $K_\nu(z)$ is the modified Hankel function of ν-th order with argument z.

Using these equalites and (9.7) in (9.6), we obtain

$$j_{11} = \frac{e^2 \sigma N_o \xi \omega_H}{8\pi^2 \sqrt{3}\, nc} \zeta F^{\perp}(z),$$

$$j_{22} = \frac{e^2 \sigma N_o \xi \omega_H}{8\pi^2 \sqrt{3}\, nc} \zeta F^{\parallel}(z), \qquad (9.10)$$

$$j_{12} = -j_{21} = -i \frac{e^2 \sigma N_o \omega_H \cos\theta}{4\pi^2 \sqrt{3}\, nc} F^{\perp\parallel}(z),$$

where $\sigma = N_o'/N_o$ and N_o is the electron number density of the ambient plasma.

Since we consider synchrotron radiation from a homogeneous radiating source, if the source depth along the line of observation is L, we can form a polarization tensor as

$$I_{ij} = j_{ij} L. \qquad (9.11)$$

Then, the incoherent radiation intensity emerging from the source region will be

$$I_o = Sp(I_{ij}) = (j_{11} + j_{22})L, \qquad (9.12)$$

i.e. the radiation intensity in watts per steradian per unit frequency interval per unit area of radiating surface.

In Fig. 9.3, we show the incoherent radiation intensity emerging from a group of monoenergetic electrons as a function

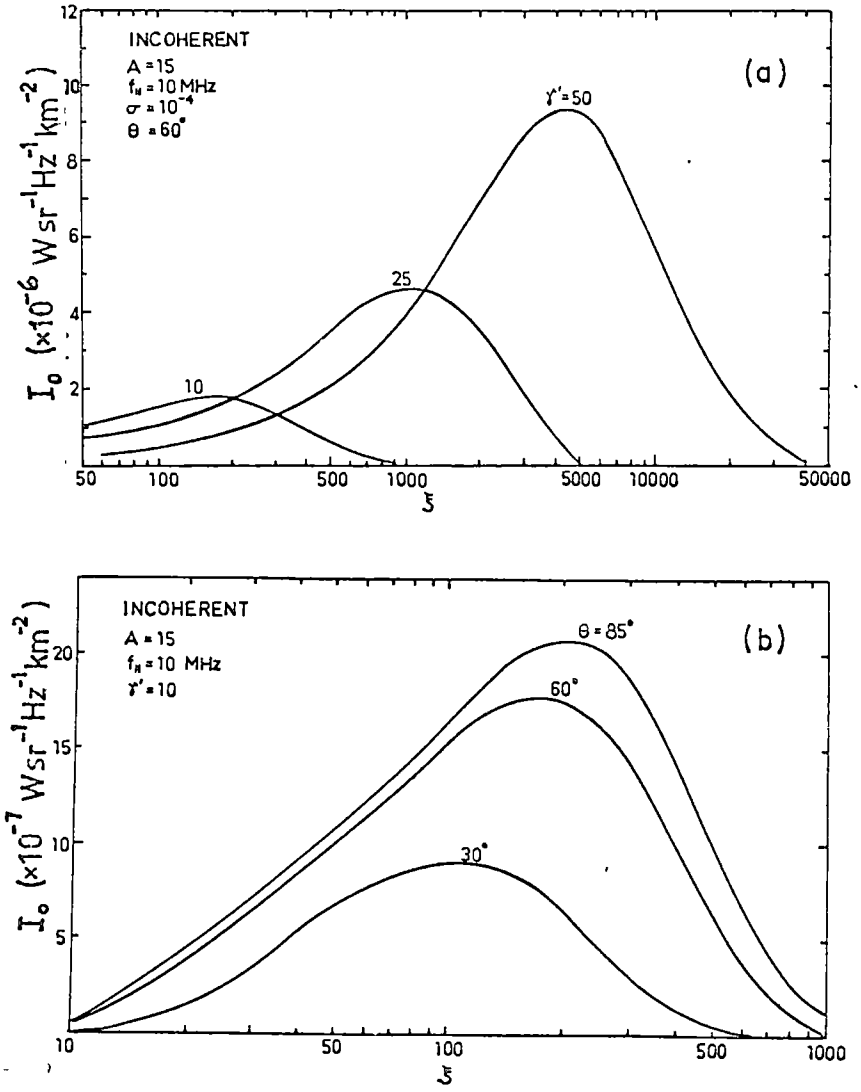

Fig.9.3 Assuming A = 15, f_H = 10 MHz, $\sigma = 10^{-4}$, the intensity of incoherent synchrotron radiation is shown as a function of normalized frequency ξ for

(a) a system of monoenergetic electeons with γ' = 10, 25, 50, $\theta = 60^{\circ}$;

(b) a system of monoenergetic electrons with γ' = 10, $\theta = 30^{\circ}, 60^{\circ}, 85^{\circ}$.

of normalized radiation frequency ξ for A = 15, f_H = 10 MHz, L = 10^5 km, $\theta = 30^o, 60^o, 85^o$, $\sigma = 10^{-4}$ and $\gamma' = 10, 25, 50$. The radiation intensity tends to maximize in the direction transverse to the magnetic field line of force and the maximum occurs at higher frequencies for higher electron energies.

In order to study the polarization character of the synchrotron radiation from an ensemble of electrons, we relate the components of the polarization tensor (9.11) to the Stokes parameters (I,Q,V,U) for the synchrotron radiation emerging from the source in the following way (Korchakov and Syrovat-skii, 1962):

$$I = I_{11} + I_{22}\ , \quad Q = I_{11} - I_{22}\ , \qquad (9.13)$$

$$V = -i(I_{12} - I_{21}),\ U = I_{12} + I_{21}\ .$$

I is the radiation intensity emerging from the source region and is equivalent to that given by (9.12). Q is the difference of the intensities of the radiations with the two principal polarization axes, $\hat{e}_1$ and $\hat{e}_2$. V gives the difference in intensities between two oppositely rotating elliptical (circular) components. If the radiation is completely polarized, the four Stokes parameters are related by $I = Q^2 + V^2 + U^2$. In the absence of elliptical or circular polarization, V=0 and for completely random polarization, Q = V = U = 0.

Since, for the relativistic electrons, the angular distribution of synchrotron radiation emitted by a single electron is symmetrical about the electron velocity vector, the synchrotron radiation from a system of isotropic and homogeneous distributed electrons is linearly polarized (Korochakov and Syrovat-skii, 1962). The degree of polarization of the incoherent synchrotron radiation is defined as

$$P = \frac{(Q^2+U^2)^{\frac{1}{2}}}{I} = \left| \frac{I_{11} - I_{22}}{I_{11} + I_{22}} \right| = \left| \frac{j_{11} - j_{22}}{j_{11} + j_{22}} \right| . \qquad (9.14)$$

Since $\eta_{11} >> \eta_{22}$ in the direction $\theta \simeq \emptyset$, the synchrotron radiation emerging from the source region is almost completely linearly polarized on the plane perpendicular to the magnetic field.

C. Reabsorption of Synchrotron Radiation

If the emission source size is sufficiently large, the synchrotron radiation emitted by individual electrons will experience absorption by the relativistic electrons in the source region. The process of reabsorption leads to a redistribution of the intensity over the spectrum of the incoherent synchrotron radiation from a system of relativistic electrons. When the effect of the ambient plasma is taken into account, negative reabsorption of the synchrotron

radiation can occur and hence the system of relativistic electrons amplifies rather than attenuates its own synchrotron radiation. As a result of negative reabsorption, the intensity level of the synchrotron radiation from a system of relativistic electrons exceeds the summed intensity of the spontaneous synchrotron radiation from all individual electrons, i.e. we have coherent synchrotron radiation. However, reabsorption would play a significant role in the radio emission from the solar corona only if $|\alpha L| \geq 1$, where α is the reabsorption coefficient. The linear sizes of most radiating sources situated in the solar corona are observed to be of the order of 10^5 km and the sources can be regarded to be optically thick if $|\alpha| \geq 10^{-5}$ per km. In this section, using the quantum approach, we study the reabsorption of synchrotron radiation in a system of mono-energetic electrons.

Firstly we consider the reabsorption of synchrotron radiation without taking account of the effects of the magnetic field on the propagation of electromagnetic waves in the plasma. In this case, the plasma is isotropic and there exists two independent modes of transverse electromagnetic waves; either the two plane-polarized modes whose planes of polarization are mutually perpendicular, or the two oppositely rotating circularly polarized modes (Spitzer, 1962, p.53). The polarization states of the electromagnetic

waves in these modes are unchanged and these waves can be regarded as the two normal waves in the isotropic plasma. In view of the fact that the synchrotron radiation emitted by a single electron maximizes in the direction along the principal axis $\hat{e}_1$, we may consider that the single electron can emit two independent normal waves polarized on the planes perpendicular to and parallel to the static magnetic field $\bar{H}_o$ with emissivities $\eta^{\perp}$ and $\eta^{\parallel}$. Then the reabsorption coefficients for the two independent normal waves in a system of isotropic electrons are given by (Bekefi, 1966,p.54)

$$\alpha^{\perp,\parallel} = -\frac{8\pi^3 c^2}{n^2\omega^2}\int \eta^{\perp,\parallel}\frac{\partial f_o(p)}{\partial E}\,d\bar{p} \qquad (9.15)$$

which are obtained by means of the Einstein coefficient method. From (9.3) and (9.5), the absorption coefficients $\alpha^{\perp,\parallel}$ can be expressible in the form

$$\alpha^{\perp} = -\frac{\pi e^2 c}{n\omega^2}\int_o^{\infty} E^2\frac{\partial}{\partial E}\left[\frac{f_o(E)}{E^2}\right]dE\,2\pi\int_o^{\pi}\frac{\omega^2 n^2\gamma'}{\omega_H}\beta_{\perp}^2 J_s'^2 \sin\phi\,d\phi, \quad (9.16)$$

$$\alpha^{\parallel} = -\frac{\pi e^2 c}{n\omega^2}\int_o^{\pi} E^2\frac{\partial}{\partial E}\left[\frac{f_o(E)}{E^2}\right]dE\,2\pi\int_o^{\pi}\frac{\omega^2 n^2\gamma'}{\omega_H}\left(\frac{\cos\theta - n\beta_{\parallel}}{n\sin\theta}\right)^2 J_s^2\sin\phi\,d\phi. \qquad (9.16)$$

With the assumption that $f_o(E)$ tends to zero rapidly as E tends to infinity, and the approximated expressions (9.8) taken into account, (9.16) are reduced to

$$\alpha^{\perp,\parallel} = -\frac{\pi e^2 c}{\sqrt{3}\,n^3 \xi \omega_H}\left\{-\int_0^\infty \frac{f_o(E)}{E}\left[\left[2\left(\frac{A}{\xi^2}+\frac{1}{\gamma'^2}\right)-\frac{2}{\gamma'^2}\right]F^{\perp,\parallel}+ z\left(\frac{A}{\xi^2}-\frac{2}{\gamma'^2}\right)F_p^{\perp,\parallel}\right] dE\right\} \qquad (9.17)$$

where $F_p^{\perp,\parallel}(z) = \frac{\partial F^{\perp,\parallel}(z)}{\partial z} = -K_{5/3}(z) \pm K'_{2/3}(z)$ and $F^{\perp,\parallel}(z)$ are defined in (9.9). For further simplication, we consider two limiting cases: (1) $\omega > \gamma'\omega_p$ (Region I) and (2) $\omega < \gamma'\omega_p$ (Region II).

In Region I, the influence of the medium on the synchrotron radiation is insignificant and the absorption coefficient (9.17) reads

$$\alpha^{\perp,\parallel} = \frac{e^2 c}{\sqrt{3}\,n^3}\int_0^\infty \frac{f_o(E)2z}{E\,\gamma'^2}\left[K_{5/3}(z) \mp K'_{2/3}(z)\right] dE \qquad (9.18)$$

where $z \simeq 2\xi/3\gamma'^2\sin\theta$. Using the recurrence relations for the modified Hankel functions, one can show that

$$z[K_{5/3}(z) - K'_{2/3}(z)] = 2[K_{2/3}(z) + zK_{1/3}(z)]\ ,$$

and $z[K_{5/3}(z) + K'_{2/3}(z)] = \frac{2}{3}K_{1/3}(z)$.

Since $K_\nu(z)$ is positive for all z, $\alpha^{\perp,\parallel}$ are always positive regardless of choice of energy spectrum. With $f_o(E)$ given by (9.7),

$$\alpha^{\perp,\parallel} = \frac{\sigma A \omega_H z}{2\sqrt{3}\, n^3\, \gamma'^3} \left[K_{5/3}(z) \mp K'_{2/3}(z)\right] . \qquad (9.19)$$

In Fig. 9.4, the absorption coefficient $\alpha^{\perp,\parallel}$ for the frequency in the Region I is shown as a function of normalized frequency with $\gamma' = 10$, $A = 15$, $f_H = 10$ MHz and $\theta = 30^\circ, 60^\circ, 85^\circ$. This figure clearly illustrates that electrons, which strongly emit synchrotron radiation with principal polarization axis $\hat{e}_1$ and at large wave-normal angles, also strongly absorb radiation of the same character.

The condition $\omega < \omega_p \gamma'$ (Region II) suggests that the medium has a significant effect on the synchrotron radiation from the relativistic electrons. Taking this limiting condition, the absorption coefficients (9.17) become

$$\alpha^{\perp,\parallel} = -\frac{\pi e^2 A c}{\sqrt{3}\, n^3 \xi^3 \omega_H} \left[-\int_0^\infty \frac{f_o(E)}{E} (2F^{\perp,\parallel} + zF_p^{\perp,\parallel}) dE \right] , \qquad (9.20)$$

with $z \simeq 2\gamma' A^{3/2}/\xi^2 \sin\theta$. Putting (9.7) into (9.20), we have

$$\alpha^{\perp,\parallel} = -\frac{\sqrt{3}\, \sigma\sqrt{A}\, \omega_H \sin\theta}{8 n^3 \xi \gamma'^2 c} G^{\perp,\parallel} , \qquad (9.21)$$

where $G^{\perp,\parallel}(z) = -(2zF^{\perp,\parallel} + z^2 F_p^{\perp,\parallel})$.

Negative reabsorption occurs when $G^{\perp,\parallel}(z) > 0$. In Fig. 9.5, the variation of the function $G^{\perp,\parallel}(z)$ with z is shown. It can be seen that $G^{\perp,\parallel}(z) > 0$ provided that

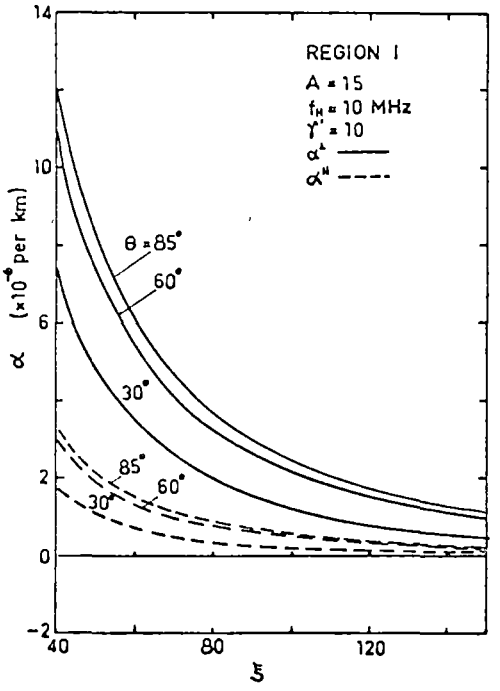

Fig.9.4. Variation of synchrotron absorption coefficient $\alpha^{\perp,\parallel}$ with normalized frequency in Region I for a system of monoenergetic electrons with $\gamma' = 10$, $\sigma = 10^{-4}$ and for A = 15, f_H = 10 MHz, θ = 30°, 60°, 85°.

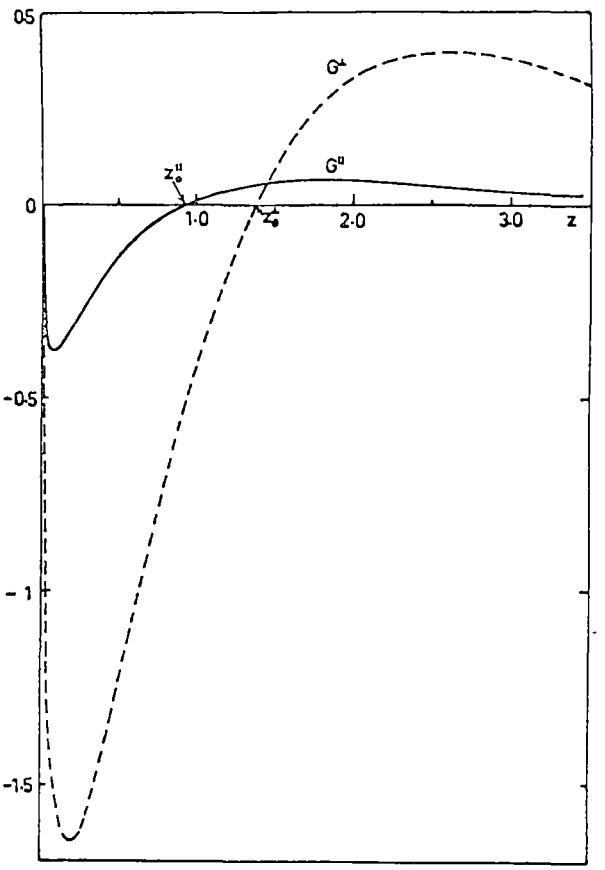

Fig.9.5. Dependence of the function $G^{\perp,\parallel}$ on z.

$z > z_o^{\perp,\parallel}$ where $z_o^{\perp,\parallel}$ is the root of the equation $G^{\perp,\parallel}(z) = 0$. Referring to this figure, we find that $z_o \simeq 1.38$ and $z_o \simeq 0.92$. Thus, for a given energy of the electrons, the value of A and the wave-normal angle θ, there is an upper cut-off frequency above which the absorption becomes positive.

In Fig. 9.6(a), we present the absorption coefficient as a function of normalized frequency ξ for A = 15, f_H = 10 MHz $\gamma' = 10$, $\sigma = 10^{-4}$ and for $\theta = 30^o, 60^o, 85^o$. The synchrotron radiation at lower frequencies but at larger wave-normal angles will be amplified at a greater rate. Fig. 9.6(b) shows the variation of the absorption coefficient $\alpha^{\perp,\parallel}$ with the normalized frequency for different electron energies $\gamma' = 10,25,50,100$. It can be seen that the synchrotron radiation emitted by electrons of higher energy will grow at the higher frequencies. However, the rate of growth in space decreases with the increase of electron energy although the incoherent synchrotron radiation would increase with the electron energy (see Fig. 9.3(a)). Moreover, the magnitude of $\alpha^{\perp}$ is much greater than that of $\alpha^{\parallel}$.

The transfer equation describing the variation of the intensity of the radiation in one normal mode on passing through the radiation source can be written in the form (Ginzburg and Syrovat-skii, 1969):

$$\frac{dI^{\perp,\parallel}}{dr} = j^{\perp,\parallel} - \alpha^{\perp,\parallel} I^{\perp,\parallel} , \qquad (9.22)$$

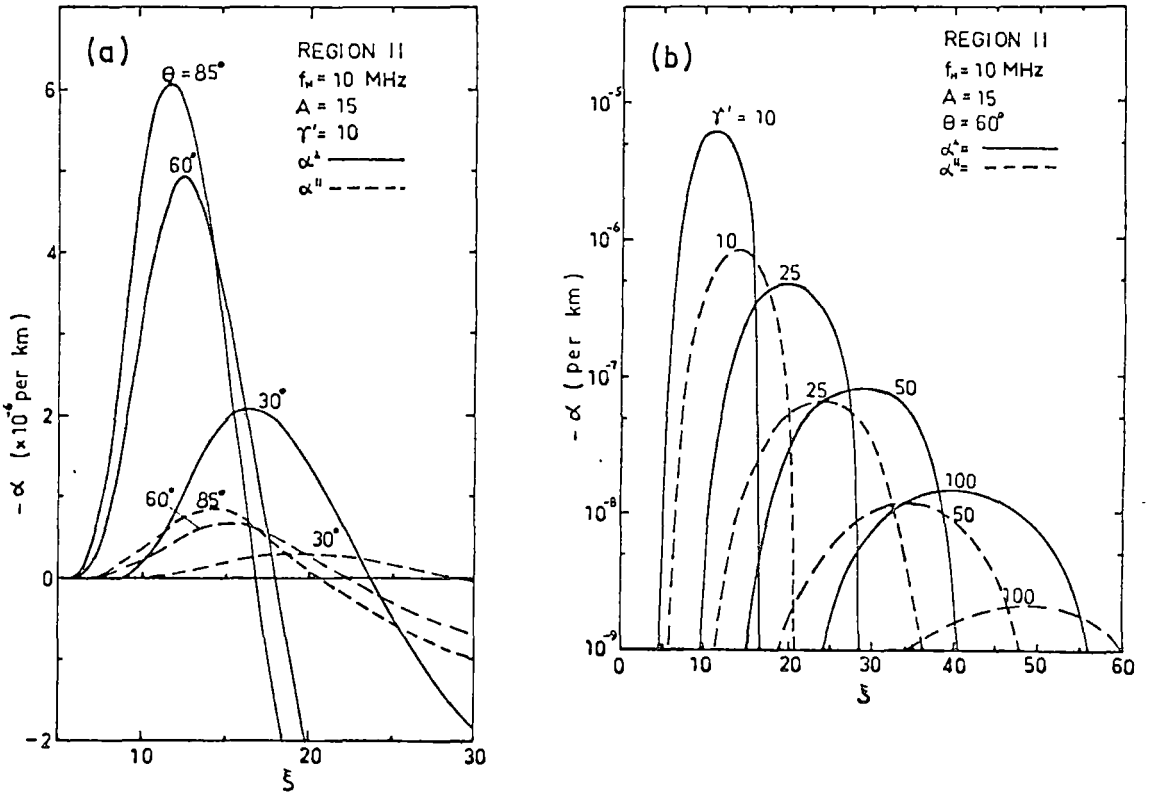

Fig.9.6. Assuming A = 15, f_H = 10 MHz and $\sigma = 10^{-4}$, the synchrotron absorption coefficient is shown as a function of normalized frequency ξ in Region II for a system of monoenergetic electrons and for

(a) $\gamma' = 10$, $\theta = 30^\circ, 60^\circ, 85^\circ$;

(b) $\gamma' = 10, 25, 50, 100$, $\theta = 60^\circ$.

where $j^{\perp,\parallel} = j_{11,22}$. In terms of Stokes parameters, (9.22) is re-written in the form

$$\frac{d}{dr}\begin{pmatrix} I \\ Q \end{pmatrix} = \begin{pmatrix} j_I \\ j_Q \end{pmatrix} - \begin{pmatrix} \mu & \lambda \\ \lambda & \mu \end{pmatrix}\begin{pmatrix} I \\ Q \end{pmatrix}, \qquad (9.23)$$

$$V = U = 0,$$

where $\mu = \frac{1}{2}(\alpha^{\perp} + \alpha^{\parallel})$, $\lambda = \frac{1}{2}(\alpha^{\perp} - \alpha^{\parallel})$,

$$j_I = j_{11} + j_{22}, \quad j_Q = j_{11} - j_{22} .$$

Since we consider the intrinsic radiation of the source, we take the boundary condition that all the Stokes parameters vanish at r=0. Then the solutions of (9.23) are found to be

$$I = \frac{j^{\perp}}{\alpha^{\perp}}(1 - e^{-\alpha^{\perp}L}) + \frac{j^{\parallel}}{\alpha^{\parallel}}(1 - e^{-\alpha^{\parallel}L}),$$

$$Q = \frac{j^{\perp}}{\alpha^{\perp}}(1 - e^{-\alpha^{\perp}L}) - \frac{j^{\parallel}}{\alpha^{\parallel}}(1 - e^{-\alpha^{\parallel}L}), \qquad (9.24)$$

$$V = U = 0 .$$

The degree of linear polarization is given by

$$P = \frac{(Q^2)^{\frac{1}{2}}}{I} = \left| \frac{j^{\perp}\alpha^{\parallel}(1 - e^{-\alpha^{\perp}L}) - j^{\parallel}\alpha^{\perp}(1 - e^{-\alpha^{\parallel}L})}{j^{\perp}\alpha^{\parallel}(1 - e^{-\alpha^{\perp}L}) + j^{\parallel}\alpha^{\perp}(1 - e^{-\alpha^{\parallel}L})} \right| . \qquad (9.25)$$

For an optically thick source, if $\alpha^{\perp,\parallel} \leq 0$, then

$$P \simeq \left| \frac{j^{\perp}\alpha^{\parallel}(1 - e^{-\alpha^{\perp}L})}{j^{\perp}\alpha^{\parallel}(1 - e^{-\alpha^{\perp}L})} \right| = 1 ,$$

since $|\alpha^{\perp}| >> |\alpha^{\parallel}|$. On the other hand, if $\alpha^{\perp,\parallel} > 0$,

$$P \simeq \left| \frac{j^{\perp}\alpha^{\parallel} - j^{\parallel}\alpha^{\perp}}{j^{\perp}\alpha^{\parallel} + j^{\parallel}\alpha^{\perp}} \right| \to 0$$

for both $j^{\perp,\parallel}$ and $\alpha^{\perp,\parallel}$ are proportional to $\eta^{\perp,\parallel}$. Therefore, without taking the birefringence of the medium into account, the main synchrotron radiation is either linearly polarized or randomly polarized. However, the omission of the effects of the magnetic field on synchrotron radiation by relativistic electrons is permissible only when the magnetic field is very weak such that the plasma can be regarded as isotropic. For optically thin source, the intensity and the polarization of the synchrotron radiation will be approximately given by (9.12) and (9.14).

In a magnetoactive plasma, there are only two normal waves; the extraordinary wave and the ordinary wave. In general, the electric field vector is not transverse to the wave vector but the electric induction is (Shafranov, 1967, p.7). Therefore, it is more convenient to define the polarization tensor for the electromagnetic radiation consisting of the o-mode and the x-mode components as (Zheleznyakov, 1968)

$$I_{ij} = \overline{D_i D_j^*}, \quad i,j = 1,2, \tag{9.26}$$

with $$D_i = \int_{\Delta\omega} D_i^o d\omega + \int_{\Delta\omega} D_i^e d\omega ,$$

where $$D_i^{e,o} = A^{e,o} n_i^{e,o} \exp(-K^{e,o} r) \exp[-i(\omega t - k^{e,o} r + \phi^{e,o})].$$

where $k^{e,o}$, $n_i^{e,o}$, $A^{e,o}$ and $\phi^{e,o}$ are the wave numbers, polarization vectors, arbitrary amplitudes and phases of the two normal waves. The bar denotes the average of the quantity (over the time). The absorption coefficients of the waves in amplitude are related to the absorption coefficients in intensity by

$$\alpha^{e,o} = 2K^{e,o} \cos\tilde{\phi}^{e,o} ,$$

where $\tilde{\phi}^{e,o}$ is the angle between the wave vector and the wave group velocity vector. Using this definition of the polarization(radiation) tensor, Zheleznyakov (1968) obtained the radiative transfer equation for the case of homogeneous, stationary magnetoactive plasma

$$\frac{dI_{ij}}{d r} = j_{ij} - K_{ijkl} I_{kl} + R_{ijkl} I_{kl} , \tag{9.27}$$

where $$K_{ijkl} = (K^e + K^o)(n_i^e n_j^{o*} n_k^{e*} n_l^o + n_i^o n_j^{e*} n_k^{o*} n_l^e)$$

$$+ 2 K^e n_i^e n_j^{e*} n_k^{e*} n_l^e + 2K^o n_i^o n_j^{o*} n_k^{o*} n_l^o ,$$

$$R_{ijkl} = i(k^e - k^o)(n_i^e n_j^{o*} n_k^{e*} n_l^o - n_i^o n_j^{e*} n_k^{o*} n_l^e) ,$$

and j_{ij} is defined in (9.4).

In general, (9.27) is extremely complicated. However, for quasi-longitudinal propagation, the two normal waves are both circularly polarized with opposite direction of rotation of the electric field vector and

$$k^o - k^e \simeq \frac{\omega_p^2 \omega_H \cos\theta}{\omega^2 c} = R,$$

and $n_i^e = \frac{1}{\sqrt{2}}(1,i)$, $n_i^o = \frac{1}{\sqrt{2}}(i,1)$.

Moreover, $\cos\tilde{\phi}^{e,o} = 1$. Taking these into account, (9.27) can be greatly simplified as

$$\frac{dI^{e,o}}{dr} = j^{e,o} - \alpha^{e,o} I^{e,o} \quad , \tag{9.28}$$

$$\frac{d}{dr}\begin{pmatrix} Q \\ U \end{pmatrix} = \begin{pmatrix} j_Q \\ 0 \end{pmatrix} - \begin{pmatrix} \alpha & R \\ -R & \alpha \end{pmatrix}\begin{pmatrix} Q \\ U \end{pmatrix} \quad ,$$

where $I = I^e + I^o$, $V = I^o - I^e$, $\alpha = \frac{1}{2}(\alpha^e + \alpha^o)$.

$j^{e,o}$ are the volume emissivities in the x-mode and the o-mode respectively.

Taking the same boundary condition as mentioned above, we find the solutions for the Stokes parameters as

$$I^{e,o} = \frac{j^{e,o}}{\alpha^{e,o}}\left[1 - \exp(-\alpha^{e,o} L)\right] , \tag{9.29}$$

$$\begin{aligned} I &= I^e + I^o, \\ V &= I^o - I^e, \end{aligned} \tag{9.30}$$

$$Q = -[P_Q\cos(RL) + P_U\sin(RL)]\exp(-\alpha L) + P_Q\ ,$$

$$U = [P_Q\sin(RL) - P_U\cos(RL)]\exp(-\alpha L) + P_U, \qquad (9.30)$$

where $P_Q = \alpha j_Q/(\alpha^2 + R^2)$ and $P_U = Rj_Q/(\alpha^2 + R^2)$.

Then the degree of polarization and the degree of circular polarization will be

$$P = \frac{(Q^2 + V^2 + U^2)^{\frac{1}{2}}}{I} \qquad (9.31)$$

and $$P_C = \frac{V}{I}$$

respectively. When P_C is negative, the circularly polarized component is in the x-mode. For an optically thick source, P_C can be approximated as

$$P_C \simeq \frac{|\alpha^e|j^o - |\alpha^o|j^e\exp[-(\alpha^e - \alpha^o)L]}{|\alpha^e|j^o + |\alpha^o|j^e\exp[-(\alpha^e - \alpha^o)L]} \text{ (for } \alpha^{e,o} < 0), \qquad (9.32)$$

$$\text{or } P_C \simeq \frac{\alpha^e j^o - \alpha^o j^e}{\alpha^e j^o + \alpha^o j^e} \quad (\text{for } \alpha^{e,o} > 0). \qquad (9.33)$$

Since both the volume emissivities $j^{e,o}$ and absorption coefficients $\alpha^{e,o}$ are proportional to the electron emissivities in the x-mode and the o-mode $\eta^{e,o}$, from (9.32), it is not difficult to see that the circularly polarized synchrotron radiation will be emitted only when the reabsorption coefficients are negative and $|\alpha^e - \alpha^o|$ differs from zero

significantly; the radiation will be polarized in the x-mode if $|\alpha^e| > |\alpha^o|$ and in the o-mode if $|\alpha^e| < |\alpha^o|$. On the other hand, if $\alpha^{e,o} > 0$, the degree of circular polarization given by (9.33) is insignificantly small.

If the radiation source is optically thin, i.e. $|\alpha^{e,o}L| \ll 1$, the solutions of (9.28) for $I^{e,o}$ are

$$I^{e,o} = j^{e,o}L \tag{9.34}$$

and the corresponding degree of circular polarization will be

$$P_C = \frac{j^o - j^e}{j^o + j^e} \quad . \tag{9.35}$$

In this case, the appearance of the strongly circularly polarized synchrotron radiation requires that the volume emissivity (or the electron emissivity) polarized in one of the two normal modes must be greater than that polarized in the other mode significantly. Therefore, once the volume emissivities and the absorption coefficients for the two normal waves in the magnetoactive plasma are known, the characteristics of the synchtron radiation emerging from a system of relativistic electrons can be determined.

According to (9.28) and (9.13), the electron emissivities, the volume emissivities and the absorption coefficients for the case of longitudinal propagation are

$$\eta^{e,o} = \tfrac{1}{2}[\eta_{11} + \eta_{22} \mp i(\eta_{21} - \eta_{12})] \ , \qquad (9.36)$$

$$j^{e,o} = \int \eta^{e,o} f_o(p) d\bar{p} \ ,$$

and $$\alpha^{e,o} = -\frac{8\pi^3 c^2}{n^2\omega^2} \int \eta^{e,o} \frac{\partial f_o(p)}{\partial E} d\bar{p} \ ,$$

where the upper sign is for the x-mode and η_{ij} is given by (9.2). Using (9.8) and (9.9), we find the volume emissivities and the absorption coefficients for the synchrotron radiation in the case of isotropic electron momentum distribution,

$$j^{e,o} = \frac{e^2\omega_H}{16\pi^2\sqrt{3}\ nc} \int_o^\infty f_o(E)[\xi\zeta(F^\perp + F^{||}) \pm \frac{4}{\gamma'}\cos\theta F^{\perp||}]\, dE, \qquad (9.37)$$

and $$\alpha^{e,o} = \frac{\pi e^2\omega_H}{2\sqrt{3}\ n^3\omega^2 c} \int_o^\infty f_o(E)\{\frac{2A}{\xi}(F^\perp + F^{||}) \pm \frac{4\cos\theta}{\gamma'} F^{\perp||} + z(\frac{A}{\xi^2} - \frac{2}{\gamma'^2})$$

$$\times [\xi \frac{\partial}{\partial z}(F^\perp + F^{||}) \pm \frac{4\cos\theta}{\gamma'}\zeta^{-1}\frac{\partial}{\partial z} F^{\perp||}]\}\, dE, \qquad (9.38)$$

with $$\frac{\partial}{\partial z}(F^\perp + F^{||}) = -2K_{5/3}(z) \ ,$$

$$\frac{\partial}{\partial z} F^{\perp||} = \frac{4}{3} K_{1/3}(z) - zK_{4/3}(z) + 2K'_{2/3}(z) + K_{5/3}(z) \ .$$

Then, for monoenergetic electron spectrum (9.7), we obtain

$$j^{e,o} = \frac{e^2 \sigma N_o \omega_H}{16\pi^2\sqrt{3}\, nc} \{\xi\zeta[F^{\perp}(z)+F^{||}(z)] \pm \frac{4\cos\theta}{\gamma'} F^{\perp||}(z)\} \ , \quad (9.39)$$

and $$\alpha^{e,o} = \frac{\sigma A \omega_H}{8\sqrt{3}n^3\xi^2 c\gamma'} \{ \frac{2A}{\xi} (F^{\perp} + F^{||}) \pm \frac{4\cos\theta}{\gamma'} F^{\perp||}$$

$$+ z(\frac{A}{\xi^2} - \frac{2}{\gamma'^2}) [\xi\frac{\partial}{\partial z} (F^{\perp} + F^{||}) \pm \frac{4\cos\theta}{\gamma'} \zeta^{-1} \frac{\partial}{\partial z} F^{\perp||}]\} \quad (9.40)$$

Using (9.10), (9.39) and (9.40) in (9.29) and (9.30), we can study the characteristics of the synchrotron radiation emitted from a system of monoenergetic relativistic electrons.

Taking $\sigma = 8\times10^{-3}$, $f_H = 10$ MHz, $A = 15$ and $\gamma' = 10$, 25, 50, 100, we illustrate the variations of the absorption coefficients $\alpha^{e,o}$ with the normalized emission frequency in Fig. 9.7(a) and (b). Firstly, negative reabsorption of synchrotron radiation in both modes occurs in the low frequency region of the synchrotron radiation spectrum. The variations of α^e and α^o with ξ are similar. Secondly, the magnitudes of $\alpha^{e,o}$ increase with the wave-normal angle. Thirdly, in general, the magnitude of α^e is greater than α^o and $|\alpha^e - \alpha^o|$ decreases with increasing wave-normal angle. Finally, the magnitude of the reabsorption coefficient decreases with increasing electron energy, but negative reabsorption occurs at higher frequencies for higher electron energy. Fig. 9.7 (c) demonstrates the suppression of

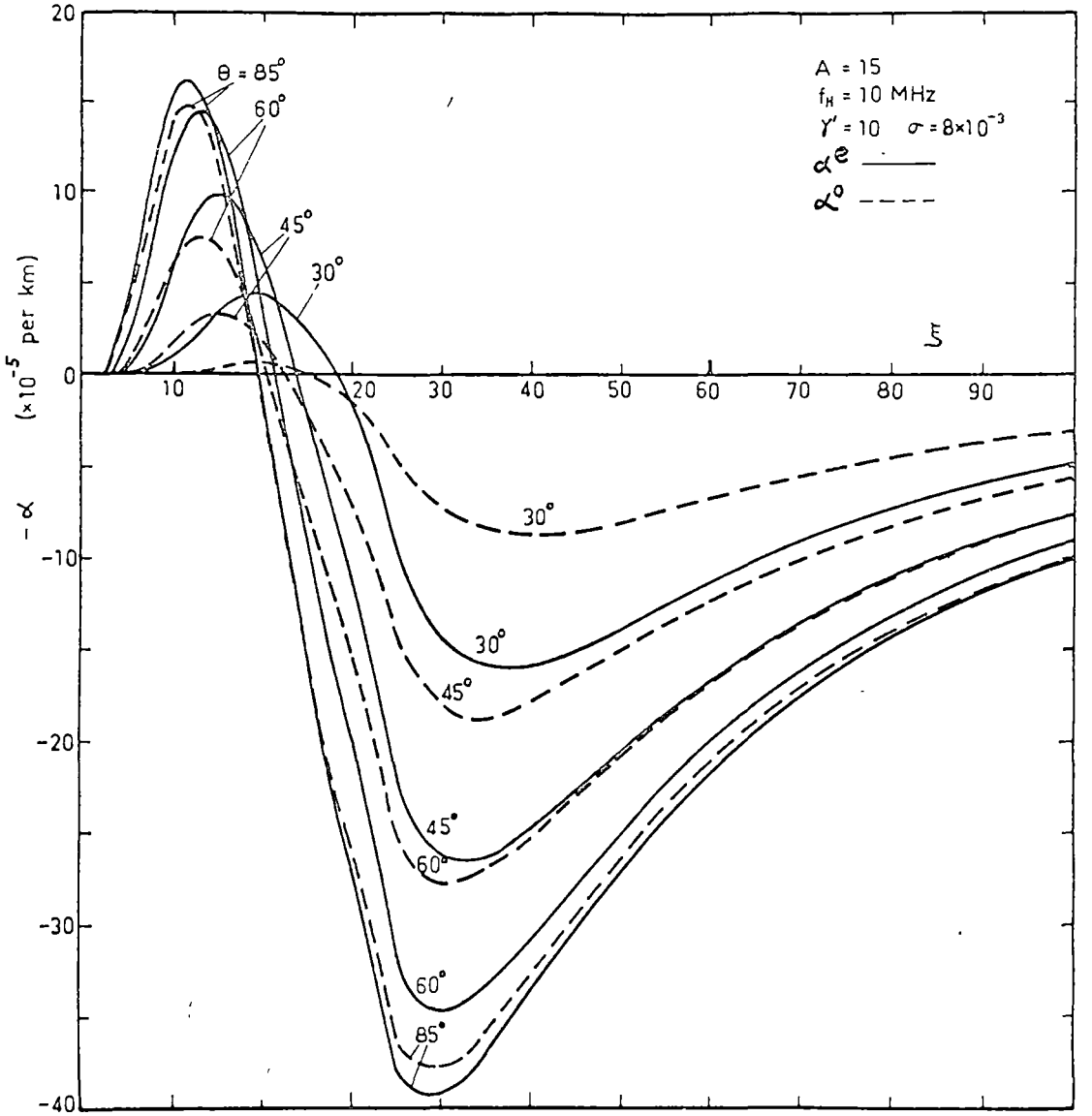

Fig.9.7(a) Assuming A = 15, f_H= 10 MHz and σ = 8×10^{-3}, the synchrotron absorption coefficient for the radiation in the x-mode (and the o-mode) is shown as a function of normalized frequency ξ for a system of monoenergetic electrons and for γ'= 10, θ = 30°, 45°, 60°, 85°.

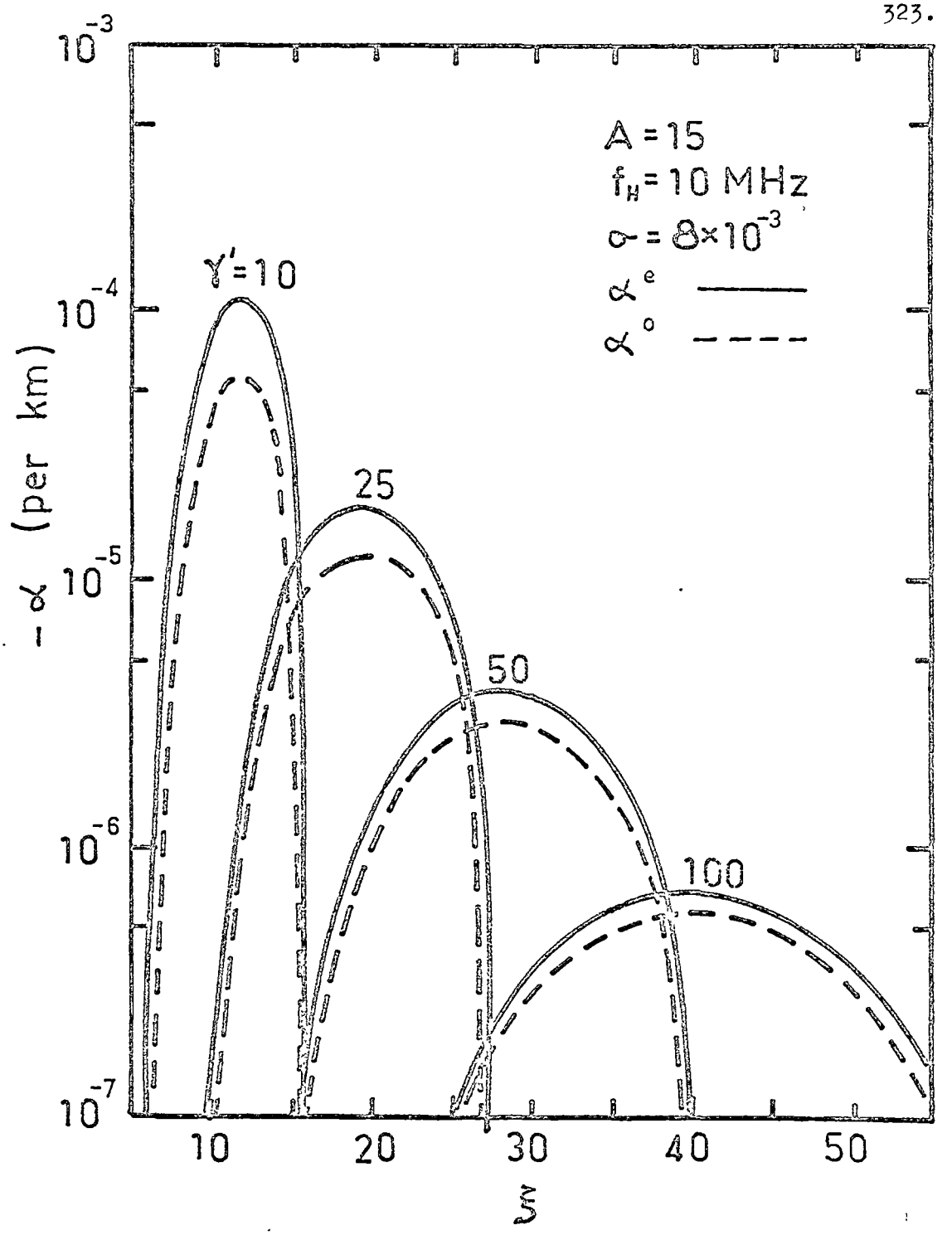

Fig.9.7(b) Assuming A = 15, f_H = 10 MHz and $\sigma = 8\times10^{-3}$, the synchrotron absorption coefficients for the radiations in the x-mode and the o-mode are shown as functions of normalized frequency ξ for a system of monoenergetic electrons and for γ' = 10, 25, 50, 100 and $\theta = 60^\circ$.

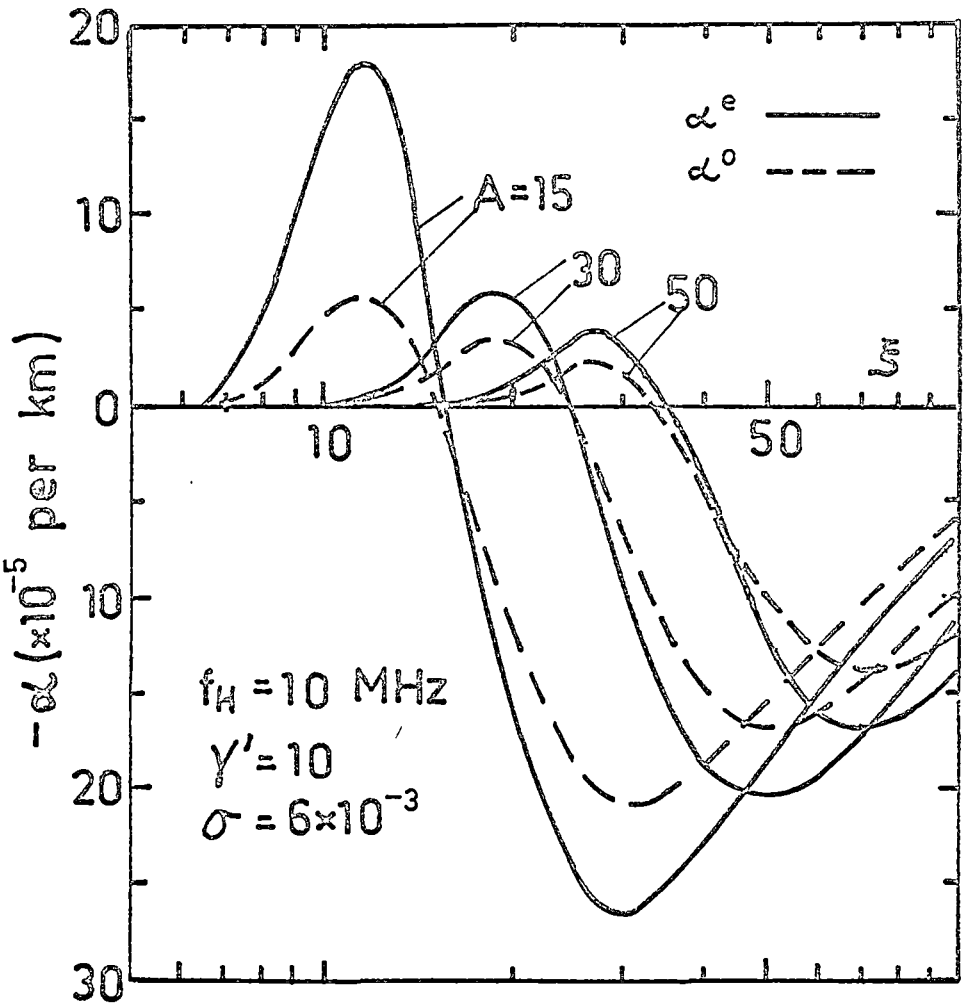

Fig.9.7 (c) Variations of the synchrotron absorption coefficients for the radiations in the x-mode and the o-mode with the normalized frequency ξ for a system of monoenergetic electrons and for $\gamma' = 10$, $\theta = 60^{\circ}$, A = 15, 30, 50, f_H = 10 MHz and $\sigma = 6\times10^{-3}$.

reabsorption due to the influence of the ionized medium on the reabsorption process. For larger values of A i.e. higher number densities of the ambient plasma and the radiating electrons, the absorption coefficients become smaller.

With the volume emissivities and the absorption coefficients given by (9.39) and (9.40), Fig. 9.8(a) emphasizes the effects of the negative reabsorption on the frequency spectrum and the polarization state of the synchrotron radiation for a given wave-normal angle while Fig. 9.8(b) demonstrates the dependence of the frequency spectrum of the synchrotron radiation on the direction of observation. The angular distribution of the intensity of the synchrotron radiation at a given frequency is shown in Fig. 9.8(c) for various values of the number density of radiating electrons and for various emission frequencies.

Fig. 9.9 (a) shows that for an optically thick radiation source, the intensity distribution of the synchrotron radiation across the spectrum changes greatly if the reabsorption is taken into account. Furthermore, the peak synchrotron radiation in the low frequency region arising from negative reabsorption will dominate. In this figure, the intensities of the incoherent synchrotron radiations in the x-mode and the o-mode ($j^{e}L$ and $j^{o}L$ respectively) are also plotted as functions of emission frequency. Both

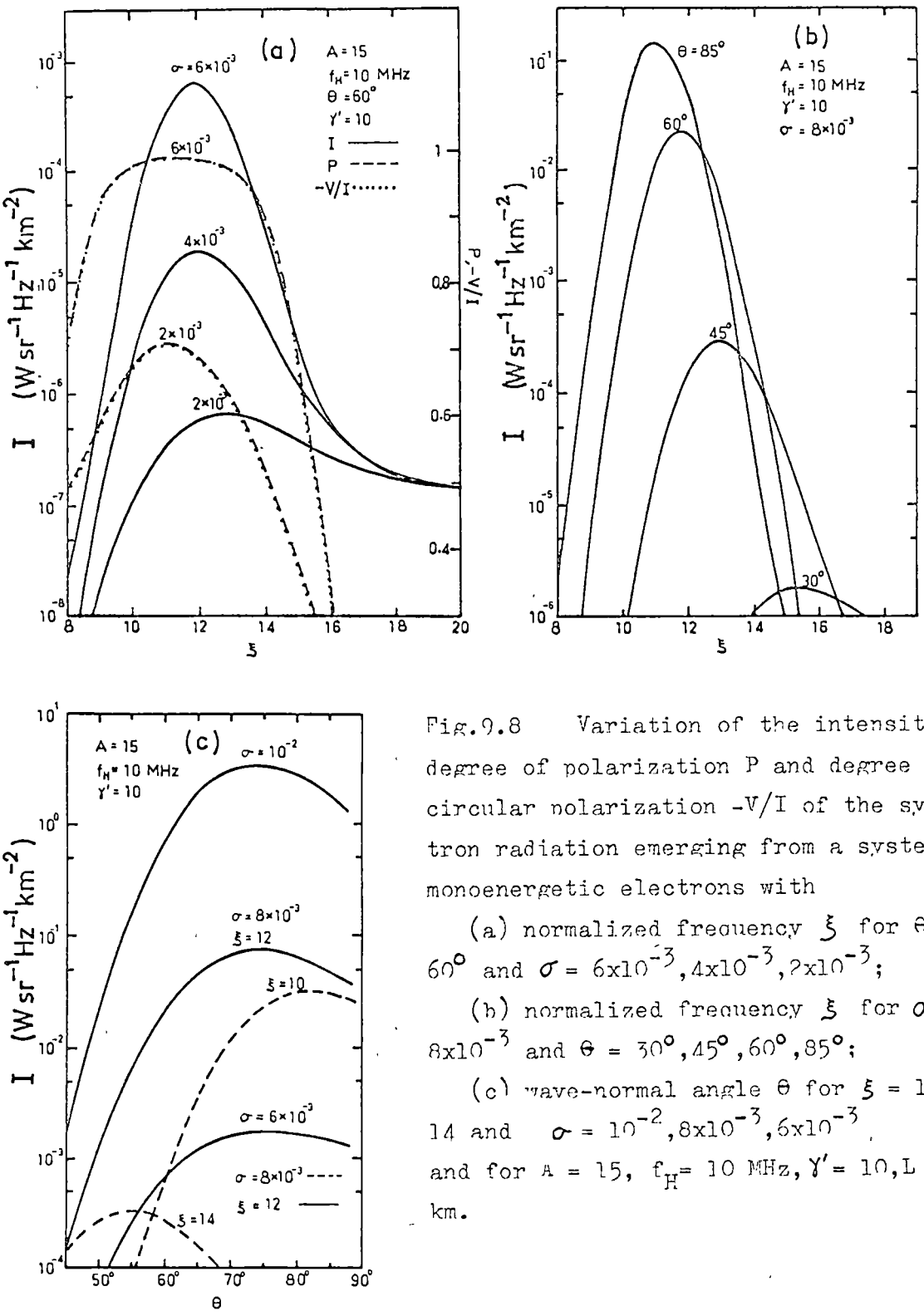

Fig.9.8 Variation of the intensity I, degree of polarization P and degree of circular polarization -V/I of the synchrotron radiation emerging from a system of monoenergetic electrons with

(a) normalized frequency ξ for $\theta = 60^{\circ}$ and $\sigma = 6\times10^{-3}, 4\times10^{-3}, 2\times10^{-3}$;

(b) normalized frequency ξ for $\sigma = 8\times10^{-3}$ and $\theta = 30^{\circ}, 45^{\circ}, 60^{\circ}, 85^{\circ}$;

(c) wave-normal angle θ for $\xi = 10, 12, 14$ and $\sigma = 10^{-2}, 8\times10^{-3}, 6\times10^{-3}$

and for A = 15, f_H = 10 MHz, $\gamma' = 10$, L = 10^5 km.

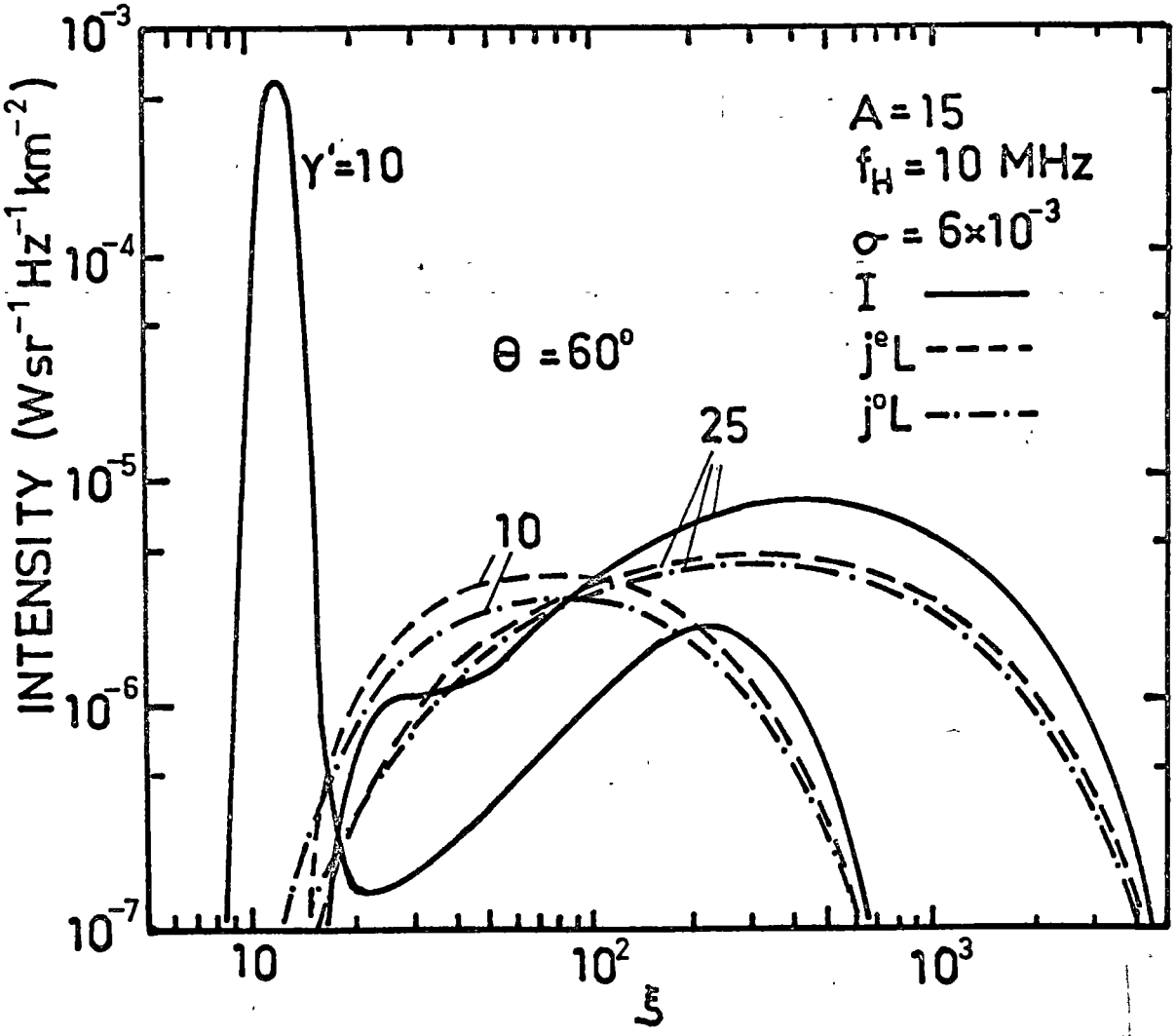

Fig.9.9 (a) Variations of the intensity of coherent synchrotron radiation and the intensities of incoherent synchrotron radiations in the x-mode (j^eL) and the o-mode (j^oL) from a system of monoenergetic electrons with normalized frequency ξ for $\theta = 60^o$, $\gamma' = 10, 25$, $A = 15$, $f_H = 10$ MHz, $\sigma = 6\times10^{-3}$ and $L = 10^5$ km.

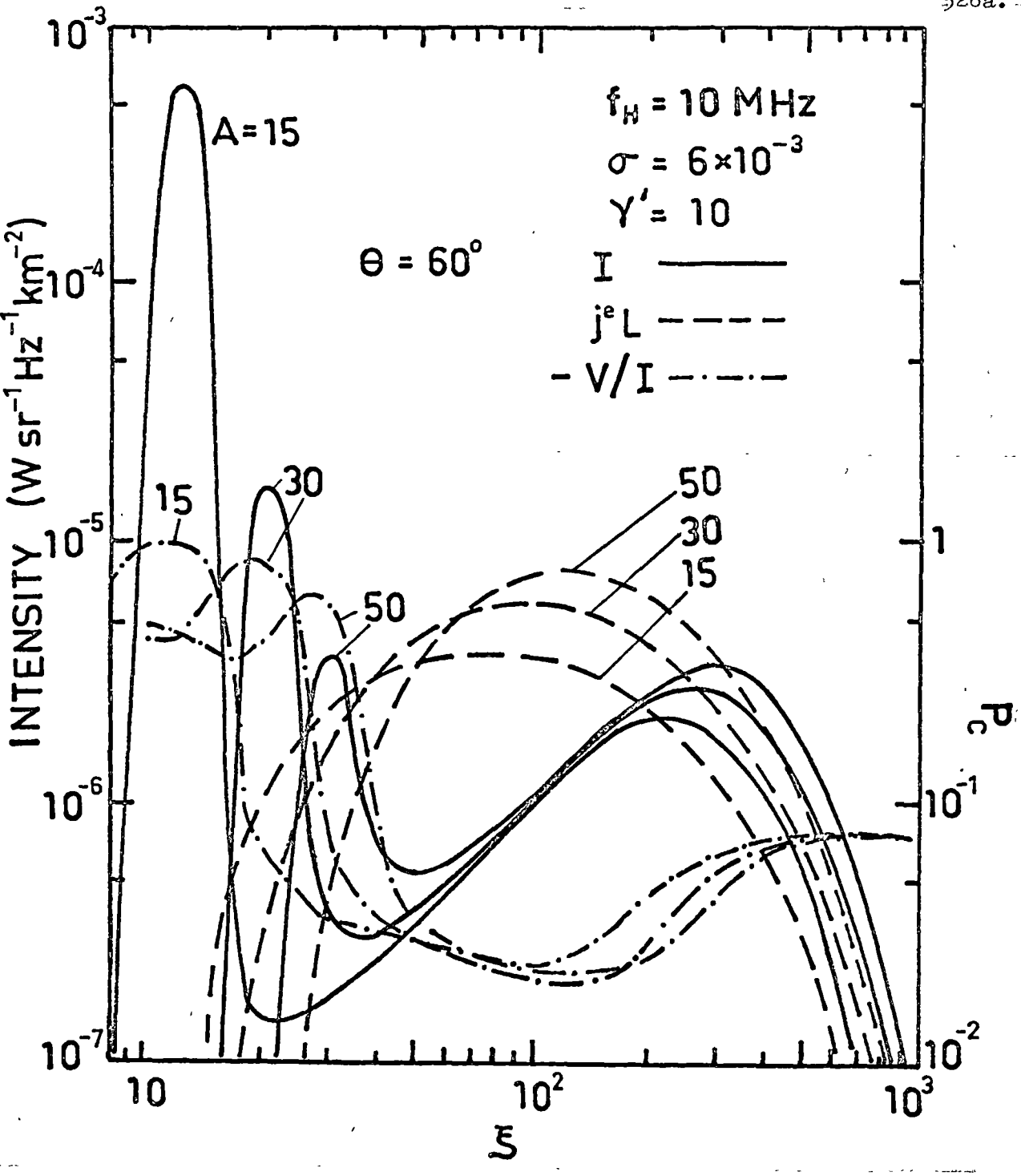

Fig.9.9 (b) Variations of the intensity I and the degree of circular polarization P_C of the coherent synchrotron radiation, the intensity of the incoherent synchrotron radiation in the x-mode j^eL emerging from a system of monoenergetic electrons with normalized frequency ξ for $\theta = 60^\circ$, $\gamma' = 10$, $A = 15, 30, 50$, $f_H = 10$ MHz, $\sigma = 6\times10^{-3}$ and $L = 10^5$ km.

the coherent and incoherent synchrotron radiation spectra have sharp low frequency cut-offs; the cut-off frequencies for the coherent and the incoherent synchrotron radiations are different. In the case of incoherent synchrotron radiation, the low frequency cut-off is due to the influence of the ionized medium, generally referred to the Razin effect. For the same system of radiating electrons and the same intensity of the magnetic field of the ambient plasma, the cut-off frequency of the incoherent (or coherent) synchrotron radiation spectrum observed at a given direction increases with increasing number density of the ambient plasma electrons. This is illustrated in Fig. 9.9 (b) where the degree of circular polarization is also shown.

From Fig. 9.7 and Fig. 9.8, it can be seen that for an optically thick radiation source, strongly circularly polarized synchrotron radiation will be emitted in the frequency region where the negative reabsorption occurs. The polarization will be in the extraordinary mode. Since at any given frequency, the magnitude of the synchrotron absorption coefficient and the volume emissivity for the x-mode are similar to those for the o-mode, positive reabsorption cannot give rise to strongly circularly polarized synchrotron radiation (see expression (9.33)). Moreover, the degree of circular polarization of the synchrotron radiation emitted from an optically thin radiation

source will be insignificant.

We have studied the characteristics of the synchrotron radiation emerging from a radiation source in the solar corona. Since the emission frequency of the synchrotron radiation satisfies the conditions: $\xi^2 >> 1$ and $\xi^2 >> A$, subsequent propagation from the source to the Earth would not cause any significant change of the spectral characteristics of the synchrotron radiation and the observed spectral characteristics of the synchrotron radiation from the solar corona will be as those mentioned above.

D. Synchrotron Radiation from Relativistic Electrons in The Solar Corona

During the recent years, solar energetic electrons with energies from a few tens of keV to a few MeV have been observed (Fichtel and McDonald, 1967; Cline and McDonald, 1968a). However, at present the problem of production of energetic charged particles in the solar corona has not been settled although several suggestions have been put forward. The Fermi acceleration or the Sweet mechanism (acceleration in the annihilation of anti-parallel magnetic fields) can lead to the production of energetic electrons in the solar corona. Since the plasma can support hydrodynamic-type turbulence as well as high frequency turbulence connected with the generation of electron oscillations relative to ions,

electrons can be accelerated by longitudinal plasma waves and by low frequency hydrodynamic-type oscillations. Tsytovich (1966) pointed out that Fermi acceleration is a limiting case of acceleration by low frequency hydrodynamic-type turbulence and is not the most effective one of all possible acceleration mechanisms in a turbulent plasma.

The quasi-regular appearance of the type III bursts indicated that the energetic electrons ejected from the flare region are likely to be accelerated by a process similar to the Sweet mechanism. Severnyi (1960) has reported optical evidence in favour of this idea. However, Tverskoi (1967), after studying the main properties of Fermi acceleration, showed that observational evidence favoured the idea of acceleration of solar energetic electrons by means of the Fermi mechanism. Laboratory experiments have shown that when an electron beam penetrates into a plasma, some of the beam electrons can be accelerated to higher energy by the plasma waves excited by the beam itself (Stix, 1964; Fainberg, 1968). Since different acceleration processes would require different conditions, the solar energetic electrons responsible for the radio emissions (or X-ray emission) and those observed on the Earth may be accelerated by these processes in different regions of the solar corona at different times. The region of acceleration is not necessarily restricted to the flare region.

The observation of solar relativistic electrons near the Earth indicates that their energy spectrum could be characterized by a certain power law (Cline and McDonald, 1968b). If the energy spectrum of the solar relativistic electrons is very steep at the high energies, the spectrum can be represented by

$$f_o(E)dE = \begin{cases} N_o'(1+\Gamma)E_o^{-(1+\Gamma)}E^{\Gamma}dE, & \text{for } E_1 < E < E_o \\ 0, & \text{for } E > E_o \text{ and } E < E_1 \end{cases} , \qquad (9.41)$$

where Γ is a positive number. If Γ is not small; that is most of the electrons have energies close to E_o, (9.41) can be approximated by the monoenergetic spectrum (9.7). So far there has been no observation data suggesting the existence of highly anisotropic relativistic electron streams in the solar corona.

Whenever sufficient electrons are accelerated to energies about a few MeV and trapped in the sunspot magnetic field, these electrons generate synchrotron radiation which would eventually be observed as a broad band smooth continuum radio emission on the Earth. Among various spectral types of solar radio emissions, the type V and type IV (both components A, B, and C) are of wide bandwidth smooth continuum emissions. Previously, these solar radio emissions were interpreted as the consequence of synchrotron radiation by

relativistic electrons. However, the simple synchrotron radiation theory cannot fully explain the spectral features of these radio emissions. In the following paragraphs, we shall examine the question of the origin of these emissions.

(a) Solar Type V Burst Emission

The solar type V burst is closely associated with the spectral type III burst; it occurs after a type III burst (see Fig. 6.1). In most cases, the type V burst is observed at frequencies below 150 MHz and is weakly polarized. Usually, the bandwidth is comparable to the centre radiation frequency and the intensity may reach values of the order of 10^{-18} W $m^{-2}Hz^{-1}$ which is considerable higher than that of the type III burst. A type V burst often occurs as the continuous diffuse prolongation of a type III burst, lasting approximately 0.5 - 3 min. The average source size of the type V at half power is about 5' at a frequency of 40 MHz. Most of the type V sources are seen near the radio limb. The source height in general agrees well with the height of the type III sources at the same frequencies.

The plasma radiation caused by solar electron streams has been proposed as the origin of type V burst emission (Weiss and Stewart, 1965; Zheleznyakov and Zaitsev, 1968). Since at the type V burst emission source height, the variation of the coronal electron density is very small, it is difficult to

account for the wide bandwidth of the type V burst on the basis of the theory of plasma radiation. So the suggestion that the type V burst emission is caused by synchrotron radiation by relativistic electrons (Wild et al., 1959) should be re-examined.

We assume a group of isotropic monoenergetic electrons with energy about 2 - 4 MeV trapped in the sunspot magnetic field at altitude about $\rho \simeq 1.9$. Taking the model of the active solar corona given by Fig. 6.1, we find the value of A and the gyrofrequency at this height is about 15 and 10 MHz respectively; these parameters are the same as those used in various figures in this chapter. If these relativistic electrons radiate incoherently, then, in order to achieve the observed intensity 10^{-18} Watts/m^2-Hz, the source volume must be $10^{10} \times 10^5 km^3$ and the number density of the radiating electrons is not less than 10^3 cm^{-3}. The centre frequency of the type V burst and the frequency of the type III burst emitted at the same height are widely separate since the incoherent synchrotron radiation maximizes at frequencies $\xi \simeq 200$ for $\theta = 85^o$ (Fig. 9.3 (a)) but the type III burst's frequency is $\xi_{2f_p} \simeq 2\sqrt{A} \simeq 8$ (cf. Chapter VI). Hence in order for the frequency of the incoherent synchrotron radiation of maximum intensity to be close to the second harmonic local plasma frequency, the local gyrofrequency must be much

smaller than 10 MHz and the electron energy should be lower than 4.5 MeV ($\gamma' = 10$).

On the other hand, if negative reabsorption is important, the peak synchrotron radiation occurs in the low frequency interval of the spectrum. From Fig. 9.7 and Fig. 9.8, the peak intensity is found to occur at $\xi_m \simeq 12$ which is close to the second harmonic of the local plasma frequency. (If $\gamma' = 5$, we find that $\xi_m < 12$ but the intensity is greater.) The half-power frequency bandwidth will be $\Delta f = \Delta\xi \times f_H \simeq 60$ MHz. However, we should note that the low frequency peak arising from negative reabsorption will dominate only if the number density of the radiating electrons exceeds 5×10^4 cm^{-3} and the source depth must be of the order of 10^5 km (The source volume may be less than $10^{10}\times10^5$ km.) (see Fig. 9.3 and Fig. 9.7 (a)). Moreover, when negative reabsorption is significant, fraction of the synchrotron radiation emerging from the source region will be circularly polarized. At present, observational data are insufficient for definitely determining the polarization character of the type V bursts (Weiss and Stewart, 1965).

The difficulty in interpretating the type V burst emission as the result of synchrotron radiation by relativistic electrons lies in the problem of production of these relativistic electrons. There is no observational report suggesting the

existence of a sharp shock front in the outer layers of the solar corona during the type V bursts emission period. We believe that the relativistic electrons responsible for the type V burst emission are not produced by the Fermi-like mechanism. Alternatively, the occurrence of the type V burst immediately after the type III burst leads us to consider acceleration of energetic electrons by high frequency plasma waves. The electron stream ejected from the flare region travels through the solar corona and excites Cerenkov plasma waves of which a very small amount of energy is converted into electromagnetic radiation by means of combination scattering on the thermal fluctuations of the electron density and eventually observed as the type III burst (cf. Chapter VI).

Meanwhile, the plasma waves excited by the stream are scattered to plasma waves of larger phase velocity and with different directions of propagation. Those scattered plasma waves with wave vectors transverse to the electron's trajectory can accelerate a small fraction of stream electrons to higher energy (Tsytovich, 1966). This leads to the diffusion of the stream electrons in velocity space and coherent generation of Cerenkov plasma waves will terminate. Those accelerated electrons trapped in the sunspot magnetic field produce the wide bandwidth type V burst through the synchrotron radiation process. Since only a small fraction of the stream electrons (a several

to ten per cent, say) can be accelerated, to secure a group of relativistic electrons of density $10^3 - 10^4$ cm^{-3} requires the density of the original electron stream not less than 10^5 cm^{-3} (i.e. $N_o'/N_o = 10^{-2}$ at $\rho \simeq 1.9$). Such a large value of stream density has been assumed in the theory of type III burst emission (Wild, Smerd and Weiss, 1963). Nevertheless, a satisfactory theory of type V burst emission on the basis of synchrotron radiation by relativistic electrons should include a detailed investigation of the possibility of accelerating a few per cent of the mildly relativistic stream electrons to energies of a few MeV by plasma waves (or by other means) and also explanations of other features of the type V burst emission. Further observational data concerning the polarization of the type V burst would be a great help in the development of the theory.

(b) Solar Type IV Emission

The type IV burst emission is a very complicated phenomenon and occurs after an important solar flare. The emission appears at the centimetre, decimetre, metre and decametre wavelengths in the spectragraph. According to Kundu (1965), this complicated radio emission can be divided into three components, namely, type IVA, type IVB (moving) and type IVC (stationary). The characteristics of type IVA component have been described in Chapter VIII. The major features of the type IVB and type IVC components are briefly

outlined in Table 9.1.

Because of their wide bandwidths, all three components have been interpreted as the results of synchrotron radiations by relativistic electrons trapped in the sunspot magnetic field or embedded in the moving plasma cloud. The energies of the electrons responsible for different components were assumed to be different (Boischot and Denisse, 1957, Takakura and Kai, 1961; etc.). Without the influence of the medium taken into account, interpretations on the basis of synchrotron radiation theory encounter difficulties in the explanation of the polarization of type IV bursts.

Firstly, in the high frequency region of the type IVA spectrum, the burst is weakly polarized in the x-mode and may be regarded as combination of the bremsstrahlung and the synchrotron radiation produced by relativistic electrons accelerated near the flare region. In the low frequency region (from 200 MHz to a few thousand MHz), the polarization state varies with the frequency; the radiation is strongly polarized in the o-mode in the decimetre wavelength region, but the polarization mode changes at the frequency in the range from 2,000 MHz to 4,000 MHz. The change in the polarization mode along the spectrum may arise from

Table 9.1 Type IV Emission
(After Kundu, 1965, p.420)

	Type IV B (Moving)	Type IV C (Stationary)
Wavelength extent	Meter and decameter waves	Meter and decameter waves
Association with type II	Occurs usually with type II	May occur without type II
Start relative to type II	A few minutes after type II	May follow type IV B, tens of minutes after type II
Altitude of emission	The source does not remain fixed in the corona; maximum altitudes vary from 10^5 to 10^6 km above the photosphere or higher	The source is situated low in the corona near the corresponding plasma level
Movement	Usually large movement with a velocity of more than 1000 km/sec	No systematic movement of the source
Angular size	About 10′ arc or larger	Usually less than 4′ arc
Variability	Smooth; may have some structure at the start	Smooth—occasionally some broadband bursts. Type I bursts gradually appear with the aging of the continuum
Polarization	Weakly circularly polarized	Strongly circularly polarized
Polarization mode (assuming field of leading spot)	Extraordinary	Ordinary
Duration	10^m to 2^h, usually longer than in phase A	Several hours to several days
Distribution on the disk	Not directive	Highly directive toward the center
Place of origin	Near the flare	Near the flare
Temperature	10^7 to 10^{10} °K	$\sim 10^{10}$ °K

differential positive reabsorption of synchrotron radiations in the x-mode and the o-mode. However, according to the discussion in the previous section, positive reabsorption cannot lead to strongly circularly polarized synchrotron radiation no matter whether the emission source is optically thick or optically thin. On the other hand, owing to the facts that $j^e > j^o$ and $|\alpha^e| > |\alpha^o|$, negative reabsorption can give rise to strongly polarized synchrotron radiation in the x-mode only. Hence the type IVA emission cannot be explained as the result of synchrotron radiation from relativistic electrons with energy about a few MeV, at least in the decimetre wavelength region.

Alternatively, we suggest that the resonance absorption by the thermal coronal plasma electrons would play an important part in the determination of the observed polarization feature of the type IVA burst emission. In other words, the radiating electrons responsible for the type IVA emission should be the low energy component of the electrons released from the flare region so that the main radiation energy in the x-mode and the o-mode concentrates in the low harmonics of the Doppler-shifted gyrofrequency. The concurrent appearance of the type III bursts in the frequency range from 600 MHz to a few MHz and the fast drifting elements superimposed on the decimetre wavelength continuum suggest that the mildly relativistic electrons organize as an electron

stream gyrating along the strongest sunspot magnetic field or travelling in the neutral plane between two sunspot fields of opposite polarity. Cyclotron radiation in the x-mode and the o-mode and Cerenkov radiation in the plasma mode by those electron streams trapped in the bipolar sunspot magnetic field configurations at the base of the solar corona result in the type IVA emission (Chapter VIII).

The moving type IV burst emission is characterized by a very large source size and the right-handed polarization. Now it is believed that the moving type IV burst is generated by electrons embedded in a moving plasma cloud expelled from the flare region (Kundu, 1965, p.598). Recently, Boischot and Clavelier (1967) observed a moving type IV burst at the frequencies 408 MHz and 169 MHz emitted from a single source having a linear size about several 10^5 km and moving with a speed about 530 km/sec. During the same period, relativistic electrons with energies up to 8 MeV were also observed at the Earth (Cline and McDonald, 1968a). Thus it is possible that the observed relativistic electrons and those responsible for the moving type IV burst emission are of the same origin.

Lacombe and Mangeney (1969) showed theoretically that the relativistic electrons responsible for this observed burst emission were accelerated by the turbulent ion acoustic waves generated by a shock wave. According to various

figures given in previous sections, we can find that negative reabsorption of the synchrotron radiation emitted by these relativistic electrons is not required for interpreting the observed intensity of the moving type IV burst (of the order of 10^{-20} W m^{-2} Hz^{-1}). On the contrary, interpretation of the moving type IV burst emission based on the coherent synchrotron mechanism requires a higher number density of the radiating electrons and stronger magnetic field intensity forzen in the moving plasma cloud. However, if the radiation source is optically thin, the synchrotron radiation theory fails to explain the strong circular polarization (in the x-mode) of many observed moving type IV bursts (degree of polarization as high as 85% (Kai, 1969)). On the other hand, the theory of cyclotron radiation in the o-mode and the x-mode by mildly relativistic electron streams trapped in some strong magnetic fields frozen in the plasma cloud can also account for most of the spectral characteristics of the moving type IV bursts.

The nature of the source and some of the spectral characteristics of the stationary type IV emission are remarkably distinct from those of the moving type IV emission although their occurrences are closely correlated. Weiss (1963b) suggested that the moving type IV emission and the stationary type IV emission should be regarded as separated events. The feature of the stationary type IV burst emission

in which a wide range of frequency is emitted from a stationary source in the solar corona can be explained by the theory of synchrotron radiation. But the strong polarization in the o-mode of the stationary type IV burst rejects the possibility of synchrotron radiation by relativistic electrons as the origin of the emission. The cyclotron radiation by mildly relativistic electron bunches is likely to be responsible for the stationary type IV emission.

If we assume the electron energy to be 20 - 30 keV, say, the second harmonic cyclotron radiation in the x-mode and the o-mode will dominate. For not too large electron pitch angle, the peak intensity of the second harmonic cyclotron radiation will be emitted at the wave-normal angles $\theta_m \simeq 50^o - 70^o$ (cf. Chapter VIII). Then the cyclotron radiation in the x-mode will be prevented from escaping from the solar corona due to the third harmonic resonance absorption. If the coronal plasma where the radiating electron bunches reside is characterized by a value of A about 3 to 4, the frequencies associated with the peak cyclotron radiation will be close to the plasma frequency, and generation of the cyclotron radiation at the second harmonic Doppler-shifted gyrofrequency and in the x-mode by the electron bunch may not be possible. Since the true escape level is higher at the solar limb than near the

centre of the solar disk (Fig. 8.12), electromagnetic radiation at the frequencies close to the plasma frequency and emitted from a limb source cannot escape from the solar corona. Thus the stationary type IV burst source will be highly directive.

Meanwhile, the same electron bunch can also excite Cerenkov plasma waves at the frequencies $f \simeq f_p$ which, after being transformed into the o-mode waves by incoherent scattering, will be observed as a narrow bandwidth drifting burst superimposed on the smooth continuum emission in the o-mode. Since the Cerenkov plasma radiation at the frequencies $f \simeq f_p$ by the electron stream with $\beta_{\parallel} \simeq 0.1 - 0.3$ maximizes at small wave-normal angles (Chapter VI), it will probably pass through the resonance absorption layers at small wave-normal angles and harmonic resonance absorption may not be important. Consequently, the wide bandwidth stationary type IV continuum emission is superimposed with fine structures occassionally.

Although theories of cyclotron radiation and Cerenkov plasma radiation by mildly relativistic electron streams can satisfactorily explain the spectral characteristics of the stationary type IV burst emission, the origin of these electron streams is not clear. These stream electrons cannot be regarded as the same electrons responsible for the moving

type IV emission since it is unlikely that a system of isotropic relativistic electrons can decay into mildly relativistic electron streams. On the other hand, if these mildly relativistic electron streams are ejected from the flare region near the base of the solar corona, then we have to explain why the electron streams cannot give rise to any radio emission on passing through the lower layers of the active solar corona.

E. Conclusion

Synchrotron radiation from a system of monoenergetic electrons has been studied in previous sections. There is no strongly circularly polarized synchrotron radiation from isotropic relativistic electrons unless the source is optically thick such that the negative reabsorption is important; i.e. the coherent synchrotron radiation is dominant. The coherent synchrotron radiation is emitted at low frequencies of the spectrum and polarized in the x-mode. Referring to the characteristics of the synchrotron radiation from electrons with energy about a few MeV, we find that the moving type IV bursts can be attributed to the result of synchrotron radiation by relativistic electrons embedded in the plasma cloud; but it is more appropriate to interpret the type IVA and the stationary type IV emissions as the consequence of cyclotron radiation by

mildly relativistic electron streams.

Finally we should point out that the low frequency cut-off of the observed moving type IV burst has been used to deduce the coronal magnetic field intensity by assuming that this low frequency cut-off is due to the suppression of the synchrotron radiation resulting from the influence of the ionized medium (Boischot and Clavelier, 1967; Ramaty and Lingenfelter, 1968). However, this method of deducing the coronal magnetic field intensity is adequate only if the observed burst is not circularly polarized since otherwise the sharp low frequency cut-off will arise from the strong negative reabsorption.

CHAPTER X

CONCLUSIONS

A. Concluding Remarks

Based on the kinetic approach, theory of plasma radiation by an electron stream in a magnetoactive plasma has been formulated. The explicit expressions for the power spectra in the plasma mode emitted from a single electron, the rate of growth of the plasma wave in a stream-plasma system and the coefficients of transformation of plasma waves into electromagnetic waves in the x-mode and the o-mode by thermal fluctuations have been obtained. The linearized kinetic equation has also been used in the study of the excitation of cyclotron radiation in the subluminous mode in the stream-magnetoactive plasma system. On the other hand, by means of the quantum treatment, the synchrotron radiation from a system of relativistic electrons is studied taking into account the influence of the medium.

With the optical observational data on the structure of the solar atmosphere, the quantitative studies of the characteritics of the electromagnetic radiations generated by solar energetic electrons through various coherent radiation processes and the propagation conditions of the electromagnetic waves in the solar corona lead to the following

conclusions:

1. The broad band continuum-type emission is caused by the mildly relativistic electron stream moving at the base of the corona where the value of A is generally much smaller than unity(see Fig. 8.3). The emission is expected to be right-handed polarized (leading spot hypothesis).

2. The narrow bandwidth drifting bursts at the frequency about (or double) the local plasma frequency and the continuum-type emission polarized in the left-handed sense can be emitted from a helical electron stream concurrently when the electron stream spirals through the layers where the value of A is in the range from unity to four. These two types of emissions will be superimposed upon each other in the dynamic spectral records if the electron pitch angle is small ($\sim 10^{o} - 30^{o}$, say) and the electron energy is about a few tens of keV to 100 keV.

3. The mildly relativistic electron stream passing through the layers where $A \geq 4$ will emit a pair of drifting bursts with similar intensities and with a frequency ratio ~ 1:2 through the Cerenkov plasma radiation process. The first harmonic component is stronger polarized than the second harmonic. If the radiation source is located near the solar limb, the second harmonic component will dominate but its polarization will be insignificant.

4. In the outer layers of the solar corona where the value of A is expected to be very large, a system of relativistic electrons will emit the wide bandwidth continuum-type emission by the synchrotron mechanism. The continuum emission may be strongly circularly polarized in the right-handed sense when the radiation source is optically thick; this requires the electron energy about a few or ten MeV and a comparatively large value of $\sigma = n_o'/n_o$.
Based on these informations and other observational data, consistent theories of the polarized type III burst and U burst emission event, the drift pair burst and hook burst emission event and the type IVA emission at centimetre and decimetre wavelengths have been put forward. The plausible mechanisms responsible the type V emission and the type IVm emission have also been suggested.

B. Suggestions for Further Research

As mentioned in Chapter III, the use of the linear instability theory in the interpretation of solar radio emissions requires a special assumption that the non-equilibrium features of the electron distribution are maintained by an efficient process. On the other hand, the use of non-linear theory does not require such assumption and would be more appropriate to the real situation. Therefore, investigation of the conditions of non-linear generation of the

electromagnetic radiation in a magnetoactive plasma (e.g. Livshiftz and Tsytovich, 1968) is of great value. This does not only allow us to justify the validity of the theories of solar radio emissions on the basis of linear mechanism but also lead us to investigate the plausible origins of some solar radio emissions which are not yet understood, e.g. split pairs (Ellis, 1969).

The tentative suggestions of the origin of the type IVm emission given in Chapter IX need detailed investigations. We should firstly investigate the properties of the synchrotron radiation from a system of electrons with a more realistic energy spectrum and secondly study the conditions for the production of the radiating electrons in the solar corona.

APPENDIX A

RANDOM FLUCTUATIONS OF PHYSICAL QUANTITIES IN A PLASMA AND THE SPECTRAL DISTRIBUTION OF MICROCURRENT DENSITY

The physical quantities in a plasma may be well approximated but not exactly given by their averages. The random deviation δx from its average $< x >$ is defined as $\delta x = x - < x >$. The mean value of this fluctuation vanishes but the mean square deviation is non-vanishing. Therefore, macroscopic physical phenomena associated with quantities proportional to the mean squares of the fluctuations of physical parameters will exist. For instance, the fluctuation current due to the random thermal electrons in the resistor which is connected across the input terminals of a linear amplifier will give rise to a random output signal (or "noise") in the amplifier (Nyquist's theorem). In a stable plasma, fluctuation of electron density and fluctuation of electron current density are responsible for the emission of various fluctuation waves. If the plasma is of thermal dynamical equilibrium, the amplitude of the fluctuation wave is determined by the plasma temperature and the radiation is generally known as fluctuation radiation or thermal radiation. On the other hand, the energy of an external wave propagating in the thermal plasma will be absorbed as in the case that the

energy from an impressed periodic voltage will be absorbed by an electrical resistor. The absorption of the energy of the propagating wave is due to the existence of the anti-hermitian part of the dielectric tensor for the thermal plasma (Sitenko and Kirochkin, 1966). For a general linear dissipative system*, the fluctuations are connected to the dissipative properties of the system. Hence in a thermal plasma, the thermal radiation is expressible in terms of anti-hermitian part of the dielectric tensor and the temperature as in the case of thermal noise of a resistor in terms of its resistence and temperature. Rostoker (1961) then defined the plasma impedence whose real part is associated with the anti-hermitian part of the dielectric tensor and he obtained the fluctuation-dissipation theorem for plasmas, in analogy with the well known Nyquist theorem.

In a non-equilibrium plasma, in which the electrons and ions are characterized by non-Maxwellian distribution functions for a long period of time, the fluctuations of various parameters can also be studied if distribution functions are known.

---

* According to Callen and Welton (1951), the system may be said to be dissipative if it is capable of absorbing energy when subjected to a time-periodic perturbation. The system may be said to be linear if the power dissipation is quadratic in the magnitude of the perturbation.

The full description of the fluctuations of a quantity is given by the correlation function which is defined as the mean value of the product of the fluctuations of the quantity at different points of space at different instants of time. If the state of the unperturbed medium is spatially homogeneous and stationary, i.e. there is no preferred origin in time and in space for the statistical description of the fluctuations, the quadratic space-time correlation function will depend only on the relative distance and the absolute value of the time interval between the points at which the fluctuations are considered. In practice, the Fourier transform of the correlation function - spectral distribution (or spectral density) - is more important. Using the correlation function to describe the averaged macroscopic quadratic fluctuations of quantities such as energy, radiation intensity, etc. in an ionized plasma is essentially to replace the time average by an average over phase (i.e. an average over an ensemble of non-interacting particle). This is possible only for a medium having stationary state and spatially homogeneous.

For fully ionized plasma, there are only rare binary collisions and each particle is influenced by so many other particles in the plasma simultaneously at all times (long range interaction) that its correlations with one other particle

(binary interaction) are partially drowned out. In this case, the particles remain far from each other at all times and the change in momentum that arises in time interval t is small. The trajectories of the interacting particles are not affected to any great extent. Therefore, the long range interaction can be analyzed by assuming that the trajectories of the interacting particles are specified beforehand and there is no position correlation. Under this condition, the spectral distribution of the microcurrent density is given by (Shafranov, 1967, p.74)

$$G_{\alpha\beta}(\bar{k},\omega) = \frac{e^2 n_o}{(2\pi)^4} \iint v_\alpha(t) v_\beta(0) e^{-i\bar{k}.\int_o^t \bar{v}(t')dt' - i\omega t} F_o(\bar{p}^o) dt d\bar{p}^o \qquad (A.1)$$

where the subscript "o" denotes the quantity at time $t = 0$. This expression holds for arbitrary unperturbed distribution function $F_o(\bar{p}^o)$ that satisfies stationarity and spatial homogeneity for the unperturbed medium.

For a thermal plasma,

$$F_o(p) = \left(\frac{m_o}{2\pi KT}\right)^{3/2} \exp\left(-\frac{E}{KT}\right) ,$$

with $E = \frac{p^2}{2m_o}$, $G_{\alpha\beta}(\bar{k},\omega)$ can be obtained from the dielectric tensor (1.7) which can be expressed as

$$\varepsilon_{\alpha\beta}(\bar{k},\omega) = \delta_{\alpha\beta} + i\,\frac{4\pi}{\omega}\,\sigma_{\alpha\beta} \ ,$$

$$\text{where } \sigma_{\alpha\beta}(\bar{k},\omega) = \frac{e^2 n_o}{\kappa T}\int d\bar{p}^{o} \int_{o}^{\infty} v_\alpha(t)v_\beta(0)F_o(\bar{p}^{o})e^{i\omega t - i\bar{k}.\int_o^t v(t')dt'}\,dt \qquad \text{(A.2)}$$

It has been shown that (Shafranov, 1967, p.51)

$$\kappa T\ \sigma_{\alpha\beta}(\bar{R},t) = G_{\alpha\beta}(\bar{R},t) \text{ with } \sigma_{\alpha\beta}(-\bar{R},-t) = \sigma_{\beta\alpha}(\bar{R},t).$$

If we separate the tensors into hermitian and anti-hermitian parts in the form

$$\varepsilon_{\alpha\beta}(\bar{k},\omega) = \varepsilon^{H}_{\alpha\beta}(\bar{k},\omega) + i\varepsilon^{A}_{\alpha\beta}(\bar{k},\omega) \ ,$$

$$\sigma_{\alpha\beta}(\bar{k},\omega) = \sigma^{H}_{\alpha\beta}(\bar{k},\omega) + i\sigma^{A}_{\alpha\beta}(\bar{k},\omega) \ ,$$

we can easily show that

$$\sigma^{H}_{\alpha\beta}(\bar{k},\omega) = \frac{\omega}{4\pi}\,\varepsilon^{A}_{\alpha\beta}(\bar{k},\omega) \quad \text{and}$$

$$2\sigma^{H}_{\alpha\beta}(\bar{k},\omega) = \int_{-\infty}^{\infty}\int_{-\infty}^{\infty} \sigma_{\alpha\beta}(\bar{R},t)e^{-i(\bar{k}.\bar{R}-\omega t)}\,d\bar{R}dt.$$

Hence, we find

$$G_{\alpha\beta}(\bar{k},\omega) = \frac{1}{(2\pi)^4}\int_{-\infty}^{\infty}\int_{-\infty}^{\infty} G_{\alpha\beta}(\bar{R},t)e^{-i(\bar{k}.\bar{R}-\omega t)}d\bar{R}dt$$

$$= \frac{\kappa T}{(2\pi)^4}\int_{-\infty}^{\infty}\int_{-\infty}^{\infty} \sigma_{\alpha\beta}(\bar{R},t)e^{-i(\bar{k}.\bar{R}-\omega t)}d\bar{R}dt,$$

$$= \frac{\omega\kappa T}{(2\pi)^5}\varepsilon^{A}_{\alpha\beta}(\bar{k},\omega) = \frac{\omega\kappa T}{(2\pi)^5}\frac{(\varepsilon_{\alpha\beta} - \varepsilon^{*}_{\beta\alpha})}{2\,i} \qquad (A.3)$$

which is of the same form as the Nyquist theorem. The microcurrent density (A.3) arises from the random thermal motions of the free plasma electrons moving in the free space.

APPENDIX B

SPECTRAL DISTRIBUTION OF ELECTRON DENSITY FLUCTUATIONS

(cf. Sitenko, 1967, Chapter 5; Shafranov, 1967,p.131)

The expression (A.1) is the spectral density of the correlation function for the fluctuation current density of one species of independent charged particles in the plasma. The interaction between the particles of the same species and that between the particles of different species have been neglected. However, the fluctuation of electric fields at some points generated by fluctuations in electron and ion current densities will react back on the ions and electrons through the self-consistent field equations and cause further current densitites in the plasma.

Let us assume $\bar{E}^e$ and $\bar{E}^i$ be the random fields inducing the independent fluctuations of electron and ion current densities in the plasma and $\delta\bar{E}^e$ and $\delta\bar{E}^i$ be the fluctuations of electric fields produced by the fluctuations of electron and ion current densities respectively. From (1.4) and the wave equation with source current term, we have

$$j_\alpha^{eM} = -i\omega K^e_{\alpha\beta} E^e_\beta \; ; \quad j_\alpha^{iM} = -i\omega K^i_{\alpha\beta} E^i_\beta \qquad \text{(B.1)}$$

and

$$\begin{aligned} \delta E^e_\alpha(\bar{k},\omega) &= i\,\frac{4\pi}{\omega}\,\lambda_{\alpha\beta} j^{eM}_\beta(\bar{k},\omega) \\ \delta E^i_\alpha(\bar{k},\omega) &= i\,\frac{4\pi}{\omega}\,\lambda_{\alpha\beta} j^{iM}_\beta(\bar{k},\omega) \end{aligned} \qquad \text{(B.2)}$$

where $\lambda_{\alpha\beta}$ is the inverse of the Maxwell's tensor $\hat{}_{\alpha\beta}$, i.e. $\lambda_{\alpha m}\hat{}_{m\beta} = \delta_{\alpha\beta}$. Thus the total fluctuation electron current density will be

$$j^e_\alpha = j^{eM}_\alpha - i\omega K^e_{\alpha\beta}\,\delta E^e_\beta - i\omega K^e_{\alpha\beta}\delta E^i_\beta \quad ,$$

$$= - i\omega K^e_{\alpha i}\,[(\delta_{i\beta}+4\pi\lambda_{ik}K^e_{k\beta})E^e_\beta + 4\pi\lambda_{ik}K^i_k\,E^i_\beta] \,. \qquad (B.3)$$

Since the ions and the electrons interact through the self-consistent field equations only, the electron and ion current density fluctuations are statistical independent;

$$< j^{iM}_\alpha j^{eM}_\beta >_{\bar{k},\omega} = < j^{eM}_\alpha j^{iM}_\beta >_{\bar{k},\omega} = 0 \quad .$$

Then the spectral distribution of fluctuations of electron current density in a plasma will be expressed in the form

$$< j^e_\alpha j^e_\beta >_{\bar{k},\omega} = (\delta_{\alpha k}+4\pi K^e_{\alpha i}\lambda_{ik})\,(\delta_{\beta m}+4\pi K^e_{\beta j}\lambda_{jm})^* G^e_{km}$$

$$+ 16\pi^2 K^e_{\alpha i}K^{e*}_{\beta j}\lambda_{ik}\lambda^*_{jm}G^{iM}_{km} \quad . \qquad (B.4)$$

The spectral density of the fluctuations of longitudinal electron density, obtained by multiplying $\kappa_\alpha\kappa_\beta\kappa_r\kappa_s\kappa_k\kappa_m\,\hat{}_{kr}\,\hat{}^*_{ms}$ on both sides of (B.4) (κ_α being k_α/k), reads

$$< j^{e2}_{||} >_{\bar{k},\omega} = \frac{1}{|\varepsilon_{||}|^2}\{|1 + 4\pi K^i_{||}|^2 G^e_{||} + 16\pi^2 |K^e_{||}|^2 G^i_{||}\} \,. \qquad (B.5)$$

Making use of the equation of continuity for electron charge density, we find

$$< \delta n^{e2} >_{\bar{k},\omega} = \frac{k^2}{e^2\omega^2|\varepsilon_{||}|^2} \{|1 + 4\pi K^i_{||}|^2 G^e_{||} + 16\pi^2 |K^e_{||}|^2 G^i_{||}\}. \quad \text{(B.6)}$$

The spectral distribution of the fluctuations of electron density (B.6) can be used for any medium with distribution function whose state is spatially homogeneous and stationary. It was also obtained by the "dressed" test particle approach (Bekefi,1966,p.260). Because of screening, a test charged particle moving in the plasma can be considered as a freely moving particle with a comoving polarization cloud of the extent about Debye length D in which there is a deficiency of charges of the same type that attached to the test charged particle. Such a test particle which includes a charge plus its attendant polarization cloud is called a "dressed" test particle (or a quasi-particle). The total electric field at a point produced by all the charged particles of the same species is the sum of the shielded fields of all the "dressed" particles when they are considered statistically independent, i.e. the field given by (B.2). It has been pointed out that a test charged particle can be considered as carrying a well-established screening cloud for most of the time during two successive short range collisions if $n_o D^3 >> 1$, n_o is the equilibrium

electron density of the plasma (Ichimaru, 1965). This condition is generally satisfied for the fully ionized plasma.

Based on the "dressed" test particle concept, the electron density fluctuation spectrum (B.6) may be interpreted as being due to the motion of fully dressed electrons (terms proportional to G_{11}^{e}) and motion of fully "dressed" ions (term proportional G_{11}^{i}). When $k < k_D$, in the high frequency region, term proportional to K_{11}^{i} is small compared with unity and the contribution comes from the collective plasma wave-like fluctuations of electron density brought about by the long range Coulomb interaction. In the low frequency region, the last term is essential. Although the main contribution to the central maximum comes from those electrons around the ions and acting to screen out the Coulomb field of the ions, the fluctuation of electron density arises from the random thermal motion of ions. Therefore, the width of the central maximum is characteristic of the ion thermal motion rather than electron thermal motion. In this case, collective low frequency magnetic sonic wave can be excited at the frequency given by dispersion equation for the low frequency wave. However, as long as $T^{e} \simeq T^{i}$, this collective mode is highly damped and cannot be meaningfully distinguished from those fluctuations caused by the individual ion thermal motion. The fluctuations at other

frequencies not restricted by the dispersion equation are due to the random motion of individual ions (Bohm and Gross, 1949; Pines and Bohm, 1952). For $k > k_D$, the second term in (B.6) becomes most important. That is the main contribution to $< \delta n^2 >_{\vec{k},\omega}$ is caused by random motion of the electrons with the comoving polarized clouds and the width of the fluctuation spectrum is characteristic of the electron thermal motion. In this case, the wavelength of the fluctuation is less than Debye length and there is no collective mode of fluctuation resulting from long range Coulomb interaction and the sharp spike disappears in the electron density fluctuation spectrum.

APPENDIX C

ELECTRON EMISSIVITY FOR SYNCHROTRON RADIATION

Starting with the wave equation with source current density, we have

$$\left[\frac{k^2c^2}{\omega^2}(\delta_{\alpha\beta} - \kappa_\alpha\kappa_\beta) - \varepsilon_{\alpha\beta}\right]E_\beta = -i\frac{4\pi}{\omega}j_\alpha \ , \qquad (C.1)$$

where $\alpha, \beta = x,y,z$ are the position co-ordinates. E_β and j_α are the Fourier components of the electric field $E_\beta(\bar{r}_q,t)$ and electron current density $j_\alpha(\bar{r}_q,t)$. In the co-ordinate system as shown in Fig. 9.1, $\bar{k} = (0,k\sin\theta,k\cos\theta)$, and when (9.1) holds, the Maxwell's tensor will be

$$\hat{}_{\alpha\beta} = \begin{pmatrix} n^2-\varepsilon_\perp & 0 & 0 \\ 0 & n^2\cos^2\theta-\varepsilon_\perp & -n^2\sin\theta\cos\theta \\ 0 & -n^2\sin\theta\cos\theta & n^2\sin^2\theta-\varepsilon_\perp \end{pmatrix} \qquad (C.2)$$

where $\varepsilon_\perp = 1 - \omega_p^2/\omega^2 = 1 - A/\xi^2$ and $n^2 = k^2c^2/\omega^2$. Therefore, the Fourier component of the electric field produced by the electron is

$$E_\beta(\bar{k},\omega) = -i\frac{4\pi}{\omega}\hat{}^{-1}_{\beta\alpha}\, j_\alpha(\bar{k},\omega) \ , \qquad (C.3)$$

with $$\hat{}^{-1}_{\beta\alpha} = \frac{T'_{\beta\alpha}}{\varepsilon_\perp(n^2 - \varepsilon_\perp)} \ ,$$

$$T'_{\beta\alpha} = \begin{pmatrix} \varepsilon_\perp & 0 & 0 \\ 0 & \varepsilon_\perp - \sin^2\theta n^2 & -n^2\sin\theta\cos\theta \\ 0 & -n^2\sin\theta\cos\theta & \varepsilon_\perp - n^2\cos^2\theta \end{pmatrix} . \quad (C.4)$$

The current density of a gyrating electron can be represented by

$$\bar{j}(\bar{r},t) = q\bar{v}_q(t)\ \delta(\bar{r} - \bar{r}_q) ,$$

where the instantaneous velocity $\bar{v}_q(t)$ and the electron position $\bar{r}_q(t)$ are

$$\begin{aligned} \bar{v}_q(t) &= (-v_\perp \sin\frac{\omega_H}{\gamma'}t,\ v_\perp\cos\frac{\omega_H}{\gamma'}t,\ v_{||}) , \\ \bar{r}_q(t) &= (\frac{v_\perp\gamma'}{\omega_H}\cos\frac{\omega_H}{\gamma'}t,\ \frac{v_\perp\gamma'}{\omega_H}\sin\frac{\omega_H}{\gamma'}t,\ v_{||}t), \end{aligned} \quad (C.5)$$

q is the electron charge and the Lorentz factor γ' is given by

$\gamma' = (1 - \beta_\perp^2 - \beta_{||}^2)^{-\frac{1}{2}}$. The subscripts $||$, $\perp$ denote the components parallel to and perpendicular to $\bar{H}_o$. The Fourier transform of the current density becomes

$$j_\alpha(\bar{k},\omega) = \frac{q}{(2\pi)^4}\int v_{q\alpha}(t)\ \delta(\bar{r}-\bar{r}_q)\ \exp(i\bar{k}.\bar{r}-i\omega t)d\bar{r}dt ,$$

$$= \frac{q}{(2\pi)^3}\sum_{s=-\infty}^{\infty}(iv_\perp J'_s,\ \frac{sv_\perp}{X}J_s,\ v_{||}J_s)\ \delta(\omega-k_{||}v_{||} - \frac{s\omega_H}{\gamma'}), \quad (C.6)$$

where J_s is the Bessel function of s-th order and with argument

$X = \gamma' k_\perp v_\perp / \omega_H$ and J_s' is its derivative with respect to X. Thus, the electric field of the radiation emitted by the electron at $\bar{r} = \bar{r}_q$ will be

$$E_\beta(\bar{r}_q,t) = \frac{-i4\pi q}{(2\pi)^3} \sum_{s=-\infty}^{\infty} \int_{-\infty}^{\infty} \int_0^{4\pi} \int_0^{\infty} \frac{T'_{\beta j} u_j^{(s)} k^2}{\omega \varepsilon_\perp (n^2-\varepsilon_\perp)} \exp(-i\bar{k}.\bar{r}_q + i\omega t)$$

$$\times \delta(\omega - k_\parallel v_\parallel - \frac{s\omega_H}{\gamma'}) dk d\Omega d\omega \ ,$$

where $u_j^{(s)} = (iv_\perp J_s', \frac{sv_\perp}{X} J_s, v_\parallel J_s)$. Taking (C.4) into account, $E_\beta(\bar{r}_q,t)$ can be expressed as

$$E_\beta(\bar{r}_q,t) = \frac{-i4\pi q}{(2\pi)^3} \sum_{s=-\infty}^{\infty} \int_{-\infty}^{\infty} \int_0^{4\pi} \int_0^{\infty} \frac{T_\beta k^2}{\omega \varepsilon_\perp (n^2-\varepsilon_\perp)} \exp(-i\bar{k}.\bar{r}_q + i\omega t)$$

$$\times \delta(\omega - k_\parallel v_\parallel - \frac{s\omega_H}{\gamma'}) dk d\Omega d\omega \ , \qquad (C.7)$$

where $T_\beta = [i\varepsilon_\perp v_\perp J_s', \ (\varepsilon_\perp - n^2\sin^2\theta) \frac{sv_\perp}{X} J_s - n^2 \sin\theta\cos\theta v_\parallel J_s \ ,$

$$-n^2\sin\theta\cos\theta \frac{sv_\perp}{X} J_s + (\varepsilon_\perp - n^2\cos^2\theta) v_\parallel J_s].$$

Now, we transform the electric field $E_\beta(\bar{r}_q,t)$ to the co-ordinate system formed by the three mutually orthogonal unit vectors $\hat{e}_1$, $\hat{e}_2$ and $\bar{\kappa}$ with $\hat{e}_2$ lying on the $\bar{k}$-$\bar{H}_o$ plane and $\hat{e}_1$ transverse to it as shown in Fig. 9.1. $\hat{e}_1$ and $\hat{e}_2$ are called the principal polarization axes. The transformation tensor is

(cf. Chisholm and Morries, 1964, p.453)

$$a_{i\beta} = \begin{pmatrix} -1 & 0 & 0 \\ 0 & -\cos\theta & \sin\theta \\ 0 & \sin\theta & \cos\theta \end{pmatrix} \qquad i = 1,2,3.$$

So in the new co-ordinate system,

$$E_i(\bar{r}_q,t) = \frac{-i4\pi q}{(2\pi)^3} \sum_{s=-\infty}^{\infty} \int_{-\infty}^{\infty} \int_0^{4\pi} \int_0^{\infty} \frac{k^2 S_i(s)}{\omega\varepsilon_\perp(n^2-\varepsilon_\perp)} \exp(-i\bar{k}.\bar{r}_q+i\omega t)$$

$$\times \delta(\omega-k_{\parallel}v_{\parallel} - \frac{s\omega_H}{\gamma'})dkd\Omega d\omega \qquad (C.8)$$

where $S_i^{(s)} = [-i\varepsilon_\perp v_\perp J_s', -\varepsilon_\perp(\frac{sv_\perp}{X}\cos\theta + v_{\parallel}\sin\theta)J_s$,

$$(\varepsilon_\perp-n^2)\ (\frac{sv_\perp}{X}\sin\theta + v_{\parallel}\cos\theta)J_s] \ .$$

In the transparency region, we take $i(n^2-\varepsilon_\perp)^{-1}=\pi\delta(\frac{k^2c^2}{\omega^2} - \varepsilon_\perp)$.

Then,

$$E_i(\bar{r}_q,t) = \frac{ie}{4\pi c^2} \sum_{s=-\infty}^{\infty} \int_{-\infty}^{\infty} \int_0^{4\pi} n\omega^2[\beta_\perp J_s'\ \hat{e}_1 - i\ (\frac{\cos\theta-n\beta_{\parallel}}{n\sin\theta})J_s\ \hat{e}_2]$$

$$\times \exp(-i\bar{k}.\bar{r}_q+i\omega t)\ \delta(\omega-k_{\parallel}v_{\parallel} - \frac{s\omega_H}{\gamma'})d\Omega d\omega \qquad (C.9)$$

and for the synchrotron radiation ($s > 0$)

$$\mathrm{Re}[E_i(\bar{r}_q,t)] = \frac{e}{4\pi c^2}\sum_{s=1}^{\infty}\int_{-\infty}^{\infty}\int_{0}^{4\pi} n\omega^2[\beta_\perp J_s' \cos(\omega t-\bar{k}.\bar{r}_q+\pi/2)\hat{e}_1$$

$$+ \left(\frac{\cos\theta-n\beta_{//}}{n\sin\theta}\right)J_s\sin(\omega t-\bar{k}.\bar{r}_q+\pi/2)\,\hat{e}_2]\,\delta(\omega-k_{//}v_{//}-\frac{s\omega_H}{\gamma'})d\Omega d\omega\ .$$

Therefore, the electric field vector of the electromagnetic radiation lies on the plane of polarization (i.e. the figure plane II in Fig. 9.1).

Since $E_i(\bar{r}_q,t)$ is a transverse electric field, only the transverse current density will be responsible for the radiation of the transverse wave (cf. Shafranov, 1967, p.55). For the sake of complete description of the polarization properties of the radiation, it is most convenient to express the instantaneous radiation power in the form of a tensor,

$$P_{ij}(\bar{r}_q,t) = -qv_{qi}^{\perp}E_j(\bar{r}_q,t)\ ,\quad i,j = 1,2 \qquad (C.10)$$

where $v_{qi}^{\perp}$ is the electric velocity component perpendicular to the wave vector. From (C.8) and (C.10), we have

$$P_{ij}(\bar{r}_q,t) = \frac{i4\pi q^2}{(2\pi)^3}\sum_{s=-\infty}^{\infty}\int_{-\infty}^{\infty}\int_{0}^{4\pi}\int_{0}^{\infty}\frac{k^2v_{qi}^{\perp}S_j\exp(-i\bar{k}.\bar{r}_q+i\omega t)}{\omega\varepsilon_\perp(n^2-\varepsilon_\perp)}$$

$$\times\,\delta(\omega-k_{//}v_{//}-\frac{s\omega_H}{\gamma'})dkd\Omega d\omega\ . \qquad (C.11)$$

By means of direct computation, we can show

$$v_{qi}^{\perp}\exp(-i\bar{k}.\bar{r}_q+i\omega t) = \sum_{m=-\infty}^{\infty} w_i^{(m)}\exp\left[i(s-m)\frac{\omega_H}{\gamma'}t\right] \qquad (C.12)$$

where $w_i^{(m)} = \left[iv_{\perp}J_m' \ , \ -\frac{mv_{\perp}}{X}J_m\cos\theta + v_{\parallel}J_m\sin\theta\right]$.

Hence,

$$P_{ij}(\bar{r}_q,t) = \frac{i4\pi q^2c^2}{(2\pi)^3}\sum_{s=-\infty}^{\infty}\int_{-\infty}^{\infty}\int_0^{4\pi}\int_0^{\infty}\sum_{m=-\infty}^{\infty}\frac{k^2Q_{ij}\delta(\omega-k_{\parallel}v_{\parallel}-\frac{s\omega_H}{\gamma'})}{\omega\varepsilon_{\perp}(n^2-\varepsilon_{\perp})}$$

$$\times \exp\left[i(s-m)\frac{\omega_H}{\gamma'}t\right] dk d\Omega d\omega \qquad (C.13)$$

with $Q_{ij} = w_i^{(m)}S_j^{(s)}/c^2$.

The time factor $\exp[i(s-m)\frac{\omega_H}{\gamma'}t]$ involved in the integrand is eliminated by taking the average of $P_{ij}(\bar{r}_q,t)$ over one period of time $T = 2\pi\gamma'/\omega_H$. We find that P_{ij} is non-zero if $m = s$. Therefore P_{ij} is reduced to

$$P_{ij}(\bar{r}_q,t) = \frac{i4\pi q^2c^2}{(2\pi)^3}\sum_{s=-\infty}^{\infty}\int_{-\infty}^{\infty}\int_0^{4\pi}\int_0^{\infty}k^2LQ_{ij}\ \delta(\omega-k_{\parallel}v_{\parallel}-\frac{s\omega_H}{\gamma'})dk d\Omega d\omega$$

where $L(\omega) = \dfrac{i}{\omega(n^2-\varepsilon_\perp)}$,

$$Q_{ij} = \begin{pmatrix} \beta_\perp^2 J_s'^2 & -i\beta_\perp J_s J_s' \left(\dfrac{\cos\theta - n\beta_{//}}{n\sin\theta}\right) \\ i\beta_\perp J_s J_s' \left(\dfrac{\cos\theta - n\beta_{//}}{n\sin\theta}\right) & J_s^2 \left(\dfrac{\cos\theta - n\beta_{//}}{n\sin\theta}\right)^2 \end{pmatrix} .$$

After summation over the harmonic numbers s by means of the delta function, we find that

$$Q_{ij}(-\omega) = Q_{ij}^*(\omega) \quad \text{and} \quad L(-\omega) = L^*(\omega) \quad .$$

Thus, we can re-write P_{ij} for the positive frequency and take the positive harmonic number for the synchrotron radiation,

$$P_{ij}(\bar{r}_q, t) = \mathrm{Re}\, \frac{8\pi q^2 c^2}{(2\pi)^3} \sum_{s=1}^{\infty} \int_0^{\infty} \int_0^{4\pi} \int_0^{\infty} k^2 L Q_{ij} \delta\left(\omega - k_{//} v_{//} - \frac{s\omega_H}{\gamma'}\right) dk\, d\Omega\, d\omega \qquad (C.15)$$

Then after integration over k by means of the relation

$$\mathrm{Re}\, L(\omega) = \frac{\pi}{\omega}\, \delta\left(\frac{k^2 c^2}{\omega^2} - \varepsilon_\perp\right) ,$$

we obtain

$$P_{ij}(\bar{r}_q, t) = \frac{e^2}{2\pi c} \sum_{s=1}^{\infty} \int_0^{\infty} \int_0^{4\pi} \omega^2 n Q_{ij} \, \delta(\omega - k_{\parallel} v_{\parallel} - \frac{s\omega_H}{\gamma'}) d\Omega d\omega \quad . \qquad (C.16)$$

The electron emissivity tensor for the synchrotron radiation will be

$$\eta_{ij} = \frac{dP_{ij}}{d\Omega d\omega} = \frac{e^2 \omega^2 n}{2\pi c} \sum_{s=1}^{\infty} C_{ij} \delta(\omega - k_{\parallel} v_{\parallel} - \frac{s\omega_H}{\gamma'}) \quad . \qquad (C.17)$$

APPENDIX D

STOKES PARAMETERS

(Zheleznyakov, 1968)

In this appendix, it is shown that the Stokes parameters I,V defined conventionally by (9.13) give the sum and the difference of the two oppositely polarized electromagnetic radiation in a magnetoactive plasma under the quasi-longitudinal propagation condition. Therefore, we consider the electromagnetic radiation consisting of x-mode and o-mode radiations in a cold and collisionless magnetoactive plasma. The polarization tensor is defined as

$$I_{iq} = \overline{D_i D_q^*}$$

where $D_i = \int_{\Delta\omega} A^e n_i^e \exp(-i\omega t + i\alpha^e + i\underline{k}^e \cdot \underline{r}) d\omega +$

$$\int_{\Delta\omega} A^o n_i^o \exp(-i\omega t + i\alpha^o + i\underline{k}^o \cdot \underline{r}) d\omega .$$

The bar denotes the time average of the quantity. $A^{e,o}, n_i^{e,o}$ and $\underline{k}^{e,o}$ are defined in Chapter IX (p.316). Then

$$\overline{D_i D_q^*} = \int_{\Delta\omega}\int_{\Delta\omega} A^e A^e n_i^e n_q^{e*} \exp\left[-i(\omega - \omega')t + i(\alpha^e - \alpha^e) + i(\underline{k}^e - \underline{k}^{e'}) \cdot \underline{r}\right] d\omega \, d\omega'$$

$$+ \int_{\Delta\omega}\int_{\Delta\omega} A^o A^{o'} n_i^o n_q^{o'*} \exp\left[-i(\omega - \omega')t + i(\alpha^o - \alpha^{o'}) + i(\underline{k}^o - \underline{k}^{o'}) \cdot \underline{r}\right] d\omega \, d\omega'$$

$$+ \int_{\Delta\omega}\int_{\Delta\omega} A^e A^{o'} n_i^e n_q^{o'*} \exp\left[-i(\omega - \omega')t + i(\alpha^e - \alpha^{o'}) + i(\underline{k}^e - \underline{k}^{o'}) \cdot \underline{r}\right] d\omega \, d\omega'$$

$$+ \int_{\Delta\omega}\int_{\Delta\omega} A^{o}A^{e\prime}n_i^{o}n_q^{e\prime *}\exp\left[-i(\omega-\omega')t+i(\alpha^{o}-\alpha^{e\prime})+i(\underline{k}^{o}-\underline{k}^{e\prime})\cdot\underline{r}\right]d\omega d\omega' \tag{D.1}$$

Then the time average of the polarization will be

$$\begin{aligned}
\overline{D_i D_q^*} = \int_{\Delta\omega}\int_{\Delta\omega}\Big\{ & A^{e}A^{e\prime}n_i^{e}n_q^{e\prime *}\exp\left[i(\alpha^{e}-\alpha^{e\prime})+i(\underline{k}^{e}-\underline{k}^{e\prime})\cdot\underline{r}\right]+ \\
& + A^{o}A^{o\prime}n_i^{o}n_q^{o\prime *}\exp\left[i(\alpha^{o}-\alpha^{o\prime})+i(\underline{k}^{o}-\underline{k}^{o\prime})\cdot\underline{r}\right] \\
& + A^{e}A^{o\prime}n_i^{e}n_q^{o\prime *}\exp\left[i(\alpha^{e}-\alpha^{o\prime})+i(\underline{k}^{e}-\underline{k}^{o\prime})\cdot\underline{r}\right] \\
& + A^{o}A^{e\prime}n_i^{o}n_q^{e\prime *}\exp\left[i(\alpha^{o}-\alpha^{e\prime})+i(\underline{k}^{o}-\underline{k}^{e\prime})\cdot\underline{r}\right]\Big\} \\
& \cdot \lim_{T\to\infty}\frac{1}{T}\int_{-T/2}^{T/2}\exp\left[-i(\omega-\omega')t\right]dt\,d\omega\,d\omega' \\
= \int_{\Delta\omega}\int_{\Delta\omega}\Big\{ & A^{e}A^{e\prime}n_i^{e}n_q^{e\prime *}\exp\left[i(\alpha^{e}-\alpha^{e\prime})+i(\underline{k}^{e}-\underline{k}^{e\prime})\cdot\underline{r}\right]+ \\
& + A^{o}A^{o\prime}n_i^{o}n_q^{o\prime *}\exp\left[i(\alpha^{o}-\alpha^{o\prime})+i(\underline{k}^{o}-\underline{k}^{o\prime})\cdot\underline{r}\right] \\
& + A^{e}A^{o\prime}n_i^{e}n_q^{o\prime *}\exp\left[i(\alpha^{e}-\alpha^{o\prime})+i(\underline{k}^{e}-\underline{k}^{o\prime})\cdot\underline{r}\right] \\
& + A^{o}A^{e\prime}n_i^{o}n_q^{e\prime *}\exp\left[i(\alpha^{o}-\alpha^{e\prime})+i(\underline{k}^{o}-\underline{k}^{e\prime})\cdot\underline{r}\right]\Big\}\delta(\omega-\omega')\,d\omega\,d\omega' \\
= A^{e2}n_i^{e}n_q^{e *} & + A^{o2}n_i^{o}n_q^{o\prime *} + A^{e}A^{o}n_i^{e}n_q^{o *}\exp\left[i(\alpha^{e}-\alpha^{o})+i(\underline{k}^{e}-\underline{k}^{o})\cdot\underline{r}\right] \\
& + A^{o}A^{e}n^{o}n^{e *}\exp\left[i(\alpha^{o}-\alpha^{e})+i(\underline{k}^{o}-\underline{k}^{e})\cdot\underline{r}\right]
\end{aligned} \tag{D.2}$$

The polarization tensors for the x-mode and the o-mode are obtained by putting $A^o=0$ and $A^e=0$ in (D.2) respectively,

$$I^e_{iq} = A^{e2} n^e_i n^{e*}_q, \tag{D.3}$$

$$I^o_{iq} = A^{o2} n^o_i n^{o*}_q \ . \tag{D.4}$$

In the case of quasi-longitudinal propagation, the polarization vectors for the x-mode and the o-mode electromagnetic radiations are

$$n^e_1 = \frac{1}{\sqrt{2}} \ , \quad n^e_2 = \frac{i}{\sqrt{2}} \tag{D.5}$$

$$n^o_1 = \frac{i}{\sqrt{2}}, \quad n^o_2 = \frac{1}{\sqrt{2}} \ . \tag{D.6}$$

Thus for the case of presence of only one normal wave, the x-mode, say, the Stokes parameters I and V are

$$I^e = I^e_{11} + I^e_{22} = A^{e2}(n^e_1 n^{e*}_1 + n^e_2 n^{e*}_2) = A^{e2}$$

$$V^e = i(I^e_{21} - I^e_{12}) = iA^{e2}(n^e_2 n^{e*}_1 - n^e_1 n^{e*}_2) = -A^{e2},$$

and the degree of circular polarization is

$$P_C = \frac{V^e}{I^e} = -1.$$

Therefore the polarization $P_C = -1$ corresponds to the case that

the electromagnetic radiation is completely polarized in the x-mode. Similar calculation shows that $P_C = 1$ corresponds to the case that the electromagnetic radiation is completely polarized in the o-mode.

Now if the electromagnetic radiation consists of both the x-mode and the o-mode radiations, the quantities I and V are

$$\begin{aligned} I = I_{11}+I_{22} &= A^{e2} + A^{o2} - iA^eA^o\exp\left[i(\alpha^e-\alpha^o)+i(\underline{k}^e-\underline{k}^o)\cdot\underline{r}\right] \\ &\quad +iA^eA^o\exp\left[i(\alpha^o-\alpha^e)+i(\underline{k}^o-\underline{k}^e)\cdot\underline{r}\right] \\ &\quad +iA^oA^e\exp\left[i(\alpha^e-\alpha^o)+i(\underline{k}^e-\underline{k}^o)\cdot\underline{r}\right] \\ &\quad -iA^oA^e\exp\left[i(\alpha^o-\alpha^e)+i(\underline{k}^o-\underline{k}^e)\cdot\underline{r}\right] \\ &= A^{e2}+ A^{o2} = I^e + I^o, \end{aligned} \tag{D.7}$$

$$\begin{aligned} V = i(I_{21}-I_{12}) &= \frac{i}{2}\Big\{iA^{e2}-iA^{o2}+A^oA^e\exp\left[i(\alpha^e-\alpha^o)+i(\underline{k}^e-\underline{k}^o)\cdot\underline{r}\right. \\ &\quad +A^oA^e\exp\left[i(\alpha^o-\alpha^e)+i(\underline{k}^o-\underline{k}^e)\cdot\underline{r}+iA^{e2}-iA^{o2}-A^eA^o\exp\left[i(\alpha^e-\alpha^o)\right.\right. \\ &\quad \left.\left.+i(\underline{k}^e-\underline{k}^o)\cdot\underline{r}\right]-A^eA^o\exp\left[i(\alpha^e-\alpha^o)+i(k^e-k^o)\cdot\underline{r}\right]\Big\} \\ &= A^{o2} - A^{e2} = I^o - I^e. \end{aligned} \tag{D.8}$$

Hence when $P_C = V/I$ is negative, the circular component of the electromagnetic radiation in polarized in the x-mode while it is polarized in the o-mode when P_C is positive.

PUBLICATIONS

A considerable portion of this thesis has been set in paper forms for publications in appropriate journals.

Yip, W.K. "A Theory of Solar Type IV Emission on Centimetre and Decimetre Wavelengths", Aust. J. Phys. 20, 421 - 43 (1967).

Yip, W.K. "Radiation of Plasma Waves by an Electron Stream in the Solar Corona", Aust. J. Phys. (in press).

Yip, W.K. "Transformation of Plasma Waves in a Magnetoactive Plasma", Planet. Space Sci. (in press).

Yip, W.K. "Theory of polarized Type III and U Burst Emissions from the Solar Corona", Planet. Space Sci. (in press).

Yip, W.K. "The Origin of Drift Pair Burst and Hook Burst Emissions from the Solar Corona", submitted to Aust. J. Phys.

Yip, W.K. "On Synchrotron Radiation by Relativistic Electrons as the Origin of the Solar Type IV Emission", submitted to Aust. J. Phys.

REFERENCES

Akabane, K., and Cohen, M.H. (1961) - Astrophys. J. 133, 258.

Akhiezer, A.I., Prokhoda, I.G., and Sitenko, A.G. (1958) - Soviet Phys. JETP 6, 576.

Akhiezer, A.I., Akhiezer, I.A., and Sitenko, A.G. (1962) - Soviet Phys. JETP 14, 462.

Akhiezer, I.A., Daneliya, I.A., and Tsintsadze, N.L. (1964). - Soviet Phys. JETP 19, 208.

Allen, C.W. (1947). - Mon. Not. Roy. Ast. Soc. 107, 426.

Aller, L.H. (1963). - "The Atmosphere of The Sun and Stars". 2nd edition, (Ronald Press: New York).

Bass, F.G., and Blank, A.Ya. (1963). - Soviet Phys. JETP 16, 1045.

Bekefi, G. (1966). - "Radiation Processes in Plasmas", (J. Wiley: New York.)

Bhonsle, R.V., and McNarry, L.R. (1964). - Astrophys. J. 139,1312.

Bohm, D., and Gross, E.P. (1949). - Phys. Rev. 75, 1851.

Boischot, A. (1957) - Compt. Rend. 244, 1326.

Boischot, A., and Denisse, J.F. (1957). - Compt. Rend. 245, 2199.

Boischot, A., and Clavelier, B. (1967). - Astrophys. Letter. 1, 7.

Bray, R.J., and Loughhead, R.E. (1962). - Aust. J. Phys. 15, 482.

Bray, R.J., and Loughhead, R.E. (1964). - "Sunspot". (Chapman and Hall: London).

Bumba, V. (1960). - Izv. Crim. Astrophys. Obs. 23, 212.

Callen, H., and Welton, T. (1951). - Phys. Rev. 83, 34.

Chapman, S. (1943). - Mon. Not. Roy. Astr. Soc. 103, 117.

Chawla, B.R., and Unz, H. (1966). - Radio Sci. 1, 1055.

Chisholm, J.S.R., and Morries, R.M. (1964). - "Mathematical Methods in Physics." (north-Holland: Amsterdam).

Christiansen, W., Mathewson, D., Pawsey, J., Smerd. S.F., Boischot, A., Denisse, J.F., Simon, P., Kakinuma, T., Dodson-Prince, H., and Firor, J.W. (1960). - Ann. Astrophys. 23, 75.

Cline, T.L., and McDonald, F.B. (1968a). - Solar Phys. 5, 507.

Cline, T.L., and McDonald, F.B. (1968b). - Cand. J. Phys. 46, S761.

Cohen, M.H. (1960). - Astrophys. J. 131, 664.

Daneliya, I.A., and Tsintsadze, N.L. (1965). - Soviet Radio-Phys. 8, 334.

De Jager, C. (1960). - "Space Research I." (Ed. H. Kallmann-Bijil) p. 628. (North-Holland: Amsterdam.)

Delcroix, J.L. (1965). - "Plasma Physics." (J. Wiley: London.) first published under Delcroix, "Physique des Plasmas" Tome I, by Dunod Éditeur, Paris, 1963.

Denisse, J.F., and Delcroix, J.L. (1963), - "Plasma Waves." (Interscience Publishers: New York.); translated into English from the French original by Marcel Weinrich and David J. BenDaniel.

Eidman, V.Ya. (1958). - Soviet Phys. JETP 7, 91.

Eidman, V. Ya. (1959). - Soviet Phys. JETP 9, 947.

Eidman, V.Ya. (1962). - Soviet Phys. JETP 14, 1401.

Ellis, G.R.A. (1964). - Aust. J. Phys. 17, 63.

Ellis, G.R.A. (1969). - Aust. J. Phys. 22, 177.

Ellis, G.R.A., and McCulloch, P.M. (1967). - Aust. J. Phys. 20, 583.

Erichson, W.C. (1962). - General Dynamics/Astronautics Report ERR-AN-233.

Fainberg, Ya.B. (1968). - Soviet Phys. Usp. 10, 750.

Fichtel, C.E., and McDonald, F.B. (1967). - Ann. Rev. Astron. Astrophys. 5, 351.

Fokker, A.D. (1964). - "Solar System Radio Astronomy." (Ed. J. Aarons) p. 171. (Plenum Press: New York, 1965)

Fomichev, V.V., and Chertok, I.M. (1968). - Soviet Astr. AJ 12, 477.

Fung, P.C.W., and Yip, W.K. (1966). - Aust. J. Phys. 19, 759.

Gershman, B.N. (1953). - ZETF 24, 659.

Gershman, B.N. (1957). - Soviet Phys. JETP 4, 582.

Gershman, B.N. (1960). - Soviet Phys. JETP 11, 657.

Ginzburg, V.L. (1946). - DAN SSSR 52, 491.

Ginzburg, V.L. (1960). - Soviet Phys. Usp. 2, 874.

Ginzburg, V.L. (1964). - "The Propagation of Electromagnetic Waves in Plasmas." (Pergamon Press: New York.); translated from V.L. Ginzburg's book entitled "Rasprostraneniye elektromagnitnykh voln v plazme" (Fizmatgiz: Moscow, 1960).

Ginzburg, V.L., and Zheleznyakov, V.V. (1958). - Soviet Astra. AJ 2, 653.

Ginzburg, V.L., and Zheleznyakov, V.V. (1959). - Soviet Astr. AJ 3, 235.

Ginzburg, V.L., Zheleznyakov, V.V., and Eidman, V.Ya. (1962). - Phil. Mag. 7, 451.

Ginzburg, V.L., and Zheleznyakov, V.V. (1965). - Phil. Mag. 11, 197.

Ginzburg, V.L., and Syrovat-skii, S.I. (1966). - Soviet Phys. Usp. 8, 674.

Ginzburg, V.L., Sazonov, V.N., and Syrovat-skii, S.I. (1968) - Soviet Phys. Usp. 11, 34.

Ginzburg, V.L., and Syrovat-skii, S.I. (1969). - Ann. Rev. Astron. Astrophys. 7, 375.

Gold, T., and Hoyle, F. (1959). - Mon. Not. Roy. Astr. Soc. 120, 89.

Gopala Rao, U.V. (1965). - Aust. J. Phys. 18, 283.

Gulyaev, R.A., Nikol'skaya, K.I., and Nikol'skii, G.M. (1963). - Soviet Astr. AJ 7, 332.

Haddock, F.T. (1958). - Proc. IRE 46, 1.

Haddock, F.T. (1959). - Symp. IAU No. 9 (Paris, 1958). p.188.

Hale, G.E., and Nicholson, S.B. (1938). - Pub. Carnegie Inst., No. 498.

Hatanaka, T. (1966). - "Pro. Rad. Sci. (Ed. E. Herbays) Vol.5, p.72 (Elsevier Publishing Co.: New York.)

Hewish, A. (1962). - Joint Discussion on "Solar Magnetic Fields." Trans. IAU, II B.

Hogbom, J.A. (1960). - Mon. Not. Roy. Astr. Soc. 120, 530.

Hughes, M.P., and Harkness, L. (1963). - Astrophys. J. 138, 239.

Ichimaru, S. (1965). - "Fluctuation Phenomena in Solids." (Ed. R.E. Burgess). Chapter 4, p.103. (Academic Press: New York.)

Ivanov-Kholodnyi, G.S., and Nikol'skii, G.M. (1962). - Soviet Astr. AJ 6, 609.

Jackson, J.D. (1962). - "Classical Electrodynamics." (J. Wiley: New York.)

Jaeger, J.C., and Westfold, K.C. (1950). - Aust. J. Sci. Res. A3, 376.

Kai, K. (1964). - Publ. Astr. Soc. Japan 17, 309.

Kai, K. (1969). - Proc. Astr. Soc. Aust. 1, 189.

Kaplan, S.A., and Tsytovich, V.N. (1968). - Soviet Astr.AJ 11,956.

Kawabata, K. (1964). - Publ. Astr. Soc. Japan 16, 30.

Komesaroff, M. (1958). - Aust. J. Phys. 11, 201.

Korchak, A.A., and Syrovat-skii, S.I. (1962). - Soviet Astr. AJ 5, 678.

Klüber, H. von (1948). - Z. Astrophys. 24, 121.

Kundu, M.R. (1959). - Annals Astrophys. 22, 1.

Kundu, M.R. (1961). - Astrophys. J. 134, 96.

Kundu, M.R. (1962a). - J. G. R. 67, 2695.

Kundu, M.R. (1962b). - J. Phys. Soc. Japan, Supplement A-II 17, 215.

Kundu, M.R. (1965). - "Solar Radio Astronomy." (Interscience Publishers: New York.)

Kundu, M.R., Roberts, J.A., Spencer, C.L., and Kuiper, J.W. (1961). - Astrophys. J. 133, 255.

Kundu, M.R., and Firor, J.W. (1961). - Astrophys. J. 134, 389.

Kundu, M.R., and Spencer, C.L. (1963). - Astrophys. J. 137, 572.

Lacombe, C., and Mangeney, A. (1969). - Astr. and Astrophys. 1, 325.

Liemohn, H.B. (1965). - Radio Sci. 69D, 741.

Livshiftz, M.A., and Tsytovich, V.N. (1968). - Soviet Phys. JETP 26, 927.

Malville, J.M. (1961). - Doctoral Thesis, University of Colorado.

Malville, J.M., and Smith, S.F. (1963). - J. G. R. 68, 3181.

Mansfield, V.N. (1967). - Astrophys. J. 147, 672.

Martyn, D.F. (1946). - Nature 158, 632.

Maxwell, A. (1963). - "The Solar Spectrum." (Ed. C. De Jager) p. 342. (D. Reidel Publishing Co.: Holland, 1965).

Maxwell, A., and Swarup, G. (1958). - Nature 181, 36.

McLean, D.J. (1959). - Aust. J. Phys. 12, 404.

Michard, R. (1963). - Symp. IAU No. 22 (Rottach-Eggern, 1963). p.373.

Molechanov, A.P., (1962). - Sov. Astr. AJ 5, 651.

Morimoto, M. (1963). - Ann. Tokyo Astr. Obs. 8, 125.

Morimoto, M., and Kai, K. (1962). - J. Phys. Soc. Japan, Supplement A-II 17, 220.

Newkirk, G. (1961). - Astrophys. J. 133, 983.

Newkirk, G. (1967). - Ann. Rev. Astron. and Astrophys. 5, 213.

Ondoh, T. (1966). - J. Radio Res. Lab. 13, 173.

Pakhomov, V.L., and Stepanov, K.N. (1963). - Soviet Phys. Tech. Phys. 8, 325.

Pick, M. (1961). - Annls. Astrophys. 24, 183.

Piddington, J.H., and Minnett, H.C. (1951). - Aust. J. Sci. Res. A4, 131.

Pines, D., and Bohm, D. (1952). - Phys. Rev. 85, 338.

Ramaty, R., and Lingenfelter, R.E. (1968). - Solar Phys. 5, 531.

Ratcliffe, J.A. (1959). - "The Magnetoionic Theory and Its Applications to The Ionosphere." (Cambridge Uni. Press: London.)

Roberts, J.A. (1958). - Aust. J. Phys. 11, 215.

Rosenbluth, M.N., and Rostoker, N. (1962). - Phys. Fluids 5,776.

Rostoker, N. (1961). - Nuclear Fusion 1, 101.

Rukhadze, A.A., and Silin, V.P. (1962). - Soviet Phys. Usp. 5, 37.

Sazonov, V.N., and Tsytovich, V.N. (1968). - Izv. Vuzov (Radiofizika) 11, 1287.

Schatzman, E. (1963). - Ann. Astrophys. 26, 234.

Sagdeev, R.Z., and Shafranov, V.D. (1961). - Soviet Phys. JETP 12, 130.

Severnyi, A.B. (1960). - Trans. Intern. Astron. Union, Moscow, 1958. p.647. (Cambridge, 1960).

Severnyi, A.B. (1966). - Soviet Phys. Usp. 9, 1.

Shafranov, V.D. (1967). - "Electromagnetic Waves in Plasma." "Reviews of Plasma Physics." Vol.3, p.1 (Consultants Bureau: New York.); translated from Report No. 194, Institute for Atomic Energy, USSR (1960).

Shain, C.A., and Higgins, C.S. (1959). - Aust. J. Phys. 12, 357.

Shapiro, V.D. (1963). - Soviet Phys. JETP 17, 416.

Shklovskii, I.S. (1946). - Astronomicheskii zhurnal 23, 333.

Sitenko, A.G. (1967). - "Electromagnetic Fluctuations in Plasma." (Academic Press: New York.). English translation from A.G. Sitenko's book entitled "Elektromagnitnye Fliuktuatsii v plazme" (Kharkov University Press: Kharkov, 1965).

Sitenko, A.G., and Stepanov, K.N. (1957). - Soviet Phys. JETP 4, 512.

Sitenko, A.G., and Radzievskii, V.N. (1966). - Soviet Phys. Tech. Phys. 10, 903.

Sitenko, A.G., and Gurin, A.A. (1966). - Soviet Phys. JETP 22, 1089.

Sitenko, A.G., and Kirochkin, Yu. A. (1966). - Soviet Phys. Usp. 9, 430.

Slysh, V.I. (1967). - Soviet Astr. AJ 11, 389.

Smerd, S.F. (1963). - "The Solar Spectrum." (Ed. C. De Jager) p. 398. (D. Reidel Publishing Co.: Holland, 1965).

Smerd, S.F. (1964). - "Research in Geophysics." (Ed. H. Odishaw) Vol. 1, p.89. (M. I. T. Press: Cambridge, Mass.).

Smerd, S.F. (1968). - Proc. Astr. Soc. Aust. 1, 124.

Smerd, S.F., Wild, J.P., and Sheridan, K.V. (1962). - Aust. J. Phys. 15, 180.

Spitzer, L. (1962). - "Physics of Fully Ionized Gases." Second Edition, (Interscience Publishers: New York.)

Stepanov, K.N. (1960). - Soviet Phys. JETP 11, 192.

Stepanov, K.N., and Kitsenko, A.B. (1961). - Soviet Phys. Tech. Phys. 6, 120.

Stewart, R.T. (1965). - Aust. J. Phys. 18, 67.

Stix, T.H. (1964). - Phys. Fluids 7, 1960.

Sweet, P.A. (1958). - Symp. IAU No. 6 (Stockholm, 1956) p. 128.

Tanaka, H., and Kakinuma, T. (1961). - Publ. Astr. Soc. Japan 13, 94.

Takakura, T. (1960a). - Publ. Astr. Soc. Japan 12, 55.

Takakura, T. (1960b). - Publ. Astr. Soc. Japan 12, 325.

Takakura, T. (1960c). - Publ. Astr. Soc. Japan 12, 352.

Takakura, T. (1962). - J. Phys. Soc. Japan, Suppl. A-II 17,243.

Takakura, T. (1963). - Publ. Astr. Soc. Japan 15, 327.

Takakura, T. (1967). - Solar Phys. 1, 304.

Takakura, T., and Kai, K. (1961). - Publ. Astr. Soc. Japan 13,94.

Thomas, R.N., and Athay, R.G. (1961). - "Physics of the Solar Chromosphere." (Interscience Publishers: New York.)

Thompson, A.R., and Maxwell, A. (1962). - Astrphys. J. 136,546.

Tidman, D.A., Birmingham, T.J., and Stainer, H.M. (1966). - Astrphys. J. 146, 207.

Tsintadze, N.L. (1965). - Soviet Phys. Tech, Phys. 9, 1397.

Tsytovich, V.N. (1966). - Soviet Phys. Usp. 9, 370.

Tverskoi, B.A. (1967). - Soviet Phys. JETP 25, 317.

Vedenov, A.A., Velikhov, E.P., and Sagdeev, R.Z. (1961). - Nucl. Fusion 1, 82.

Warwick, J.W. (1964). - "Solar System Radio Astronomy." (Ed. J. Aarons) p.131. (Plenum Press: New York, 1965.)

Weiss, A.A. (1963a). - Aust. J. Phys. 16, 240.

Weiss, A.A. (1963b). - Aust. J. Phys. 16, 526.

Weiss, A.A., and Stewart, R.T. (1965). - Aust. J. Phys. 18,143.

Wentzel, D.G. (1963). - Astrphys. J. 137, 135.

Wild, J.P. (1950). - Aust. J. Sci. Res. A3, 541.

Wild, J.P., Sheridan, K.V., and Neylan, A.A. (1959). - Aust. J. Phys. 12, 369.

Wild, J.P., Smerd, S.F., and Weiss, A.A. (1963). - Ann. Rev. Astr. Astrophys. 1, 291.

Young, C.W., Spencer, C.L., Moreton, G.E., and Roberts, J.A. (1961). - Astrophys. J. 133, 243.

Zaitsev, V.V. (1966). - Soviet Astr. AJ 9, 572.

Zaitsev, V.V. (1967). - Soviet Astr. AJ 10, 919.

Zayed, K.E., and Kitsenko, A.B. (1968a). - Plasma Phys. 10, 147.

Zayed, K.E., and Kitsenko, A.B. (1968b). - Plasma Phys. 10, 673.

Zheleznyakov, V.V. (1959). - Radiofizika 2, 14; Engl. Transl.: News of Higher Education Institutes- Radiophysics Series 2, 29 (1960).

Zheleznyakov, V.V. (1960). - Radiofizika 3, 180; Engl. Transl.: News of Higher Ed. Institutes- Radiophysics Series 3, 33 (1960).

Zheleznyakov, V.V. (1962). _ Soviet Astr. AJ 6, 3.

Zheleznyakov, V.V. (1965). - Soviet Astr. AJ 9, 191.

Zheleznyakov, V.V. (1968). - Astrophys. and Space Sci. 2, 417.

Zheleznyakov, V.V., and Zlonik, E.Ya. (1964). - Soviet Astr. AJ 7, 485.

Zheleznyakov, V.V., and Zaitsev, V.V. (1968). - Soviet Astr. AJ 12, 14.

SYMBOLS

All symbols are defined in the body of the thesis when they first occur. Those which are used more extensively and which may occur somewhat apart from their definitions are listed below:

$A = f_p^2/f_H^2$,

$\bar{a}_j$ = polarization vector for the electromagnetic wave in the j-mode

c = speed of light in vacuum

D = Debye length

D_α = electric induction

e = charge of an electron

$\hat{e}_1, \hat{e}_2$ = principal polarization axes for the transverse wave (Fig. 9.1)

f = wave frequency

$f_p = \omega_p/2\pi = (e^2 n_o/\pi m_o)^{\frac{1}{2}}$ = electron plasma frequency

$f_H = \omega_H/2\pi = |e|H_o/(2\pi m_o c)$ = magnitude of the electron gyrofrequency

$$f_\pm = \omega_\pm/2\pi = \sqrt{\tfrac{1}{2}}\{f_p^2 + f_H^2 \pm [(f_p^2 + f_H^2)^2 - 4f_p^2 f_H^2 \cos^2\theta]^{\frac{1}{2}}\}^{\frac{1}{2}}$$

= plasma resonance frequencies

$f_o(\bar{p})$ = particle momentum distribution function normalized to particle number density

$f_o(E)$ = particle energy spectrum

$F_o(\bar{p})$ = particle momentum distribution function normalized to unity

H_o = static magnetic field intensity

H_s = magnetic field intensity at the centre of the sunspot

I,Q,V,U = Stokes parameters

$I^{e,o}$ = intensity of electromagnetic radiations in the x-mode and the o-mode respectively

I_{ij} = polarization tensor

j_α = current density

j_{ij} = volume emissivity tensor

$j^{e,o}$ = volume emissivities in the x-mode and the o-mode respectively

$J_s(X)$ = Bessel function of s-th order with the argument $X = k_\perp v_\perp / \gamma\omega_H$

$\bar{k}$ = wave vector

$k_\perp, k_{||}$ = transverse and longitudinal components of the wave vector $\bar{k}$ respectively

$K^{e,o}$ = absorption coefficients in amplitude for the x-mode and the o-mode waves respectively

$k_D = (4\pi e^2 n_o/\kappa T)^{\frac{1}{2}}$

$K_{\alpha\beta}$ = polarizability tensor

K_{ijkl} = absorption tensor of the plasma

$K_\nu(z)$ = modified Hankel function of ν-th order with the argument z

L = source depth along the line of observation

m_o = rest mass of an electron

n_o (or N_o) = electron number density of the ambient plasma

n_o' (or N_o') = electron number density of the non-thermal electrons

n_j = refractive index

$\langle \delta n \rangle_{\bar{k},\omega}$ = spectral distribution of fluctuations of electron density

$P(\theta)$ = power of electromagnetic wave

P = degree of polarization

$p_\perp, p_{||}$ = perpendicular and parallel components of the particle momentum $\bar{p}$ respectively

$(q/k)_s$ = specific s-th harmonic resonance absorption coefficient

R_o = solar radius

s = harmonic number

T = temperature in ^oK

$v_\perp, v_{||}$ = perpendicular and parallel components of a particle respectively

$X = \omega_p^2/\omega^2$

$Y = \omega_H/\omega$

$\alpha^{e,o}$ = absorption coefficients in intensity for waves in the x-mode and the o-mode respectively

$\beta_T = (\kappa T/m_o c^2)^{\frac{1}{2}}$ = normalized mean thermal speed of the plasma electrons

$\beta_\perp = v_\perp/c$, $\beta_{||} = v_{||}/c$

$\beta = (\beta_\perp^2 + \beta_{||}^2)^{\frac{1}{2}}$

$\gamma' = (1 - \beta_\perp^2 - \beta_{||}^2)^{-\frac{1}{2}}$ = Lorentz factor

$\gamma = \gamma'^{-1}$

$|\mathrm{Im}\frac{\delta}{\omega_H}|$ = temporal growth rate of electromagnetic wave (normalized by angular gyrofrequency)

$\delta_{o1}, \delta_{o2}, \delta_o$ = coupling parameters

$\delta_{\alpha\beta}$ = Kronecker's delta

$\epsilon_{\alpha\beta} = \delta_{\alpha\beta} + 4\pi K_{\alpha\beta}$ = dielectric tensor of a plasma

$\xi = \omega/\omega_H = f/f_H$

$\tilde{\xi}_\pm = f_\pm/f_H$

$\zeta = A/\xi^2 + 1/\gamma'^2$

$\phi = \arctan(\beta_\perp/\beta_{||})$ = pitch angle of gyrating particle

ψ = azimuthal angle for a vector in a Cartesian coordinate system

ω_p' = angular electron plasma frequency of the stream in the reference frame in which the stream is at rest

$\rho = R/R_o$ = radiatial distance from the centre of the Sun in units of solar radius

ν = electron-ion collision frequency

κ = Boltzmann constant

$\bar{\kappa} = \bar{k}/k$

ω = angular wave frequency = $2\pi f$

$\hat{}_{\alpha\beta} = \frac{c^2}{\omega^2}(k^2\delta_{\alpha\beta} - \frac{\omega^2}{c^2}\varepsilon_{\alpha\beta} - k_\alpha k_\beta)$ = Maxwell's tensor

η_j = coefficient of transformation of the plasma wave into the electromagnetic wave in the j-mode

η_{ij} = electron emissivity tensor

$\eta^{e,o}$ = electron emissivity in the x-mode and the o-mode respectively

$\sigma = n_o'/n_o = N_o'/N_o = \omega_p'/\omega_p$

θ = wave-normal angle; angle between static magnetic field and wave vector